Title

A Comprehensive Study of the Physical Properties of Isolated Zymogen Granules Using Scanning Transmission X-ray Microscopy

Author

Goncz, K.K.

Publication Date

1994

LBL-35088
UC-406/408

Lawrence Berkeley Laboratory
UNIVERSITY OF CALIFORNIA

Materials Sciences Division

A Comprehensive Study of the Physical Properties of Isolated Zymogen Granules Using Scanning Transmission X-Ray Microscopy

K.K. Goncz
(Ph.D. Thesis)

January 1994

Prepared for the U.S. Department of Energy under Contract Number DE-AC03-76SF00098

DISCLAIMER

LBL-35088
UC-406/408

A COMPREHENSIVE STUDY OF THE PHYSICAL PROPERTIES OF ISOLATED ZYMOGEN GRANULES USING SCANNING TRANSMISSION X-RAY MICROSCOPY

KAARIN KERR GONCZ
Ph.D. Thesis

DEPARTMENT OF BIOPHYSICS
University of California

and

MATERIALS SCIENCES DIVISION
Lawrence Berkeley Laboratory
University of California
Berkeley, CA 94720

DECEMBER 1993

This work was supported by the Director, Office o fEnergy Research, Office of Basic Energy Sciences, Materials Sciences Division, of the U.S. Department of Energy under Contract No. DE-AC03-76SF00098.

A COMPREHENSIVE STUDY OF THE PHYSICAL PROPERTIES OF ISOLATED ZYMOGEN GRANULES USING SCANNING TRANSMISSION X-RAY MICROSCOPY

by

KAARIN KERR GONCZ

Abstract

A Comprehensive Study of the Physical Properties of Isolated Zymogen Granules Using Scanning Transmission X-Ray Microscopy

by

Kaarin Kerr Goncz

Doctor of Philosophy in Biophysics

University of California at Berkeley

Professors Stephen S. Rothman and Harold Lecar, Chairs

Zymogen granules isolated from pancreatic acinar cells were observed at 50 nm resolution using scanning transmission X-ray microscopy. Granules were suspended in isosmotic medium at pH 6.0 immediately after isolation and, using a specially designed environmental sample chamber, individual granules were imaged periodically over time for up to 4 hours without the use of stains or fixative. In other experiments, granules were exposed to different solutions - isosmotic sucrose, hyperosmotic sucrose, water, isosmotic salt - and 0.025% & 0.05% Triton X-100, 5μM Nigericin and two concentrations of chymotrypsinogen all in isosmotic sucrose - perfused through the sample chamber and again individual granules were imaged repeatedly over the time course. The solutions (pH 6.0) were: In addition, the effects of glutaraldehyde were studied by comparing fresh to fixed granules.

The diameter, protein content (mass) and concentration of each granule was measured from the images. The rate of protein efflux from individual granules was determined. On average, granules continuously decreased in size and protein mass towards a final protein concentration characteristic of the preparation. An increase in protein mass and diameter was observed for granules expose to solutions containing chymotrypsinogen. The

decrease (or increase) in size and protein varied with the particular solution. Protein was determined to be released (or taken up) by the granule according to mass action and the permeability of the granule membrane. Lysis of the granules, or sudden loss of protein content, was not observed.

The protein permeability coefficient (P) for individual granules was calculated and an average permeability coefficient of 2-7 x 10^{-6} cm/sec estimated. The relatively large value of P suggests that a protein transport mechanism exists in the granule membrane. A single aqueous channel large enough to allow single file diffusion of protein through the membrane gives a similar value. Currently, there are two reports of pores in granule membrane large enough to accommodate proteins, although their function remains to be shown. These results provide direct visual and quantitative confirmation of the hypothesis that the membrane enclosing this object is permeable to its various contained proteins, although the mechanism of transport remains to be proven.

Stephen S. Rothman

Harold Lecar

Harold Lecar

To the water signs who were as invaluable to me
in the realization of
this thesis as
the water window is to X-ray microscopy:

My Mum, major advisor and, husband - Robert

First of all I would like to thank my major advisor, Stephen Rothman, for his unique contribution to my thesis. Steve initially proposed this project to me and although he had his own stake in the work, he allowed me the freedom to develop the research according to my interests. He also made sure that I could still see the forest when it seemed all I was doing was running into the trees. In Steve's lab, I would also like to thank both Bill Loo and Hsien-Chen Tseng who spent many hours with me at Brookhaven helping in the experiments.

I would also like to thank the people at the Center for X-ray Optics, who have supported me throughout the entire project. Especially David Attwood, who introduced me to X-rays. Also, Phil Batson and René Delano whose machine shop wizardry produced our sample holders. Finally, all of the computer people who have helped in both the hardware and software aspects of this project - Ron Tackaberry, William Lin and Rolf Behrsing. I would still be trying to print images if it weren't for you all. I would also like to thank Eric Gullikson and Malcolm Howells for several enlightening conversations about the interactions of X-rays with material. And, Jim Underwood for his unique perspective.

This experience would not have been half as pleasurable if it weren't for the friendliness of the people at Brookhaven National Laboratory. I appreciate the time Janos Kirz, a true scientist, was willing to spend helping out at the beam line, no matter what hour. Chris Jacobsen, whose great sense of humor and knowledge combined for some interesting interactions. Shawn Williams, another biophysicist whose enthusiasm is completely infectious. Steve Lindaas, as near to a graduate student peer as I have and may his filing date be as close to mine as our birthdays. Also, Ian McNulty for his willingness at any time to put aside his tasks and help with mine, and Harold Ade for conversation. Oh yes, and Sue Wirick, the inexhaustible lab technician.

There are also three other X-ray microscopists I would also like to thank. The first is Nasif Iskander, who originally began the project many years ago and has helped me finish it. The second is John Gilbert whose path I only crossed because of Brookhaven but I am glad to find that our friendship has escaped "the island." And finally, Mario Moronne, whose eclectic skills range from great scientific discussions to fantastic pasta!

The research for this dissertation was supported by the Director, Office of Health and Environmental Research and the Office of Basic Energy Sciences, Material Sciences Division, of the U.S. Department of Energy under contract No. DE-AC03-76SF00098; by the U.S. Department of Defense, Air Force Office of Scientific Research under Contract No. F49620-87-K-0001.

Table of Contents

List of Figures and Tables

Introduction

In the examination of this thesis, I would ask the reader to keep in mind that there are two purposes to this particular project. The first was to design an experiment that would help resolve a biological question. This question concerned the permeability of isolated zymogen granules from the acinar cell of the exocrine pancreas to their contained proteins. But, because this experiment involved the new and relatively untested technique of X-ray microscopy, the second goal, which actually predated the first goal, was to be able to adapt the experiment to the physical constraints of the machine and understand its limitations and benefits well enough to be able to perform the experiments.

In this chapter, I would like to briefly introduce the particular question about zymogen granules that we sought to answer and why we chose the X-ray microscope as an investigative instrument. The final section is a brief overview of the chapters contained in the thesis.

What about Zymogen Granules?

For three hundred years it has been known that the mammalian pancreas secretes a juice into the small intestines, via a duct, and that this juice is associated with the digestive function (Thomas, 1930). One hundred years ago, Heidenhain (1875) was the first to identify and characterize the cells of the pancreas. By performing extensive research using the light microscope on fixed and stained dog pancreas he observed the acinar cells and identified features within these cells. Some features were common to other mammalian cells, such as the nucleus, but he also discovered that a large volume of each acinar cell was occupied by dense spherical granules (~1μm in diameter) clustered at one end of the cell, the apical region. He also observed that many of these cells would group together with their apical ends oriented towards the center of the cluster forming what he called an acinus. The center of this cluster surrounds a lumen which is a duct leading into the small intestine.

He compared changes in appearance of acinar cells from fasted and fed dogs and noted that the size and number of these granules were different. Fasted animals had many large granules and fed animals appeared to have fewer granules that were smaller. From these observations and many other experiments, he concluded that the granules within the acinar cell were the site of storage for the digestive enzymes that the pancreas produced and that upon stimulation (e.g. eating) the enzymes were released from the granules into the duct and passed into the small intestine. The granules were called "zymogen granules" because Heidenhain believed that they contained only the precursors (zymogens) of the active digestive enzymes; although, it was not until the 1940's and the development of biochemistry that this could be verified (Northrop and Kunitz, 1948).

It is obvious that understanding the mechanisms by which the zymogen granule accumulates, stores and releases the digestive enzymes is critical to our understanding of the function of the acinar cell and the process of digestion. But on a much larger scale, the acinar cell is only one of many different secretory cells in the mammalian system. There are many other secretory cells in epidermis, endocrine and nervous systems. Therefore, by understanding the mechanisms of protein transport in the acinar cell we learn something about the general process of protein transport. This information can then be applied to the many other fields of research concerning these and other cells in general.

In the past 100 years, there have been many technological advances which have contributed to our understanding of the process of protein transport. The first widely accepted model of the process of protein transport through the acinar cell was based in part on the results of the electron microscopic autoradiography techniques (Jamieson and Palade, 1971). This model, which will be described in greater detail in chapter I, proposed that the digestive enzymes are manufactured in the endoplasmic reticulum (ER) of the cells, transported to the Golgi apparatus and from the Golgi apparatus, transported to the

condensing vacuoles, which are precursors to zymogen granules. The condensing vacuoles undergo condensation and are transformed into the mature zymogen granules that were originally identified by Heidenhain. It was proposed that the enzymes are then released into the duct lumen by a process called exocytosis. When the acinar cell is stimulated to secrete, the zymogen granule membranes fuse with the apical membrane of the cell and the granule extrudes its contents.

Although this model of protein transport through the cell is still generally accepted, there are a variety of experimental observations that challenge the exocytosis model of secretion. The primary alternative being what is called "the equilibrium model" (Rothman, 1975). This model is based in part on the observation that when isolated zymogen granules are suspended in isosmotic solution (0.3M sucrose, pH 6.0) for a period of time (0-4hr) enzymes can be detected in the suspending solution using enzyme assay techniques. Based on this observation and many others, including in situ experiments (which are described in chapter 1), Rothman and colleagues proposed that the zymogen granule membrane is permeable to its enclosed proteins and protein molecules can move through the cell individually, in response to mass action. The equilibrium model was not presented as an alternative to the exocytosis model, but as another possible route for protein transport. The two models are shown in figure 1.

There were two major criticisms of Rothman's proposal and the measurements. The first was that, at the time, it was considered highly unlikely that a large polar protein molecule (average MW ~35,000) would be able to pass through the hydrophobic membrane. And the second was that because the measurement of protein release was indirect (e.g. as detected by an enzyme assay and not directly observed) it was impossible to be certain how individual granules were releasing protein. Theoretically, the same results could have been attained if some of the granules in the population lysed (i.e. broke open and released their contents into the suspending solution) while the other granules

remained intact instead of all of the granules responding to mass action. At the time, there was no technique that could distinguish between the two possibilities. Light microscopy does not provide the resolution to adequately observe 1 μm sized objects. The electron microscope (EM) offers the needed resolution, but it is not possible to observe the same granule over a period of time. Therefore, the proposal that the zymogen proteins could cross the enclosing membrane of the granule remained speculative in the eyes of many scientists. The observations were discounted as artifact even though, as mentioned above, there were other in situ experiments that supported this conclusion.

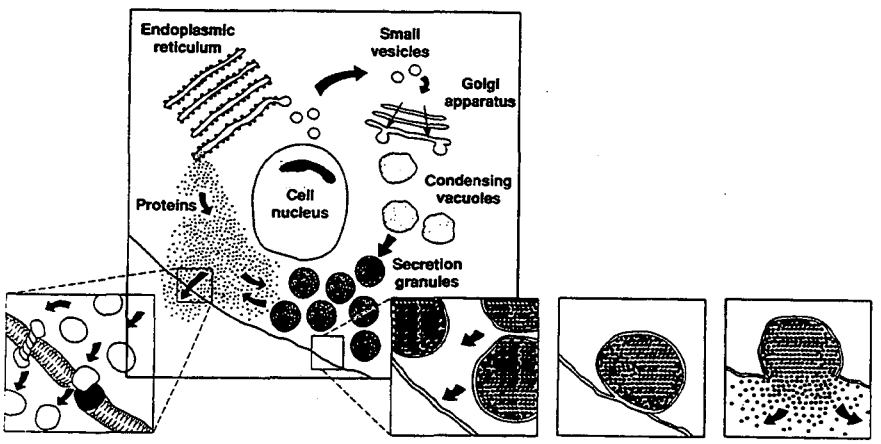

Figure 1 A schematic drawing of two views of the secretion process. The exocytosis model is outlined on the right, showing protein products being moved through a series of membrane bound compartments, culminating in the exocytosis of the granule (inset). The equilibrium model is shown on the left, and shows individual proteins crossing the membrane of the zymogen granule and the cell. In this model, some proteins destined for secretion may not necessarily be stored in the zymogen granule but instead pass directly through the cell membrane (inset).

Recently, it has been become evident that the direct trans-membrane transport of proteins is a common process; for example in mitochondria and the nucleus. With the

discovery of specialized pores through which proteins can pass, membrane porter molecules for proteins and cytoplasmic helper molecules or chaperones; there is a growing realization that the complex physically and chemically diverse structures of bio-membranes and proteins are variously adapted to carry out protein transport functions. There is even evidence of a 5nm pore in the zymogen granule membrane (Cabana, 1988) and work is currently underway to isolate a large membrane protein that may be this pore (Tseng).

So, given that there is now much evidence indicating that direct membrane transport of proteins is possible, we were interested in addressing the second point of contention regarding Rothman's proposal - the uncertainty regarding the mode of protein release from zymogen granules. Our intention was to re-examine isolated zymogen granules, but by direct observation on a visual and quantitative level and follow individual granules as they released their contained proteins. We would witness lysis, if it occurred. The newly developed technique of X-ray microscopy, at least in theory, offered us the opportunity to make these type of observations and test Rothman's observation.

Why X-ray microscopy?

The concept of using X rays as the light source for a microscope has been around for many decades (Lamarque, 1936). It is an attractive alternative to both light and electron microscopy for a variety of reasons. First, because the resolution of any microscopy ultimately depends on the wavelength of the illuminating source, and because X-rays have a shorter wavelength than with visible light, we can expect to achieve a higher resolution than light microscopy, although not as high as with the electron microscope. Second is that in the range of X-ray wavelengths (2.3 - 4.4nm, called the water window) water transmits X rays by a factor of 10 more efficiently than organic material (primarily carbon). This results in a natural contrast in a biological specimen between its organic

content and water. Therefore, samples can be imaged *in vitro* without the use of the stains that are necessary for EM.

A graph of the absorption of water and protein in the water window is shown in figure 2. The final advantage of X-ray microscopy is that there is a quantitative relationship between the number of X-ray photons that are transmitted through a sample and the amount of material that is present, making it possible to calculate the exact amount of a specific material in our sample.

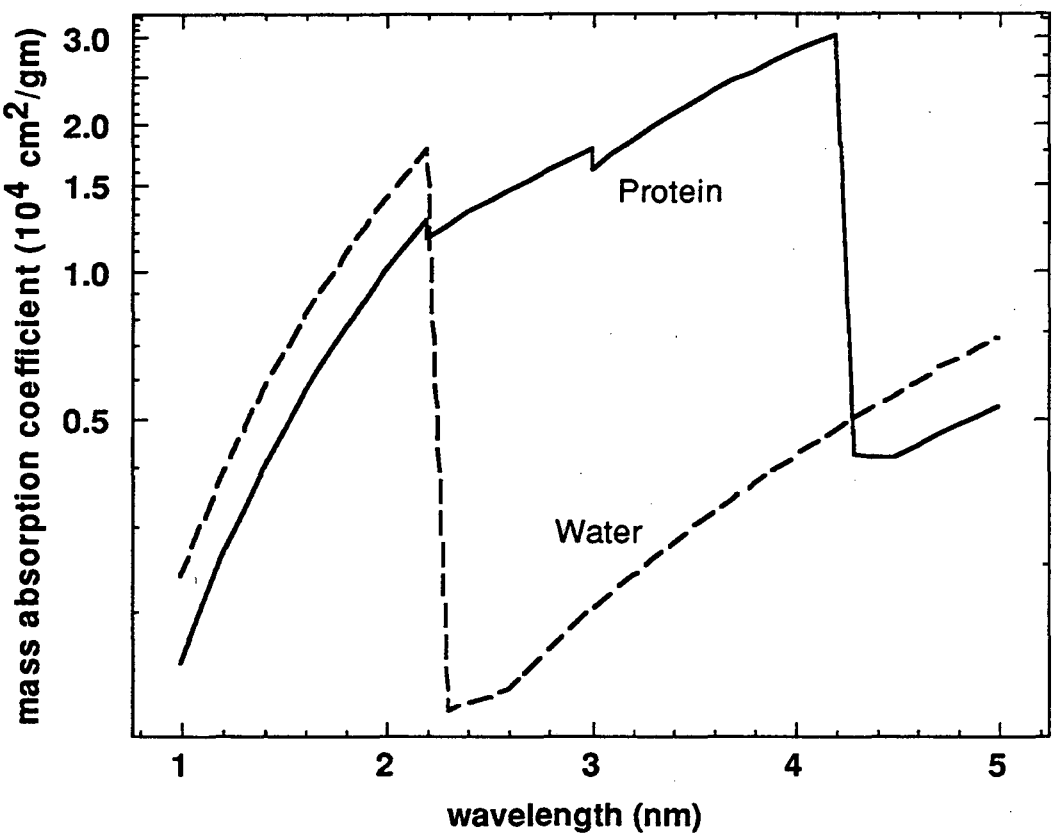

Figure 2 The mass absorption coefficients versus the wavelength for both protein and water. We can see that in the range between 2.3 and 4.4nm, the mass absorption coefficient is approximately a factor of 10 greater than water. This means that protein will absorb more X-ray photons than water which results in a natural contrast between biological samples and their aqueous environments without the use of stains. This wavelength region is referred to as the "water window." The data from this graph is from Kirz and Rarback (1985).

These three aspects of X-ray microscopy offered us the possibility of making the needed measurements on the zymogen granules by 1) providing high resolution, ~ 50 nm currently (Howells et. al., 1991), which is high enough to observe the morphologic consequences of protein release from individual granules, 2) allowing the needed aqueous environment and ambient pressure and temperature in which to suspend whole granules so that protein release can occur and 3) permitting the simultaneous quantitative measurement of protein release from individual granules on the order of femtograms.

It has only been the availibility of two relatively recent technological advances - high brightness, partially coherent soft X-ray radiation sources (e.g., synchrotrons) and diffractive X-ray lenses capable of focusing such radiation to a small spot size - that make high resolution X-ray microscopy a practical reality. When we first began our work in 1988, there were 11 soft X-ray microscopes in the world (Howells, 1985) and biological research was on the level of imaging diatoms or dried, fixed biological samples (Sayre et. al., 1988). While it was clear that the microscopes could produce images of certain biological samples, it was not known whether we would be able to image individual zymogen granules over a period of time as our experiment required.

Rothman et al. (1988, 1989) had done some previous preliminary work examining zymogen granules at one of the facilities mentioned above (Rothman, 1988, 1989). This facility, located at the NSLS synchrotron in Brookhaven National Lab (BNL) on Long Island, New York, is one of three facilities that have X-ray microscopes which have been committed to development for biological experiments. The other two are the Daresbury synchrotron in England and the BESSY synchrotron in Berlin, Germany.

In this preliminary work, freshly isolated zymogen granules suspended in 0.3M sucrose (pH 6.0) were imaged by sandwiching the specimen between two silicon nitride membranes sealed with epoxy cement in order to maintain a fluid environment. The microscope at that time was in a state of development and they were only able to take a

few images of granules at a resolution of ~100 nm. So, while X-ray microscopy offered promise as a technique to resolve the zymogen granule permeability question, the evidence that it *could* work was not to be had. As a result, we spent as much time developing the techniques for executing the experiments as we did actually carrying them out.

Since we began our experiments in 1988 at BNL, there has been a tremendous increase in the number of biological studies performed using X-ray microscopy. The latest conference on X-ray microscopy was held September 20-24, 1993 in Moscow and the number of biological experiments that have been performed has increased 20 fold since 1988. We are pleased to see that the pioneering efforts presented in this thesis (as well as those performed by others at the same time) are now receiving general acceptance and the field of X-ray microscopy is growing by leaps and bounds.

Review of Thesis

From the previous sections, it is clear that the challenge of this thesis project was to improve and apply the technique of X-ray microscopy in order to shed light on the twenty year old question of whether or not the membrane of isolated zymogen granules are permeable to their enclosed proteins. The first chapter is a review of the current knowledge concerning the function, composition and characteristics of the zymogen granule and in it is described the experiments that were originally performed on isolated granules which motivated this thesis work. The second chapter describes the scanning transmission X-ray microscope (STXM) that we used in the research. The third chapter explains the digital images that STXM produces and presents the image processing and mathematical manipulations that we performed on them. The fourth chapter is a description of the sample chamber which we developed for use in STXM. The fifth chapter presents our methods for isolating the zymogen granules, performing the

experiments and our imaging protocols. Included in this chapter is a brief discussion on our considerations of radiation damage to our sample but a more complete description of X-ray damage to biological specimens is given in the seventh chapter. In the sixth chapter are the results of our experiments. And the eighth chapter is the discussions and conclusions from our experiment.

Introduction - References

Cabana C, P. Magny, D. Nadeau, G. Grondin and A. Beaudoin, Freeze-fracture study of the zymogen granule membrane of pancreas: two novel types of intramembrane particles. Euro. J. Cell Biol. (1988) **45**:246-55.

Heidenhain, R., Beiträge zur Kenntniss des Pancreas, Pflüger Archiv. Phsyiol. (1875) **10**:557-632.

Howells, M.R., J. Kirz and D. Sayre, X-ray Microscopes, Sci. Am. (1991) **264**: 88-94.

Howells, M.R., J. Kirz, D. Sayre and G. Schmahl, Soft X-ray microscopes, Phys. Tod. (1985) **42**:2-11.

Kirz, J. and H. Rarback, Soft X-ray microscopy, Rev. Sci. Instrum. (1985) **56**:1-13.

Jamieson, J.D. and G.E. Palade, Condensing vacuole conversion and zymogen granule discharge in pancreatic exocrine cells: metabolic studies, J. Cell Biol. (1971) **48**:503-522.

Lamarque, P., Histologie-historadiographie, C.R. Acad. Sci. Paris (1936) **202**:684-685.

Northrop, J.H., M. Kunitz and R.M. Herriott, Crystalline Enzymes, Columbia University Press: New York (1948).

Rothman, S.S., Protein transport by the pancreas, Science (1975) **190**: 747-753.

Rothman, S.S., N. Iskander, K. McQuaid, H. Ade, D.T. Attwood, T.H.P. Chang, J.H. Grendell, D.P. Kern, J. Kirz, I. McNulty, H. Rarback, D. Shu and Y. Vladimirsky, The Biology of the cell and the high resolution X-ray microscope, In: X-ray Microscopy II (D. Sayre, M. Howells, J. Kirz and H. Rarback, Eds.), Springer-Verlag: Berlin (1988).

Rothman, S.S., N. Iskander, D. Attwood, Y. Vladimirsky, K. McQuaid, J. Grendell, J. Kirz, H. Ade, I. McNulty, D. Kern, T.H.P. Chang and H. Rarback, The interior of a whole and unmodified biological object - the zymogen granule - viewed with a high-resolution X-ray microscope, Biochim. Biophys. Acta. (1989) **991**:484-486.

Sayre, D., M. Howells, J. Kirz and H. Rarback (Eds.), X-Ray Microscopy II, Springer-Verlag: Berlin, (1988)

Thomas, J.E., The external secretion of the pancreas, In: Selected Readings in the history of physiology, Charles C. Thomas: Springfield, Ill. (1930).

Tseng, H.C. Personal communications.

Chapter I. An Introduction to zymogen granules

Zymogen granules are spherical organelles, ~1μm in diameter found in the acinar cells of the exocrine pancreas. These cells are adapted for the synthesis and secretion of digestive proteins that are used in the small intestine to digest the food that we eat. And, the zymogen granules function as "storage vesicles" for these proteins within the cell. The protein secretory mechanisms of this particular cell have been and still are the subject of extensive studies and many of our ideas about these processes in other types of cells have been derived from these studies. The acinar cells have the ability to secrete the 20 or so digestive enzymes they manufacture in varying proportions in response to a variety of stimuli or secretagogues (or to no stimuli). While it is known that zymogen granules have the role of storing and releasing the digestive enzymes, the mechanisms that underlie these processes are still not well understood and require further investigation.

What is currently understood about these mechanisms comes from many different types of experiments, from general research on the process of protein secretion to specific studies on isolated zymogen granules. In the first part of this chapter we will review some of this research, starting with the broad topic of protein secretion. We will also disucss specific observations on the behavior of zymogen granules during secretion in situ in acinar cells. And, finally we will present some of the characteristic properties of zymogen granules, their morphological and chemical structure.

The specific results of some of the isolation experiments suggested one type of mechanism by which the zymogen granule could accumulate, store and release protein (Rothman, 1975a). But at the time, these results were considered artifactual by many workers. Over the years, however, evidence has accumulated that has made it difficult, although not impossible, to discount these original observations. X-ray microscopy, at least in theory, offered to shed new light on these old experiments. We were thus

motivated to use this technique to attempt to either confirm the results and give credence to this mechanism of protein transport into and out of the zymogen granule first suggested by Rothman (1975a), or to demonstrate its falsity. Therefore, in the final section of this chapter, we will specifically discuss the isolation experiments that had been performed on isolated zymogen granules and the results that provide the background and objective for our experiments.

I.1 The process of protein secretion

The processes of protein manufacture, intra-cellular transport and extra-cellular secretion are found, to at least some degree, in almost all types of eukaryotic cell. These mechanisms were first studied in the acinar cell and given the ubiquity of these processes, many of our ideas about how these same mechanisms work in other cells has been derived from these studies. In this section, we will present the original model for the pathway of protein secretion in the acinar cell. From this model, what is known as the exocytosis mechanism by which zymogen granules release protein, was proposed. However, evidence for this mechanism in the acinar cell was sorely lacking, although it appeared to occur in other types of secretory system. Additionally, it could not wholly account for observations of "non-parallel" protein secretion from the acinar cell. We will explain what is meant by "non-parallel" secretion and present the subsequent modifications to the originally proposed exocytosis mechanism, by which zymogen granules may release their protein that have been proposed for the acinar cell.

I.1.1The secretory pathway and the vesicular model of protein transport

The general pathway for secretory proteins from their site of initial translation within the cell to their secretion outside of the cell was first proposed by Palade and his collaborators from their studies on the acinar cells of guinea pig (Jamieson and Palade, 1967, 1971a,b, 1977; Palade, 1975; Siekevitz and Palade, 1960). Using a combination of morphological, autoradiographic and cell fractionation studies they proposed the

following model. Secretory proteins are first synthesized on the endoplasmic reticulum (ER) and simultaneously translocated into its cisternae. From here, they are transported to the Golgi apparatus. Although, their studies did not establish the route taken by secretory products through the Golgi apparatus, their autoradiographic findings demonstrated that the secretory products are transported to condensing vacuoles (CV) located on the trans side of the Golgi stack. The CVs are filled with secretory product and are converted into mature zymogen granules (ZGs), where the secretory product remains until an appropriate stimulus causes the release of their content from the acinar cell. This final step was proposed to occur through a process called exocytosis in which the zymogen granule membrane would fuse with the apical membrane of the cell and the contents would be released into the lumen of a duct system which eventually leads to the small intestine. The reader is referred to a review article by Case (1978) for a further discussion of this model.

Evidence for this pathway through the cell (ER --> Golgi --> secretion granules) for proteins that are destined for secretion has accumulated for many types of cells[1] (Burgess and Kelly, 1987). However, the mechanisms by which the secretory protein is transported from organelle to organelle within the cell that were originally suggested (there was no direct evidence) in this model are still the subject of intense investigation in the acinar and other cells. For example, in order for protein to pass from the ER to the Golgi, Jamieson and Palade proposed that microvesicles containing the protein would bud off from the ER and shuttle to the Golgi, where they would fuse and release the protein into the lumen of the Golgi apparatus. There was no direct evidence for this process at the

[1]It is important to understand that this pathway is what is known today as the "regulated pathway" of secretion because a stimulus is required for protein secretion. The acinar cell is also known to have a "constitutive pathway" by means of which proteins are secreted spontaneously and without being stored in the zymogen granules. We will not discuss the constitutive pathway in this chapter and the reader is refered to a review of this pathway in the pancreas by Beaudoin and Grondin (1991). Reviews of both the regulated and constitutive pathways in other cells can be found in Chung et al. (1989) and Burgess and Kelly (1987).

time, or for many years, although some recent immunocytochemical observations now support this theory (Posthuma, et al., 1988). Also, the route taken by secretory proteins through the Golgi stack from the cis side to the trans side was not addressed by Jamieson and Palade, but has since been studied in detail by J. Rothman (1975) and others, who have described many of the chemical changes that the proteins undergo within this organelle. The mechanism by which the CVs are filled in the acinar cell is also still not well understood. It may be that the CVs originate as distention's of the Golgi membrane, but contrary to evidence for some hormonal cells, the CVs do not stay attached to the Golgi and continue to fill with secretory product. Instead, the CVs in the acinar cell are separate entities. It has been proposed that again, microvesicles may play a role by shuttling protein from the Golgi to the CVs in order to fill them. Empty microvesicles would then bud off the CV membrane and return to the Golgi in order to recycle the membrane. There is some relatively recent evidence that supports this hypothesis (Beaudoin and Grondin, 1987).

And finally, while the process of exocytosis proposed by Palade and collaborators was based on electron micrograph images that suggested granules fusing with the apical membrane, there has since been little additional evidence supporting this mechanism in the acinar cell. Geuze and Poort (1973) measured an increase in the length of the apical membrane of an acinar cell after it had been stimulated to secrete for 2hrs, during which 90% of the granules were discharged. The increased length of the apical membrane was interpreted as indicating that the granules fused with this membrane. However, in 30 years of research on this system, this is the only report of an increase in the surface area of the apical membrane. But while the evidence for exocytosis in acinar cells is not overwhelming, this process has been observed in other types of cells; e.g., mast cells (Zimmerberg, 1993), chromaffin cells (Patzak and Winkler, 1986) and neurons (von Wedel et al., 1981).

Thus, although there is a substantial literature that provides a range of evidence that is consistent with the pathway of intracellular transport first laid out by Palade and collaborators for the acinar and other types of cells, what we can see is that the mechanisms within this pathway that transport protein from organelle to organelle and eventually out of the cell are not well understood and may be different from cell type to cell type. Specifically, the evidence that exocytosis occurs in acinar cells is substantially less than from other types of cells. This leaves open the possibility of alternative mechanisms by which the zymogen granule may release its contained proteins. Indeed, this idea is reinforced from particular observations on protein secretion from the acinar cell, explained below, that are not consistent with an exocytosis mechanism. As a result, the exocytosis model for the release of protein from the acinar cell has been re-evaluated and modified.

I.1.2 Non-Parallel protein transport

One of the main problems with the Jamieson-Palade model of protein secretion as originally envisioned was that it could not explain observations of non-parallel secretion of enzymes from the pancreas. Non-parallel secretion means that the pancreas is able to secrete its twenty or so enzymes in differing proportions in response to different stimuli. The exocytosis model, as originally proposed, could not account for this observation because it predicted, and there was no reason to think otherwise, that each granule contained an undefined mixture of the digestive enzymes and that upon stimulation, the granules would randomly fuse with the apical membrane of the acinar cell and release their contents *en masse* . The secretory product of the pancreas therefore, would contain, on average, proportional or "parallel" amounts of the different enzymes. But Rothman (1967a) observed that the hormone pancreozymin, differentially enhanced the secretion of trypsinogen and chymotrypsinogen (two of the 20 enzymes) from an *in vitro* pancreas. And in subsequent experiments (Rothman, 1967b, 1969, 1970, 1974a), it was confirmed

that different enzymes (commonly trypsinogen, chymotrypsinogen and amylase were measured) were indeed secreted in varying proportions in response to a variety of different secretagogues. The observation of non-parallel secretion from the pancreas was later observed by other investigators (Singh, 1982; Sommer and Kasper, 1981; Dagorn, 1978). Rothman and Isenman (1974) proposed that there must be at least one other pool of digestive enzymes, in addition to the zymogen granules, that could be affected by a stimulus in order to account for this observation. They suggested that the relative contribution to secretion from each pool is altered by stimulants thus producing non-parallel secretion.

Rothman's experiments actually confirmed observations of non-parallel secretion that had been made much earlier by Pavlov and Walther (Pavlov, 1910). In these experiments, it was proposed that the proportions of different digestive enzymes found in pancreatic juice and in the intestines varied in a substrate-related manner. But later, Babkin (1950) was not able to confirm these results and they were considered an artifact; results of the misuse of enzyme assays. It was not until the development of more sensitive enzyme assay techniques that the process of non-parallel secretion could be confirmed.

In any event, the observation of non-parallel secretion meant that the original model of protein secretion by *en masse* exocytosis of zymogen granules needed to be modified. There were two approaches to take - one involved addressing the basic assumption of the process of exocytosis by which proteins leave the cell (the equilibrium model) and the other attempted to modify how exocytosis might occur (vesicular models).

I.1.3 Non-parallel secretion and the equilibrium model

Rothman's original observation of non-parallel secretion led to his proposal that some secretory proteins in the acinar cell were actually free to move independently of each other in response to particular stimuli. This was "the equilibrium model" of protein secretion. *Instead* of all of the proteins being constrained to move *en masse* by zymogen

granule exocytosis, they moved separately (Rothman, 1975a). In this manner, even though different type proteins were all stored in zymogen granules, particular enzymes would be influenced to leave this pool upon stimulation and pass through the cytoplasm before crossing the cell membrane into the duct. The driving force responsible for moving the proteins once they were released from the storage pool was simple concentration gradients and transport occurred by a reversible process capable of equilibrium behaviour. This model did not preclude the possibility of exocytosis but proposed an additional pathway whereby the ratios of the different types of secreted digestive enzymes could be varied.

Rothman developed this model on the basis of several observations on the movement of secretory protein, in addition to non-parallel transport itself, that suggested that these proteins could move independently. One of the more interesting observations was that acinar cells secreted protein even when there were no visible zymogen granules (Rothman, 1975b). He also found evidence that digestive enzyme was present in the cytoplasm (Rothman, 1970) and that exogeneously added chymotrypsinogen entered the cell, was found in the cytoplasm and accumulated in zymogen granules (Liebow and Rothman, 1974). These experiments suggested that indeed granule proteins could move independently through the cell.

But, perhaps the most important experiment, for our purposes, was that isolated ZGs released their contained protein into the suspending solution (Liebow and Rothman, 1972; Burwen and Rothman, 1972; Rothman, 1972, 1971). These experiments suggested that the granule proteins were able to cross membranes, at least the enclosing membrane of the zymogen granule, and therefore suggested a mechanism by which the proteins could independently move through the cell. Moreover, the experiments confirmed that proteins moved in response to concentration gradients since protein moved from the zymogen granule to the suspending solution, where there was no protein. However, over

time as the protein concentration increased in the suspension medium, the rate of protein release from the granules was measured to decrease, suggesting that the system was approaching an equilibrium or stationary steady-state; the protein efflux rate was the same as the influx. As such, this phenomenon also suggested a process by which the zymogen granules could be filled. Protein from the cytoplasm could enter the granules and be bound to the osmotically inactive aggregate that was already accepted to be a part of the structure of the granules. As these aggregates did not contribute to the protein concentration within the granule, protein would continue to move into the granule until filling was complete, i.e. additional binding to the aggregate was no longer possible. But, the model did not gain much support at the time because there was a reluctance to accept its premise that secretory proteins could "diffuse" through membranes.

I.1.4 Non-parallel secretion and the exocytosis model

Researchers reluctant to accept that proteins were able to cross cell membranes, especially since there was no established mechanism by which this could occur, concentrated their efforts on understanding how non-parallel secretion could occur by exocytosis. Two general hypothesis have resulted from these efforts - one in which the process of exocytosis is controlled at the cellular level and one where it is controlled at the zymogen granule level.

At the cellular level, it was proposed that although the pancreas appears to be composed of homogeneous acinar cells it is actually a heterogeneous organ, a mixture of different types of secretion cells, which respond differently to different stimuli. These different cells would individually produce secretory proteins in different proportions and so non-parallel secretion would occur as a result of different cells being stimulated. The attraction of this model was that the original notion of exocytosis as a random process is maintained; granules would be filled "normally" and, the only difference would be that only certain stimulated cells would secrete at a given time. But naturally, this model

requires the existence of different types of acinar cells that would produce more of one type of enzyme than another in some sort of ordered fashion. Since it was known that all of the enzymes are present in all of the cells (Bendayan et al., 1980; Kraehenbuhl et al., 1977), the enzyme production for all of the various enzymes would have to be regulated in each cell. It has been shown that there are variations in the rate of synthesis of different secretory proteins at the ER level (Scheele and Tartakoff, 1985; Geuze and Slot, 1980), and that rates of synthesis of each protein can be affected by different secretagogues (Rausch et al., 1985; Schick et al., 1984). This would have a long term effect on the proportions of enzymes in each cell (see reviews by Pfeffer and Rothman (1987); Rothman (1987)). So, it is possible for different cells to produce different amount of the enzymes, but is there evidence for a heterogeneous population of cells within the pancreas? There has always been a natural distinction between acinar cells that are located near islets of Langerhans and those found further away. These cells are called "peri-" and "teleinsular" cells, respectively. The peri-insular cells are actually larger on average and have more zymogen granules. Several groups have reported finding differences in the proportions of enzyme in situ in these cells as compared to the teleinsular region (Gingras and Bendayan, 1992; Malaisse-Lagae et al., 1975). However, there are also reports that show no difference between them (Beaudoin et al., 1981). But even if there are such differences, given the small percentage of peri-insular cells relative to the total population of acinar cells, they make up only ~1% of the cells of the pancreas, it is not likely that their contribution to the secretory product would result in a measurable non-parallel effect. Moreover, it would limit the notion of non-parallel secretion to a single type of non-parallel effect (peri- versus teleinsular) and the evidence indicates a variety of non-parallel responses. There is also a report that there are two different types of acinar cells, this time distinguished by different blood group antigens . These different cell types are distributed more uniformly throughout the pancreas (Uchida

et al., 1986). But these cells have yet to be evaluated for difference in their enzyme content.

For non-parallel secretion by exocytosis to be controlled at the zymogen granule level, there should be multiple kinds of zymogen granules containing different amounts of the digestive enzymes. Each granule would be stimulated to exocytotic activity in response to a different stimulus. Moreover, all cells would contain these various types of granules. The attraction of this hypothesis is that it does not require the existence of the, as yet unproven, different types of acinar cells. On the other hand, it does require the existence of an intracellular mechanism by which the different enzymes would be packaged from the Golgi into different zymogen granules. Although, it is possible that the granules would be differentially packaged as a result of the different synthesis rates of enzymes mentioned above, e.g. granules would be filled with whatever enzyme was currently being synthesized and as their synthesis rates are different, granules would be differentially filled over time. However, immunocytochemical studies (discussed below) indicate that each granule contains all of the enzymes, therefore somehow all of the proteins would still have to be packaged in a granule regardless of the synthesis rate. Furthermore, while there is some evidence that zymogen granules do contain different proportions of the 20 digestive enzymes (Tobler et al., 1991; Adelson and Miller, 1989; Mroz and Lechene, 1986), there is also evidence that they don't (Gingras and Bendayan, 1992). Even if there were different zymogen granules, there is still the problem of the mechanism by which different granules would be released in response to different stimuli.

In any event, for either the cell or the granule model, quite complex mechanisms would be required to differentially cause secretion from either different cells or zymogen granules given the number of stimuli already known to cause or alter protein secretion: - amino acids, fatty acids and glucose, cholecystokinin (CCK), vasoactive intestinal

polypeptide (VIP), gastrin inhibiting polypeptide (GIP), secretin, chymodenin, histamine, cholinergic agents, insulin, glucagen and so forth (Grendell, 1981). Many different receptors and target molecules would be required and there is no evidence that this is so.

I.2 Zymogen granule behavior during secretion in situ

From the above discussion of the equilibrium and exocytosis models, we can see that it is our lack of knowledge about how the zymogen granules actually accumulate and are able to release their enclosed secretory proteins that prevents us from understanding non-parallel secretion. One way that we can try to better understand these processes is by observing the behavior of zymogen granules during the process of secretion. Doing so was what originally led Heidenhain to his conclusion that zymogen granules were the site of protein storage in 1875. He observed dog pancreas under the light microscope both before and after feeding and noticed that the size and number of the granules decreased as a result of feeding.

In the mature rat pancreas, zymogen granules normally occupy between 5-25% of the cell volume and are usually concentrated in the apical region of the cell. The volume of the cell that the ZGs occupy, which is a combination of their number and their size, is greatly influenced by the physiological condition of the animal. If the animal has been fasted, there are apparently more granules with larger diameters than if the animal has been stimulated to secrete. The volume that the granules occupy can change as much as 95% after stimulation (Rothman, 1975b)! Whether this volume change is a result of a decrease in the number of granules alone, or if it is due to a decrease in their size with the actual number of granules remaining the same, can help distinguish between the equilibrium and exocytosis models. The exocytosis model predicts that after stimulation, the number of granules should decrease because some of them would be "lost" to

exocytosis; whereas the equilibrium model predicts a change in the size and protein content as each granule lost protein. Studies by Ermak and Rothman (1981) demonstrated a shift in the size frequency distribution of granules of rat pancreas after feeding, while the number of granules remained unchanged. This result was confirmed in response to hormonal stimulation as well (Beaudoin et al., 1984; Aughsteen and Cope, 1987). But while Ermak and Rothman proposed that the evidence was consistent with granules shrinking as their contents are released by diffusion like processes (the equilibrium model), Beaudoin et al. (1984) proposed that this shift is due to a selective discharge of large granules and the concomitant formation of smaller new granules. This view was shared by Aughsteen and Cope (1987).

However, these new small granules would have to be formed rather quickly particularly if the total number of granules is to stay the same. Regranulation is thought to be much slower than granule depletion (Geuze and Kramer, 1974; Cope and Williams, 1980, 1981). New granules usually begin to appear about 3-4 hr after the onset of secretion, then their volume rises sharply for the next 4-6 hr, during which time the rate of accumulation falls off, with complete restitution of granule stores after 12-16 hr (Cope and Williams, 1980, 1981). If this is true, then in conjunction with the observations of Ermak and Rothman (1981), it would appear that granules are shrinking during the course of secretion.

We have already mentioned that unfortunately, it has not been possible to observe the process of exocytosis in the acinar cell. However, it is possible to indirectly observe granule behavior in situ by tracking the granule membrane with membrane markers. If exocytosis occurs, then the markers will appear in the cell membrane. This technique has been successful in other types of cells and reinforces the idea that exocytosis occurs in some cells, e.g. the parotid gland (Williams and Cope, 1981). However, the results of

similar experiments in acinar cells are ambiguous (Beaudoin and Grondin, 1991) and as such, the evidence for exocytosis in the acinar cell is as yet unresolved.

While the evidence of granule behavior in situ presented supports the equilibrium model, because these results are based on EM images or indirect measurements, it is difficult to conclude with as much certainty as we could if we were actually watching the process, that granules are shrinking and losing protein content. It may well be that these results are inconclusive because both processes, exocytosis and equilibrium, are occurring.

I.3 Characteristics of Zymogen Granules

To better understand the zymogen granule, we can study the structural and chemical characteristics of isolated granules.

I.3.1 Morphology

A typical EM image of a cross section of an acinar cell is shown in Fig. 1.1. We can see that the granules appear as circular, uniformly dense objects and are roughly ~1μm in diameter. Measurements of the diameter of the zymogen granules have been made in two ways - from EM images and using light scattering methods. It is difficult to characterize an "average" size for the granule because their size varies widely in response to physiological state, e.g. fed or fasted. In general, studies that report values for granules from fasted animals (maximizing granule number and size) show an approximately Gaussian size distribution around an average diameter of 1.0 μm (Liebow and Rothman; Nadelhaft, 1973; Warashina, 1981; Beaudoin et al., 1984; Aughsteen and Cope, 1987). One study has reported a bimodal distribution of granule diameters, with a second minor peak between 0.8 and 1.0μm (Sato and Take, 1975). This was confirmed by Yoshimura (1977), who noticed, however that only the pancreata of some rats had two populations of granules while others had only the one.

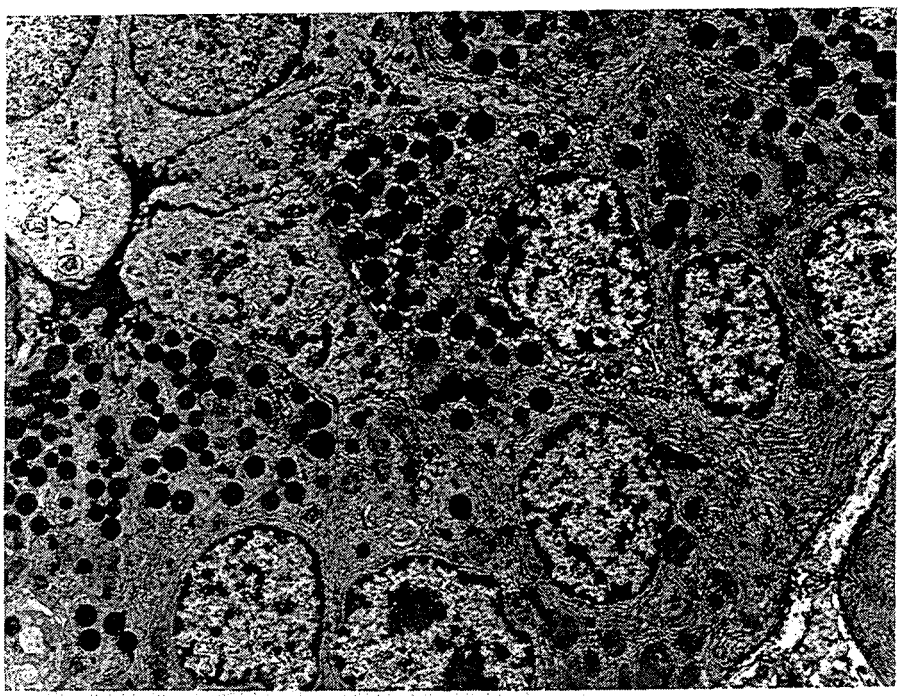

Figure 1.1 An EM image of a cross section of the pancreas. The acinar cells are visible and can be seen to contain many dark, round objects at the apical end of the cell. These zymogen granules are ~1μm in diameter. The apical ends of several cells are oriented towards a central region that forms the duct where the secretory product passes to the small intestine.

A bimodal distribution was also been observed in stimulated pancreas by Beaudoin and Grondin (1987) with the lower peak at between 2-3μm and the upper peak was at 7μm. From the previous section, it was reported that Beaudoin and Grondin attributed this new peak to the presence of newly formed zymogen granules. However, Ermak and Rothman showed that the diameter distribution of granules before and after stimulation was Gaussian. And, therefore a bimodal peak could occur from combining populations of granules, some which have released protein and some which have not. We cannot definitively distinguish between either model based on these results.

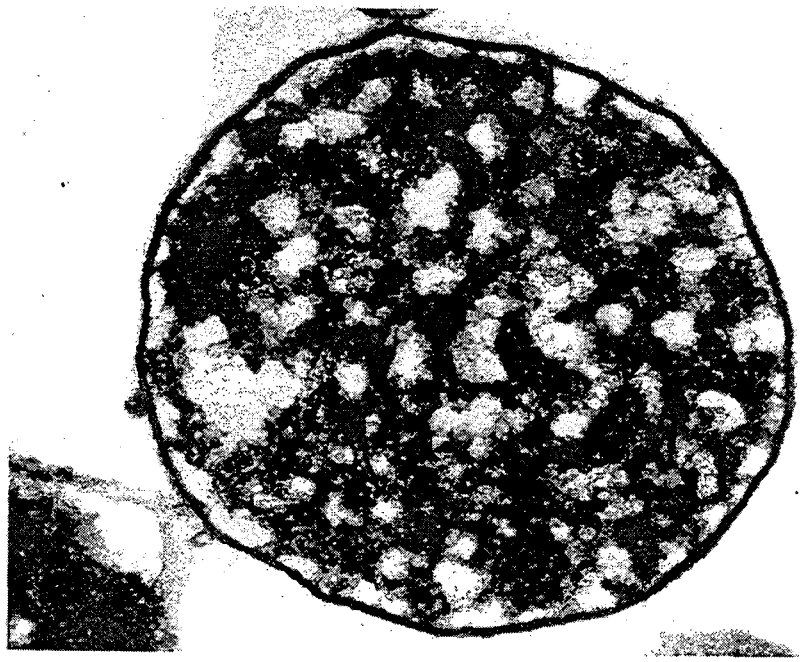

Figure 1.2 Reticulated granule containing a meshwork of electron-dense material. Reticular strands (~50nm thick) make attachments to the granule membrane and outline spherical spaces (~100 nm in diameter) and larger polymorphic spaces. x65,000.

As mentioned above, the granules appear as uniformly dense spheres with no apparent internal structure. But, another study by Ermak and Rothman (1978) showed in EM images of isolated granules that had been partially or fully depleted of their protein contents, a reticular meshwork of electron dense strands criss-crossing the granule matrix. The reticulum outlined spherical and polygonal spaces and was attached at discrete points to the internal surface of the intact granule membrane. It was suggested that this reticulum provided the framework for the bonding of the digestive proteins within the granule. The bonding interactions were shown to be electrostatic in nature (as opposed to hydrophobic). As mentioned above, proteins would bind to the aggregate according to their individual binding properties (Rothman et al., 1974).

I.3.2 Chemical Contents

This section presents the basic chemical composition of zymogen granules and is divided into the following sub-sections; the digestive enzymes, other internal proteins, and elemental distribution.

I.3.2a The digestive enzymes

In the previous section, we reported that the acinar cell manufactures 20 or so different enzymes that are used in digestion and that each zymogen granule contains an unknown mixture of these enzymes. These enzymes have been characterized by many investigators over the years. In recent work by Schick et al. (1984), proteins were pulse labeled with a mixture of 15 ^{14}C amino acids administered into pancreatic lobules in vitro for 2 hours. The soluble proteins extracted with alkaline buffer from a purified ZG fraction were separated by two-dimensional isoelectric focusing (IEF)/sodium dodecyl sulfate (SDS) polyacrylamide gel electrophoresis. Their results are shown in Table 1.1 for the rat pancreas. Different species contain the same types of proteins, they vary in molecular weight, isoelectric point and mass proportion (e.g. guinea pig, Scheele, 1975).

The fact that the proteins have different isoelectric points implies that each protein will have unique binding or solubility properties depending on the local pH or other environmental conditions. As such, this supports the equilibrium model as a mechanism by which non-parallel secretion could occur because, depending on the internal environment of the cell, different proteins would be more likely to be in solution, depending upon their isoelectric point. The environment of the cell could easily be affected differently by various secretagogues. Once the protein was in solution within the granule, then in response to mass action, it would leave the granule and eventually, be secreted.

Table I.1. The digestive enzymes produced by the acinar cell of rat pancreas.

Zymogen	Molecular Weight	Isoelectric Point	Mass Proportion
Ribonuclease	14000	9.2	0.6
Trypsinogen 1	21000	4.3	13.2
Trypsinogen 2	21000	4.4	1.6
Trypsinogen 3	22500	8.0	6.9
Chymotrypsinogen 1	25000	4.8	11.9
Chymotrypsinogen 2	25000	9.0	4.4
Proelastase 1	26000	4.9	2.5
Proelastase 2	28500	9.2	3.6
Procarboxypeptidase A1	49000	4.4	5.8
Procarboxypeptidase B1	47000	4.3	5.3
Procarboxypeptidase B2	47000	4.5	3.7
Procarboxypeptidase B3	47000	4.6	1.7
Lipase 1	50000	6.8	4.5
Amylase 1	55000	8.6	10.6
Amylase 2	53000	8.9	15.9
unidentified	13000	5.0	1.8
unidentified	54000	5.4	0.9
unidentified	56000	5.4	1.6
unidentified	77500	4.7	2.4

It is known that the enzymes that are held within the granule are in an inactive form (pro-enzyme or "zymogen", hence the name zymogen granule) and that once they are secreted, they become active after modification by one or more specific proteolytic cleavages (Neurath and Walsh, 1976). However, current research being performed using high resolution mass spectroscopy, which can determine the mass of molecules to the order of a few amino acids, has found that there are small differences between the mass of specific enzymes from the zymogen granules and their pro-enzyme form in secretion, before they are proteolytically cleaved (Tseng). This result implies that the proteins have been slightly modified during their transport to the exterior of the cell and as such, cannot be explained by the exocytosis model since proteins would be simply released. And although it is still unclear what this result indicates, it has been suggested that the proteins are being slightly modified in order to more easily cross the internal membranes of the cell.

I.3.2b Other Internal Zymogen Granule Proteins

The digestive enzymes are not the only proteins found within the zymogen granule although they do account for ~85-90% of the protein contents of the granule (Greene et al., 1963; Hokin, 1955). Sulphated glycosaminoglycans have been found in the zymogen granules of guinea pig (Reggio and Palade, 1978a; Reggio, 1978b) and have a molecular weight of ~250,000 MW. These molecules may by involved in the aggregation of the digestive enzymes within the granule because they have an excess of negative charge. Considering that Ermak and Rothman (1978) concluded that the structural components they found in the zymogen granule probably held the granule proteins in an aggregated state via the use of electrostatic interactions, these sulphated glycans are prime candidates for the observed structural components.

Other research has produced evidence that gamma aminobutyric acid (GABA) and its regulating enzymes, L-glutamate decarboxylase (GAD) and gamma aminobutyrate-α-ketoglutarate transaminase are present in zymogen granules (Garry et al., 1988). GABA has been found to have a role in activating ligand-gated Cl^- channels. The zymogen granule membrane contains one, possibly two Cl^- channels (discussed below).

I.3.2c Elemental Distribution within the Zymogen Granule

Energy dispersive X-ray micro-analysis has been used to detect Na, Mg, P, S, Cl, K and Ca in the zymogen granule. The results are shown in Table 1.2 from various references and the amounts are given in mM/kg dry weight of pancreatic tissue. None of the samples had been stimulated to secrete and cryoprotectant was used in all except for the studies of Tobler (1992) and Roos (1988, 1989).

Table 1.2. The distribution of ions in the zymogen granules. Quantities are given in mM/kg dry weight of pancreas.

Na	Mg	P	S	Cl	K	Ca	Ref
21±3	23±3	49±9	284±7	36±2	65±4	17±1	Tobler, 1992
	33±6					15±1	Wolters, 1979
36±12	29±5	166±16	173±7	105±9	342±17	16±2	Roomans, 1982
105±9	39±2	126±14	674±21	96±8	121±6	54±2	Roomans, 1985
105±7	39±4	126±12	674±10	96±4	120±6	54±2	Roos, 1988
128±8	53±3	171±15	287±9	190±9	213±11	18±2	Roos, 1989

The wide variance in elemental composition reported above may be due to various influences including: individual sample variations, physiological state of the organ and, of course, preparation. From this method it is not possible to tell whether the element is in a bound or ionic state or is part of a molecule. The amounts of all of the elements are significantly less than found in the cytoplasm of the cell , except for sulphur - which is higher in the granule, and calcium - which is similar (Tobler, 1992). The amount of Ca detected in the granule was higher than in any other organelle. The same measurements were made on stimulated animals and it was shown that the amounts of the elements Na, Cl and K increased in the granules after stimulation. As the granule is known to have ion transporters in the membrane (see below) this may indicate that ions are being transported into the granule during stimulation. Although, it is still unclear how the influx of ions is related to the process of secretion. It was proposed that this influx of ions could cause the granule to swell which would enable the granule to fuse with the cell membrane for exocytosis, but subsequent experiments were not able to confirm this observation (Green, 1987). The influx of ions in all likelihood does contribute to the partial dissolution of the protein aggregate which would result in the solubilization of enzymes (different enzymes, depending on their charge distribution, would be solubilized at different rates) within the

granule. The "free" proteins could then be individually transported across the granule membrane, as suggested by the equilibrium model.

There has been precious little research performed on the elemental content of isolated granules. In one study (Burwen, 1972) found that isolated granules contained at most 1-2mEq/L of sodium and potassium, and 2-3mEq/L of chloride. This is far less than seen above in the energy dispersive X-ray micro-analysis. It would be interesting to perform the energy dispersive X-ray micro-analysis on a preparation of isolated granules to confirm the amount of these ions that may be lost during the isolation procedure.

I.3.2d Membrane proteins and ion permeability properties

The membrane of the zymogen granule contains many proteins. Ultrastructural examination of the ZG membrane, from isolated granules, by rapid-freezing and freeze-fracture techniques reveals that the external membrane side has a density of intramembrane particles (IMPs) of 44 per μm^2 showing diameters of 9-18nm (Cabana, 1988). And, the side of the membrane exposed to the cytoplasm has even more IMPs. In this study, two new undescribed types of IMPs were found on both sides of the membrane. The first was a population of 13nm particles with an electron-lucent center and the second was a population of large IMPs (15nm)which was characterized by what appeared to be a large pore (5nm in diameter), subdivided by a delicate cross-shaped structure. This pore structure is large enough for the passage of proteins contained in the granule.

Several membrane proteins have been identified: 3 glycoprotein: γ-Glutamyl-transferase (GGT), thiamine pyrophosphatase(TPPase), ATP-diphosphorylase, protein disulfide isomerase, ADP-ribosylated protein and a GTP-binding protein.

GP2 (MW~80 kDa), one of the glycoproteins was first identified by MacDonald and Ronzio (1974) and later corroborated by Paquet et al. (1982). There appears to be two forms of GP2 found in association with the ZG. Using biochemical methods in isolated

ZG, Rindler and Hoops (1990) found that 60% of the total GP2 content was associated with the membranes ($GP2_m$) while the other 40% was found in the content ($GP2_c$). It has been suggested (Rindler and Hoops, 1990 and Paquet et al., 1986) that $GP2_m$ is linked to the membrane via glycosyl phosphatidylinositol (GPI) and $GP2_c$ is the released form of this protein. GP2 is also found on the cisternal leaflet of the trans-Golgi. Freedman et al. (1990) have suggested that GP2 plays a role in the assembly of CVs. γ–Glutamyl-transferase (GGT) is another glycoprotein found in the ZG membrane of rat pancreas (Castle et al., 1985) although its function is unknown.

Several other enzymes have been found associated with ZG membranes using cytochemical, immunological and biochemical methods, including TPPase (Paquet et al., 1982) and ATP-diphosphohydrolase (LeBel et al., 1980; Laliberté et al., 1982). TPPase is found in ZG membranes but not CV membranes (Beaudoin et al., 1983) and AcPase (acid phosphatase) is found in CV membranes but not in ZG membranes. Because the CV is presumed to be the precursor to the ZG, these chemical differences require that the AcPase be removed from the CV membrane and TPPase be added during its conversion to a ZG. It has been proposed that in the conversion step, micro-granules that contain the AcPase, bud off of the CV membrane. Not only would these micro-granules serve to remove this phosphatase, but it has also been proposed that they actually transfer the protein product they contain to the cell membrane and secrete it (Beaudoin and Grondin, 1987). This secretion pathway has been called the para-granular pathway and is thought to be a form of constitutive secretion.

The ADP-ribosylated protein (25 kDa) was identified by Lambert et al. (1990) who also confirmed the presence of a G protein (28 kDa) originally found by Padfield et al. (1990). Lambert suggests that the G protein could be involved in protein transport between intracellular compartments along the secretory pathway and/or exocytosis. A protein disulfide isomerase (Akagi et al., 1988), is also located on the ZG membrane,

which is unusual, because it is almost exclusively located in the ER and catalyzes the formation of disulfide bonds during synthesis of secretory proteins. According to the equilibrium model, proteins are able to cross the zymogen granule membrane and if they are unfolded in order to cross (this process is discussed further in the Discussion and Conclusions chapter) then these enzymes would have a role in reforming the disulfide bonds after the protein was transported. And, finally, work currently in progress has characterized a large protein that is ~170kDa and that western blot analysis has identified as the cystic fibrosis transmembrane regulator (Tseng).

While it is not known what the function is of all of the proteins in the membrane, some of them are ion transporters. This was inferred from the electrolyte permeability of zymogen granules. DeLisle and Hopfer (1986), using suspensions of zymogen granules isolated from resting rat pancreas, found that the decrease in optical density of the suspension was directly related to the permeability of the ZG membrane to various electrolytes. Ionophores were also used (CCCP[2], monensin[3] , nigericin [4], valinomycin[5] and nonactin[6]) to discern whether the effect was a result of cation or anion permeability. The results suggested that the ZGs possess an anion exchange and an anion conductance pathway. The anion exchanger could be blocked with 2mm DIDS[7]. The granules also showed some slight permeability to cations, especially K which was confirmed by Gasser et al. (1988) using similar techniques.

It has been suggested that zymogen granule permeability to ions maintains a particular internal pH, although, interestingly enough, there are no ATP-driven H^+ pumps present on the ZG membrane (Laliberté et al., 1982). Niederau (1986a) found that ZGs

---

[2]carbonylcyanide-*m*-chlorophenylhydrazone: a protonophore. Had no effect up to 13µg/ml
[3]cation exchange ionophore - increased the amount of granule lysis (5- to 50-fold) in 150 mM NaCl
[4]cation exchange ionophore - increased the amount of granule lysis (5- to 50-fold) in 150 mM NaCl
[5]electrogenic K^+ specific ionophore - effective in promoting lysis in 150 mM KCl
[6]electrogenic cation ionophore - increased the amount of granule lysis (5- to 50-fold) in 150 mM NaCl
[7]4,4' -diisothiocyanostilbene -2,2' -disulfonic acid

were acidified in comparison to other parts of the acinar cell. And, this result was confirmed by Lebel (1988) who measured the presence of a pH gradient between the cell cytoplasm of isolated acinar cells and the inside of the zymogen granules. The cell cytosol was measured to be at ~pH 7.0 and the interior of the ZG was less than pH 5.7. Maintenance of this acidic intragranular pH may be important in the condensation and inactivation of the zymogens within the granule (Rothman, 1971).

I.4. A re-analysis of the equilibrium model

From this review, we can see that although the mechanism(s) by which the zymogen granule in the acinar cell releases its protein is still not completely determined, there is substantial evidence that supports Rothman's original proposal that the proteins destined for secretion are able to move independently through the cell and cross membrane barriers (the equilibrium model). And although other secretory cells are known to release their protein by an exocytotic process, it has been surprisingly difficult to confirm this process' existence in the acinar cell.

Some of the most convincing evidence that proteins were able to cross the enclosing membrane of the zymogen granule came from Rothman and collaborator's original experiments on isolated granules, as mentioned earlier. In these experiments, protein was detected in the suspending medium when isolated granules were suspended in various solutions. In this section, we will briefly review the experiments that led to the development of the equilibrium model. We will also address the reasons why these observations were originally discounted but how now, the results from these experiments can no longer be considered artifacts. As such, they merit a re-examination and in the following section, we will propose an alternative technique by which to perform these experiments and confirm the original results.

I.4.1 Protein release from isolated zymogen granules

Since Hokin (1955) was first able to isolate zymogen granules from the acinar cell using differential centrifugation, it has been possible to study the properties of the zymogen granules in vitro. Hokin's basic procedure is still currently the most widely used and a modified version of the procedure is described in Chapter V. Hokin observed that granules retained their morphological structure for long periods of time when stored in isosmotic sucrose at 4°C at a pH between 4.5 and 6.5. But, if the pH was raised to 7.2 or above, they apparently "dissolved" and the suspending solution became clear (a suspension of granules is normally cloudy in appearance). This observation was difficult to understand because the granules are quite stable within the acinar cell cytoplasm which has a pH of 7.0 (Preissler and Williams, 1981).

In his first experiment, Rothman (1971) investigated this pH instability by measuring the amounts of chymotrypsinogen, trypsinogen, amylase and total protein released into the suspending solution at pHs ranging from 4-8.5 (0.3M sucrose, for 30min at 24°C) by enzyme assay technique . He found that when pH was plotted against the percentage of enzyme released from the granules, there were different release curves for the different enzymes (see figure 1.3) This could not occur if, as generally believed at the time, granule "instability" was a result of the granules breaking open, or lysing, and releasing their contained protein into the solution. As such, since each granule supposedly contained a mixture of all of the digestive enzymes, all of the enzymes would be present in the suspending solution in the same ratios (although not necessarily in the same amounts) at the different pH values. However, as can be seen in the figure, this is not the case - and the proportions of the different enzymes present in the solution varied as a function of pH. Therefore, it appeared that lysis was not an appropriate explanation for the observation, and it appeared that proteins were able to independently move into the solution from the granule and their solubilization rate depended on the pH of the solution.

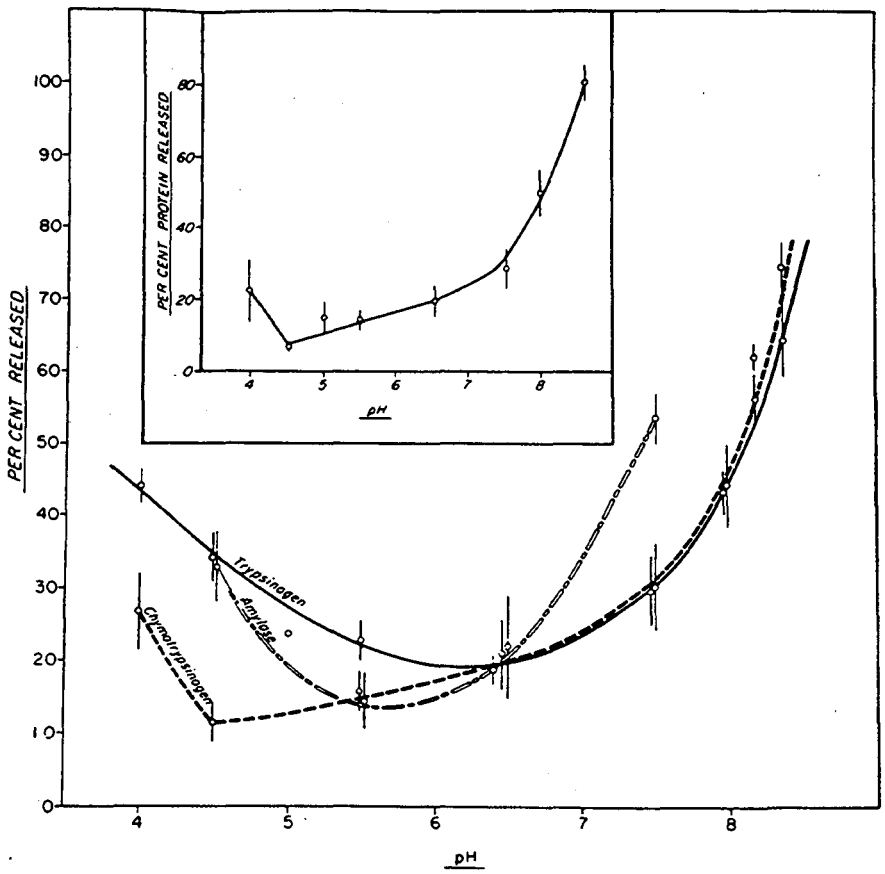

Figure 1.3. The release of protein, trypsinogen, amylase and chymotrypsinogen from suspensions of zymogen granules at various pHs'. Percent release refers to the percentage of the total enzyme activity or protein recovered in a supernatant after centrifugation at 10000g for 10min. The total yield of enzyme and protein was not altered by pH in the range presented in this figure. Results are taken from Rothman (1971)

Subsequent experiments, with different solutions, showed that the relative amounts of different enzymes detected in the suspending solution also varied with the ion content of the solution (Burwen and Rothman, 1972). The amount of release for protein, chymotrypsinogen and amylase were measured for a variety of ionic solutions (150mM NaCl, KCl; 100 mM $CaCl_2$, $MgCl_2$, $BaCl_2$, $SrCl_2$) as well as for different osmotic strength solutions (water, 0.3M sucrose and 0.3M urea). It was found again that the release curves for different proteins were not the same for a given ionic solution.

The above experiments certainly suggested that the various proteins that were contained within the granule were able to be released from the granule independently of one another. As such, this observation provided a mechanism by which non-parallel secretion could occur. In further experiments, Rothman and collaborators explored the mechanisms by which protein was released from the granule. Experiments done by Liebow and Rothman (1972, 1976) confirmed that the amount of protein released from the granule was affected by simple concentration gradients. It was already shown in the Rothman (1971) paper that the rate of release of protein reached a steady-state value after the granules had been suspended for over one-half hour. This implied that the protein release rate was affected by the increased protein concentration in the solution, as protein was released from other granules, and the rate of protein loss reached an equilibrium. In the Liebow and Rothman (1972, 1978) experiments, this theory was addressed by suspending granules at lower density numbers than the initial isolation procedure called for. If the proteins were indeed released according to the concentration of protein in solution, then an increased rate of protein release should be observed at lower density numbers since the protein concentration in the suspending solution would be reduced due to the larger suspending volume. They measured the release rates for chymotrypsinogen at two different pHs (5.5 & 7.0) and for different degrees of dilution (up to 100 times) of the original suspension. A tenfold increase in the amount of chymotrypsinogen released was detected accompanying a tenfold increase in dilution. These experiments not only showed that protein was being released from the granules, but that it was released according to concentration gradients that existed across the membrane.

Additionally, these experiments also addressed the question that if protein could be released from the granule, then uptake might be possible. The uptake of chymotrypsinogen was measured relative to a marker protein (albumin) and it was found that chymotrypsinogen was preferentially taken up by the granules. As such, the

equilibrium model was proposed by Rothman (1975) and suggested that granule protein was able to independently cross the enclosing membrane of the granule and that each type of enzyme did so in response to concentration gradients.

I.4.2 Artifact?

Unfortunately, the results of all of these experiments were considered by many workers in this area to be artifactual. The protein that was detected in the solution was assumed to be a result of the granule's lysing or breaking open and releasing their content into the suspending solution. That lysis occurred was based on two assumption; the first was that granules were not stable once they were isolated and the second was that at the time, it was considered unlikely that proteins were able to cross membranes and therefore the only manner by which protein could be detected in the solution was if the granules were breaking open or lysing.

As mentioned above, Hokin only considered the granules to be "unstable" at high pH; he found that they were stable at pH values less than 7 and would retain their morphological characteristics for long periods of time. A current explanation as to why granules may not be stable at high pH is that they have lost a "stabilizing" factor during isolation. This was first proposed by O'Conner and Matthews (1980), and Rogers et al. (1987) have reported isolating a soluble cytosolic factor which increases the stability of the ZG preparations at high pH. LeBel et al. (1988) have proposed that the "stabilizing" factor is some-how involved in regulating the internal pH of the granule. As discussed above, zymogen granules in situ have a low internal pH ($\leq$ 5.7). When this factor is "lost", the granule no longer has the ability to maintain this low pH. They concluded that isolated granules are stable if they are resuspended in a solution with a pH $\leq$ 7.2, because the Donnan equilibrium is sufficient to produce the necessary internal low pH. But if the suspending solution has a higher pH, the Donnan equilibrium is no longer sufficient to provide an internally low pH and the granules become unstable. The missing stabilizing

factor may help control the permeability of the membrane to protons and Cl^- ions and therefore be able to help produce the necessary pH gradient.

The instability of the granule was also attributed to the process of differential centrifugation itself damaging the granules in some manner which made them particularly unstable at neutral pH. DeLisle et al. (1984) developed an isolation procedure using isosmotic Percoll density gradients that they claimed produced granules that were stable in common electrolyte solutions such as NaCl or KCl and at neutral pH. But, Rogers et al. (1987) concluded that Percoll particles were actually binding to the granules and were probably contributing to their stability at the higher pH. Two other papers that critically examined this technique and the technique of differential centrifugation (Rothman and Liebow, 1985; Neiderau, 1986b) showed that granules isolated using Percoll density gradients at pH 7.0 were no more "stable" than those isolated using differential centrifugation at pH 6.0

Therefore, we can conclude that isolated granules are stable in solutions with pH < 7 - however, there is still the question of lysis to be considered. Although, it is difficult to reconcile the results of Rothman and collaborator's experiments with a lysis model. As explained above, one would expect to see parallel amounts of protein released into solution. Additionally, in the dilution experiment, if lysis was the cause of protein release, then why would increasing the volume of the suspending solution produce proportional increases in the amount of protein released? Lysis would only happen to a certain number of granules from a preparation depending on the particular granule's "stability;" it is difficult to envision how increasing the volume of the suspending solution would affect granule stability.

Recently, Rothman and collaborators have using light scattering theory to attempt to resolve the lysis issue. As mentioned above, enzyme assay techniques were often used to detect the amount of protein released into a suspending solution of isolated granules, but

it was not mentioned that it is also possible to determine the amount of protein that has been released into the solution by measuring the light scattering properties of a solution. The change in light scattering, or optical density as measured by a spectrophotometer, is directly related to the amount of protein that can be detected in the solution. According to Mie light scattering theory of small particles (Van de Hulst, 1981) and Beer's law, the change in optical density can be attributed to a change in one or all three or the following characteristics of the particles; their number, diameter and refractive index (in our case, protein concentration). Therefore, it is theoretically possible to determine if protein is being released into the solution by lysis (a change in the number of the particles) or from crossing the granule membrane and leaving the granule intact, which would mean that the size and/or protein concentration of the granules was changing. Traditionally, a change in the optical density of a solution of isolated granules has been attributed to lysis (e.g.

However, even though these results indicate that isolated granules may be decreasing in diameter and/or protein concentration and lysis is not necessarily the mechanism by which protein can be detected in the suspending solution, the problem with using Mie theory is that it is not able to definitively determine which process is occurring, only that a combination of the processes are occurring. This is a general problem with indirect techniques for measuring biological processes and as a result it is left to the direct techniques to provide the definitive answer.

I.5 Thesis Goals

From this review, we can see that there are still many unresolved questions concerning the mechanism, or mechanisms, of protein secretion from the acinar cell of the pancreas. One of these observations, the detection of non-parallel secretion from the pancreas in response to a variety of stimuli, led to the proposal that secretory proteins might be able to move through the cell as independent molecules, not *en masse*, and cross the cell and granule membranes in the process. A variety of evidence supports this model, including results of studies performed on isolated zymogen granules. Unfortunately, the results were widely attributed to lysis of the granules.

However, in light of the fact that these results do not have to be attributed to lysis, according to Mie theory and the growing body of evidence concerning the ability of proteins' to cross membranes (this will be considered in the Discussion and Conclusion chapter) we were motivated to repeat experiments on isolated granules using the newly developed technique of scanning transmission X-ray microscopy (STXM) in an attempt to provide direct evidence concerning the modality of protein release. We hoped to be able to directly observe the morphologic sequel to protein release as it occurred in STXM. We also hoped to be able to correlate such observations simultaneously with the quantitative measurement of protein flux out of single granules.

STXM could at least in theory; 1) provide a resolution ~5 times better than light microscopy , 2) allow for the needed aqueous environment in which to suspend whole granules and 3) permit the simultaneous quantitative measure of the protein contents of individual granules on the order of femtograms.

If we could apply this in practice, we planned to:

1) Measure the characteristics of diameter, protein mass and concentration of freshly, isolated zymogen granules that are suspended in 0.3M sucrose (pH 6.0) and observe individual granules over time as they released their contents, looking for any signs of lysis and changes in the diameter, protein mass and concentration that might occur.
2) If the granules were observed to change in their characteristics, we planned to characterize the permeability of the granule membrane to its enclosed proteins for individual granules.
3) In addition, we planned to explore the effects of glutaraldehyde fixation on zymogen granules detectable at STXM resolution and study the effects of radiation exposure on our specimen.
4) Finally, we had a more general goal in mind. We hoped that through these studies we would help in the development of X-ray microscopic methods for research in biology as well as better understand its potential utility and shortcomings.

Chapter I - References

Adelson, J.W. and P.E. Miller, Heterogeneity of the exocrine pancreas, Am. J. Physiol. (1989) **256**:G817-G825.

Akagi, S., A. Yamamoto, T. Yoshimori, R. Masaki, R. Ogawa and Y.Tashiro, Localization of protein disulfide isomerase on plasma membranes of rat exocrine pacnreatic cells, J. Hist. Cyto. (1988) **36**:1069-1074.

Aughsteen, A.A. and G.H. Cope, Changes in the size and number of secretion granules in the rat exocrine pancreas induced by feeding or stimulation in vitro, Cell Tiss. Res. (1987) **249**:427-436.

Babkin, B.P., In: Secretory mechanisms of the Digestive galand, (1950) Hoeber, New York.

Beaudoin, A.R. and G. Grondin, Zymogen granules of the pancreas and the parotid gland and their role in cell secretion, Int. Rev. Cyt. (1992) **132**:177-222.

Beaudoin, A.R. and G. Grondin, Secretory pathway in animal calls: with emphasis on pancreatic acinar cells, J. Electron Microscopy Tech. (1991) **17**:51-69.

Beaudoin, A.R. and G. Grondin, Pathways of secretion in the exocrine pancreas: The status of resting secretion, Life Sci. (1987) **40**:2453-2460.

Beaudoin, A.R., G. Grondin, M. Filion and A. Lord, Secretagogues cause a preferential discharge of large size granules in rat pancreas, Can. J. Biochem. Cell Biol (1984) **62**:1288-1292.

Beaudoin, A.R., G. Grondin, A. Lord, M. Roberge and P. St.-Jean, The origin of the zymogen granule membrane of the pancreatic acinar cell as examined by ultrastructural cytochemistry of acid phosphatase, thiamine pyrophosphatase and ATP diphosphohydrolase activities, Euro. J. Cell Biol. (1983) **29**:218-225.

Beaudoin, A.R., P. St.-Jean and G. Girard, Distribution of amylase and chymotrypsinogen in four regions of the rat pancreas, Can. J. Physiol. Pharmacol. (1981) **59**:884-886.

Burgess, T.L. and R.B. Kelly, Constitutive and regulated secretion of proteins, Ann. Rev. Cell Biol. (1987) **3**:243-293.

Burwen, S.J. and S.S. Rothman, Zymogen granules: osmotic properties, interactions with ions, and some structural implications, Am. J. Physiol. (1972) **222**:1177-1181.

Cabana, C., P. Magny, D. Nadeau, G. Grondin and A. Beaudoin, Freeze-fracture study of the zymogen granule membrane of pancreas: two novel types of intramembrane particles, Eur. J. Cell Biol. (1988) **45**:246-255.

Case, R.M., Synthesis, intracellular transport and discharge of exportable proteins in the pancreatic acinar cell and other cells, Biol. Rev. (1978) **53**:211-354.

Castle, J.D., R.S. Cameron, P.L. Patterson and A.K. Ma, Identification of high molecular weight anitigens structurally related to gamma-glutamyl transferase in epithelial tissues, J. Membr. Biol. (1985) **87**:13-26.

Chung, K.-N., P. Walter, G.W. Aponte and H.-P. H. Moore, Molecular sorting in the secretory pathway, Science (1989) **243**:192-197.

Cope, G.H. and M.A. Williams, Restitution of granule stores in the rabbit parotid gland after isoprenaline-induced secretion. A stereological analysis of volume parameters, Cell Tiss. Res. (1980) **209**:315-325.

Cope, G.H. and M.A. Williams, Secretion granule formation in the rabbit parotid gland after isoprenaline-induced secretion; stereological reconstructions of granule populations , Anat. Rec. (1981) **199**:377-392.

Dagorn, J.C., Non-parallel enzyme secretion from rat pancreas: in vivo studies, J. Physiol., (1978) **280**:435-448.

DeLisle, R.C. and U. Hopfer, Electrolyte permeabilities of pancreatic zymogen granules:implications for pancreatic secretion, Am. J. Physiol. (1986) **250**:G489-G496.

DeLisle, R.C., I. Schultz, T. Tyrakowski, W. Haase and U. Hopfer, Isolation of stable pancreatic zymogen granules, Am. J. Physiol. (1984) **246**:G411-G418.

Ermak, T.H. and S.S. Rothman, Large decrease in zymogen granule size in the postnatal rat pancreas, Cell Tiss. Res. (1981) **214**:51-66.

Ermak, T.H. and S.S. Rothman, Internal Organizatin of the zymogen granule: Formation of reticular structures *in vitro*, J. Ultr. Res. (1978) **64**:98-113.

Freedman, S., S.I. Fukuoka and G. Scheele, A single gene encodes membrane-bound and free forms of GP-2, the major glycoprotein in pancreatic secretory (zymogen) granule membranes, J. Cell Biol. (1990) **111**:318a.

Garry, D.J., M.G. Garry, R.L. Sorenson, Ultrastructural immunocytochemical localization of L-glutamate decarboxylase and GABA in rat pancreatic zymogen granules, Cell Tiss. Res. (1988) **252**:191-197.

Gasser, K.W., J. DiDomenico and U. Hopfer, Secretagogues activate chloride transport pathways in pancreatic zymogen granules, Am. J. Physiol. (1988) **254**:G93-G99.

Geuze, H.J. and J.W. Slot, Disproportional immunostaining patterns of two secretory proteins in guinea pig and rat exocrine pancreatic cells. An immunoferritin and fluorescence study, Euro. J. Cell. Biol. (1980) **21**:93-100.

Geuze, J.J. and M.F. Kramer, Functin of coated membranes and multivescular bodies during membrane regulation in stimulated exocrine pancreas cells, Cell. Tiss. Res. (1974) **156**:1.

Geuze, J.J. and C. Poort, Cell membrane resorption in the rat exocrine pancreas cell afterin vivo stimulation of the secretion ias studied by in vitro incubation eith extracellular space markers, J. Cell. Biol. (1973) **57**:159-174.

Gingras, D. and M. Bendayan, Differences in secretory granule content in pancreatic acinar cells from peri-insular and tele-insular regions, Pancreas (1992) **7**:477-485.

Green, D.P.L. Granule swelling and membrane fusion in exocytosis, J. Cell. Sci. (1987) **888**:547-549.

Greene, L.J., C.H.W. Hirs and G.E. Palade. J. Biol. Chem. (1963) **238**:2054.

Grendell, J.H. and S.S. Rothman, Digestive end products mobilize secretory proteins from subcellular stores in the pancreas, Am. J. Physiol. (1981) **241**:G67-G73.

Heidenhain, R., Beiträge zur Kenntniss des Pancreas, Pflüger Archiv. Phsyiol. (1875) **10**:557-632.

Hokin, L.E., Isolation of the zymogen granules of dog pancreas and a study of their properties, Biochim. Biophys. Acta (1955) **18**:379-388.

Jamieson, J.D. and G.E. Palade, Production of secretory proteins in animal cells. In: Int. Cell Biology Symp. (B.R. Brinkley and K.R. Porter, Eds.) (1976-77) pp. 308-318.

Jamieson, J.D. and G.E. Palade, Condensing vacuole conversion and zymogen granule discharge in pancreatic exocrine cells: metabolic studies, J. Cell Biol. (1971a) **48**:503-522.

Jamieson, J.D. and G.E. Palade, Sythesis, intracellular transport and discharge of secretory proteins in stimulated pancreatic exocrine cells, J. Cell Biol. (1971b) **50**: 135-158.

Jamieson, J.D. and G.E. Palade, Intracellular transport of secretory protein in the pancreatic exocrine cell. II. Transport to condensing vacuoles and zymogen granules, J. Cell Biol., (1967) **34**:597-615.

Kraehenbuhl, J.P., L. Racine and J.D. Jamieson, Immunocytochemical localization of secretory proteins in bovine pancreatic exocrine cells, J. Cell Biol. (1977) **72**:406-423.

Laliberté, J.F., P. St-Jean and A.R. Beaudoin, Kinetic effects of Ca2+ and Mg2+ on ATP hydrolysis by the purified ATP diphosphohydrolase, J. Biol. Chem (1982) **257**:3869-3874.

Lambert, M., N.D. Bui and J. Christophe, Novel GTP-binding proteins in plasma membranes and zymogen granule membranes from rat pancreas and in pancreatic AR 4-2J cell membranes, FEBS Lett. (1990) **271**:19-22.

LeBel, D. G. Grondin and J. Paquette, In vitro stability of pancreatic zymogen granules: roles of pH and calcium, Biol. Cell (1988) **63**:343-353.

LeBel, G.G. Poirier, S. Phaneuf, P. St.-Jean, J.F. Laliberté and A.R. Beaudoin, Characterization and purification if a calcium-sensitive ATP diphosphohydrolase from pig pancreas, J. Biol. Chem. (1980) **255**:1227-1233.

Liebow, C. and S.S. Rothman, Equilibrium of pancreatic digestive enzymes across zymogen granule membranes, Biochim. Biophys. Acta (1976) **455**:241-253.

Liebow, C. and S.S. Rothman, Transport of bovine chymotrypsinogen into rabbit pancreatic cells, Am. J. Physiol. (1974) **226**:1077-1081

Liebow, C. and S.S. Rothman, Membrane transport of proteins, Nature (1972) **240**:176-178.

MacDonald, R.J. and R.A. Ronzio, Phosphorylation of a zymogen granle membrane polypeptide from rat pancreas, FEBS Letters (1974) **40**:203-206.

Malaisse-Lagae, F., M. Ravazzola, P. Robberecht, A. Vandermeers, W.J. Malaisse and L. Orci, Exocrine Pancreas: Evidence for Topographic partition of seccretory function, Science (1975) **190**:795-797.

Mroz, E.A. and C. Lechene, Pancreatic zymogen granules differ markedly in Protein concentration, Science (1986) **232**:871-873.

Nadelhaft, I., Measurement of the size distribution of zymogen granules granules from rat pancreas, Biophys. J. (1973) **13**:1014-1029.

Neurath, H. and K.A. Walsh, Role of proteolytic enzymes in biological regulation, Proc. Natl. Acad. Sci. (1976) **73**:3825-3832.

Niederau, C., R.W. Van Dyke, B.F. Scharschmidt and J.H. Grendell, Rat pancreatic zymogen granules. An actively acidified compartment, Gastr. (1986a) **91**:1433-1442.

Niederau, C., J.H. Grendell, S.S. Rothman, Characteristics of rat pancreatic zymogen granules prepared by different methods, Am. J. Physiol. (1986b) **251**:G421-429.

Niederau, C., J.H. Grendell, S.S. Rothman, Digestive end products release pancreatic enzymes from particulate cellular pools, particularly zymogen granules, Biochim. Biophys. Acta (1986c) **881**:281-291.

O'Conner, M.D.L. and E.K. Matthews, Membrane surface interactions involved in insulin secretion, Horm. Metab. Res., suppl. (1980) **12**:149-153.

Oliver, C. Endocytic pathways at the lateral and basal surfaces of exocrine acinar cells, J. Cell Biol. (1982) **95**:154.

Orci, L, R.G. Miller, R. Montesano, A. Perrelet and M. Amherdt, Opposite polarity of Filipin-induced deformations in the membrane of condensing vacuoles and zymogen granules, Science (1980) **210**:1019-1020.

Padfield, P.J., T.-G. Ding and J.D. Jamieson, The effect of guanine nucleotides on Ca2+ dependent amylase secretion from permeabilized rat pancreatic acini, J. Cell. Biol. (1990) **111**:76a.

Palade, G.E., Intracellular aspects of the process of protein synthesis, Science (1975) **189**:347-358.

Paquette, J., F.A. Leblond, M. Beattie and D. LeBel, Reducing conditions induce a total degradation of the major zymogen granule membrane protein in both its membranous and its soluble form. Immunochemical quantitation of the two forms, Biochem. Cell. Biol. (1986) **64**:456-462.

Pâquet, M.R., P. St.-Jean, M. Roberge and A.R. Beaudoin, Isolation of zymogen granules from rat pancreas and characterization of their membrane proteins, Euro. J. Cell Biol. (1982) **28**:20-26

Patzk, A. and H. Winkler, Exocytotic exposure and recycling of membrane antigen of chromaffin granules: Ultrastructure evaluation after immuno-labeling, J. Cell. Biol. (1986) **102**:510-515

Pavlov, I.P. In: The work of the digestive glands, (1910) Griffin, London.

Pfeffer, S.R. and J.E. Rothman, Biosynthetic protein transport and sorting by the endoplasmic reticulum and Golgi, Ann. Rev. Biochem. (1987) **56**:829-852.

Posthuma, ,G., J.W. Slot, T. Vunendall and H.J. Geuze, Immunogold determination of amylase concentrations in pancreatic subcellular compartments, Eor. J. Cell. Biol. (1988) **46**:327-335.

Preissler, M and J.A. Williams, Pancreatic acinar cell functions; measurement of intracellular ions and their relation to secretion, J. Physiol (1981) **28**:20-26.

Rausch, U., P. Vasiloudes, K. Rüdiger and H.F. Kern, In-vivo stimulation of rat pancreatic acinar cells by infusion of secretin II. Changes in individual rates of enzyme and isoenzyme biosynthesis, Cell Tiss. Res. (1985) **242**:641-644.

Reggio, H.A. and G.E. Palade, Sulfated compounds in the zymogen granules of the guinea pig pancreas, J. Cell Biol. (1978b) **77**:288-314

Reggio, H. and J.C. Dagorn, Ionic interactions between bovine chymotrypsinogen A and chondroitin sulfate A.B.C.. A possible model for molecular aggregation in zymogen granules, J. Cell Biol. (1978a) **78**:951-957.

Rindler, M.J. and T.C. Hoops, The pancreatic membrane protein GP-2 localizes specifically to secretory granules and is shed into the pancreatic juice as a protein aggregate, Eur. J. Cell Biol. (1990) **53**:154-63.

Rogers, J., E.K. Matthews and D.B. McKay, Effects of a cytosolic protein on the interaction of rat pancreatic zymogen granules in vitro, Biochim. Biophys. Acta (1987) **897**:217-228.

Roomans, S.M. and X. Wei, X-ray microanalysis of resting and stimulated rat pancreas, Acta Physiol. Scand. (1985) **124**:353-359.

Roomans, G.M. and T. Barnard, Calcium and Magnesium in exocrine secretion - an X-ray microanalytical study, Scann. Elec. Micr. (1982) **1**:229-242.

Roos, N., Effect of stimulation of rat exocrine pancreas on subcellular element distribution, Thesis, University of Oslo, (1989).

Roos, N., A possible site of calcium regulation in rat exocrine pancreas cells: an X-ray microanalytical study, Scan. Micros. (1988) **2**:323-329.

Rothman, J.E., Protein sorting by selective retention in the endoplasmic reticulum and Golgi stack, Cell (1987) **50**:521-542.

Rothman, J.E., The compartmental organization of the Golgi Apparatus, Sc. Am. (1985) **253**:74-89.

Rothman, S.S., J. Underwood, K. McQuaid, J. Grendell, The relationship between the light scattering properties of zymogen granules and the release of their contained proteins, Biochim. Biophys. Acta (1991) **1074**:85-94.

Rothman, S.S. In: Protein Secretion: A critical analysis of the vesicle model, John Wiley and Sons (1985) New York, pp.56-58.

Rothman, S.S. and C. Liebow, Permeability of zymogen granule membrane to protein, Am. J. Physiol. (1985) **248**:G385-G392.

Rothman, S.S., Protein transport by the pancreas, Science (1975a) **190**: 747-753.

Rothman, S.S., Enzyme secretion in the absence of zymogen granules, Am. J. Physiol. (1975b) **228**:1828-1834.

Rothman, S.S., Molecular regulation of digestion: short term and bond specific, Am. J. Physiol. (1974a) **226**:77-83.

Rothman, S.S., Secretion of digestive enzyme derived from two parallel intracellular pools, Am. J. Physiol. (1974b) **226**:1082-1087.

Rothman, S.S. and L.D. Isenman, Secretion of digestive enzyme derived from two parallel intracellular pools, Am. J. Physiol. (1974) **226**:1082-1087.

Rothman, S.S., S. Burwen and C. Liebow, The zymogen granule: Intragranular organization and its functional significance, In: Advances in Cytopharmacology (Ed. B. Ceccarelli, F. Clementi and J. Meldolesi) Vol. 2, Raven Press: New York (1974).

Rothman, S.S., Association of bovine α-chymotrypsinogen and trypsinogen with rat zymogen granules, Am. J. Physiol. (1972) **222**:1299-1302.

Rothman, S.S., The behavior of isolated zymogen granules: pH-dependent release and reassociation of protein, Biochim. Biophys. Acta (1971) **241**:567-577.

Rothman, S.S., Subcellular distribution of trypsiongen and chymotrypsinogen in rabbit pancreas, Am. J. Physiol. (1970) **218**:372-376.

Rothman, S.S. and H. Wells, Selective effects of dietary egg white trypsin inhibitor on pancreatic enzyme secretion, Am. J. Physiol. (1969) **216**:504-507.

Rothman, S.S., "Non-parallel transport" of enzyme protein by the pancreas, Nature (1967a) **213**:460-462.

Rothman, S.S., Enhancement of pancreatic enzyme synthesis by pancreozymin, Am. J. Physiol. (1967b) **213**:215-218

Sato, M. and H. Take, J. Electr. Microsc. (1975) **24**:190-192.

Sesso, A., J.E.P. Assis, V.Y. Kuwajima and B. Kachar, Freeze-fracture and thin section study of condensing vacuoles in rat pancreatic acinar cells, Acta. Anat. (1980) **108**:521-539

Scheele, G. and A. Tartakoff, Exit of nonglycosylated secretory proteins from the rough ER is asynchronous in the exocrine pancreas, J. of Biol. Chem. (1985) **260**:926-931.

Scheele, G., Two dimensional gel analysis of soluble proteins: characterization of guinea pig exocrine pancreatic proteins, J. Biol. Chem. (1975) **250**:5375-5385.

Schick, J., H. Kern and G. Scheele, Hormonal stimulation in the exocrine pancreas results in coordinate and anticoordinate regulation of protein synthesis, J. Cell Biol. (1984) **99**:1569-1574.

Siekevitz, P. and G.E.Palade, A cytochemical study on the pancreas of the guinea pig. V. In vivo incorporation of leucine-l-C^{14} into the chymotrypsinogen of various cell functions, J. Biophys. Biochem. Cytol. (1960) **7**:619-630.

Singh, M., Non-parallel transport of exportable proteins in rat pancreas in vitro, Can. J. Physiol. Pharmacol. (1982) **60**:597-603.

Sommer, H. and H. Kasper, The action of synthetic secretin, cholecystokinin-octapeptide and combinations of these hormones on the secretion of the isolated perfused rat pancreas, Hepato-Gastroenterol. (1981) **28**:311-315.

Tobler, M., K. Zierold, R.W. Ammann and A.U. Freiburghaus, Element distribution in organelles of pancreatic acinar cells of rat, mouse, and pig investigated by energy-dispersive X-ray microanalysis, Pancreas (1992) **7**:686-697.

Tobler, M., J. Kassner, R.W. Ammann and A.U. Freiburghaus, Heterogeneity of zymogen granules - Are all granules filled equally?, In: Abstracts of the XXII Meeting of the European Pancreatic Club (1991) 182.

Tseng, H.C. Personal Communication.

Uchida, E., Z. Steplewski, E. Mroczek, M. Buchler, D. Burnett and P.M. Pour, Presence of two distinct acinar cell populations in human pancreas based on their antigenicity, Int. J. Pancreatol. (1986) **1**:213-225.

van de Hulst, H.C., Light scattering by small particles, Dover Publications, Inc. (1981) New York

von Wedel, R.J., S.S. Carlson and R.B. Kelly, Transfer of synaptic vesicle antigens to the presynaptic plamsa membrae during exocytosis, PNAS (1981) **78**:1014-1018.

von Zastrow, M., A.M. Castle and J.D. Castle, Ammonium chloride alters secretory protein sorting within the maturing exocrine storage compartments, J. Biol. Chem. (1987) **105**:2675-2684.

Warashina, A., Properties of pancreatic zymogen granules studied by quasi-elastic light scattering, Biochim. Biophys. Acta (1981) **672**:158-164.

White, D.A. and J.N. Hawthorne, Zymogen secretion and phospholipid metabolism in the pancreas, Biochem. J. (1970) **120**:533-538.

Williams, M.A. and G.H. Cope, Membrane dynamics in the parotid acinar cell during regranulation: a stereological study followin isoprenaline-induced secretion, Anat. Rec. (1981) **199**:389.

Wolters, G.H.J., A. Pasma, W. Konijnendijk and G. Boom, Calcium, Zinc and other elements in Islet and exocrine tisue of the rat pancreas as measured by histocehmical methods and electron-probe micro-analysis. Effects of fasting and tolbutamide, Histochemistry (1979) **62**:1-17.

Yoshimura, M., Acta Med. Univ. Kagoshima (1977) **19**:115-129.

Zimmerberg J., Simultaneous electrical and optical measurements of individual membrane fusion events during exocytosis, Meth. Enz. (1993) **221**:99-112.

Chapter II. X-Ray microscopy

In this chapter, we will the discuss the design and use of the scanning transmission X-ray microscope (STXM). The first section will review the different designs of X-ray microscopes and why we chose to use STXM. The second section will describe the basics in the design of the STXM microscope at Brookhaven National Laboratory. Because it is a developing experimental microscope, many of its features have changed over the years in which we have been using it. Therefore, the discussion here will focus more on how the microscope works as opposed to the specific design parameters. The third section describes the use of STXM in practice.

II.1 X-ray Microscopes - An overview

We mentioned in the introduction that the concept of using X rays as the light source for microscopy has been around for many decades (Lamarque, 1936). The main advantages of using X rays to image biological specimens are: a higher resolution than light microscopy can be achieved; specimens can be imaged in an aqueous environment; and quantitative information about the amount of material in the specimen can be determined from the X-ray transmission information. These aspects of X ray microscopy are discussed in the following sources (Rothman, 1990; Hasnain, 1989; Attwood, 1992, 1988; Robinson, 1987; Kirz and Rarback, 1985; Stuhrmann, 1982; Parsons, 1980).

There are three general designs of microscopes[1] that have successfully used X-rays as the illuminating source - contact microscopy; imaging microscopy, where the sample is located between the condenser and objective lenses and scanning transmission microscopy, which uses a focused spot of light to scan the sample (figure 2.1). The information in this section is based on the references (Howells et. al., 1991, 1985; Kirz

[1] In terms of imaging specimens, holographic techniques are also emplyed using X-rays. While we will not discuss this method here, the reader is refered to Jacobsen et al. (1988) and Howells et al. (1987) for further material.

and Rarback, 1985) and the reader is referred to further discussions on the development of these microscopes at specific facilities in the conference proceedings of the series of X-ray microscopy meetings that have been held every 3 years since 1984 (Schmal and Rudolph, Eds., 1984; Sayre et. al., Eds., 1988; Michette et. al., Eds, 1992 and Erko, Ed., 1993). While the basic design for the different types of X-ray microscopes is no different than those for light or electron microscopy, the difficulty in their construction has been in our ability to manufacture optics that can focus and collect the X-rays and the ability to produce a high flux source of X-rays.

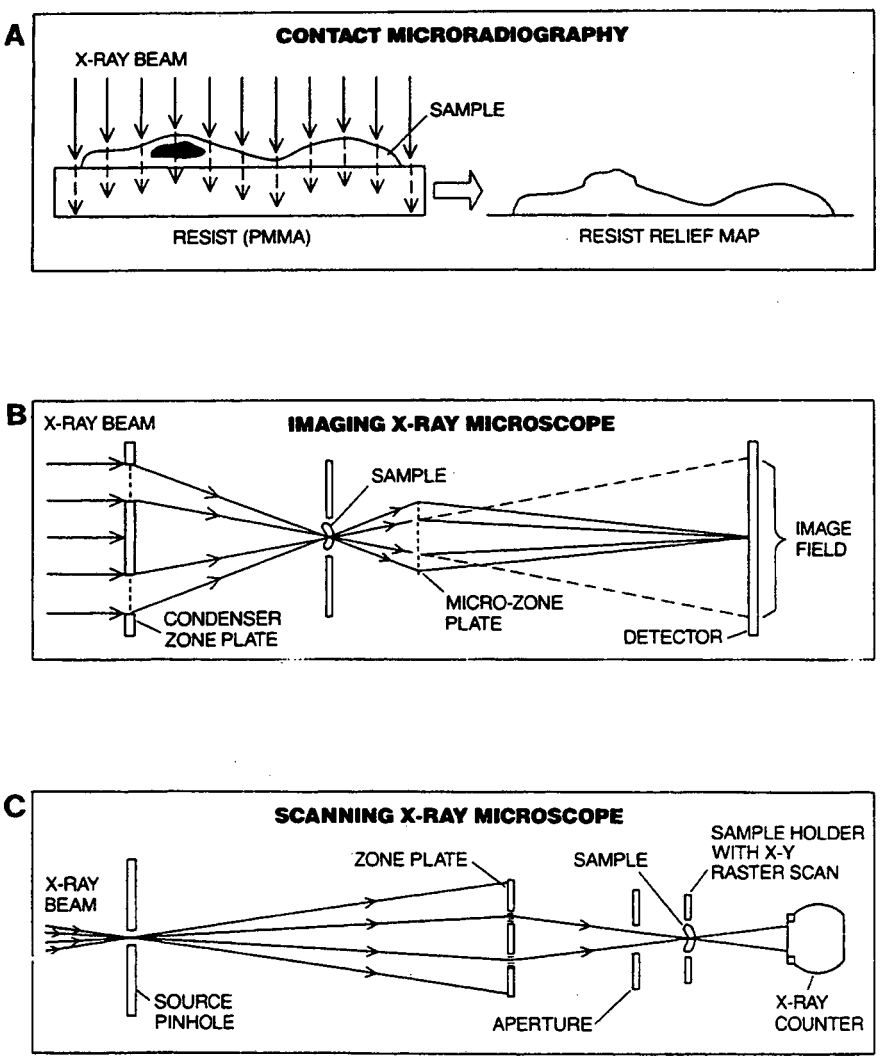

Figure 2.1 Three types of microscopy that use X rays as the illuminating source: contact microscopy (A), imaging (B) and scanning transmission (C).

The simplest microscope, which requires no X-ray optics at all, is contact microscopy (figure 2.1A). The specimen is placed on an X-ray sensitive layer (resist) and then exposed to X rays. Currently, PMMA (polymethylmethacrylate) is used as the resist material and, upon exposure to X-rays, it is damaged by chain scissions or cross-linking. After the exposed resist is "developed," the damaged material is removed leaving a relief pattern on the surface of the resist. The resolution of this method could be as low as 5nm. But there are several problems in attaining the full resolution. The first is choosing an appropriate technique to read the resist and magnify the image without compromising the resolution. Currently, scanning and transmission electron microscopy (SEM and TEM) and atomic force microscopy (AFM) have been used. Another problem is the actual development time of the resist material. Like a photograph, the resist can be over- or under-developed which in turn can produce features in the resist that are not in the sample, "artifacts." And the third problem is the X-ray exposure or "dose" required for an image which is typically of order 10^3 Mrad (the reader is referred to Chapter VII for a thorough explanation of dose). The good news is that if a very bright source of X-rays is used, then the sample can be imaged in microseconds. This is fast enough to eliminate any blurring that may occur due to normal motion in the specimen and so live, fresh specimens can be imaged. But, specimens can be imaged only once since after receiving the dose of the initial image they are permanently damaged. The inability to image the specimen more than once was the main reason that we did not choose this technique for our experiments. Further information on contact X-ray microscopy can be found in (Cheng et al., 1986; Feder et al., 1986; Feder and Sayre, 1980).

The imaging microscope and the scanning transmission microscopes both require optics that have the ability to focus X-rays. Traditional optical materials, such as glass or quartz lenses, are highly opaque to X rays and so X-ray refraction through such lenses is not a viable option for focusing X rays. The X-ray optics that have been designed rely on

the diffractive properties of X-rays and the fact that at very small glancing angles, X rays can be reflected and it is only through recent technological advances that these optics are able to be manufactured (Ceglio, 1989; Underwood, 1978; Underwood and Attwood, 1984). Diffractive lenses, called Fresnel zone plates, have been constructed which give a diffraction limited focus spot of 20nm. They will be described in more detail in the next section. Reflective optics have also been developed using mirrors with special coatings but they do not work well in the range of wavelengths in the water window and so we will not consider them here (see Underwood et al., 1986). The imaging microscopes (figure 2.1B) require two zone plates - a condensing and an imaging lens - just as in a typical light microscope. Because the diffraction efficiency of the zone plates is extremely low (< 8%) the incident X-ray flux must be extremely high for enough photons to pass through both zone plates and the specimen to be detected. The development of synchrotron sources and laser plasma X-ray sources has enabled the production of extremely bright and coherent X-rays so that imaging microscopes can be constructed (DaSilva, 1992; Attwood, 1985).

The advantage of the imaging microscope is that the entire sample can be imaged using one "shot" of X-rays. Unfortunately, in order to compensate for the loss of X-ray flux through the imaging zone plate in this design, the sample receives an extremely high dose of X rays akin to that of contact microscopy. This high dose to the sample makes it currently impossible to image fresh samples, although fixed and material science specimens are routinely imaged. A recent description of the imaging microscope at the BESSY synchrotron in Berlin, mentioned in the introduction, is given in Schmahl et al. (1993).

The scanning transmission microscope (figure 2.1C) only requires one zone plate to focus the X-rays to a small spot. This spot is scanned over the sample and the transmitted photons are detected, usually with a gas flow proportional counter. Because the optics are

only placed before the sample, it is not necessary to expose the sample to high doses of X-rays. And, depending on the sensitivity of the photon detector, the sample can actually be imaged with a relatively low dose of X-rays. The disadvantages to this technique are that 1) it requires that the illuminating X-rays be coherent so that the optics will form a diffraction limited probe and 2) scanning the specimen takes a finite amount of time. The first problem has been addressed by the use of insertion devices in synchrotron rings that produce coherent X-rays (described in the next section). And, the second problem imposes a limit on the type of sample that is being investigated. Objects that move rapidly are out of the question.

As mentioned above, all three types of microscopes are currently in use. We chose to use the scanning transmission X-ray microscope because it was the only technique with which we could image our specimens with a low enough dose to allow multiple imaging.

II.2 The Scanning Transmission X-ray Microscope at BNL

II.2.1 The production of X rays

We have been using the STXM[2] located at National Synchrotron Light Source (NSLS) in Brookhaven National Laboratory (BNL) on Long Island, NY(Kirz et a., 1990; Rarback et al., 1990a&b, 1988). Since 1989 we have been using about 8 weeks of beam time a year at this facility.

The synchrotron at NSLS is an electron storage ring with a diameter of 50ft that accelerates the electrons to an energy of 2.5GeV. It operates at a working current of ~220 mA which decays exponentially to 100mA at which time a new fill of electrons is injected. A fill can last between 8-12hrs, if there are no unscheduled beam dumps during the period. When we first began our experiments, the stability of the electron orbit was

[2] The other functioning STXM, as mentioned in the introduction, is located at the Daresbury synchrotron facility in England. A description of that microscope can be found in Morris et al. (1991)

subject to failure and beam dumps were quite common. Today, the expected duration of the electron fill is rarely interrupted.

X-rays are radiated from the electron beam as it passes through magnetic insertion devices installed in the ring. The insertion device at BNL is called an undulator and is a periodic array of magnets that wiggles the electron beam as it passes through. This acceleration and deceleration of the electron beam causes the electrons to radiate energy. The energy at which they radiate can be regulated depending on the design constraints of the undulator. For a further discussion of the theory of undulators and other types of insertion devices see (Hofmann, 1978). The undulator that is used for STXM at BNL is located at beamline X1A. It is a 35 period device and the magnetic field is generated by samarium-cobalt permanent magnets. It has been designed to produce X rays between 200 and 800eV (1.7 - 7.0nm). By adjusting the gap between the magnetic components of the undulator, we can tune the peak X-rays. The spectral brightness of X-rays produced by the undulator is $\sim 1 \times 10^{17}$ photons/[(sec)(mm^2)(mrad^2)(0.1%bandwidth)] at our working wavelength. Figure 2.2 shows the spectral brightness of the X1A undulator as well as other X-ray sources that are currently in use.

The X-rays produced from the undulator are radiated tangentially from the orbit of the electrons. The natural direction of these X-rays defines what are called "beam-lines" and there are about 30 beamlines at BNL. At the end of each beam-line is a scientific station. The electron storage ring is operated at ultra-high vacuum $\sim 10^{-11}$ Torr and the X rays that are generated from the insertion devices are also kept in vacuum along the beamlines at about 10^{-7} Torr. Typically, scientific endstations are ~20 meters from the insertion devices.

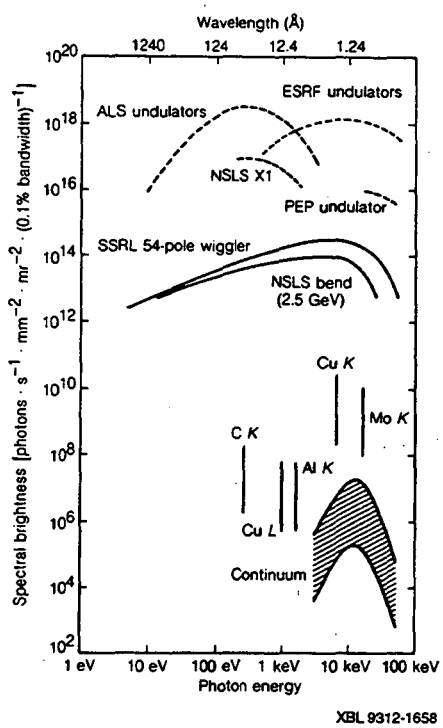

Figure 2.2 The spectral brightness for several synchroton radiation sources and conventional X-ray tube sources as a function of wavelength. The source for the microscope that we used is labeled NSLS X1. We can see that the brightness of X-rays from this source is many magnitudes higher than that from conventional X-ray tube sources which use particular emission lines from atoms as the X-ray source (C, Al, Cu & Mo K-lines and Cu L-line). We can also see that the newly built ALS synchrotron at Lawrence Berkeley Laboratory will contain an undulator that is capable of producing even brighter X-ray than at NSLS.

The direction of the X rays from the insertion device (ID) also defines the coordinate system of the beamline. The direction from the (ID) towards the endstation is considered "downstream" (+z) with the opposite direction being "upstream" (-z). Looking upstream from the endstation, the direction to one's left is "inboard" (+x) and to the right is outboard (-x). Then there is "up" (+y) and "down" (-y). This is diagrammed in figure 2.3. The components of the beamline downstream of the undulator, shown in figure 2.3, are designed to extract from this spectrum of X rays, a spot of spatially and temporally

coherent X rays that can be directed onto the focusing optics of the microscope. Immediately downstream of the undulator is a water cooled mirror which is responsible for splitting the X rays into two beamlines - X1A and X1B. X1B is a spectroscopy beamline and can be operated simultaneously with X1A, as long as both groups agree on the undulator gap setting. Further downstream in the X1A beamline is a spherical grating bichrometer (SGB). The bichrometer selects a narrow bandwidth of energy from the spectrum that the undulator produces. The width of the band defines the temporal coherence of X rays. The SGB selects both the fundamental and second harmonic of undulator energy. Because of the difference in wavelength, the two harmonics undergo different angular deviation at the grating thus forming two new beamlines, the X1A long wavelength and short wavelength branches. The long wavelength branch is essentially the fundamental peak of the undulator while the short wavelength branch is at the second harmonic of the undulator. They are able to operate at the same time. Typically the long wavelength branch operates at 350eV (3.5nm) and the short at 700eV(1.8nm). STXM is located at the end of the long wavelength branch and so the following discussion will be concerned with the components of this branch.

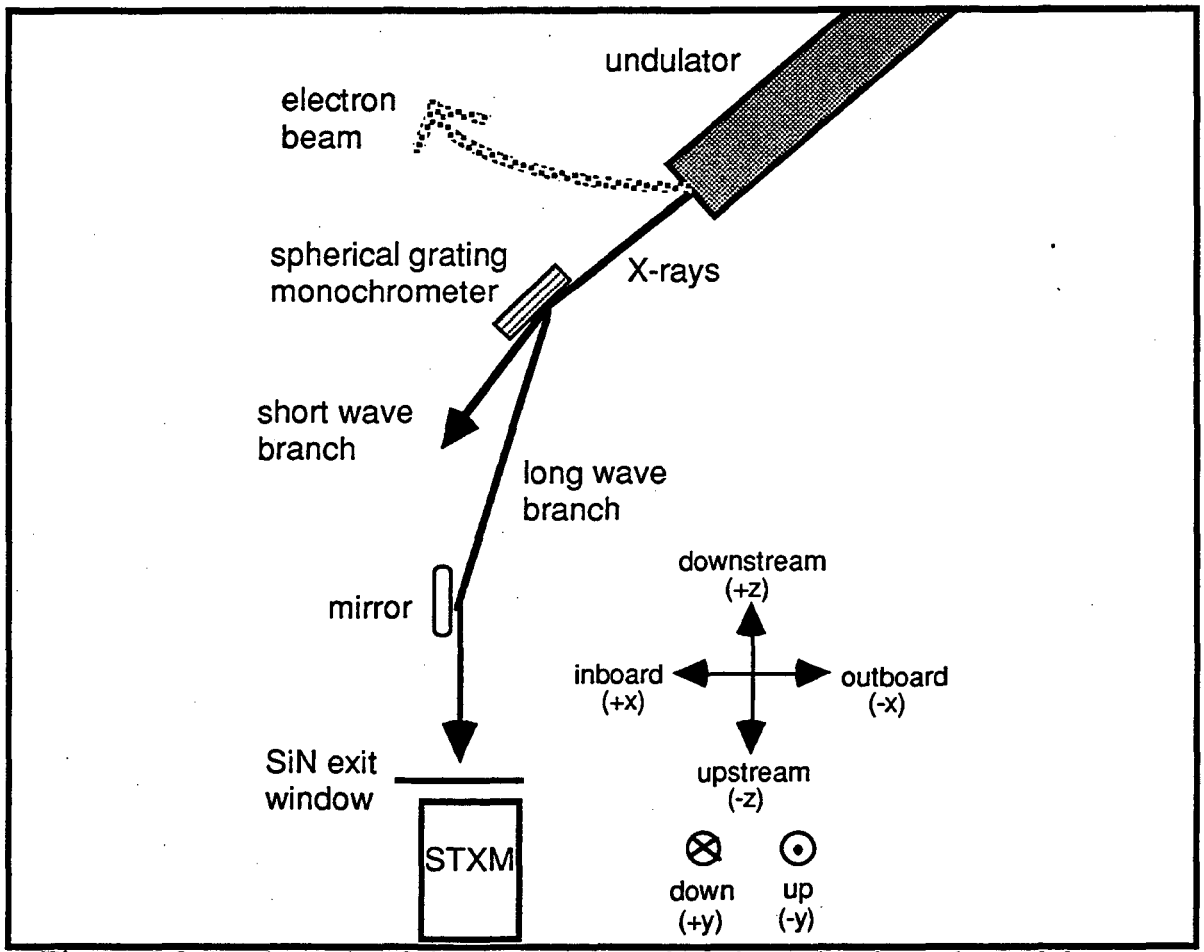

Figure 2.3 A schematic of the components of the beamline from the undulator to STXM as seen from above - components are not drawn to scale although the distance from the undulator to STXM is 24 meters. The coordinate system is also shown. The components are described in the text. Everything downstream of the SiN (silicon nitride exit window) is in vacuum; upstream of the exit window is in air.

Downstream of the SGB, the X-rays pass through an exit slit. The slit can be adjusted from 25 - 400 μm and contributes to the spatial coherence of X rays. There is one more mirror downstream of the exit slit, called the long wavelength branch mirror (LWB), that can be adjusted to help direct the X rays onto the exit window of the beamline. The exit window is a 120nm silicon nitride window about 250μm^2. After the X rays pass through the exit window, they are no longer in vacuum and because X-rays are quickly absorbed in air, the microscope is located immediately downstream from the exit window. Directly upstream from the exit window is the last component of the microscope in vacuum, and

that is a shutter. It can be automatically opened and closed at the beginning and end of an image.

II.2.2 The microscope

A schematic of the microscope is shown in figure 2.4. The four main components of the microscope are the zone plate, the order sorting aperture (OSA), the sample stage and the X ray detector or proportional counter (PC). The microscope is enclosed in a Plexiglas box and there are helium gas inlets into the general area of the microscope. The helium presents a relatively non-absorbing environment to X rays as compared to air, around the microscope. The box also serves as a barrier to fluctuating air currents.

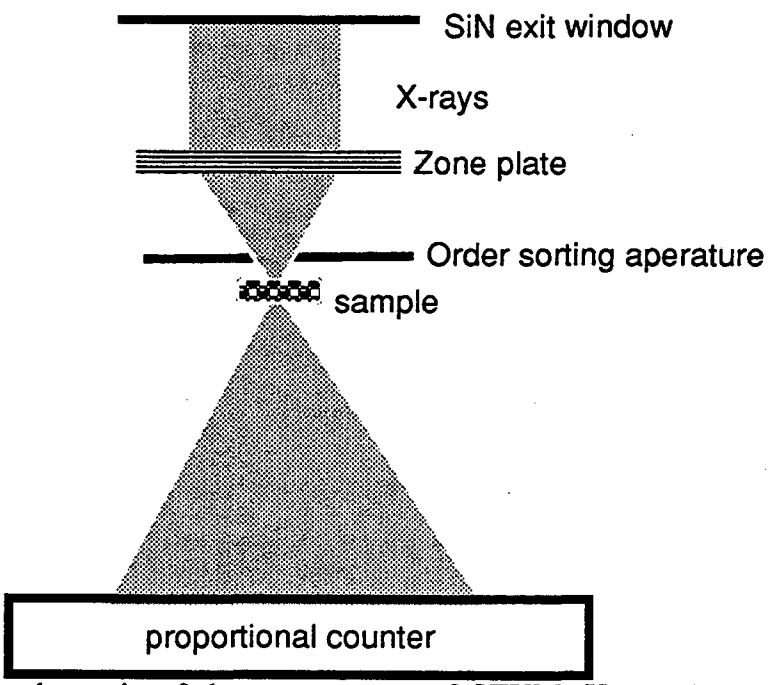

Figure 2.4 A schematic of the components of STXM. X-rays leave the vacuum environment of the beamline at the silicon nitride exit window. They are then focused by the zone plate, pass through the order sorting aperature and the focused spot of X-rays is directed onto the sample. Transmitted X-rays are detected by a gas flow proportional counter. Separations between objects are not drawn to scale. Helium is flowed around the microscope and a plexi-glass box surrounds the microscope which maintains this environment.

All of the components of the microscope are separately mounted mechanically, with independent x, y and z micrometers or stepper and piezoelectric (PZT) drivers. This is so the microscope can be aligned and focused. Some of the movements are manually controlled and some are computer controlled. This will be discussed in further detail as each component of the microscope is addressed.

The most critical component of the microscope is the Fresnel zone plate (figure 2.5) (Vladimirsky et al., 1988). This ingenious device is able to focus X rays into a small spot - no small feat because X rays are significantly absorbed by most materials and are not easily reflected. The zone plate is a circular structure with alternating opaque and transparent zones. It is designed to focus X-rays using diffraction and since every other zone is transparent, the X-rays that pass through these zones constructively interfere.

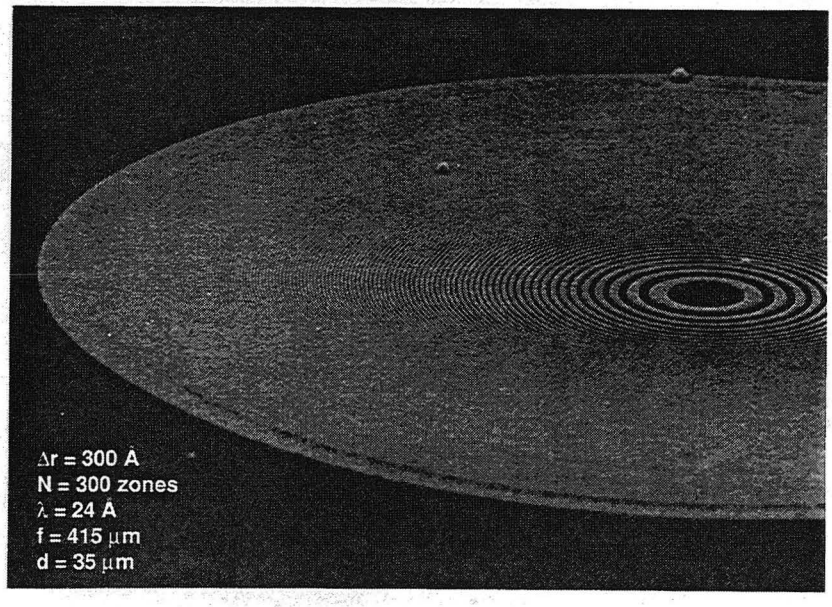

Figure 2.5 A scanning electron microscope image of a Fresnel zone plate. The diameter of this zone plate is 35μm and the width of the outermost zone 30nm. It has 300 zones and the central region of the zone plate is apodized, as will be explained in the text

The formula for the radius of each zone (r_n) is derived so that the phase over one zone varies by 180° and is described by the equation

$$r_n^2 = r_o^2 + n\lambda f \quad \text{when } r_o << f \text{ and } nf << f$$

where r_o is the radius of the first zone, n is the number of zones, λ is the wavelength of X rays and f is the focal length of the lens.

The focal length, focal spot size (S) and depth of focus (dF) are dependent on the number of zones that the zone plate contains, the diameter of the zone plate (D), the width of the outermost zone (δ) and the wavelength of light.

$$f = D \cdot \delta / \lambda$$

$$S = 1.22 \cdot \lambda f / D = 1.22 \cdot \delta$$

$$dF = \pm 1/2 \cdot (f/\delta)^2$$

The numerical aperture (N.A.) of the lens can also be defined as

$$N.A. = (\delta/f)$$

The zone plates that are used at BNL are manufactured at IBM using e-beam lithography (Anderson and Kern, 1992; Anderson, 1989). When we first began using the microscope, the zone plates were constructed of gold. Fifty percent of the incident light was initially absorbed by the opaque zones and the remaining fifty percent of the X rays was divided between the different ordered focal points (remember that the zone plate is a circular diffraction grating). Theoretically, we could only expect to receive 10% of the incident light at the 1st order focal spot and it was more like 7%. The efficiency of the zone plates has been improved by using phase shifting material in their construction instead of just opaque and transparent zones. The material used was nickel and it shifted the phase of light that passed through the opaque zones enough so that it constructively interfered with light from the transparent zones. Theoretically, these zone plates should direct 18% of the incident light into the first order; the zone plates we used had a practical

efficiency of 13% (Jacobsen, 1991). This relatively low efficiency of the zone plate is one of the reasons that extremely bright X rays are required.

A typical Ni zone plate that we worked with had the following parameters

Diameter (D)	90 μm
Number of zones (n)	300
width of outer zone (δ)	45 nm
Depth of zones	100 nm
focal length (λ=3.6nm)	1113 μm
spot size (λ=3.6nm)	~50nm
depth of focus (λ=3.6nm)	2.7 μm
N.A. (λ=3.6nm)	0.0404

As mentioned above, zone plates are able to focus X rays by diffraction but only ~10% of the light is directed into the first order focal spot and so we need to block the light from the other focal orders so as not to contaminate the image. The zeroth order light is blocked by an opaque central stop on the ZP that is 45μm in diameter. The other orders of light are blocked using the second component of the microscope, an order sorting aperture (OSA). Its function is to block X rays from the other orders and only let light through from the first order. The OSA is essentially a pinhole with a diameter (24 μm) that is only large enough to let the first order focus X rays through. This is more easily seen in figure 2.6.

The sample stage is located after the OSA. At this point, we remind the reader that because X rays are produced in a beam that is horizontal to the ground, instead of moving the mountain to Mohammed, our sample stage is in a vertical position instead of the traditional horizontal one. This is rather awkward because it requires that we fight the force of gravity in order to image our specimens. There is a magnetic mount on the sample stage to hold the sample chamber vertical. But affixing one's specimen to the sample chamber is the great challenge for the scientist and we will discuss our solution to this problem in the next section. The stage can be moved both in the x and y direction

with either coarse steps (the steppers) or fine steps (PZTs). The stepper motors are able to move in micron steps and their range is 25mm. The PZTs can move in 0.5nm steps and have a range of 75μm. The ranges determine the maximum size of the image that can be formed.

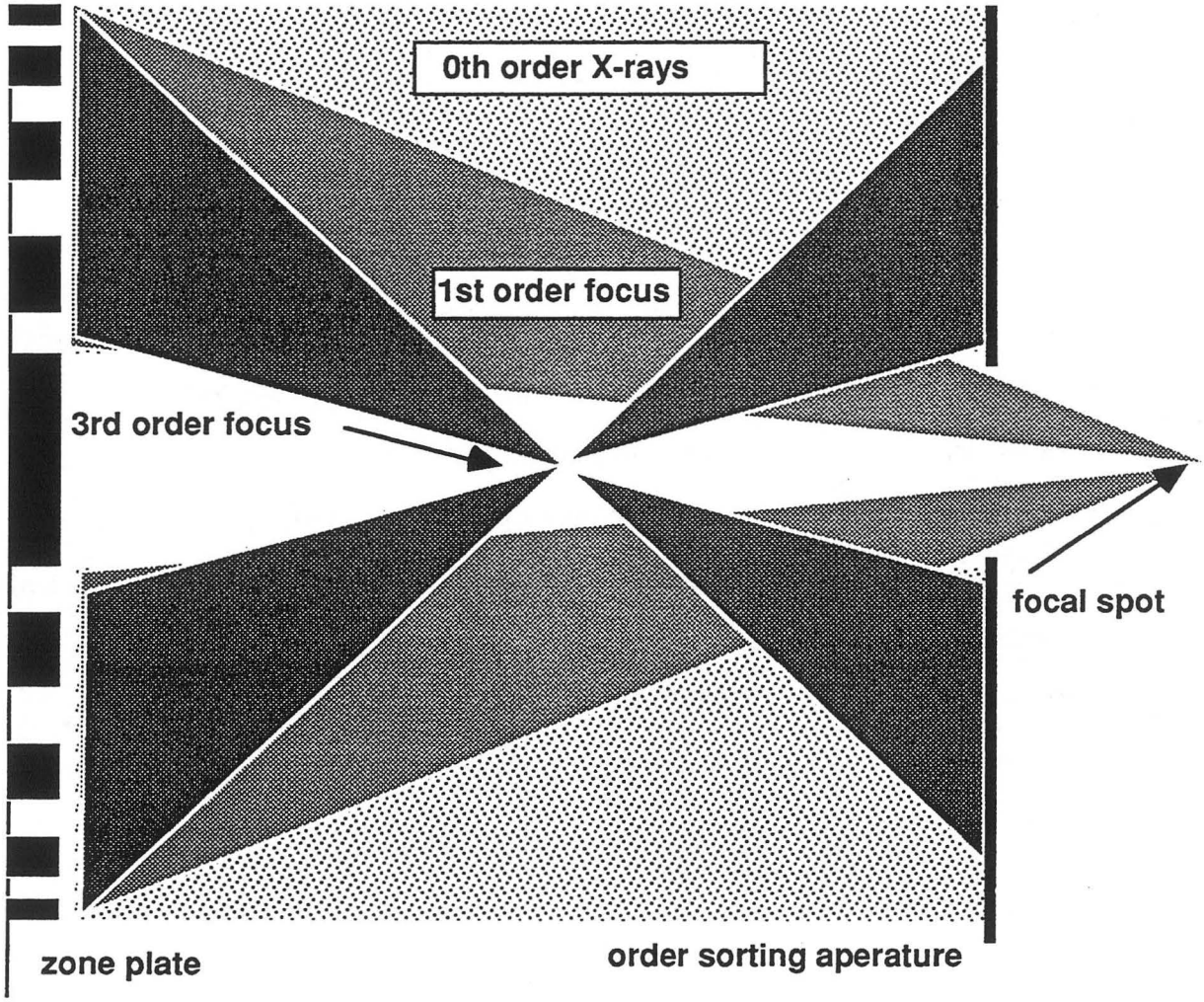

Figure 2.6 The zone plate and the order sorting aperature. From this schematic, we can see that the zone plate is able to focus several different orders of X-rays (because it is a diffraction lens). So that only the 1st order light illuminates the sample, the order sorting aperature (OSA) blocks out the other orders, as well as the non-focused zero order. The diameter of the hole in the OSA is 24μm. The distance between the zone plate & OSA is ~800μm (λ=3.6nm) and between the OSA and the focal spot, it is ~300μm. We can see that there is very little working distance between the OSA and where the sample sits, at the focal spot.

Immediately behind the sample stage is the X-ray detector. A high rate, gas flow proportional counter (PC) is used at X1A. It runs in saturation mode with a 90% Ar : 10% CO_2 gas mixture and an aluminized silicon nitride entrance window. We expect a >95% quantum efficiency in counting single photons for count rates around 1MHz although the counter will saturate at 3MHz.

There is also a visible light microscope (VLM) mounted behind the proportional counter. This microscope allows the user to view the components of the microscope when aligning and also to see the sample. The PC has to be raised when using the VLM.

A STXM image is attained by scanning the stage across the focused spot of X rays and the number of transmitted photons are detected and recorded. This is accomplished through an interactive software package called "STXM" that enables the user to choose the imaging parameters for each image. These include 1) number of pixels in a scan, which will determine the dimensions of the scan depending on their size; 2) The size of each pixel which is effectively the distance the sample stage motors are told to move between photon collecting points; 3) the dwell time or the time that the motors are held constant at a particular photon collection point. Changing the dwell time effectively changes the exposure time and the number of photons that are counted at the PC. The images are constructed pixel by pixel on the computer screen as the microscope is scanning so we have the advantage of real time imaging.

II.3 STXM in practice

II.3.1 Aligning the Microscope

Preparing the microscope for use requires adjusting all of the components of the beamline and microscope that have been mentioned in the previous sections in order to focus the X rays. Control of these components is divided between computer control and manual adjustments. There are two VAX station 3200 computers that interact with

CAMAC controllers that actually move the components; "BNLX1" controls the SGB, water-cooled mirror and the undulator positions and "BNLX1L" controls the long wavelength branch mirror, the shutter and some of the motors for the microscope components in the - z direction for the zone plate and the x &y directions for the sample stage.

The first step is an initial choice of wavelength. We generally chose to work at 3.6nm because the second harmonic of this wavelength was compatible with the group who was working on the short wavelength branch. Although, occasionally we used 3.4 or 3.5nm. The wavelength was adjusted by changing the undulator gap via BNLX1 software. The SGB position also had to be adjusted in order to direct the selected wavelength down the long wave branch. Directing the X-rays onto the exit window was achieved by adjusting the LWB mirror, controlled by BNLX1L. There is one mirror that has three independent mounts so that it can be moved in all three dimensions. There is a phosphor coating surrounding the exit window, and so a rough approximation of the position of the beam can be achieved by observing the fluorescence of this spot. But after this rough adjustment is done, the rest of the alignment is achieved by imaging the focusing optics.

Using STXM, the exit window is imaged to ensure that it is uniformly illuminated. We use a 5μm diameter pinhole mounted on the sample stage to image the exit window so as not to oversaturate the counter. If the window is not evenly illuminated, then it is possible to fine tune the illumination with slight adjustments of the LWB mirror. When the exit window appears uniformly illuminated, the zone plate is inserted. The zone plate is mounted on a silicon nitride window which in turn is on a magnetic holder which holds the zone plate to the exit window. The zone plate is imaged, again with the pinhole, and adjusted manually so that it too appears uniformly illuminated. Next, the OSA is inserted. It is mounted on micrometers that move it in all three dimensions. The distance the OSA needs to be from the zone plate (in the z direction) in order to block out the unfocused

light can be calculated geometrically (figure 2.6). This distance is determined using the VLM. The VLM has a micrometer that notes its position in z. The position when the zone plate is in focus is noted and then the VLM is moved the calculated distance that is required between the zone plate and OSA. When the OSA is inserted, its z position is adjusted until it appears in focus in the VLM.

The alignment of the OSA in the x&y planes is then checked by imaging the OSA. From figure 2.6, the reader is reminded that the zone plate diffracts the X-rays into a conical shape the apex of which is the focal spot. Therefore, if we image a cross section of this cone of X-rays, we will see a donut shape. If the OSA is misaligned with respect to this focal cone, then the donut appears to have a bite taken out of it (flatfoots on the loose). The x and y positions can then be adjusted by hand using the micrometers. This alignment step can be particularly harrowing because of the close fit of the OSA to the cone of X rays and we generally only have about ± 1.5μm of slack.

Once this alignment step is completed, the microscope is essentially ready to go. The last check is to adjust the position of the PC so that it is detecting as many photons as possible. The alignment of the beam can take anywhere from 15 minutes to literally hours. Sometimes the electron beam itself is not very stable and this in turn can affect our alignment accuracy. Also, if the position of the beam has changed from fill to fill, the components of the microscope have to all be realigned. It is also a fact that aligning at 3 in the morning takes 3 times as long as it does during the day! After the alignment is complete, we are ready to insert the sample.

II.3.2 Imaging with STXM

Once we have aligned the microscope, we are ready to image a specimen. The specimen has to first be mounted on some sort of "slide" that has a magnetic backing so that it can be attached to the sample stage. The stage can then be moved in the x&y directions so that it is in line with the zone plate/OSA. This step is usually performed

using the VLM which offers a direct line-of-sight down the microscope. The VLM also allows us to look at our specimen and choose an area that might be of interest to image. This, of course, only works if our specimen is large enough to be visible in the VLM. At this point, the sample stage is located quite a distance from the focal plane of the zone plate so that we do not run the risk of misaligning the optics by bumping them with the specimen. The next step will be to move the specimen into the focal plane, which we remember from the previous section is only ~300μm from the OSA! Not a lot or working distance. At this point, we are back to imaging the specimen in order to find the focus. The VLM will be removed and the PC inserted.

In order to move into the focal plane, the specimen theoretically has to be moved upstream. But the STXM design at BNL actually moves the ZP/OSA downstream in z. It is a matter of perspective, but something to keep in mind. In focusing, the initial images are done using the stepper motors with short dwell times in order to minimize the exposure of the sample to X rays. In our experience, we have found it extremely useful to have focusing spots on our sample window. These will be described in the next section in further detail, but are essentially 10μm sized gold squares that are ~1μm high. Not only do they have good sharp edges to focus on, but they sustain no radiation damage. When the spots are roughly in focus, we do a finer focus using a routine built into the STXM software. This routine will perform a line scan across the object one is focusing on and then move a distance in Z and repeat the scan. From the resulting image, one is able to chose, by comparison, the Z position that has the best focus. The ZP/OSA is moved to this position and we are now ready to image. Inserting the sample and focusing takes ~15 minutes.

From this point on, we are in a search and find mode in order to image our specimen. Our methodology for finding images and the parameters that we used for imaging them is discussed in further detail in the Methods - Chapter V.

Chapter II - References

Anderson, E. and D. Kern, Nanofabrication of zone plate lenses for high resolution X-ray microscopy, In: X-ray Microscopy III (A.G. Michette, G.R. Morrison and C.J. Buckley, Eds.), Vol. 67, Springer Series in Optical Sciences, Springer-Verlag: Berlin (1992)

Anderson, E.H., Fabrication technology and applications of zone plates, Proceedings of SPIE (1989) **1160**:2-11.

Attwood, D., New opportunities at soft X-ray wavelengths, Phys. Tod. (1992) **45**:24-31.

Attwood, D., Y. Vladimirsky, D. Kern, W. Meyer-Ilse, J. Kirz, S. Rothman, H. Rarback, N. Iskander, K. McQuaid, H. Ade and T.H.P. Chang, X-ray microscopy for the life and physical sciences, In: OSA Proceeding on Short Wavelength Coherent Radiation: Generation and Applications, Optical Society of America: Washington, D.C. (1988) **2**:274-276.

Attwood, D., K. Halbach and K.-J. Kim, Tunable Coherent X-rays, Science (1985) **228**:1265-1272.

Ceglio, Revolution in X-ray Optics, J. X-ray Sc. Tech. (1989)**1**:7-78.

Cheng, P.C., R. Feder, D.M. Shinozaki, K.H. Tan, R.W. Eason, A. Michette and R.J. Rosser, Soft X-ray contact microscopy, Nucl. Instr. Meth. Phys. Res. (1986) **A246**:668-674.

DaSilva, L.B., J.E. Trebes, R. Balhorn, S. Mrowka, E. Anderson, D.T. Attwood, T.W. Barbee, Jr., J. Brase, M. Corzett, J. Gray, J.A. Koch, C. Lee, D. Kern, R.A. London, B.J. MacGowan, D.L. Matthews and G. Stone, X-ray Laser microscopy of rat sperm nuclei, Science (1992) **258**:269-271.

Erko, A.I. (Ed.), X-ray Microscopy IV, (1993) To be Published.

Feder, R., J.W. McGowan and D.M. Shinozaki (Eds.), Examining the Submicron World, Plenum Press:New York (1986).

Feder, R. and D. Sayre, Recent developments in X-ray contact microscopy, Ann. New York Acad. Sci. (1980) **342**:213-229.

Hasnain, S. (Ed.), Biophysics and Synchrotron Radiation, Ellis Horwood Limited: Chichester, UK (1989).

Hofmann, A., Nucl. Instrum. Meth. (1978) **152**:17

Howells, M.R., J. Kirz and D. Sayre, X-ray microscopes. Sci. Am. (1991) **264**: 88-94.

Howells, M., C. Jacobsen, J. Kirz, R. Feder, K. McQuaid and S. Rothman, X-ray holograms at improved resolution: A study of zymogen granules, Science (1987) **238**:514-517.

Howells, J. Kirz, D. Sayre and G. Schmahl, Soft X-ray microscopes, Phys. Tod. (1985)

Jacobsen, C., S. Williams, E. Anderson, M.T. Browne, C.J. Buckley, D. Kern, J. Kirz, M. Rivers, X. Zhang, Diffraction-limited imaging in a scanning transmission X-ray microscope, Opt. Comm. (1991) **86**:351-364.

Jacobsen, C., J. Kirz, M. Howells, K. McQuaid, S. Rothman, R. Feder and D. Sayre, Progress in high-resolution X-ray holographic microscopy, In: X-ray Microscopy II (D. Sayre, M. Howells, J. Kirz and H. Rarback, Eds.) Vol. 56, Springer Series in Optical Sciences, Springer-Verlag: Berlin (1988).

Kirz, J., H. Ade, E. Anderson, D. Attwood, C. Buckley, S. Hellman, M. Howells, C. Jacobsen, D. Kern, S. Lindaas, I. McNulty, M. Oversluizen, H. Rarback, M. Rivers, S. Rothman, D. Sayre and D. Shu, X-ray microscopy with the NSLS soft X-ray undulator, Phys. Script. (1990) **T31**: 12-17

Kirz, J and H. Rarback, Soft X-ray microscopes, Rev. Sci. Instrum.(1985) **56**:1-13

Lamarque, P.C.R., Acad. Sci. (1936) **202**:684.

Michette, A.G., G.R. Morrison and C.J. Buckley (Eds.), X-ray Micrscopy III, Vol. 67, Springer Series in Optical Sciences, Springer-Verlag: Berlin (1992).

Morris, D., C.J. Buckley, G.R. Morrison, A.G. Michette, P.A.F. Anastasi, M.T. Browne, R.E. Burge, P.S. Charalambous, G.F. Foster, J.R. Palmer and P.J. Duke, Recent advances in scanning X-ray microscopy, Scann. (1991) **13**:7-10.

Parsons, D.F. (Ed.), Ultrasoft X-ray Microscopy: Its Application to Biological and Physical Sciences, The New York Academy of Sciences: New York (1980).

Rarback, H., C. Buckley, H. Ade, F. Camilo, R. DiGennaro, S. Hellman, M. Howells, N. Iskander, C. Jacobsen, J. Kirz, S. Krinsky, S. Lindaas, I. McNulty, M. Oversluizen, S. Rothman, D. Sayre, M. Sharnoff and D. Shu, Coherent radiation for X-ray imaging - The soft X-ray undulator and X1A beamline at NSLS, J. X-ray Sci. Tech. (1990a) **2:** 274-296.

Rarback, H., C. Buckley, K. Goncz, H. Ade, E. Anderson, D. Attwood, P. Batson, S. Hellman, C. Jacobsen, D. Kern, J. Kirz, S. Lindaas, I. McNulty, M. Oversluizen, M. Rivers, S. Rothman, D. Shu and E. Shang, The scanning transmission microscope at the NSLS. Nucl. Instr. and Methods. (1990b) **A291**:54-59.

Rarback, H., D. Shu, S.C. Feng, H. Ade, J. Kirz, I. McNulty, D.P. Kern, T.H.P. Chang, Y. Vladimirsky, N. Iskander, D. Attwood, K. McQuaid and S. Rothman, Scanning X-ray microscope with 75nm resolution, Rev. Sci. Instrum. (1988) **59**:52-59.

Robinson, A.L., Imaging unaltered cell structures with X rays, Science, **237**:723-724 (1987).

Rothman, S., E. Anderson, D. Attwood, P. Batson, C. Buckley, K. Goncz, M. Howells, C. Jacobsen, D. Kern, J. Kirs, H. Rarback, M. Rivers, D. Shu, R. Tackaberry and S. Turek, Soft X-ray microscopy in biology and medicine: Status and prospects, Physica Scripta. (1990) **T31**:18-22.

Sayre, D., M. Howells, J. Kirz and H. Rarback (Eds.), X-ray Microscopy II, Vol. 56, Springer Series in Optical Sciences, Springer-Verlag: Berlin (1988).

Schmahl, G., P. Guttman, G. Schneider, B. Niemann, C. David, T. Wilhein, J. Thieme and D. Rudolph, Studies of hydrated biological specimens with the X-ray microscope at BESSY, In: X-ray Microscopy IV (A.J. Erko, Ed.) To be published.

Schmahl, G. and D. Rudolph (Eds.), X-ray Microscopy I, Vol. 43, Springer Series in Optical Sciences, Springer-Verlag: Berlin (1984).

Stuhrmann, H.B. (Ed.), Uses of Synchrotron Radiation in Biology, Academic Press: San Francisco (1982).

Underwood, J.H., T.W. Barbee Jr. and C. Frieber, X-ray microscope with mutilayer mirrors, Appl. Opt. (1986) **25**:1730-1732.

Underwood, J.H. and D.T. Attwood, The renaissance of X-ray optics, Phys. Tod. (1984) 44-51.

Underwood, J.H., X-ray Optics, Am. Scientist (1978) **66**:476-486.

Vladimirsky, Y., D.P. Kern, T.H.P Chang, D.T. Attwood, N. Iskander, S. Rothman, K. McQuaide, J. Kirz, H. Ade, I. McNulty, H. Rarback and D. Shu, Zone plate lenses for X-ray microscopy, Nuc. Instr. Meth. Phys. Res. (1988) **A266**:324-328.

Chapter III. STXM Images, Computer Processing and Calculations

As mentioned in Chapter II, the STXM images are digital recordings of the number of photons transmitted through the sample at each pixel point. In this chapter, we will discuss the basis of resolution, contrast and noise sources inherent in these images. We will also discuss the computer techniques we used to display, process and print hardcopys of each image from this digital information. In addition, we will also describe the software used to perform calculations on the raw data of these images in order to measure the diameter, protein mass per pixel, total protein mass and protein concentration of each zymogen granule.

III.1 STXM Images

In this section, we will discuss in more detail the characteristics of STXM images. This involves defining the resolution, the basis of contrast and the noise inherent in this type of imaging.

III.1.1 Resolution

The resolution of STXM is limited by the diffraction efficiency of the zone plate and can therefore be described using the Rayleigh criteria. In order obtain diffraction limited performance, the zone plate illumination must have sufficient temporal and spatial coherence and the zone plate must meet certain manufacturing constraints. Jacobsen (1991) has discussed in depth these criteria and has concluded that the resolution of the Ni zone plate used at X1A is indeed diffraction limited.

The Rayleigh criteria essentially defines the resolution of a microscope based on the Airy pattern of the diffracted light. For a zone plate with > 100 zones, the 1st order diffraction pattern (spot) is approximately an Airy function (Michette, 1986). During imaging, we are essentially moving our specimen over the focal spot and the image is the X-ray absorption pattern of the sample convoluted with the Airy pattern of the focal spot.

By the Raleigh criteria, we will be able to just distinguish two points in our specimen if the first maximum of the convoluted Airy pattern from the first point falls on the first minimum of the convoluted Airy pattern from the second point. This distance, or resolution (R) is defined traditionally as $R=1.22\ f\lambda/d$ where d is the diameter of the lens. For zone plates with no obstructed zones (e.g. no central stop) ,

$$R = 1.22\ f\lambda/d = 1.22\delta \qquad (3.1)$$

where (δ) is the width of the outermost zone of the zone plate. The Rayleigh resolution for the Ni zone plate with δ=45nm is 55nm.

The spatial resolution of the zone plate has often been confirmed using high resolution test objects. A typical test object is 70nm thick, with 36nm minimum width gold features (85% opaque when λ=3.6nm) on a 100nm thick silicon nitride membrane. These objects were manufactured using the same electron beam lithography system used for zone plates. From images taken of these test objects at X1A, it is possible to see the 36nm features of the test object, although they are extremely faint. Recently, work has been done to deconvolute the zone plate point spread function from these images and this has the effect of essentially increasing the contrast of the small features so that they are more visible. Using this technique, the 36 nm features in the test object are much more visible in the image (Jacobsen, 1991).

The maximum resolution limit of the microscope is attained when the diffraction patterns of the focal spot overlap as the specimen is scanned so that the maximum of one is located at the minimum of the other. In other words, each pixel should be half the size of the Rayleigh resolution. And, actually, if we have the zone plate point spread function we can decrease the pixel size even more in order to attain additional resolution information. But, we were not usually interested in using the maximum resolution limit of the microscope for a variety of reasons. The main reason being that applying such a technique oversamples the image and this increases the radiation dose. Moreover,

although we may gain resolution information, we do not increase our sensitivity in detecting the amount of material present in the image. Generally, we imaged our samples with a pixel size that was of order the spot size of the ZP. This means that the entire sample was exposed to the X-rays once, and the image contains all of the absorption information. It was also useful to undersample. In other words, using pixel sizes much larger than the focal spot size. In this case, even though the image looks uniform, it is not uniformly illuminated. Undersampling was routinely done to give a general (low resolution) view of the specimen without exposing the sample to a substantial radiation dose.

III.1.2 The basis of contrast

The images that are produced from the X-ray microscope have a natural contrast resulting from the differential absorption of X-rays by biological material and the suspending solution. This natural contrast can be explained by understanding the absorption of the X-ray photons with different materials. In the energy range of photons that we used the absorption of the photon by an inner shell electron can be expressed by the Beer-Lambert Law in terms of the transmitted intensity (I) and the incident intensity (Io) of photons as

$$I = I_o e^{-(\mu\rho\, t)} \qquad (3.2)$$

The variables are: μ (cm^2/g), the mass absorption coefficient; ρ (g/cm^3), the density; and t (cm), the thickness of material. If more than one element is present in the material, then the contribution of each element (i) is summed in the exponent

$$I = I_o e^{-\Sigma(\mu\rho\, t)_i} \qquad (3.3)$$

The mass absorption coefficient is unique for each element and also depends on the energy of the photons. Fortunately, we can apply the Henke Tables (Henke et al., 1982) which have calculated mass absorption coefficients for the elements Z = 1-94 and the energy range of E=100-2000eV. The mass absorption coefficient of protein is

approximately 10 times that of water, which is one of the reasons why there is good contrast between a biological sample and a water background (see figure 2 in the Introduction). Of course, the amount of material present also determines photon absorption. As can be seen in figure 3.1, the relationship between the thickness (assuming uniform concentration) of the sample (t) and its relative transmissivity (I/Io) is not linear. This means that by visual inspection of the image alone, we cannot judge the relative thickness of the sample. But, as can be seen in figure 3.1, for the range of protein thickness that we have worked with, the relationship is relatively linear and so it is still possible to get a rough idea of the relative amounts of protein present by looking at the images. In any event, to measure how much material is present, mathematical manipulations on the data are performed and these will be discussed in the next section.

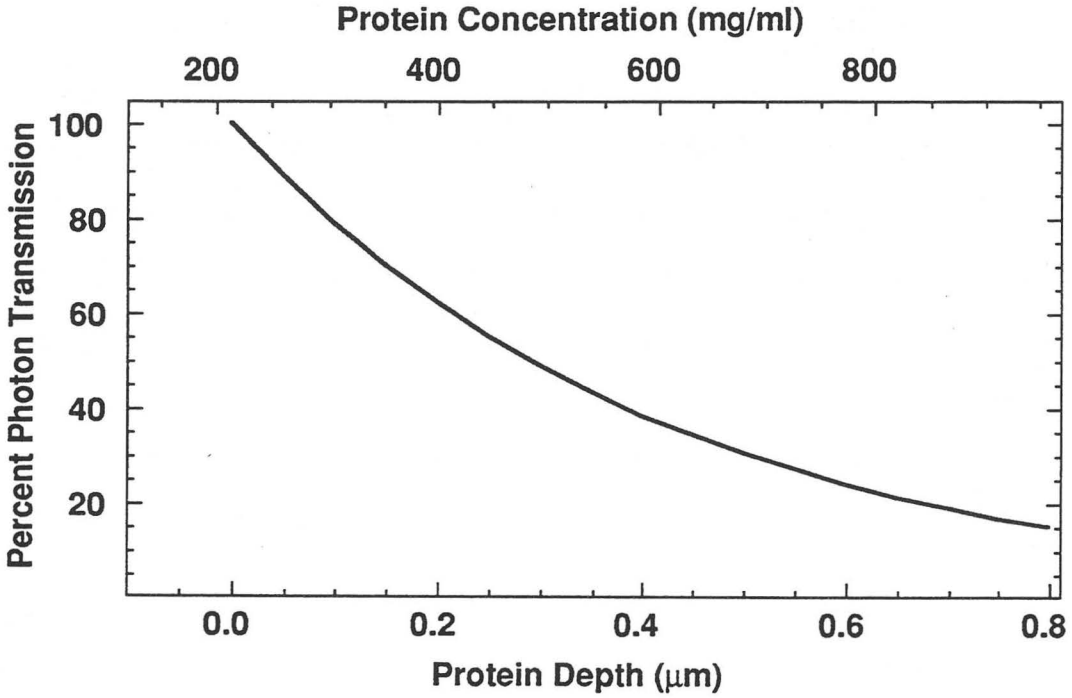

Figure 3.1 The relative X-ray transmission through a biological sample as a function to the depth (or protein concentration) of protein in the sample. We can see that in the range of protein concentrations that we can expect in our sample, that the this relationship is roughly linear and so by simple inspection of our images, we can get a general idea of the differences in protein concentration throughout the sample. However, in order to determine more exactly how much protein is present, mathematical manipulations of the images are required.

Even though we can expect good contrast using this technique, we are interested in a quantitative way of establishing what the best contrast is for our system. Ultimately, the level of contrast visible in an image is a function of how good the signal is as compared to the noise level. In STXM, our signal (Ns) is the number of photons that are detected at each pixel. And the noise, because we are dealing with Poisson statistics in counting the number of photons, is shot noise (N). Shot noise can be expressed in terms of the signal as $N = \sqrt{Ns}$. The standard criteria for establishing a certain contrast level is called the Rose criterion (Rose, 1948) and it states that a feature will be detectable if the contrast (C) is at least 5 times the noise to signal ratio, or

$$C > 5*\frac{N}{Ns} \tag{3.4}$$

We can define the contrast between the protein (p) in our sample and the background (b) using the following formula:

$$C = \frac{[(A)_p - (A)_b]}{(A)_b} \tag{3.5}$$

where "A" represents the absorption of X rays. From equation 3.3, we can determine the absorption of the protein and background;

$$A = 1 - \text{transmission} = 1 - \frac{I}{I_o} = 1 - e^{-\Sigma(\mu\rho\, t)i} \tag{3.6}$$

and therefore determine the contrast for different densities (ρ).

Obviously, from equation 3.4, the bigger the signal we detect the more sensitive our contrast measurements are. Unfortunately in STXM, an increased signal corresponds to exposing the sample to a higher radiation dose. As a result we are interested in determining what the best contrast is that could be attained with a given signal. From our previous experience and that of other investigators, we tried to keep the radiation dose below 50Mrad and as close to 5Mrad as possible. This corresponds to counting a signal of ~1000 photons at our detector (for further discussion, see the Radiation Damage

Chapter VII). Using this signal value (Ns) in equation 3.4, we determine that the minimal detectable contrast would be 0.158 or 15.8% between our sample and the background. To determine what protein concentration this corresponds to, we solve equation 3.5. In doing so, we assume that the background is a 0.3M sucrose solution (our most common suspending solution) and that we are interested in determining what the protein concentration is within the depth of a zymogen granule (diameter ~ 1μm) that can be detected "above" an equivalent depth of the background solution. From equation 3.5 and 3.6 we get

$$C = \{[1 - \exp-[(\mu\rho\, t)_p + (\mu\rho\, t)_b]] - [1 - \exp-(\mu\rho\, t)_b]\} / [1 - \exp-(\mu\rho\, t)_b] \qquad (3.6)$$

We have determined the values of μ for protein and 0.3M sucrose using the Henke Tables. These and the value for the density of 0.3M sucrose is given in Table 3.2. Using a thickness (t) of 1μm, we get (for λ=3.6nm)

$$C = \{[1 - \exp-[(1.97\rho)_p + 0.49]] - [1 - \exp-(0.49)_b]\} / [1 - \exp-(0.49)_b]$$

$$= \{[1 - \exp-[(1.97\rho)_p + 0.49]] - 0.36\} / [0.36]$$

where C = 0.158 so,

$$0.584 = \exp-[(1.97\rho)_p + 0.49]$$

applying the natural log to both sides, we get

$$0.538 = 1.97(\rho)_p + 0.49$$

$$(\rho)_p = 24 \text{ mg/ml at } 3.6\text{nm}$$

Thus we can determine the minimum protein concentration that we can expect to detect using the Rose criterion for an average signal of 1000 photons.

III.1.3 Noise

There are three main sources of noise in the STXM images. We discussed the shot noise in the previous section. The other sources of noise come about because it takes a finite time for an image to be generated. In this time, if there are beam fluctuations or variations in the gas environment around the microscope, they appear on the image. The

beam fluctuation noise is due to beam oscillations during the imaging time. They can be seen in figure 3.2A and often appear as stripes across the image. It is still not clear what the cause of these oscillations at BNL are. Everything from electrical noise from other machines in the facility to vibrations from the reactor located at BNL were taken into consideration in determining the source, but their appearance was still random. During later runs, we were able to reduce their appearance by careful alignment of the beam on the mirrors. Because they are quite regular in frequency, ~60Hz, these stripes can easily be removed through image processing techniques. The variations in gas flow, which are usually due to motion around the stage, e.g. people walking by, appear as streaks in the image. See figure 3.2B. This problem was greatly reduced when the microscope was entirely encased in a Plexiglas box.

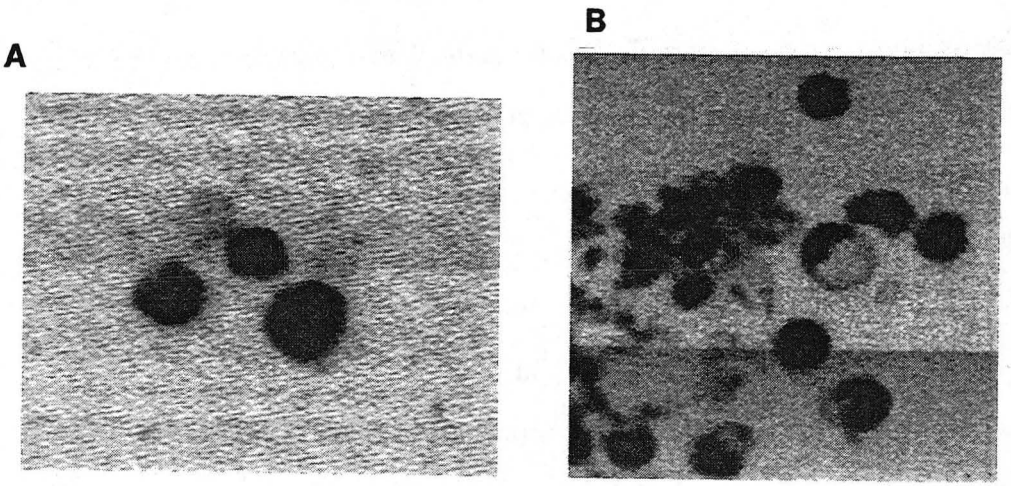

Figure 3.2 The appearance of noise in our STXM images. In (**A**) we can see stripes across the image that are a result of beam oscillations. In (**B**) we can see variations in the intensity of the image as a result of air or helium fluctuations around the microscope.

While these noises are inherent to the technique of scanning X-ray microscopy, they can be greatly reduced so as not to substantially affect the quality of the image. The shot

noise is less noticeable by counting more photons per pixel. The beam fluctuation noise can be essentially eliminated by proper alignment of the microscope components. And, the gas fluctuation noise is greatly reduced by encasing the microscope.

III.2 Computer Processing

The image files generated by STXM are stored in Brookhaven Standard Image Format (BSIF) on the VMS Vax station at Brookhaven National Laboratory. These files can be readily transferred to our Sun system via FTP. A typical file is 320kbytes for an image that is 400x400 pixels in size. We chose to use the software package IDL for displaying and processing the images.

IDL has built in routines that allow the user to display and manipulate the image from the command line or by using a scripting language. We constructed a software program call "Cell," using these routines in conjunction with the built in scripting capabilities to perform some of the more complex mathematical manipulations on the images. These procedures will be described later in the chapter.

We have chosen to display most of the images in the thesis with no image processing. This is done in order to present the reader with an accurate description of the primary images that STXM produces. Some of nosier images have been subjected to a Smooth Robert's Edge Enhancement (SREE). This routine first smooths the variations in the background by dynamically adding radially adjacent pixels; the radius being user selected, and then performs a weighted average with the center pixel. The value of this pixel is replaced with the computed result and the result is a reduction in high frequency background noise. Next, a Robert's edge enhancement subtracts the first derivative of an image from itself, thereby enhancing areas in the image that change from light to dark, i.e. edges.

In figure 3.3 we see a primary image of a group of granules and then the same image after two image processing routines have been performed on it. In the first image (figure 3.3A) the background has been smoothed by a standard deviation routine which first calculates an average value of the background pixels and then replaces the value of all pixels that are ± 2 standard deviations, with this average value. The SREE routine has then been performed and we can see this in the second image (figure 3.3B). As can be seen, the background in smoothed and the edges are clearer. This sort of processing clearly enhances distinctions in contrast within an object. Image processing is obviously a powerful technique but at the same time, it can be distracting and so we have limited the amount of processing performed on these particular images. Any image processing that was performed is noted in the figure caption. Images were printed out on a Kodak printer with a grey scale of 0-255 at 200 dots/inch.

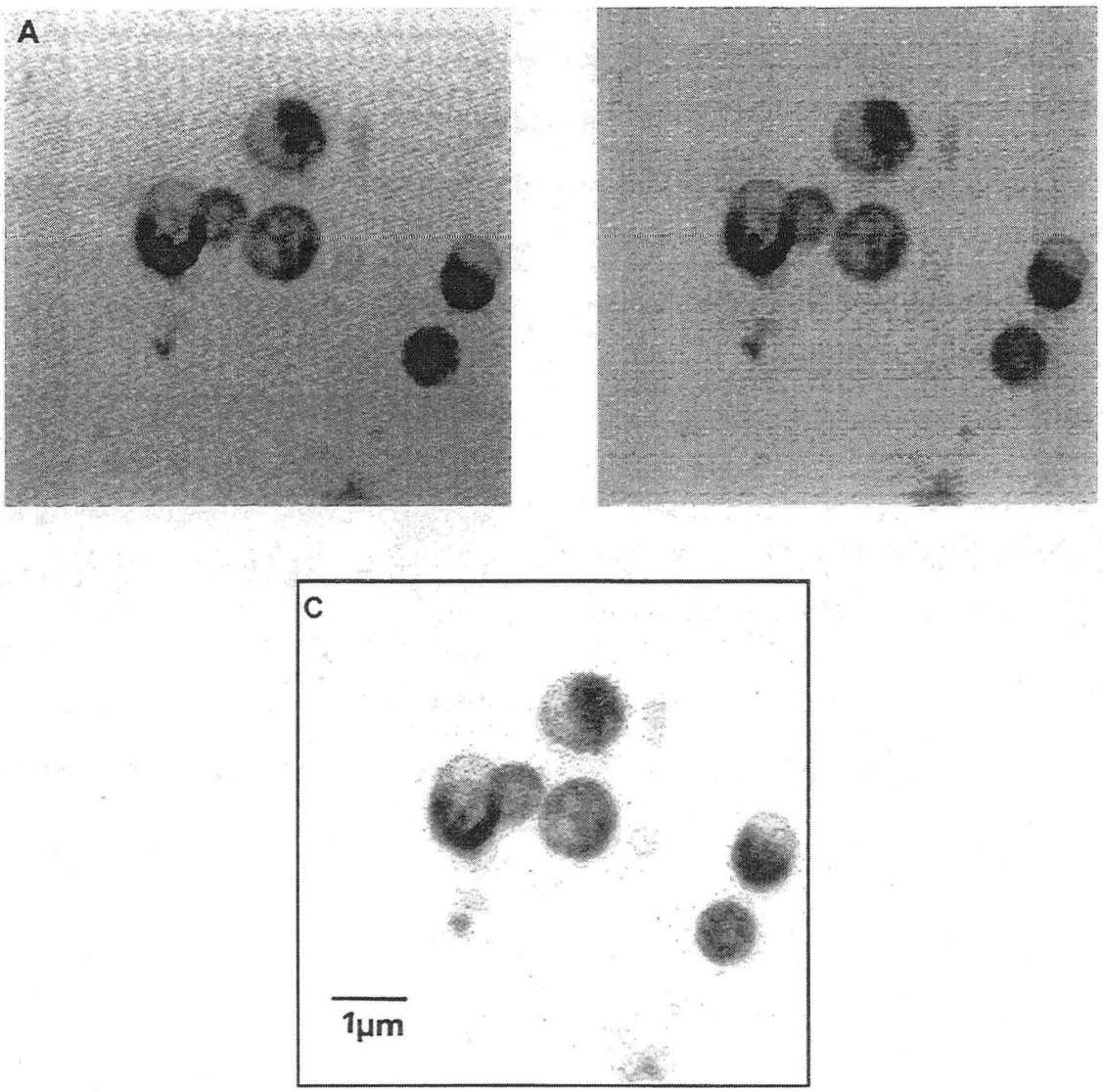

Figure 3.3 Using image processing to enhance the STXM images. In this figure, the original image has been processed using several routines described in the text. The original image can be seen in **A**. The image has undergone a standard deviation routine in **B** and we can then see in **C**, after smoothing and a Robert's Edge Enhancement, how easily we can determine the edges of the granule and variations in density.

III.3 Computer Calculation

III.3.1 Calculating the diameter, protein mass and concentration of zymogen granules

As mentioned earlier, STXM not only offers high resolution images of natural biological specimens but is a digital record of the number of photons that are transmitted through the specimen. Equation 3.3 shows the relationship between the number of photons that are transmitted through a specimen (I) and the amount of biological material that is present in the specimen (ρt = density • thickness). Therefore by using STXM images and equation 3.3, we should be able to determine the amount of biological material contained within the granules.

Unfortunately, in order to use equation 3.3 as presented, we need to know both the number of photons incident on the sample (Io) and the number transmitted through the sample (I); as illustrated in figure 3.4 (A). STXM does not have an Io detector and the photons that the proportional counter (PC) does count have not only passed through the sample but have also passed through other elements in the microscope. This is shown in figure 3.4(B).

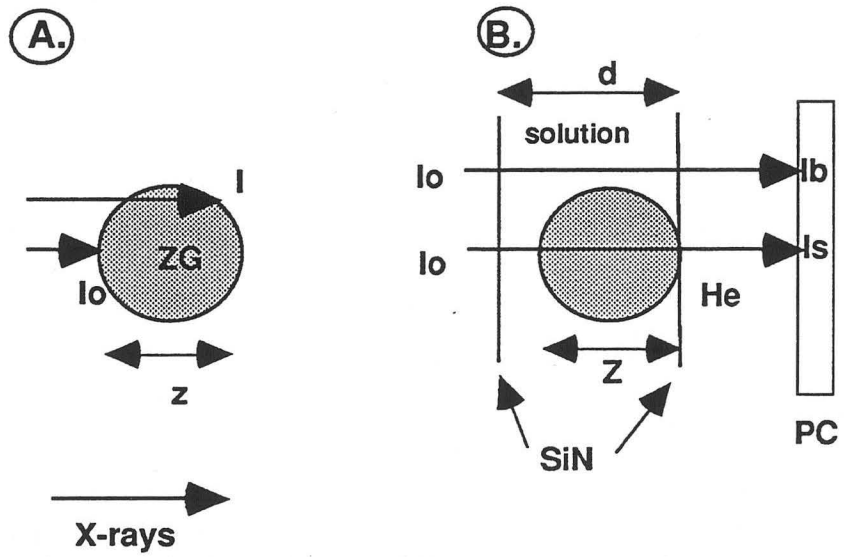

Figure 3.4 Transmission of X-rays. The circles represent zymogen granules. **A** diagrams what is meant in equation 3.3 by transmitted intensity (I) and incident intensity (Io) where z is the thickness of the zymogen granule the X-rays pass through. **B** diagrams what photons STXM is actually recording. The X-ray detector (**PC**) records the number of photons that have passed through the silicon nitride windows (**SiN**) of the sample chamber, solution in the chamber, the sample itself (**ZG**) and the **He** filled space between the sample chamber and the PC. Photons that have passed through the sample are designated Is and those that have only passed through the background solution are designated Ib.

For these reasons, we have redefined the variables I and Io from equation 3.3 in terms of the photons that STXM actually records. The variables in the following equations are explained in figure 3.4 except for "t" which represents an undefined thickness.

Let Is = I (through sample)

$$= Io * \exp^{-(\mu\rho\, t)}_{SiN} * \exp^{-(\mu\rho\, t)}_{sol} * \exp^{-(\mu\rho\, t)}_{He} * \exp^{-(\mu\rho\, t)}_{ZG} \qquad (3.7)$$

or,

$$Is = Io * [\exp^{-(\mu\rho\, t)}]_{SiN}[\exp^{-(\mu\rho(d-z))}]_{sol}[\exp^{-(\mu\rho\, t)}]_{He}[\exp^{-(\mu\rho\, z)}]_{ZG} \qquad (3.8)$$

and let Io be the number of detected of photons (Ib) from regions in the image that are clear of any sample i.e., where there is only background solution present so that,

$$Ib = I \text{ (through sol)} = Io * [\exp^{-(\mu\rho\, t)}]_{SiN}[\exp^{-(\mu\rho\, d)}]_{sol}[\exp^{-(\mu\rho\, t)}]_{He} \qquad (3.9)$$

If we then divide Is by Ib, the variables for SiN and He, as well as the unknown value (Io), are canceled out, and we get a simplified equation

$$I(\text{sample}) / I(\text{Background}) = [\exp^{-(\mu\rho(d-z))}]_{sol}[\exp^{-(\mu\rho\, z)}]_{sample} / [\exp^{-(\mu\rho\, d)}]_{sol}$$
$$= [\exp^{(\mu\rho\, z)}]_{sol}[\exp^{-(\mu\rho\, z)}]_{sample} \qquad (3.10)$$

The values for μ and ρ for both the solution and the sample can be determined (this will be discussed shortly) thus allowing us to solve for z, which is the thickness of the zymogen granule. From this value we were able to determine the mass of material within the granule by solving for the density (mass = thickness * density). But the zymogen granule is not composed of one solid material; it contains both organic material and internal, empty spaces filled primarily with the suspending solution and dissolved solutes. The organic material is composed of 90% protein (digestive enzymes); the remainder is lipid and carbohydrates. But for our calculations, we assume that the organic material is composed entirely of protein. Because we want to know the mass of the protein within the granule, we divide the thickness "z" of the granule into the thickness of protein "a" and the thickness of solution within the granule "z-a". This is diagrammed in figure 3.5

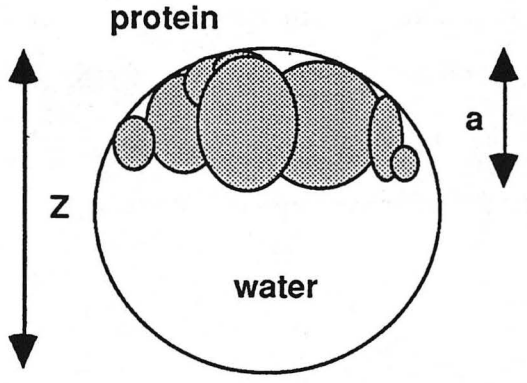

Figure 3.5 Model zymogen granule. Zymogen granules are known to contain a combination of protein and "water" (suspending solution). In a model granule, we can call the total thickness of protein "a".

In this figure, all of the protein is on one side of the granule. This is not usually the case in a real granule, but we can use this type of representation in the equation since the X-rays are not influenced by the spatial position of the protein; they are only affected by how much protein is present. Thus equation 3.10 becomes

$$\begin{aligned} I(\text{sample}) / I(\text{background}) &= [\exp(\mu\rho\, z)]_{sol}[\exp^{-}(\mu\rho\, z)]_{sample} \\ &= [\exp(\mu\rho\, z)]_{sol}[\exp^{-}(\mu\rho\, a)]_{protein}[\exp^{-}(\mu\rho\, (z-a))]_{sol} \\ &= [\exp(\mu\rho\, a)]_{sol}[\exp^{-}(\mu\rho\, a)]_{protein} \end{aligned} \qquad (3.11)$$

We can now solve for "a" - the thickness of protein and by multiplying this value times the density of protein, we will get the mass of protein.

$$a = \ln \frac{[I(\text{sample}) / I(\text{background})]}{[(\mu\rho)_{back} - (\mu\rho)_{protein}]} \qquad (3.12)$$

The values for the mass absorption coefficients (μ) for the solution and protein depend on the elemental composition of the material and the energy of the X-rays used. They are derived from the Henke Tables and are shown below in Table 3.1, along with density values (ρ). We have used a generic formula for animal protein ($C_{313}H_{498}N_{85}O_{101}S_3$) because the protein within each zymogen granule is an unknown combination of the 20 or so different digestive enzymes they contain.

Table 3.1 Mass Absorption Coefficients. The values for the mass absorption coefficients are given for the different materials and solutions that were used in the experiments. These values were calculated from the Henke Tables based on the molecular formula of the material. The density values of materials were obtained from the CRC except for protein (Bohm).

Materials	Density (g/cm^3)	Mass Absorption Coefficient (cm^2/g)			
		3.4 nm	3.5 nm	3.55nm	3.6nm
protein	1.2	16940	18080	18660	19740
SiN	3.44	12080	12960	13410	14250
Helium	2.00×10^{-4}	1430	1564	1633	1765
Solutions					
water	1.00	2716	2922	3027	3224
0.3M sucrose	1.10	3787	4064	4205	4468
0.6M sucrose	1.20	4680	5015	5188	5505
50 mg/ml ChTg[1]	1.15	4284	4594	4751	5045
250 mg/ml ChTg[1]	1.35	6933	7419	7668	8130

[1] bovine α-chymotrypsinogen (Sigma). $C_{1157}H_{2378}N_{318}O_{585}S_{22}$, in 0.3M sucrose solution

Using the appropriate mass absorption coefficients - we can solve equation 3. 12 for the

depth of protein per pixel = a

mass of protein per pixel = m = a • $\rho_{protein}$ • pixel area

total mass of the granule = M = Σm

The Cell program automates the above mathematical expressions. The program prompts the user to select a region of the image to be used as I(background) and then averages the pixel values in this region to obtain a final value. Next, the program provides a movable/resizable circle with which the user selects a granule. The diameter of the circle can be increased or decreased until the best fit is found. Once the granule has been

selected, Cell performs the calculation of equation 3.12. The diameter of the granule, average mass per pixel, total mass of the granule and granule protein concentration (total mass divided by volume of the granule) are given by the program. One other calculation that is performed is the **protein concentration of each pixel**. This value is calculated by dividing the mass per pixel by the volume of the pixel (or voxel) passing through the granule. By using a perfect spherical model of the granule and some basic geometry, we can determine what the chord length through the sphere of the granule would be by the location of the pixel on the 2-D projection that is the image of the granule.

III.3.2 Accuracy of the calculations

This section is divided into two parts. In the first part is a discussion of the accuracy of our calculations for diameter, protein mass and concentration from the data in our STXM images. Accuracy in this sense refers to the absolute measurement of these characteristics using STXM and any error is a systematic error for all of our values. However, as we were primarily interested in comparing these properties between populations of granules, the second section discusses how precisely we can reproduce each measurement and to what degree we can determine whether or not two populations have significantly different characteristics.

The most significant source of error in the accuracy of our measurements as calculated by the Cell program from the STXM images is in the selection of the granule to be analyzed. As we mentioned earlier, a granule is chosen by fitting a circle around the circumference. The program then calculates the diameter of the granule and then the protein concentration and mass as described earlier. As the images are pixelated, it can be difficult to exactly fit a circle around the granule. We have determined the limits to the error in our choice of the diameter of the circle (granule) to be ± one, two or three pixels, depending on the pixel size. The larger the pixel, the more confident we are that the diameter we have selected is the best possible fit. We have then calculated the protein

mass and concentration for 10 granules using 3 different pixel sizes in order to determine to what extent this error in diameter will affect these characteristics. This error, in terms of a percentage, is shown in Table 3.2 below.

Table 3.2 The error in the accuracy of our calculations for diameter, protein mass and concentration as determined from the error in the initial selection of the diameter of the granule from a STXM image.

Pixel size	Error in Diameter	Error in Mass (fg)	Error in Conc. (mg/ml)
18.8 nm	± 3 pixels	+7 / -10%	-12 / +6%
39.9 nm	± 2 pixels	+5 / -6%	-11/ +14%
63.3 nm	± 1 pixels	+5 / -6%	-6 / +15%

From the table, we can see that for a 1μm diameter granule, the maximum error in the diameter is about ±6% for all three pixel sizes. The error in the protein mass is similar, however we can see that the error in the protein concentration is higher. This is because the protein concentration has been calculated by dividing the total mass by the total volume (as determined by the diameter), which propagates the error. Three other sources of error that affect the accuracy of our calculation are the shot noise in the image, the minimum amount of protein we can detect in our image and our choice of the mass absorption coefficient for protein. As we are counting ~1000 photons per pixel in our images, the error in the value for the transmitted intensity (I) at each pixel is shot noise, and as mentioned earlier can be expressed as, $\sim \sqrt{1000}/1000$ or ~3%. From our discussion on the Rose criteria earlier, we determined that we could detect a minimum of ~24mg/ml protein in a pixel. This means that any amount below this value, would not be detected above the background and if we add up this amount of protein from each pixel in an average image, then we determine that our total protein mass value could be lower, on average, by ~9fg; an accuracy error of ~6% for the average protein mass values. Finally, the accuracy of our measurements in determining the amount of material present in our

object depends on our ability to determine the correct mass absorption coefficient to be used in equation (3.12). As we do not know the actual mixture of the 20 different enzymes that are contained in the zymogen granule, we cannot exactly determine what the mass absorption coefficient is. However, by using the mass absorption coefficient of generic protein, we have calculated the protein mass and concentration of granules to be in the range of those reported using other methods (see results Chapter VI.1) and therefore we can conclude that this approximation is reasonable for determining the protein mass for the granules. Further discussions on the potential accuracy of this technique for determining the amount of a specific material present in a sample can be found in Sayre et al. (1977) and Gilbert (1992).

As mentioned above, we were primarily interested in comparing these characteristics between populations, and so the absolute accuracy of the measurements was not as relevant to our results as how reproducible our technique was in determining these characteristics. In other words, taking into account the systematic errors , to what certainty could we determine if there was a *significant difference* between the measured characteristics of two granules or two populations of granules. As I performed all of the data reduction, the selection of the granule diameters was therefore "observer consistent" and highly reproducible. That is, I would consistently choose the same defining border of a granule. I estimate the potential error in this determination from object to object was, at most ±1 pixel; and in images that had larger pixels (i.e. 63.3nm) I would consistently chose exactly the same defining region of the granule.

Therefore, we have determined that at the 95% confidence level, we can statistically determine whether the characteristics of diameter, protein concentration or mass are significantly different between either two granules or two populations of granules and have applied parametric statistics accordingly.

Chapter III - References

Bohm, Andrew, private communication

Buckley, C.J., Measurements of resolution in zone plate X-ray microscopy, In: X-ray microscopy II (D. Sayre, M. Howells, J. Kirz and H. Rarback, Eds.)Vol. 56, Springer Series in Optical Sciences, Springer-Verlag, Berlin (1988).

Gilbert, J. Soft X-ray Microimaging of Whole Wet Cells, Ph.D. dissertation, California Institute of Technology: Pasadena, California (1992).

Henke, B.L., P. Lee, T.J. Tanaka, R.L. Shimabukuro and B.K. Fujikawa, Low-energy X-ray interaction coefficients: Photoabsorption, scattering and reflection, At. Data Nucl. Data Tables (1982) **27**.

Jacobsen, C., S. Williams, E. Anderson, M.T Browne, C.J. Buckley, D. Kern, J. Kirz, M. Rivers and X. Zhang, Diffraction-limited imaging in a scanning transmission X-ray micrscope, Opt. Comm. (1991) **86**:351-364.

Michette, A.G., Optical Systems for Soft X Rays, Plenum Press: London (1986).

Rose, A., Television pick up tubes and the problem of noise, Advan. Elect. (1948) **1**:131.

Sayre, D., L. Kirz, R. Feder, D.M. Kim and E. Spiller, Transmission microscopy of unmodified biological materials: Comparative radiation dosages with electrons and soft X-rays, Ultramicroscopy (1977) **2**:337-348.

Chapter IV. The Sample Chamber

In order to image the zymogen granules and perform our experiments using STXM we first had to design a special specimen holder specifically for our experiments. This was because there were no standardized samples holders and moreover, prior to our studies no other group had tried imaging specimens suspended in an aqueous environment while changing the experimental conditions of the experiment during imaging. So, besides the previous work that had been done on zymogen granules (Rothman, 1988, 1989) we had little to go on in designing the holder. Primarily fixed and dried or non-biological specimens requiring no special environmental conditions had been imaged in these microscopes either on electron microscope grids or in sealed, inaccessible chambers (Morrison et al., 1992; Rudolph et al., 1992). Although, concurrent with our experiments, another group (Gilbert, 1992) was imaging whole cells. They designed a sample chamber that was capable of maintaining a humid as opposed to aqueous environment for their sample during imaging. Their sample chamber is especially well suited for cell culture.

In designing our sample holder, we had to keep certain specifications in mind. These are:

1: The working distance between the sample holder and the focusing optics could be no more that 250 μm. This is akin to the distance that an 100x oil immersion objective requires. This constraint is dictated by current manufacturing methods for zone plate lenses. To increase the working distance it is necessary to fabricate larger lenses with the same, accurately placed small zones. Although attempts have been made to do this, it is a difficult technical task and one that is still in a state of research and development.

2: There must be a thin viewing window penetrable by X rays that is large enough to provide a substantial viewing area, and yet strong enough to support the sample and its

fluid environment. It would also be helpful if cells in culture could be grown on these windows.

3: In order to perform our experiments on suspended, isolated zymogen granules, the sample holder must have the capability of containing fluid in small amounts that will not evaporate and which can be changed conveniently while viewing.

4: The water depth within the chamber must be minimal, of the same order of thickness as the sample itself, to allow penetration of the sample by X rays (a 3.4 μm thick water layer absorbs 63% of 3.5 nm X rays).

5: Because we have to work with a vertical stage we needed a method of attaching our specimen to the viewing window or otherwise immobilize it so that it would not settle due to gravity.

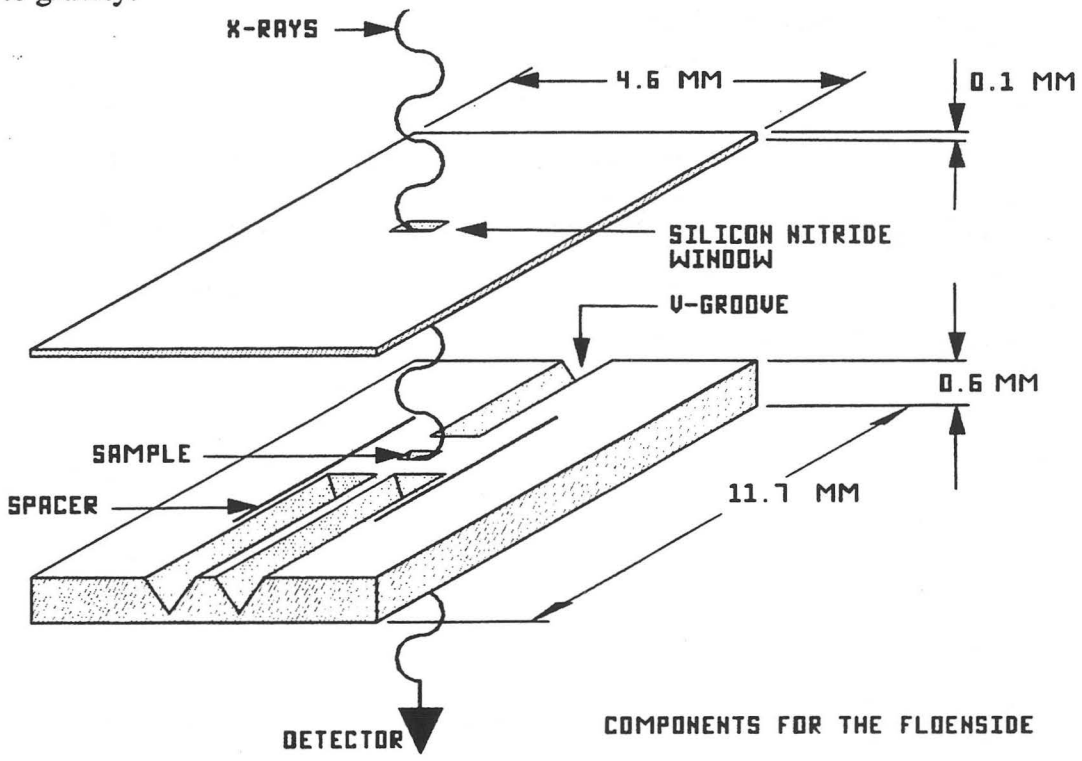

Figure 4.1: An isometric drawing of the two silicon wafers which comprise the LBL-WC. The "top" wafer lies between the focusing optics and the sample and therefore must be very thin because of the short working distance. However, there is no thickness constraint on the "bottom" wafer so it supports the V-grooves and other structural fabrications. The V-grooves serve as inlet and outlet ports after the sample chamber is assembled.

We were able to meet these specifications by modifying an earlier design of a sample chamber that was used by our group to image samples wholly suspended in water (Rothman, et. al, 1989). Whereas the previous design was a sealed chamber, our sample holder (called the Lawrence Berkeley Lab Wet Cell or, LBL-WC) provided both an aqueous environment for the sample and allowed the investigator to change that environment during periods of observation

Although the LBL-WC is also a sealed chamber, it contains an inlet and outlet port through which a sample in suspension can be flowed (figure 4.1). The components of the LBL-WC are fabricated from silicon wafers using lithographic microfabrication methods (done at Lawrence Livermore Laboratory by Dino Ciarlo). The chamber body is made by sealing together two silicon wafers (Goncz et al., 1992).

A 60 nm silicon nitride film is deposited on both sides of the wafers using a low pressure chemical vapor deposition system (LPCVD). And, the viewing windows, 400 μm x 400 μm, are formed by etching through one side of each silicon wafer until the silicon nitride layer is reached. The result is that each wafer contains a window that is flush with one surface ("front" surface) and recessed from the other ("back" surface). The front surfaces face each other when the LBL-WC is sealed together. X-ray transmission of silicon nitride membranes is shown in figure 4.2 for various thicknesses at varying wavelength. The effectiveness of the LBL-WC is crucially dependent upon the windows being sufficiently transmissive. Beam attenuation through both the entrance and exit windows must be kept to a minimum. Our measurements indicate that the windows we have used are approximately 60 nm thick, and have ranged from about 40 to 100 nm, depending upon fabrication conditions. While a thin window is desirable from the standpoint of X-ray penetration, such very thin windows are, of course, quite fragile. We have found that for windows approximately 50-100 nm thick with areas as great as one mm^2 are sufficiently sturdy (will hold a pressure differential of about one atmosphere).

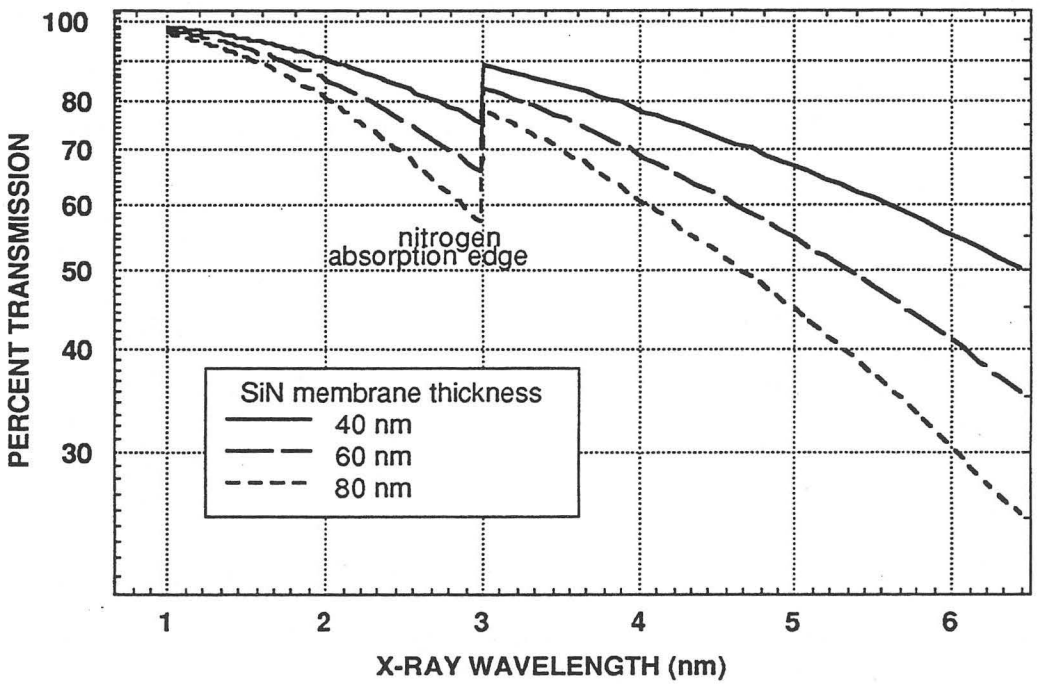

Figure 4.2: A graph of the transmissivities of various thicknesses of silicon nitride membranes to different wavelengths of X rays. The values are calculated and assume a silicon nitride density of 3.44 g/cm^3. The nitrogen absorption edge is located at 3.1 nm. We have been using a 60 nm thick silicon nitride membrane at a wavelength of 3.5 nm.

In order to define the internal spacing of the chamber we used "spacer bars" as shims. Gold is evaporated onto the front surface of one of the wafers, over the silicon nitride layer and a 10 nm chromium adhesion layer, and is etched to form the bars. These spacers are set at 2 μm height. This meant that we had a 2 μm thick layer of water within the LBL-WC at all times. The attenuation of the X rays through this layer was acceptable.

Constructing inlet and outlet ports was difficult because we were limited by the availability of tubes to fit into the ports. The smallest tubes that were useful were 31 gauge (0.25 mm OD, 0.13 mm ID) stainless steel tubes (Small Parts Inc., Miami, FL.). These are much larger than the internal spacing of the LBL-WC and so it was necessary

to etch grooves into one of the silicon wafers into which the tubes would fit without affecting the internal spacing. Etching was accomplished by a KOH etching procedure; an anisotropic method that produces a characteristic V-groove angle in the silicon substrate. Other areas of the silicon piece are protected from the etching with resist. Figure 4.3 is a scanning electron micrograph of a double V-groove. Because of the grooves, the silicon wafer into which the grooves were etched had to be 600 μm thick. This is too thick to fit between the sample stage and the focusing optics. But, since we only needed one wafer to hold the tubes, the other wafer could be much thinner, 100 μm, so that we would have sufficient working distance. The spacer bars were also placed on the thick wafer located just lateral to the V-grooves, so that the entering fluid is directed over the windows as it flows through the chamber.

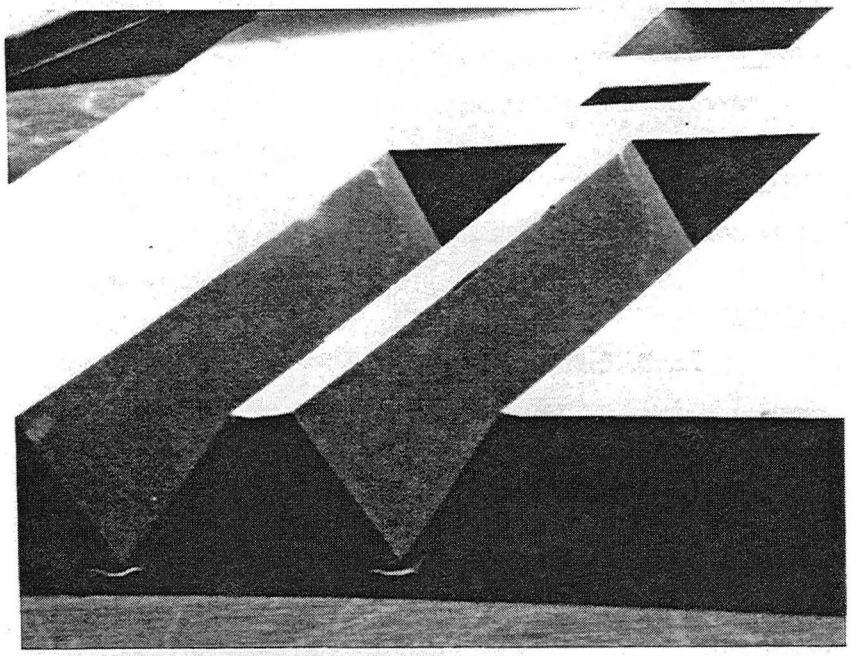

Figure 4.3: A scanning electron micrograph of the double V-groove located on the "bottom" wafer (magnification = x30). The window where the silicon nitride membrane is located can also be seen and the spacer bars are located just lateral to the V-grooves so that the flow of fluid is directed over the windows.

Focusing squares were placed on the windows of both of the wafers. They were formed by evaporating a 250 nm layer of gold (over a 5 nm layer of chromium) directly

onto both windows on the front surfaces of the pieces. The gold was then chemically etched, through a mask, to form small objects, usually squares and rectangles (10 nm x 20 nm), that are convenient for focusing on. This etching is carried out before the silicon nitride windows themselves are formed. Double sided alignment is used to assure that the focusing objects are located in the center of the window. Figure 4.4 shows the entire fabrication sequence.

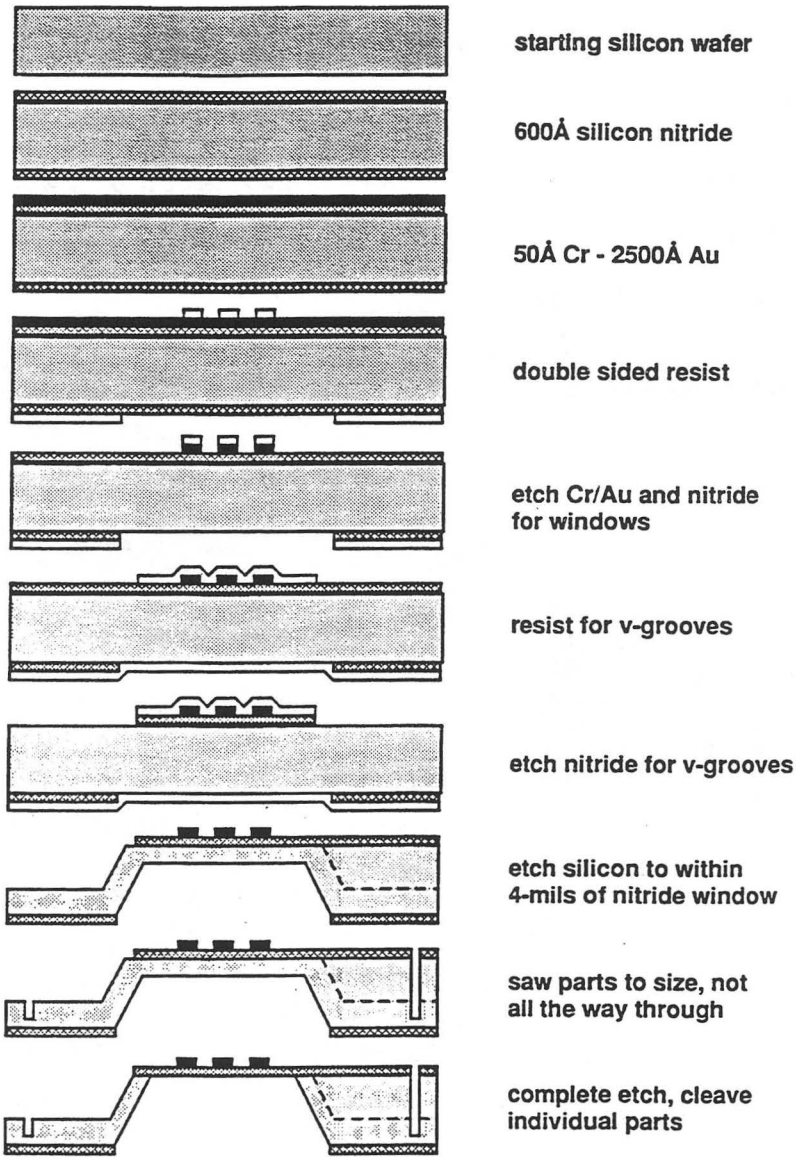

Figure 4.4: Steps in the fabrication of the "bottom" component of the LBL-WC. The starting silicon wafer is 0.6 mm thick, single side polished. The "top" wafer is double side polished and goes through the same treatment except for the V-grooves and the gold spacer bars.

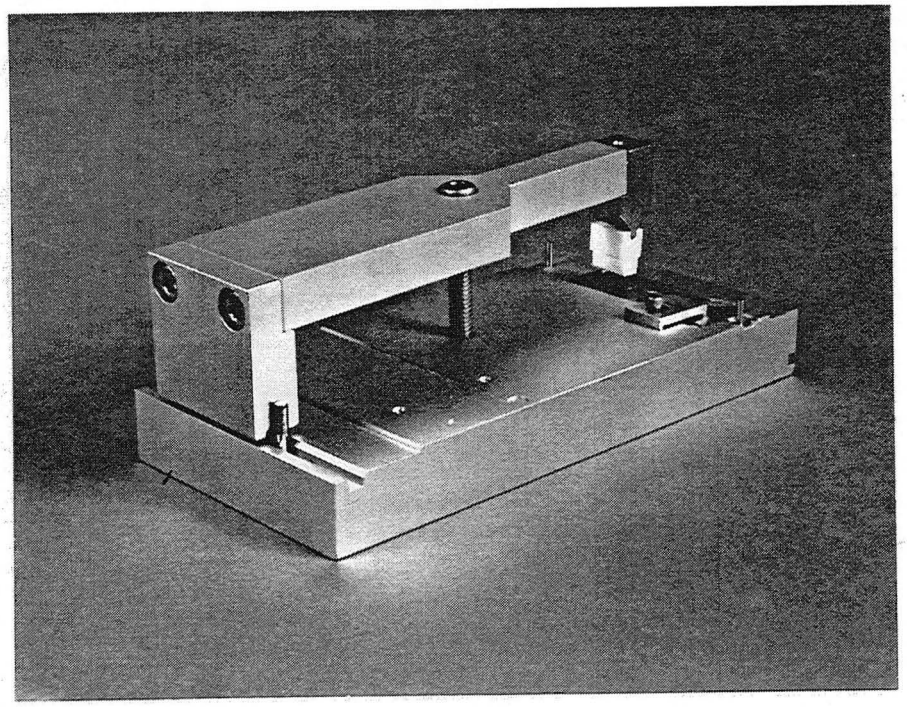

Figure 4.5: The specially designed fixture for assembling the LBL-WC. A normal force is applied to the LBL-WC by tightening the screw in the center of the fixture. The Teflon piece is flexible enough so that the pressure does not crack the silicon wafers and while in place, the edges of the LBL-WC can be glued without contaminating the front surface.

In order to assemble the LBL-WC, a specially designed assembly fixture was designed (figure 4.5). The two silicon wafers are pressed together with a Teflon press, until the spacers on the thick piece are touching the front surface of the thin silicon wafer. The Teflon piece on the end of the fixture is flexible enough not to shatter the silicon when pressure is applied. Spacing can be checked in the visible light microscope through a hole in the fixture. Light interference fringes will be visible when the windows are within about 3 μm of each other. The tubes are then inserted into the holes formed from the V-grooves. The edges of the LBL-WC are sealed with a 5 minute epoxy cement and allowed to dry for 2-4 hours. Epoxy does not adhere to Teflon, and by making the Teflon piece slightly larger than the silicon pieces, only the edges of the chamber are exposed to

the glue. In this way the epoxy cannot be deposited on the top (or optics-facing) surface of the LBL-WC. This is important. Because of the very short working distance, even a small amount of substance on the surface of the silicon wafer can prevent proper positioning of the chamber. The LBL-WC is also simultaneously attached to a piece of aluminum (5 cm x 1.8 cm) which acts as a mounting plate. On the back of the mounting plate is a piece of steel by which the whole assembly is magnetically attached to the STXM stage.

Initially, we were concerned about the effect of gravity on the positional stability of our sample, but fortunately we found that our particular specimens adhered relatively well to clean silicon nitride windows. However, this it is not a general solution to the problem of holding samples in place within the LBL-WC. Individual specimens require developmental work to determine how they can best be immobilized.

For use in STXM, the specimen is introduced into the chamber via the tubes using a peristaltic pump. These tubes can be primed with other solutions that may be used during an experiment.

We experimented with recycling the LBL-WC components after the chamber was used for an experiment. It was possible to dissolve the epoxy, holding the wafers together, using laboratory glassware detergent. Then we attempted to clean the wafers with a pirhana bath (four parts concentrated sulphuric acid to one part 30% hydrogen peroxide). Although the silicon nitride windows looked clean in the light microscope, the transmission through the silicon nitride membranes appeared changed in STXM and objects looked fuzzy. We believe that this was a result of a film of epoxy being deposited on the windows. In the future a better method for cleaning the components should be developed in order to save time and effort in making the wafers.

Chapter IV - References

Gilbert, J. Soft X-ray Microimaging of Whole Wet Cells, Ph.D. dissertation, California Institute of Technology: Pasadena, California (1992).

Goncz, K.K., P. Batson, D. Ciarlo, B.W. Loo, Jr. and S.S. Rothman, An environmental sample chamber for X-ray microscopy, J. Micr. (1992) **168**:101-110.

Morrison, G.R., P.A.F Anastasi, M.T. Browne, C.J. Buckley, R.E. Burge, P.S. Charalambous, G.F. Foster, A.G. Michette, D. Morris, J.R. Palmer, G.E. Slark, P.M. Bennett and P.J. Duke, Recent progress with the King's College scanning transmission X-ray microscope, In: X-ray Micrscopy III (A.G. Michette, G.R. Morrison and C.J. Buckley, Eds.), Vol. 67, Springer Series in Optical Sciences, Springer-Verlag:Berlin (1992).

Rothman, S.S., N. Iskander, K. McQuaid, H. Ade, D.T. Attwood, T.H.P. Chang, J.H. Grendell, D.P. Kern, J. Kirz, I. McNulty, H. Rarback, D. Shu and Y. Vladimirsky, The Biology of the cell and the high resolution X-ray microscope, In: X-ray Microscopy II (D. Sayre, M. Howells, J. Kirz and H. Rarback, Eds.), Springer-Verlag: Berlin (1988).

Rothman, S.S., N. Iskander, D. Attwood, Y. Vladimirsky, K. McQuaid, J. Grendell, J. Kirz, H. Ade, I. McNulty, D. Kern, T.H.P. Chang and H. Rarback, The interior of a whole and unmodified biological object - the zymogen granule - viewed with a high-resolution X-ray microscope, Biochim. Biophys. Acta. (1989) **991**:484-486.

Rudolph, D., G. Schneider, P. Guttman, G. Schmahl, B. Biemann and J. Thieme, Investigations of wet biological specimens with the X-ray microscope at BESSY, In: X-ray Micrscopy III (A.G. Michette, G.R. Morrison and C.J. Buckley, Eds.), Vol. 67, Springer Series in Optical Sciences, Springer-Verlag: Berlin (1992).

Chapter V. Experimental Methods

The first section of this chapter includes the zymogen granule isolation procedure, a discussion of the different experiments we performed on the granules and how we physically accomplished these experiments in the microscope. The second section discusses our protocol for imaging the sample with STXM.

V.1 Experimental Protocol

V.1.1 Zymogen Granule Isolation

The zymogen granule sample was prepared from acinar cells of rat pancreas. Male Sprague-Dawley rats (Taconic Farms, Germantown, NY), 200-225g, were fasted prior to removal of the pancreas. The rats were anesthetized with CO_2 and sacrificed quickly and painlessly by cervical dislocation. The pancreas was then quickly dissected out. Fat, lymph nodes and connective tissue were removed as much as possible. The resulting tissue was weighed and homogenized (1:10 w/v) in 0.3M sucrose (5mM $NaHPO_4$, pH 6.0) in a glass mortar with a motor-driven glass-embedded teflon pestle (clearance 0.11-0.13mm) at an average speed of 4,000 rpm. Homogenization was complete with 4 to 5 passes of the pestle. The homogenate was centrifuged at 600g, 4°C, for 10 minutes to sediment nuclei, intact cells and cell debris. The supernatant was decanted from the sediment and then centrifuged at 1000g, 4°C, for 10 minutes. The result is a whitish pellet (zymogen granules) with a yellowish edge. The yellowish edge is removed by adding 1ml of sucrose solution to the pellet , gently swirling and pouring off the solution. The remaining pellet is resuspended in the sucrose solution (1:5 w/v) and centrifuged at 1000g, 4°C, for 10 minutes. The final pellet is again resuspended in the sucrose solution (1:2.5w/v). The average rat pancreas was ~1g, leaving us with ~5ml of a suspension of granules at a number density of ~1 x 10^9/ml. This procedure for the isolation of granules

is essentially the same as that used by many different investigators over many years: e.g. Hokin (1955), Jamieson and Palade (1967), Meldolesi et al. (1971) and Rothman (1971).

The constitution of the pellet has been examined by electron microscopy and by chemical composition. A few mitochondria are seen when examining the upper layers of the pellet, and an occassional nucleus is found at its base. No microsomes are present. Nuclear and microsomal contamination is chemically insignificant based on nucleic acid measurements. Overall the purity of the pellet is estimated to be ~95% zymogen granules (Rothman, 1971).

After isolation, the zymogen granule suspension was kept on ice until it was used in an experiment. The suspension would then be removed from ice and the experiments were all carried out at room temperature, 24°C. Currently, we have no means of controlling the temperature of the specimen, besides maintaining a constant room temperature, while using STXM.

V.1.2 Fresh Granule Experiments

The general purpose of these experiments was to observe individual granules in a fluid environment over a period of time using STXM. Based on the results of the experiments on isolated granules presented in Chapter I (Neiderau et al., 1986a&b, Liebow and Rothman, 1972, 1976; Burwen and Rothman, 1972; Rothman, 1972, 1971), we expected to observe granules decreasing in protein mass and possibly size over the time course of the experiment. This loss rate would depend on the particular solution or conditions the granules were exposed to.

The experiments differed primarily in the particular fluid to which the granules were exposed. This simple manipulation of the experimental situation lent itself well to developing an experimental protocol that could be reproduced exactly for each different experiment. Ten different solutions that we used were: **1**) the original suspension, or "control"(0.3M sucrose, 5mM $NaHPO_4$, pH 6.0), **2&3**) 0.3M & 0.6M sucrose (5mM

$NaHPO_4$, pH 6.0), water, **4&5**) 0.025% & 0.05% Triton-X in 0.3M sucrose (5mM $NaHPO_4$, pH 6.0), **6&7**) 50 & 250 mg/ml chymotrypsinogen A (bovine, Sigma) in 0.3M sucrose (5mM $NaHPO_4$, pH 6.0), **8**) 150mM NaCl (pH 6.0), **9**) 5μM Nigericin in 0.3M sucrose (5mM $KHPO_4$, pH 6.0) and **10**) 1 1/2% glutahaldehyde in 0.3M sucrose (5mM $NaHPO_4$, pH 6.0).

A fraction of the zymogen granules suspension is drawn from the original preparation and introduced into the LBL-WC by use of a peristaltic pump (Gilson, Middleton, WI.) and through fine surgical tubing attached to the stainless steel tubes of the LBL-WC. Care must be taken not to introduce air bubbles into the LBL-WC when attaching the peristaltic pump tubing to the stainless steel tubes. The viewing window is simultaneously examined in a light microscope as the specimen is flowed into the chamber. Typical volume flows are ~1 μl/min, which is slow enough to observe objects moving past the viewing window. When a large enough sample population adheres to the window, the chamber is ready to be inserted into STXM.

If the experiment calls for granules to be exposed to some other solution besides the initial suspending medium, then the surgical tubing was primed with the particular solution and attached to the LBL-WC. In this way, when the time came, we could flow the new solution past the granules without having to take the LBL-WC out of the microscope. It would have been impossible to find the original field of granules if it were necessary to reposition the chamber.

Once the LBL-WC was loaded and inserted into the microscope, the Plexiglas box was sealed around the microscope (although the peristaltic pump was located outside of the box). The routine for bringing the viewing window into focus was described in the previous section. After the viewing window was in focus in STXM, we chose an initial field(s) of granule(s) to image. Our method for selecting a field of granules to image will be described in the following section.

Once an initial field(s) of granules was chosen, this same field would be imaged sequentially for a period of time. We usually tried to perform the experiment over 4 hours, imaging the field once every hour. If the protocol called for a new solution to be flowed past the granules, we would begin this flow after the initial image was taken. In calibration experiments, it was determined that a pump rate of 3rpm for 10 minutes would ensure that the old fluid within the chamber had been completely replaced with the new fluid. Both the inlet and outlet ports were connected to the pump at the "push" and "pull" ends respectively, so that a constant volume of fluid is always being moved since a small increase in the internal pressure can cause the windows to bow outwards which thickens the water layer and reduces X-ray transmission.

V.1.3 Fixed Granules

The general purpose of this experiment was the same as for the fresh granules, but instead of observing *individual* granules over a period of time after their initial isolation and resuspenstion in 0.3M sucrose (5mM $NaHPO_4$, pH 6.0), we performed population studies on different groups of granules that had been kept at room temperature for different periods of time to see how the population characteristics changed. We used fixation to "arrest" the zymogen granules after they had been at room temperature for their alloted time period. All of the different specimens came from the same preparation. After the final resuspension of the pellet in 0.3M sucrose (pH 6.0), the material was divided into 5 aliquots, each ~1ml in volume. The aliquots were treated as follows:

aliquot no.	name	treatment
1	0 hr	fixed immediately
2	1/2 hr	left at 24°C for 1/2 hour, then fixed
3	4 hr	left at 24°C for 4 hours, then fixed
4	4i hr	left at 4°C for 4 hours, then fixed

Fixation was performed by adding glutahaldehyde to the suspension of granules to a final concentration of 1 1/2% and the specimen was left overnight.

V.1.4 Radiation Damage Studies

Granules were loaded into the LBL-WC as described in the previous section and an initial image of a field(s) was taken. Granules were exposed to large X-ray doses by directing the focused spot of X-rays onto a particular region in a granule.

V.2 Imaging Protocol

The description of the imaging protocol consists of two parts. The first part describes our technique for finding possible fields of fresh granules to image within the imaging window as quickly as possible and the second part presents the imaging parameters we used when imaging these fields in order to minimize the radiation exposure to the specimen.

Because the goal of our experiments with the fresh granules was to be able to observe changes over time, it was critical to take the initial image as soon as possible after the specimen had been taken off of ice. The viewing window of the LBL-WC could be quickly brought into focus, using the techniques described in the previous chapter, because of the focussing spots on the window. A stepper image of the window, 200x200 pixels and 1μm pixel size could be imaged in ~40 sec using a dwell time of 1msec per pixel. This pixel size insured that we could identify the granules (their diameters are ~1μm) as black dots in the STXM image while receiving only a minimal exposure of X-rays. From the initial image, we chose a region that contained as many granules as possible. The software for the microscope allows the user to "click" on a particular spot of an image and the stage motors will move to that spot. These areas can also be saved and often we saved several areas so that we would have a few different fields of granules to observe. We would then immediately take a higher resolution image of the field and

this would be our initial image. Refocussing on the specimen was not generally required because the depth of focus of the microscope is of order 2μm and from the stepper image, we knew that the gold squares were in focus.

We tried to include as many granules in an initial image as possible. Unfortunately, the adherence properties of the granules was not always reliable and whereas sometimes we had experiments where the granules were virtually covering the silicon nitride window, in others granules were few and far between. This density of granules would dictate the size of our initial image. From the initial stepper image, we could get a rough idea of the size of the field that was to be imaged. Then we would have to decide how many pixels and what size the pixels should be in order to image as many granules as possible in as little time as possible. We were limited to image sizes of no more than 516x516 pixels, using the PZTs, and we generally would use pixel sizes of between 20 and 60nm, so with these parameters, our image fields range between $10x10\mu m^2$ to $30x30\mu m^2$. Generally between 2-5 intial fields of granules were taken during the first hour after being taken off of ice and the locations of all the fields were saved in the software. After the intial images were taken, then the experimental solution was flowed past the granules. Subsequent images of the same fields of granules were taken, usually about an hour apart, for up to 5 hours. These fields were easily revisited because their location was saved in the STXM software.

As discussed in Chapter III, we attempted to image our sample consistently using 1000 counts/pixel. This gave us minimal exposure with sufficient statistics for our purposes.

V.3 Analysis of Data

The images were analyzed as described in Chapter III. The data for each granule diameter, protein mass and concentration was transfered to an excel spreadsheet (version 4.0) and analyzed on a Macintosh IIfx. Statistics were performed on the data using statistical routines in Excel. Plots were done using the Passage program (version 2.1) which also supplied the least square fit curves.

Chapter V - References

Burwen, S.J. and S.S. Rothman, Zymogen granules: osmotic properties, interactions with ions, and some structural implications, Am. J. Physiol. (1972) **222**:1177-1181.

Hokin, L.E., Isolation of zymogen granules of dog pancreas and a study of their properties, Biochim. Biophys. Acta. (1955) **18**:379-388.

Jamieson, J.D. and G.E. Palade, Intracellular transport of secretory proteins in the pancreatic exocrine cell II. Transport to condensing vacuoles and zymogen granules, J. Cell. Biol. (1967) **34**:597-615.

Liebow, C. and S.S. Rothman, Equilibrium of pancreatic digestive enzymes across zymogen granule membranes, Biochim. Biophys. Acta (1976) **455**:241-253.

Liebow, C. and S.S. Rothman, Membrane transport of proteins, Nature (1972) **240**:176-178.

Meldolesi, J., J.D. Jamieson and G.E. Palade, Composition of cellular membranes in the pacnreas of the guinea pig. III. Enzymatic activities, J. Cell. Biol. (1971) **49**:109-129.

Niederau, C., J.H. Grendell, S.S. Rothman, Characteristics of rat pancreatic zymogen granules prepared by different methods, Am. J. Physiol. (1986b) **251**:G421-429.

Niederau, C., J.H. Grendell, S.S. Rothman, Digestive end products release pancreatic enzymes from particulate cellular pools, particularly zymogen granules, Biochim. Biophys. Acta (1986c) **881**:281-291.

Rothman, S.S., Association of bovine α-chymotrypsinogen and trypsinogen with rat zymogen granules, Am. J. Physiol. (1972) **222**:1299-1302.

Rothman, S.S., The behavior of isolated zymogen granules: pH-dependent release and reassociation of protein, Biochim. Biophys. Acta (1971) **241**:5667-577.

Chapter VI: Results

In this chapter, the results of our experiments are presented. Our data set consists of the diameter, protein mass and concentration values for individual zymogen granules. These characteristics were obtained by analyzing the STXM images generated from each experiment, according to the protocol described in Chapter III. The first section provides a general description of isolated zymogen granules; their appearance in STXM images, the identification of two sub-classes of granules and the measured population averages of diameter, protein mass and concentration. In the second section we show how these characteristics change over the time course for different experimental protocols. The third section looks at how fixation with glutaraldehyde affects the zymogen granules as seen by STXM. And the fourth section presents the calculated permeability coefficient of the zymogen granule membrane to its enclosed protein as derived from our data.

VI.1 A STXM description of granules - The General Population

Every new scientific technique allows us to "see" nature from a new perspective; scanning transmission X-ray microscopy (STXM) is no exception and we will use this section to familiarize the reader with what typical images of zymogen granules look like and the range of values we measured from these images for the characteristics (diameter, protein concentration and mass) of a population of isolated granules studied. We will also discuss some of the basic relationships that exist between these characteristics of zymogen granules.

Several STXM images are shown in figure 6.1. The granules are easily identifiable and stand out clearly from the background. As expected from electron microscopy (EM) studies (figure 6.2), they appear roughly circular in shape with a diameter of ~1μm. From Chapter I, we discussed that EM images also show the granules as being uniformly dense or dark in appearance. No discernible internal structures are visible at this high magnification. However, the STXM images paint a different picture. While some of the granules appear uniformly dark or dense (figure 6.1, granules marked "UG"), others only have regions that are dense. The remaining regions are lucent in appearance. If the variations between the dense and lucent areas in the granule are frequent, the granule takes on a honey-comb or reticulated appearance (figure 6.1, granules marked "NUG"). If the variations are less frequent, the granules appear clumpy (figure 6.1, granules marked "CG") and in extreme cases, the clumpiness is located on only one edge of the granule (figure 6.1, granules marked "EG").

That granules may have more of a heterogeneous appearance than normal EM images suggest, has already been addressed. Ermak and Rothman (1978) showed EM images of granules with reticulated structures (see figure 1.2) not unlike our STXM images. The reticulation was made visible by suspending isolated granules in large volumes of an isosmotic solution to cause the release of protein. It is possible that these structures are

only visible in electron micrographs when granules contain less protein (e.g. as a result of release of protein) because the normally high concentration of protein combined with the effects of staining and fixation, necessary for EM, mask these reticular structures. We discuss how fixation affect the appearance of fresh granules in STXM in the third section of this chapter. Nevertheless, the difference in appearance allowed an initial separation of the population into two broad sub-groups of granules - **uniform** (UG) and **non-uniform** (NUG). The NUG granules included all granules in which we could see any obvious variation in the density across the granule. That we properly can sort granules into these two types is reinforced in the analysis that follows.

Table 6.1 contains the measured characteristics of 388 isolated granules imaged within 1 hour of being taken off ice. These granules were prepared by the protocol described in Chapter III and were suspended in isosmotic solution (0.3M sucrose, pH 6.0). The table shows the average values (± standard error of the mean, s.e.m) for the diameter, protein concentration and mass of the each of the two classes of granules, UG and NUG, as well as the combined average.

Table 6.1. General Population. This table presents the average values for the characteristics of a population of zymogen granules. The granules have been divided into two sub-classes; uniform and non-uniform. Values with the same letter between UG and NUG groups are not significantly different (P>0.05, t test).

	Diameter (μm) average ± (s.e.m.)	**Protein Concentration (mg/ml)** average ± (s.e.m.)	**Protein Mass (fg)** average ± (s.e.m.)
Uniform (N=300)	1.00 ± 0.01	294 ± 17	153 ± 5[a]
Non-Unif. (N=88)	1.36 ± 0.04	115 ± 6	142 ± 10[a]
All (N=388)	1.08 ± 0.02	253 ± 7	150 ± 4

From the table we can see that the NUG granules represent about 23% of the population of granules. They have a much larger average diameter value, 36% bigger

than the UG granules and a lower protein concentration, ~40%. Consequently, as can be seen, the protein mass for both populations is not significantly different.

We can compare the characteristics of the population taken as a whole ("All") to results from other techniques mentioned in Chapter I. The best average range of protein concentration for a preparation of isolated zymogen granules has been measured using specific activity enrichment to be 135-270 mg/ml (Ho and Rothman, 1983). Additionally, Burwen (1972) measured the protein concentration of isolated granules using a Petroff Hauser chamber to be 280mg/ml. And, the average diameter for our General Population is within the range of results attained by other investigators, as mentioned in the first chapter, at around 1μm. However, because both of these characteristics depend on the state of the animal (fasted or fed) it is difficult to directly compare values. Nonetheless, the STXM technique has a distinct advantage over other methods in measuring these characteristics because it is possible to directly measure the diameter and protein mass of each individual granule. This is the first time such direct measurements have been made on bio-objects this small!

Diameter

A histogram of the distribution of diameter values for all of the granules is shown in figure 6.3. Also shown is a normal curve based on the average diameter of the population taken as a whole and its standard deviation. As can be seen, the curve is not a very good fit to the data. If instead we acknowledge the UG and NUG granules as two separate populations, in figure 6.4, we can see that a normal distribution now fits both populations relatively well. From the work of others, we expect the diameters to fit a normal distribution (Liebow, 1973). One final point to notice is that while both types of granules have different diameter distributions, the range of values within those distributions is about 3 fold for both. The UG granules range from 0.56-1.80μm and the NUG granules range from 0.73 - 2.37μm.

Protein Concentration

A histogram of the distribution of protein concentration for both types of granules is shown in figure 6.5. From the figure, we can see that although the two distributions are statistically distinct, they share a region of overlapping values, between 100 and 250 mg/ml. This overlap is a consequence of combining several preparations in one graph. For the results presented later in this chapter, where one or two preparations were used for each experiment, the distinction between the protein concentration distributions of the two types of granules is much clearer (see for example figure 6.19).

We can examine the distribution of protein concentration further for both types of granules by graphing the data in two other plots, figure 6.6 and figure 6.7. Figure 6.6 is protein concentration plotted against diameter. We have divided the ranges of diameter and protein concentration in half resulting in a graph with 4 quadrants that represent A: large granules (diameter > 1.4μm) with high protein concentrations (> 300 mg/ml), B: small granules high protein concentration, C: small granules with low protein concentration and D: large granules with low protein concentration. Immediately we notice that there are no granules in quadrant A, large granules with high protein concentration. There are only small granules with high protein concentrations (quadrant B) and these are exclusively UG granules. Both types of granules are equally represented in quadrant C, small granules with low protein concentration. And, in quadrant D, the majority of the granules are the NUG type.

The other graph, figure 6.7, plots protein mass against volume for all of the granules. This type of plot is particularly useful because the slope of a straight line drawn through the origin will represent a specific protein concentration. Data points above the line have a protein concentration greater than the slope, and those lying below the line a lower protein concentration. Lines that designate values of 25, 100 and 600mg/ml are shown. These lines were chosen because, as we can see, they represent the limits of the protein

concentration values for the UG and NUG granules; the UG granules lie exclusively between 100 and 600mg/ml and most of the NUG granules lie between 100 and 25mg/ml. This is a concentration range of some 25 fold overall and is due to pooling the results from multiple preparations. We will see that in experiments where only 1 or 2 preparations of granules are used, the range of protein concentration of the granules is considerably less.

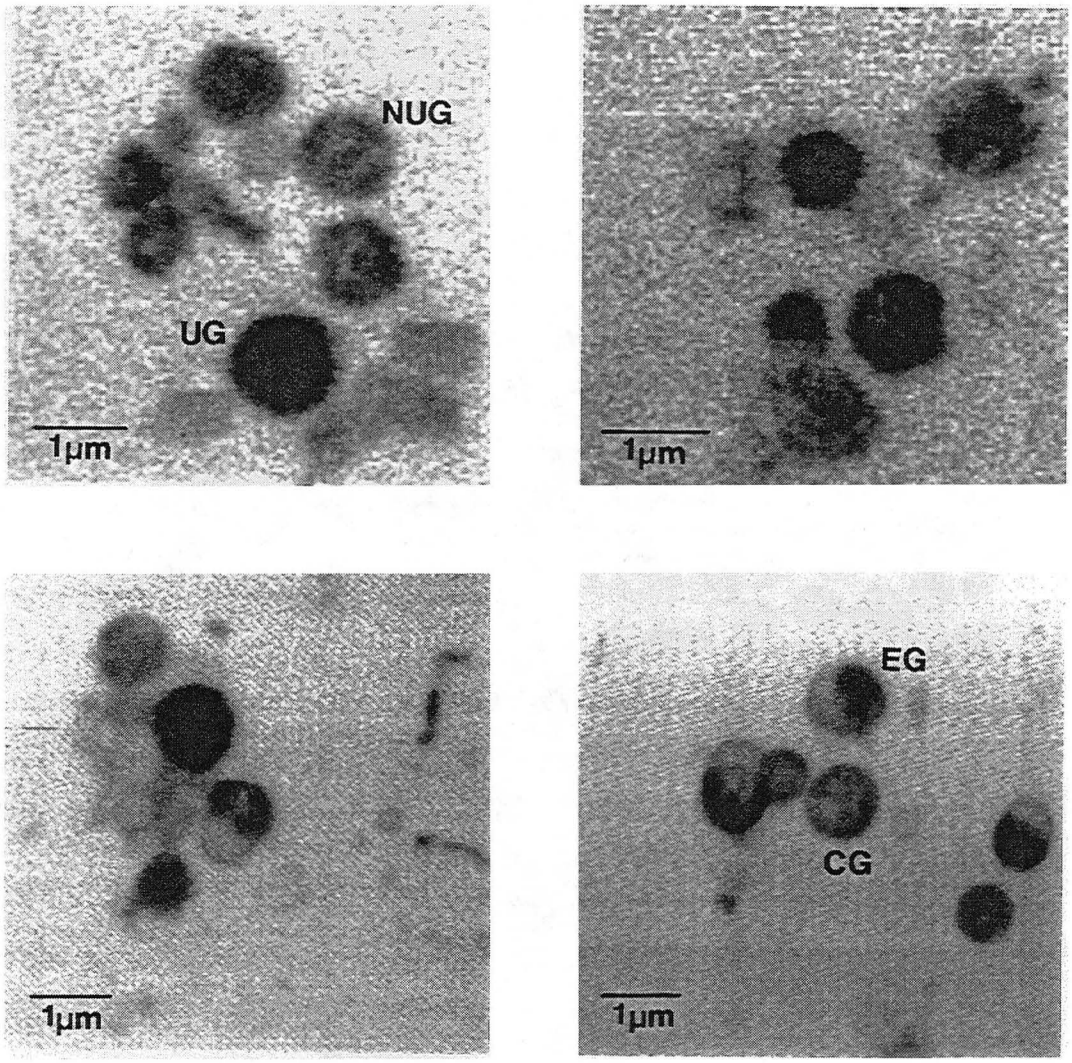

Figure 6.1 Four STXM images of freshly isolated zymogen granules suspended in 0.3M sucrose (pH 6.0). All of the images are from different preparations. We can identify four types of granules - UG (uniform), NUG (non-uniform), CG (clumpy) and EG (edge clumpy). The CG and EG granules are considered to be NUG granules in the presentation of the data. Different pixel sizes were used for each of the images: A-27nm, B-18.8nm, C&D-31.6nm.

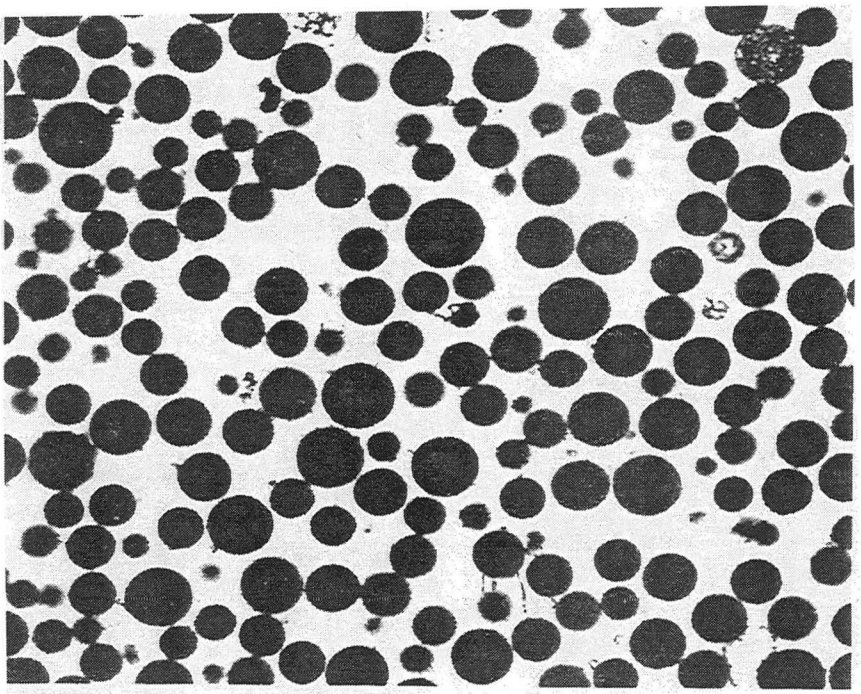

Figure 6.2 Low magnification electron micrograph of zymogen granule pellet, obtained from the protocol described in Chapter V, illustrating the morphology of the granules. The granules have a circular profile and a relatively homogeneous, dense content. Magnification: x9,000

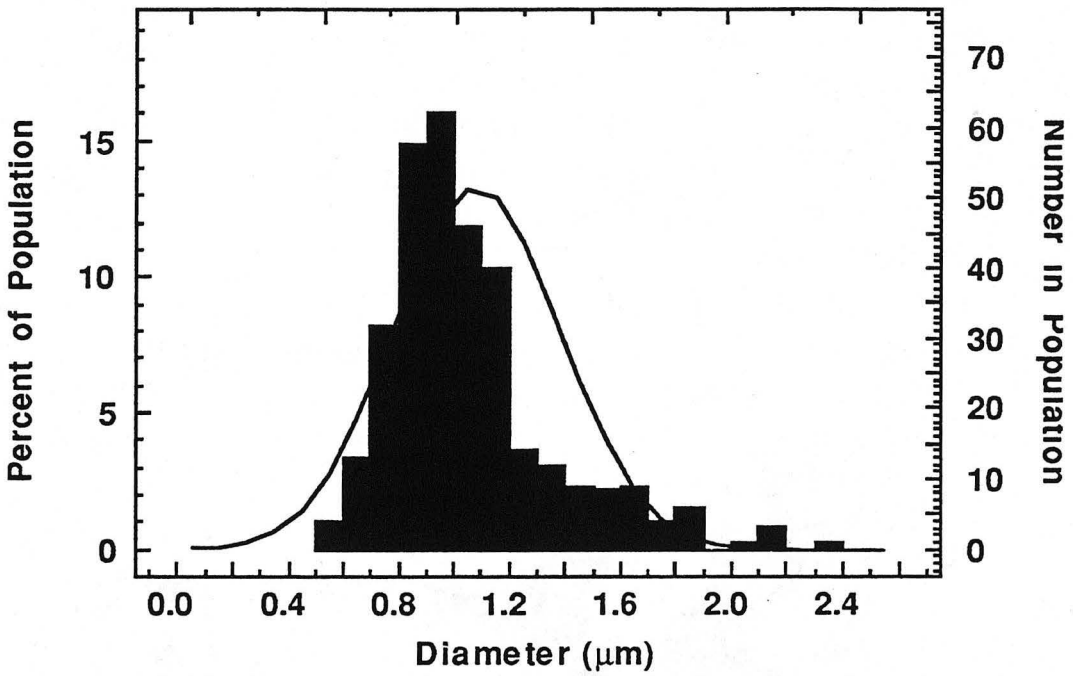

Figure 6.3 Distribution of all zymogen granule diameter values from the general population. Also shown is a normal curve based on the average diameter of the population and the standard deviation.

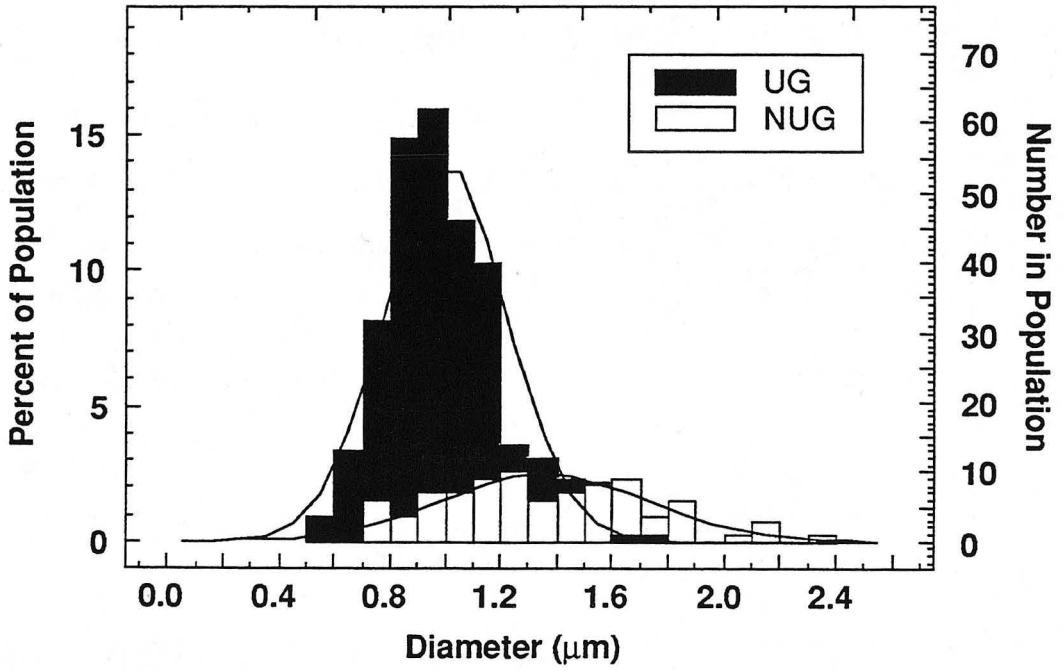

Figure 6.4 Distribution of zymogen granule diameter from the general population. The distributions for the UG and NUG granules are shown separately and normal curves based on the values for each population are also shown.

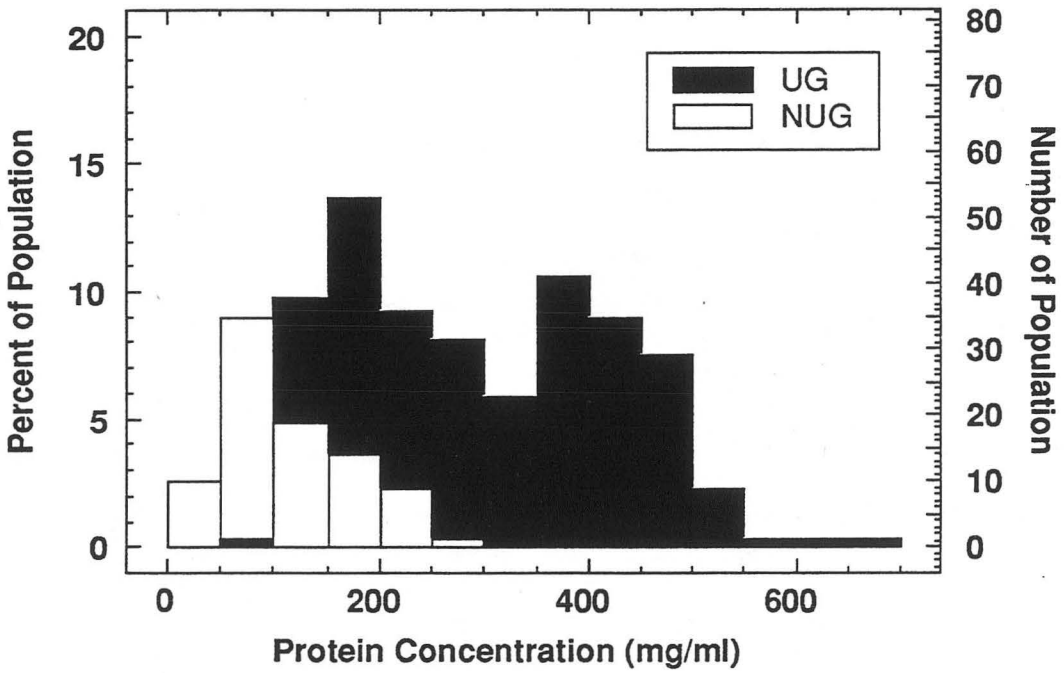

Figure 6.5 Distribution of zymogen granule protein concentration from the general population. The distributions for the UG and NUG granules are shown separately. The average protein concentration for the UG granules is 294 ± 17mg/ml (±s.e.m.) and for the NUG granules it is 115 ± 6mg/ml.

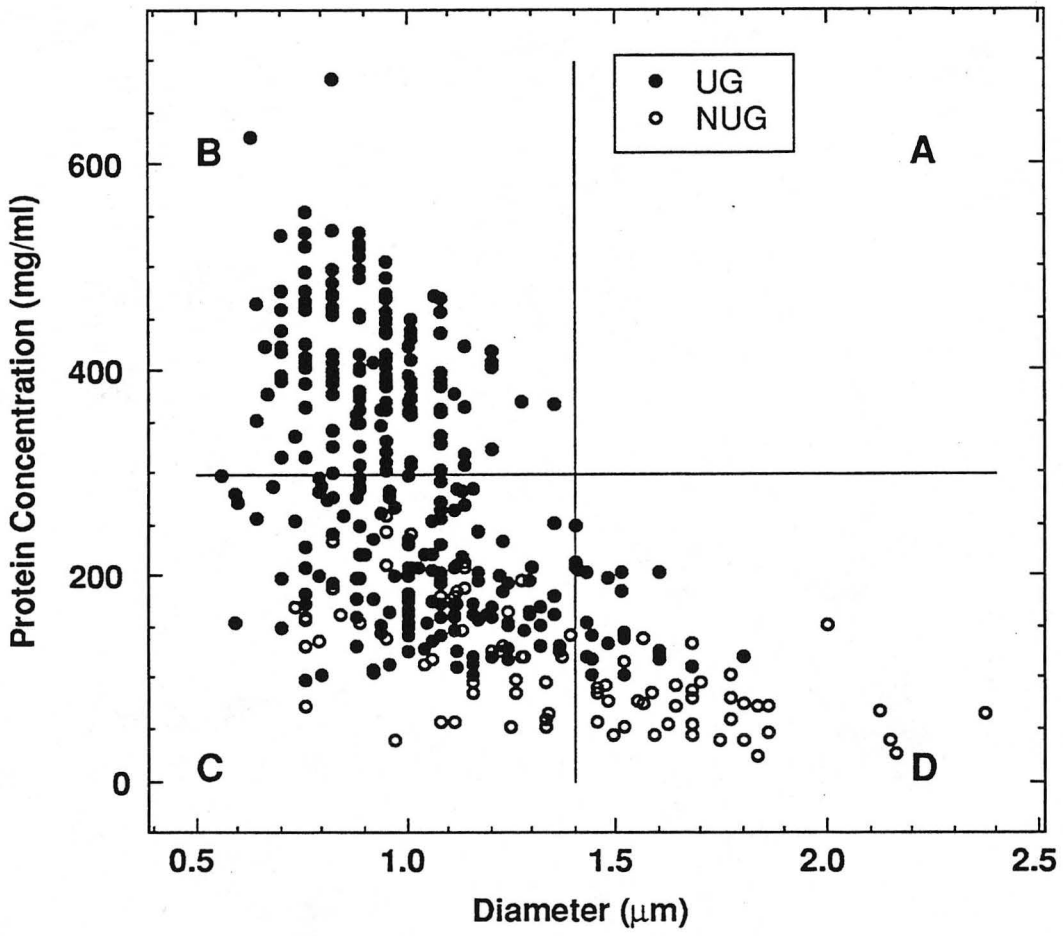

Figure 6.6 The relationship between the protein concentration and the diameter of the granules from the General Population. The graph has been divided into quadrants by demarking the median protein concentration and diameter values. Quadrant A is for large granules with a high protein concentration, quadrant B is for small granules with a high protein concentration, quadrant C is for small granules with a low protein concentration and quadrant D is for large granules with a low protein concentration.

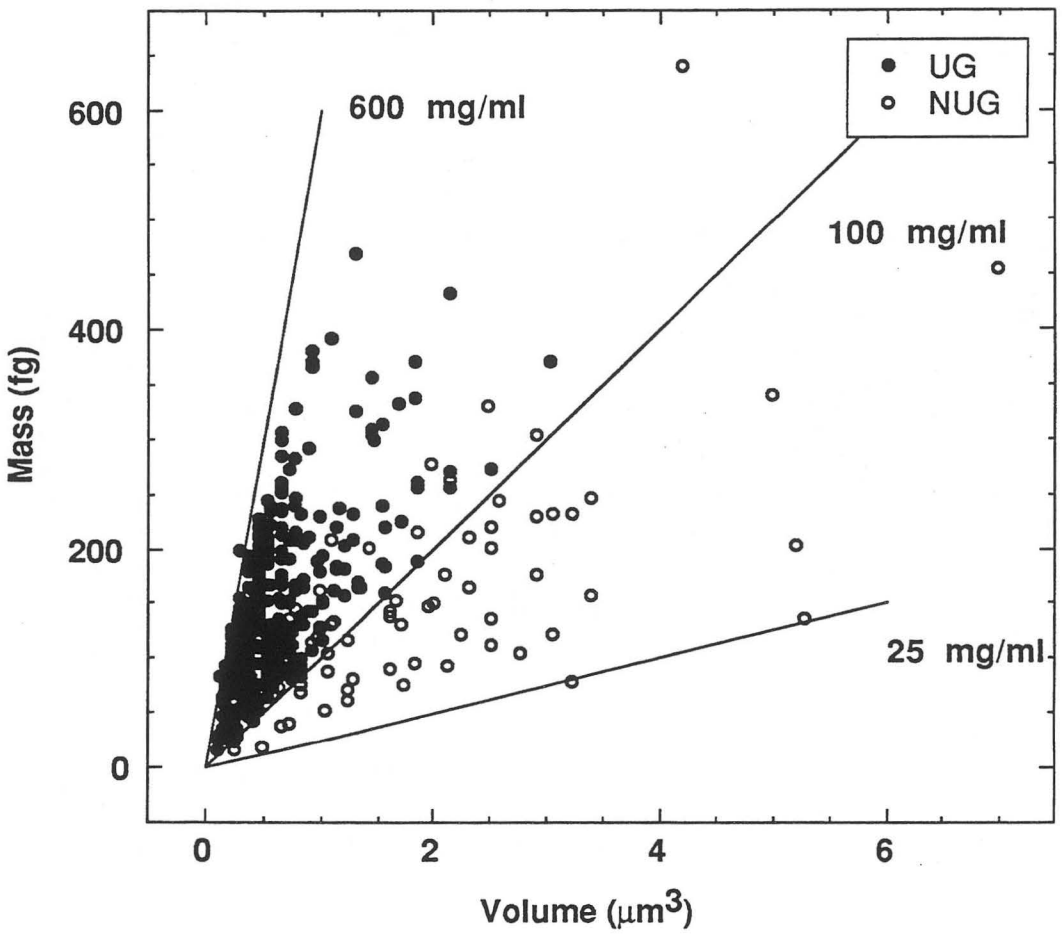

Figure 6.7 The relationship between protein mass and granule volume for all of the granules from the General Population. The slope of a line drawn through the origin represents a protein concentration value. Three lines have been drawn showing protein concentration values of 25, 100 and 600mg/ml.

VI.2 Time Resolved Studies on Zymogen Granules.

This section presents the results of the time-resolved experiments that were performed using STXM on isolated zymogen granules suspended in various aqueous solutions as described in Chapter V. The characteristics of diameter, protein concentration and mass of each individual granule in the experiment were measured several times over the time course of the experiment and the results pooled for the granule population in each experiment. From the results of similar experiments performed on isolated granules using different techniques as discussed in Chapter I, we expected the characteristics of diameter and protein mass of each granule to steadily change over time, and that this rate of change would depend on the particular solution in which the granules were suspended.

The experimental protocol was described in Chapter V, but we will briefly review it here. Isolated granules were introduced into the sample chamber (LBL-WC) and an initial image of several fields of granules were taken. If we were interested in observing the effect of a different solution than the original isolation, suspension solution on the granules, then after the initial image was taken, the experimental solution was flowed into the LBL-WC until it displaced the original solution. Another image of each field of granules was taken afterwards and then subsequent images were taken, approximately once every hour for the duration of the time course. In most of the experiments, unless otherwise noted, time was measured from the point that the granule suspension was taken off ice and introduced into the LBL-WC. The initial image was generally taken within 1 hr. In order to compare the data from all the images, we have binned the time points as follows: time 1 means that the image was taken between 0 and 1 hour after the suspension was taken off of ice, time 2 is between 1 and 2 hours, time 3 is between 2 and 3 hours, time 4 is between 3 and 4 hours and time 5 is between 4 and 5 hours.

In these experiments we did not observe lysis, or the sudden loss of mass from any individual granule. All of the granules were observed to individually change in their diameter and/or protein mass over the time course of the experiment; although as mentioned above, the combined results for all of the granules in the experiment are presented. Additionally, the rates of change of the characteristics of diameter and protein mass were different for the various experimental solutions to which the granules were subject. The results from these different solutions are presented in the following subsections - **control** (original suspension), **0.3M & 0.6M sucrose** (5mM $NaHPO_4$, pH 6.0), **water, 0.025% & 0.05% Triton-X** in 0.3M sucrose (5mM $NaHPO_4$, pH 6.0), **50 & 250 mg/ml chymotrypsinogen** A (bovine, Sigma) in 0.3M sucrose (5mM $NaHPO_4$, pH 6.0), **15μM Nigericin** in 0.3M sucrose (5mM $KHPO_4$, pH 6.0) and **150mM NaCl** (pH 6.0). STXM images of only some of the experiments are shown.

VI.2.1 Control Experiments

In the control experiments, we observed changes in the diameter, protein mass and concentration over time in isolated zymogen granules that had been resuspended in an isosmotic solution of 0.3M sucrose (pH 6.0) according to the standard isolation protocol. The results of four experiments are presented in this section.

The first experiment used fixation to arrest the granules at a particular time point after they had been resuspended and then the granules from each "time population" were observed in STXM and their diameter, protein concentration and mass were measured. The following three experiments were performed on fresh granules. Isolated granules were introduced into the LBL-WC and initial images were taken. These same granules were then imaged once every hour for the time course.

VI.2.1a Control Experiments - Fixed

In this experiment, a preparation of isolated zymogen granules was divided into 4 aliquots; three remained at room temperature for different amounts of time (0hr, 1/2hr and 4hr) and one was held for 4 hours at 4°C. All of the "time populations" were fixed with 1 1/2% glutaraldehyde overnight and then examined in STXM. We expected to observe the characteristics of diameter and/or protein mass gradually decrease for the time populations - except for the 4hr-4°C population. Because this population was maintained at a low temperature, it was assumed that its transport processes should have been arrested or slowed down and we would therefore expect that the characteristics of diameter, protein mass and concentration of this population would not be significantly different from the 0hr population.

Figure 6.8 shows a typical STXM image of each zymogen granule time population. From this figure, we can easily identify the two populations of granules, UG and NUG granules, that were mentioned in the General Population section (VI.1). Table 6.2 shows the measured characteristics for the UG and NUG granules for the different time points. The 339 granules from the 0hr time point come from 24 separate images with 63.3nm pixel sizes, the 210 granules from the 1/2hr time point came from 10 separate images with 63.3nm pixel sizes, the 66 granules from the 4hr time point came from 9 separate images that had 31.6nm pixel sizes and the 72 4hr-4°C granules came from 13 separate images with 63.3nm pixel sizes. Table 6.2 shows the average (± s.e.m.) of the characteristics - diameter, protein concentration and mass for each population. A notation is made on the chart when particular characteristics are not shown to be statistically significantly different between either the two groups of granules at a particular time point, or between the time points for a particular type of granule (UG or NUG).

Table 6.2. The characteristics of fixed granules for the different time groups mentioned in the text. All granules came from the same preparation. Values with the same letters are not significantly different (P>0.05, t test).

	Diameter (μm) average ± (s.e.m.)	Protein Concentration (mg/ml) average ± (s.e.m.)	Protein Mass (fg) average ± (s.e.m.)
Uniform			
t=0hr (N=251)	1.06 ± 0.01	267 ± 5	175 ± 5[f,g]
t=1/2hr (N=167)	1.03 ± 0.02[a]	300 ± 5	180 ± 7[f,h]
t=4hr (N=52)	1.00 ± 0.02[a,b]	388 ± 9	211 ± 13
t=4hr-4° (N=52)	0.98 ± 0.02[b]	348 ± 9	181 ± 12[g,h]
Non-Uniform			
t=0hr (N=88)	1.57 ± 0.03[c]	74 ± 4[e]	152 ± 10[i]
t=1/2hr (N=43)	1.49 ± 0.05[c]	96 ± 6	163 ± 13[i]
t=4hr (N=14)	1.10 ± 0.07[d]	152 ± 14	105 ± 16
t=4hr-4° (N=20)	1.13 ± 0.05[d]	81 ± 6[e]	69 ± 11
All			
t=0hr (N=339)	1.19 ± 0.02	217 ± 6	169 ± 5
t=1/2hr (N=210)	1.13 ± 0.02	256 ± 7	176 ± 6
t=4hr (N=66)	1.02 ± 0.02	388 ± 14	189 ± 12
t=4hr-4° (N=72)	1.02 ± 0.02	274 ± 16	150 ± 11

From the table we can see that the initial characteristics of diameter, protein mass and concentration for this population of granules overall ("All") are similar to those of the General Population. Also, we see that NUG granules represent a similar fraction of the population as in the General Population (20 & 23% respectively) and in this study, they are also larger in diameter and have a lower protein concentration than UG granules.

What is interesting to note is that we can now see that these properties, just mentioned between NUG and UG granules, remain the same even over the time course of the experiment. The NUG granules represent 20, 20, 21 and 28% of the population of granules for the respective time points. They also have a larger average diameter than UG granules for all of the time points, although the difference becomes less pronounced over time. For 0hr they are 48% larger but by 4hr they are only 10% larger. The protein concentration for NUG granules is lower than UG granules for all time points, but again

the difference becomes smaller at the later time point. At 0hr the UG granules are 3.5 times more concentrated than the NUG granules but by 4hr the difference is only 2.5 times. We also see that the protein mass for both populations remains approximately the same for the respective time points.

Over time (0, 1/2 and 4hr time points) the average diameter of both types of granules progressively decreases and as expected we see that NUG granules decrease in protein mass (~30% from 0hr to 4hr). However, UG granules showed an unexpected small, but significant increase in protein mass over the time course. This result may occur because some granules take up protein that has been released into solution by other granules. This phenomenon is expected, as results from (Liebow and Rothman, 1972) show that granules are able to take up exogeneously added protein.

The results from the 4hr-4°C experiment are intriguing. On the one hand, we can see that the protein mass of UG granules at 0hr is not significantly different from that at 4hr-4°C which implies that maintaining these granules at 4°C prohibits the uptake (or release) of protein. However, NUG granules at 4hr-4°C show a significant difference in protein mass than at 0hr and it appears that at 4°C protein release occurs even faster than at room temperature (4hr). Temperature does not appear to affect the rate of diameter decrease as UG and NUG granule diameters are not significantly different between 4hr and 4hr-4°C.

Diameter

Histograms of the distributions of diameters for the initial and final time points (0 & 4hr) are shown in figure 6.9. As can be seen, a normal distribution seems to fit both populations at both time points. The initial (t=0hr) range of diameter values, for both UG and NUG granules is, as expected, smaller than for the General Population because only one preparation has been used in this experiment (~2.5fold as compared to 3 fold). These initial ranges for both types of granules decrease between 0hr and 4hr; from 0.63-1.71μm to 1.00-1.33μm and 0.89-2.34μm to 0.57-1.51μm respectively. For UG granules, this is

due to an increase in the size of the smallest granules as well as a decrease in the size of the largest; whereas for NUG granules both upper and lower limits decrease with the upper limit falling by a greater extent. By 4 hr, the ranges of both types of granules overlap, although the NUG granules have a wider range of diameters. Although, because we are dealing with population statistics, the differences may be at least in part attributable to sampling differences.

Protein Concentration

Histograms of the distribution of protein concentration for the initial and final time points (0 & 4hr) are shown in figure 6.10. The difference between the protein concentration ranges of NUG and UG granules for both time points is obvious and clearer than in the General Population of pooled data (see figure 6.5). We can also see that the range of protein concentration is smaller for both types of granules, especially UG granules. In the General Population, UG granule concentration ranged almost 7fold and in this population, we see that the range is only 3fold. Once again this is because the results from only one preparation are used here.

The protein mass versus granule volume plots for each time point are shown in figure 6.11 as well as the calculated least squares function. The UG granules show quite a tight fit to the calculated line for all of the time points as compared to the General Population (see figure 6.6), although NUG granules still show a substantial variability. We can see that the relationship between protein mass and volume appears to be maintained irrespective of the fact that the granules have lost (or gained) protein and decreased in diameter over time as they have been sitting at room temperature or 4°C. However, because this is a population study, it remains to be shown in the following sections that this relationship is also maintained for individual granules over time.

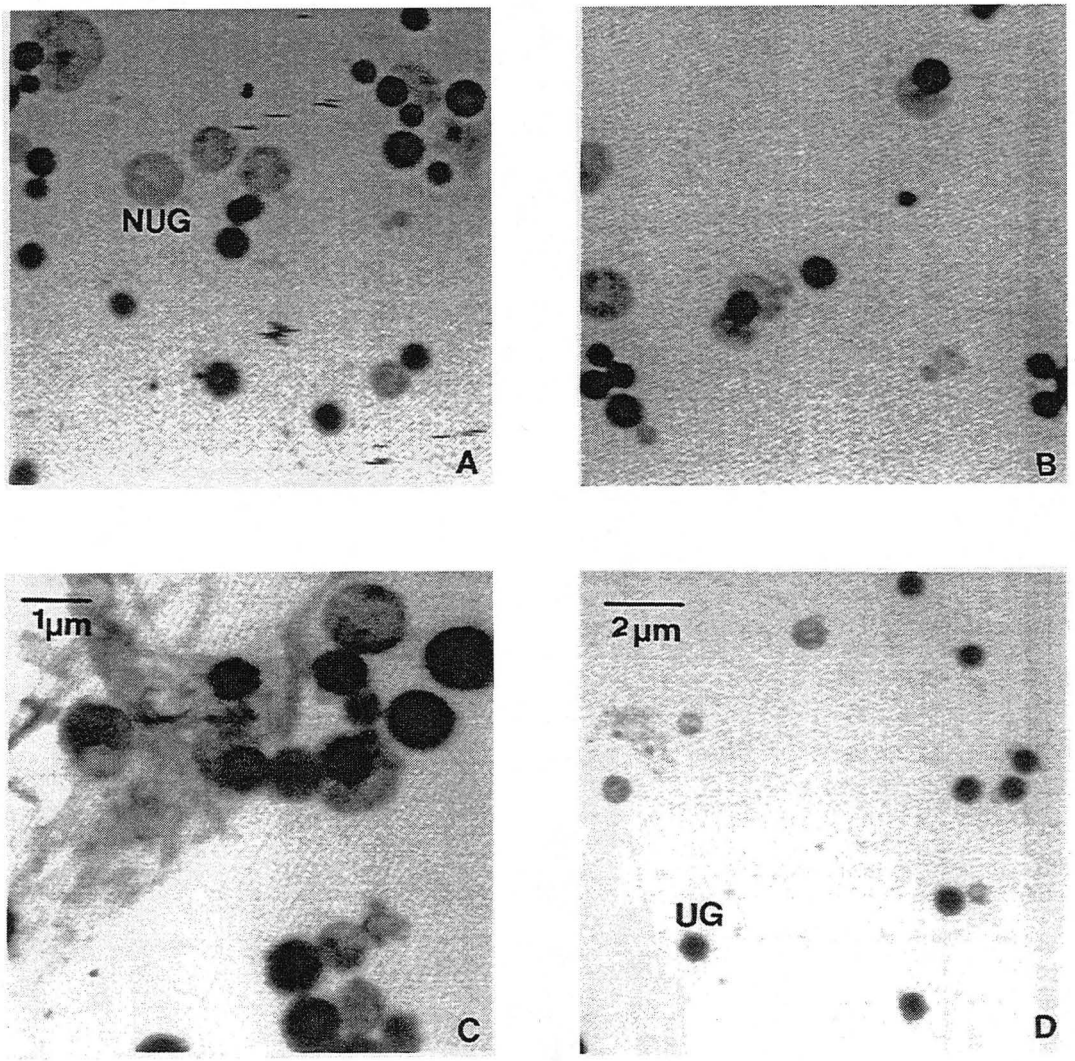

Figure 6.8. Typical STXM images of the 4 different groups of fixed granules. UG and NUG granules are visible in all of the images and are marked. **A** shows the 0hr population; **B** shows the 1/2hr population; **C** shows the 4hr population and **D** shows the 4hr-4°C population. All of the images were taken with 63.3nm pixel sizes except **C** which used 31.6nm pixel sizes.

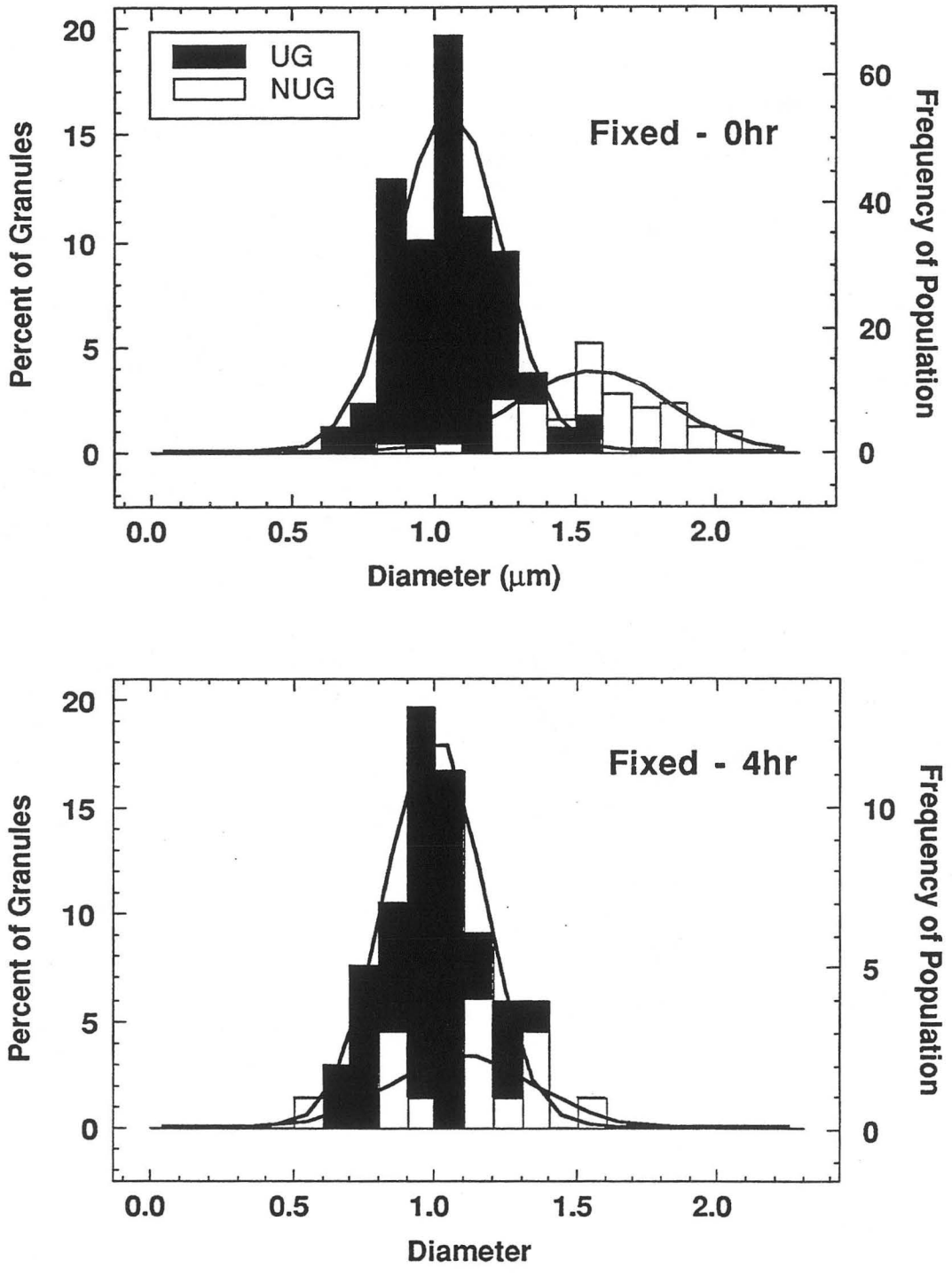

Figure 6.9 Distribution of the diameter for fixed UG and NUG granules from 0hr and 4hr groups. A normal curve fit to the average value for the diameter and the standard deviation of each group is also shown.

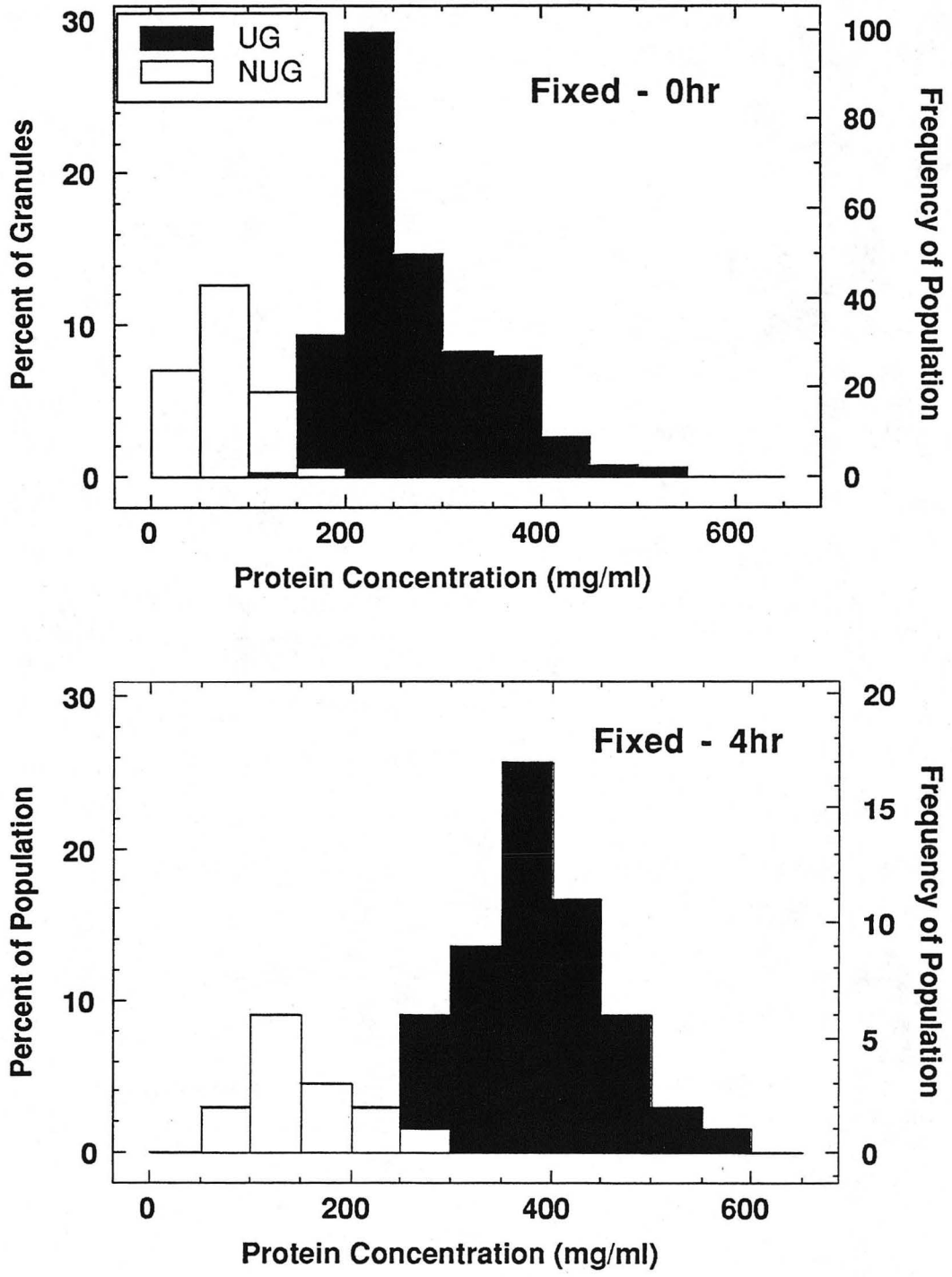

Figure 6.10 The distribution of protein concentration for the UG and NUG granules from the 0hr and 4hr groups.

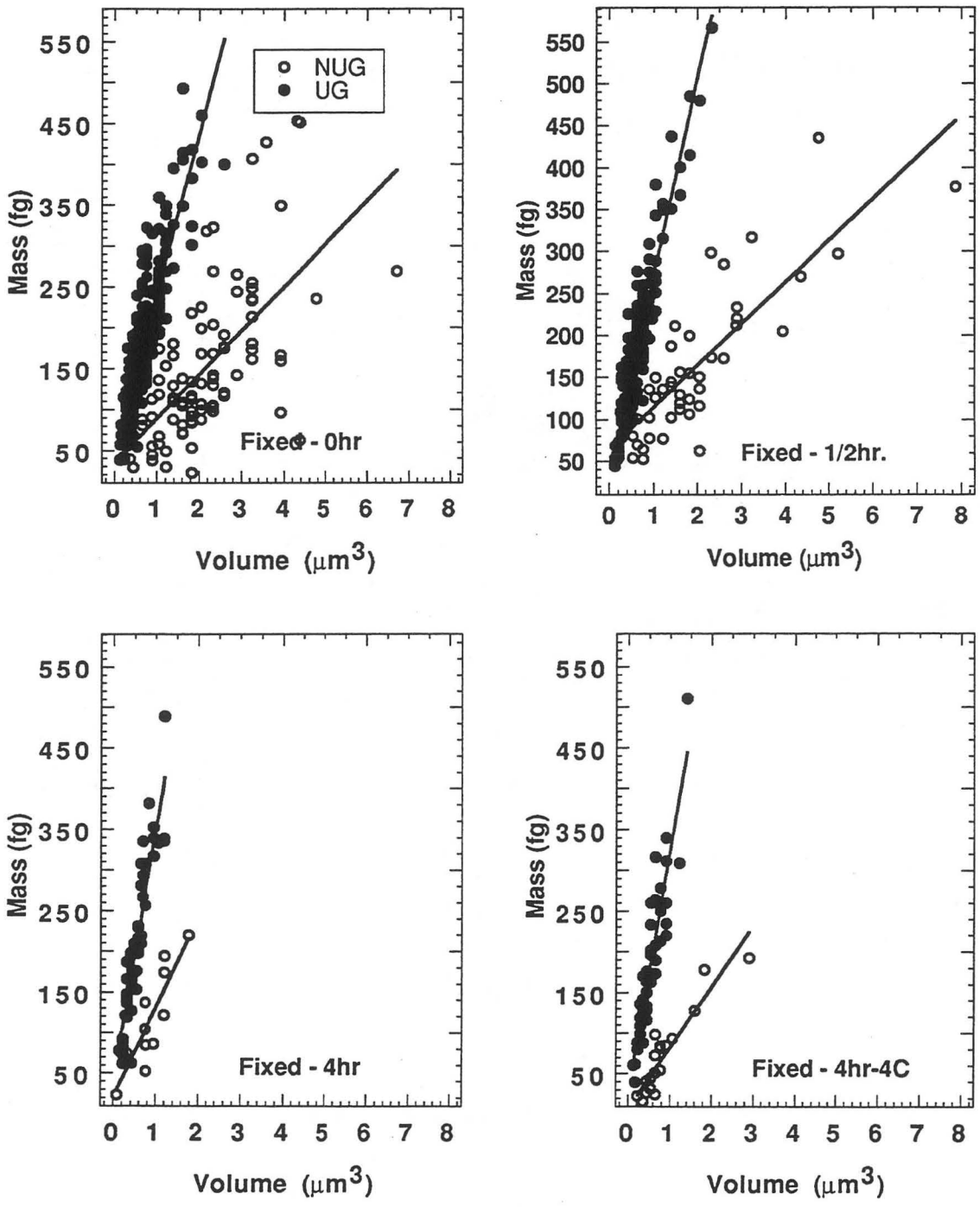

Figure 6.11. Protein mass versus granule volume for each time point. Lines drawn are least squares best fit. The correlation coefficient (r) for each of the lines is as follows: UG(0hr)=0.79, NUG(0hr)=0.60, UG(1/2hr)0.92=, NUG(1/2hr)=0.70, UG(4hr)=0.91, NUG(4hr)=0.87, UG(4hr-ice)=0.91, NUG(4hr-4°C)=0.92 ($P << 0.01$ for all of the data).

VI.2.2 b Control- Fresh Granules

As mentioned above, the control experiments entail observing granules over a period of time in the same suspending solution they were originally isolated in and the changes in their diameter and protein mass noted. The results of the previous section were obtained by examining populations of granules that had been fixed at particular time points after the initial isolation and was therefore a "population study." In this section (and the remaining sections), we observe the changes in diameter, protein mass and concentration of *individual* fresh granules over the time course of the experiment.

The first experiment on fresh granules was performed in May 1990, and was essentially a trial run to establish that we could indeed image the same granules over a period of time. We have included it for historical interest because it was the first time we were able to take multiple images of the same granule over time and observe changes in the characteristics. These experiments set the stage for further investigation. The second experiment was performed in June 1991 and the third experiment was performed in December of 1991 and is reported separately for reasons that will be explained in that section.

May Control

The results from the five zymogen granules that were analyzed for the control experiments in May 1990 are shown in Table 6.3. All of the granules, except one - may29.002, were from the same preparation and were contained within the same LBL-WC. All of the granules were imaged in separate fields with pixel sizes of 31.6nm. The granules were distinctly visible in each image and the imaging did not appear to change the structural appearance of the granules, e.g. they maintained their circular appearance and we did not observe any holes or artifacts in the granules. This was the first time that an unfixed object suspended in an aqueous environment had been imaged more than twice using STXM.

From Table 6.3, we can see that all of the granules decreased substantially, although slowly in protein concentration and mass over time. Moreover, four of the five granules were observed to decrease slightly in diameter over time and one granule was not observed to change at all. Protein loss is not necessarily correlated with a change in diameter.

Table 6.3. Results from the May control experiment. Each granule's characteristics are reported separately.

Granule Image	Init. Time (hr)	Final Time (hr)	Initial Diam. (μm)	Final Diam. (μm)	Initial Con. (mg/ml)	Final Con. (mg/ml)	Initial Mass (fg)	Final Mass (fg)
may25.006	0.73	4.85	1.36	1.36	127	60	166	79
may25.007	0.78	4.90	1.55	1.52	77	41	150	74
may29.002	0.85	1.18	1.52	1.45	52	43	95	69
may25.012	1.48	5.17	1.04	0.88	114	62	68	23
may25.013	1.65	5.05	1.01	0.98	120	82	65	40

Figure 6.12 shows the percent mass loss as a function of time for each granule. From the figure, we can see that the rate of mass loss is not the same for all granules and is independent of the frequency of imaging. May25.012 was imaged 6 times whereas may25.013 was imaged only twice in the same period of time and they show a similar rate of protein loss.

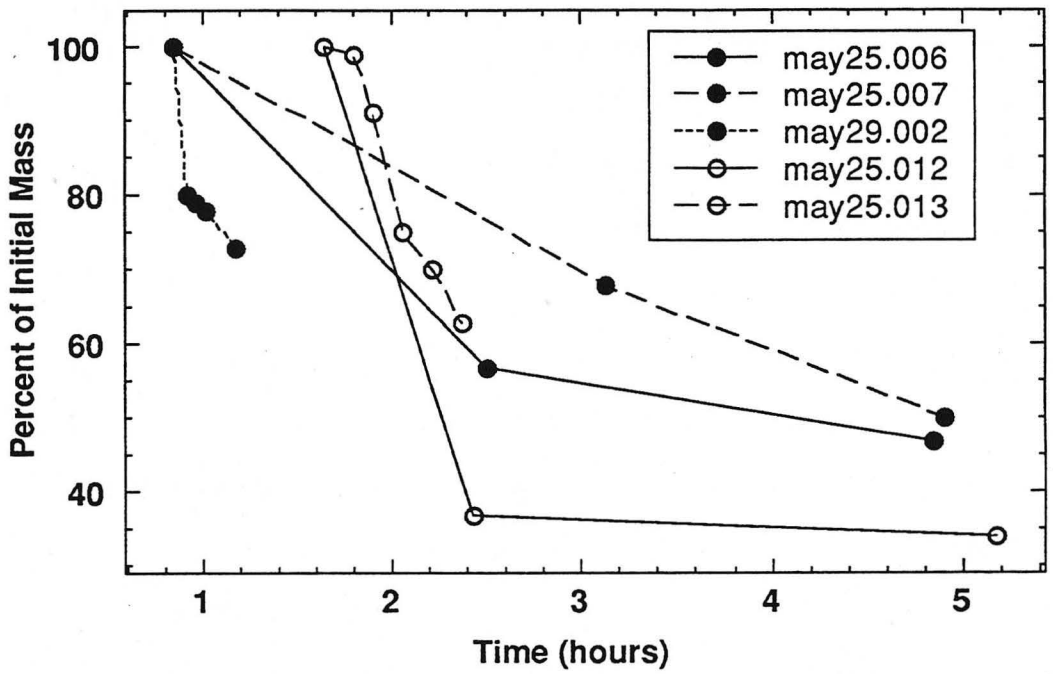

Figure 6.12 Percent mass loss for the May control experiment. All of the granules decreased in protein mass over time . Three of the granules (may25.006, may25.007 and may25.013) were imaged long enough to show that the rate of protein loss appears to approach a steady-state.

June Control

The June control data set consisted of 49 granules, observed in 8 different fields from 2 different granule preparations once every hour over a period of 4 hours from the initial image. All of the images were taken with 39.9nm pixels. Figure 6.13 - 6.16 show four of these fields at each of the time points during the experiment. By looking at the figures, we can see that individual granules are easily recognized and can be identified in each of the images through the time series. Only granules that were present in images of all of the time points were selected for analysis. The two types of granules, UG (uniform) and NUG (non-uniform) are present in these fields and what is interesting to note is that their gross structure does not change over the time course, although they are obviously

shrinking[1]. Figure 6.17 shows protein density contour maps of four granules from figure 6.13. The internal protein density of each granule was calculated on a pixel by pixel basis as described in Chapter III. From these images, it can be more clearly visualized how the distribution of protein changes within each granule over time. In general, we can see that all of the regions within the granules become more dense, and that the lucent areas in the initial images appear to become smaller.

Table 6.4 shows the diameter, protein concentration and mass data for the 49 granules over the time course. The data from the UG and NUG granules are reported separately as well as in combined form. From the table we can see that NUG granules represent 16% of the total population, which is slightly smaller than from the General Population (23%). They are as expected, significantly different than the UG granules in diameter and protein concentration. The NUG granules are on average 33% bigger than the UG granules for all of the time points and the UG granules remain twice as concentrated for all of the time points. The protein mass for both types of granules is similar throughout the experiment.

This particular population of granules shows significantly higher initial diameters and lower protein concentrations for both NUG and UG granules than the General Population (GP) - although, the protein mass values are similar (June-all 152 ± 10 fg and GP 150 ± 4 fg). We will see that granule preparations for each experiment can be quite different in terms of their initial characteristics.

Both types of granules in this experiment decreased in diameter and protein mass over the time course, although protein concentration increased. A notation is made on the chart when particular characteristics are not shown to be statistically significantly

---

[1] Unfortunately, some of these images show streaks which may have been a result of uneven He flow around the sample chamber. At this point, STXM was not isolated from the environment by the Plexiglas box that exists now and for some reason, the gas flow was particularly uneven. This is one of the problems with performing time sensitive experiments using STXM. That is, if something is wrong with the image, it is not possible to retake it because 1) that particular time point has passed and 2) it is important to expose the sample as little as possible to the X rays.

different between either the two groups of granules at a particular time point, or between the time points for a particular type of granule (UG or NUG).

Table 6.4 Results from the June control experiment. Values with the same letters are not significantly different (P>0.05, t-test)

		Diameter (μm) average ± (s.e.m.)	Protein Concentration (mg/ml) average ± (s.e.m.)	Protein Mass (fg) average ± (s.e.m.)
Uniform				
(N=41)	**t=1hr**	1.21 ± 0.03	159 ± 6	151 ± 12[b]
	t=2hr	1.06 ± 0.03	229 ± 7	145 ± 11[b]
	t=3hr	0.98 ± 0.03	267 ± 7	138 ± 10[c]
	t=4hr	0.95 ± 0.02	287 ± 9	134 ± 10[c,d]
	t=5hr	0.92 ± 0.02	312 ± 9	132 ± 10 [d]
Non-Uniform				
(N=8)	**t=1hr**	1.64 ± 0.09	76 ± 10	158 ± 11
	t=2hr	1.40 ± 0.07	106 ± 11	145 ± 11[e]
	t=3hr	1.31 ± 0.05	123 ± 12	141 ± 14[e,f]
	t=4hr	1.24 ± 0.04	138 ± 10[a]	136 ± 15[f]
	t=5hr	1.21 ± 0.05	140 ± 17[a]	126 ± 18
All				
(N=49)	**t=1hr**	1.28 ± 0.04	145 ± 7	152 ± 10
	t=2hr	1.11 ± 0.03	209 ± 9	145 ± 9
	t=3hr	1.04 ± 0.03	244 ± 10	138 ± 8
	t=4hr	1.00 ± 0.03	262 ± 11	135 ± 9
	t=5hr	0.97 ± 0.03	284 ± 12	131 ± 9

Diameter

The distribution of diameter for UG and NUG granules for four of the time points is shown in figure 6.18. The UG granules range in diameter values from 0.76-1.68μm for the initial time point to 0.64-1.28μm for the final time point. The NUG granules range in diameter values from 1.28-2.16μm for the initial time point to 1.00-1.44μm for the final time point. We can see that for both types of granules, the diameter ranges decrease over time, in other words the variance of the values decreases and the diameter range gets tighter. From the figure, we can also see that over time, the two distributions begin to overlap in diameter .

Protein Concentration

The distribution of protein concentration for UG and NUG granules for four of the time points is shown in figure 6.19. The UG granules range in protein concentration from 103-258mg/ml for the initial time point to 214-431mg/ml for the final time point. The average value of protein concentration increased over time by a factor of two. The distribution also became "tighter" and the variance of protein concentration between the initial and final time point were significantly different ($P<0.05$, F test). The NUG granules range in protein concentration from 26-123mg/ml for the initial time point to 49-183mg/ml for the final time point. On average, they too became more concentrated over time by a factor of 1.8, although the variance remained the same.

A plot of protein mass versus granule volume is shown in figure 6.20. We can see that the UG and NUG granules are well correlated and have distinctive distributions. Overtime, the slope (which is in units of protein concentration) of the best fit line changes as the average protein concentration of the population increases but we can see that the relationship between the protein mass and granule volume still holds for both types of granules. This indicates that decreases in protein mass and granule diameter over time occur in a manner that maintains the relationship between protein mass and volume. The protein concentration of the population is tightly grouped around the average value for each time point and this average value increases progressively for each time point, as can be seen by the slope of the best fit line in each graph. Previously, in the control-fixed section, we could only show that different populations were correlated in this fashion for all time points (figure 6.12), but not individual granules. Furthermore, the distinction between the two populations is maintained through the time course indicating that the UG and NUG are unique groups. This phenomenon will be discussed further in the Discussions and Conclusion chapter (VIII).

Protein Mass and Diameter Change

Protein mass and diameter loss over time is shown for both types of granules in figure 6.21 expressed as a percent of the initial value. On average, both types of granules decrease in protein mass and diameter between the initial and the final time. However, from looking at Table 6.4, we can see that the protein mass values for UG and NUG granules are not significantly different ($P>0.05$, t test) between adjacent time points indicating that protein loss in this control experiment occurs slowly. The protein loss rate appears to reach a "semi-equilibrium" state at the end of the experimental period. Overall, UG granules decreased in diameter to $76 \pm 1\%$ (ave. $\pm$ S.E.M) of the initial value and the NUG granules to $74 \pm 1\%$ over the 4 hours of study. This is a decrease of ~ 6.5%/hr and ~7%/hr, respectively. The UG granules decreased in mass to $89 \pm 2\%$ of the initial values and NUG granules to $77 \pm 6\%$ over the 4 hours. This is equivalent to a mass loss rate of ~2.5%/hr and ~6%/hr, respectively.

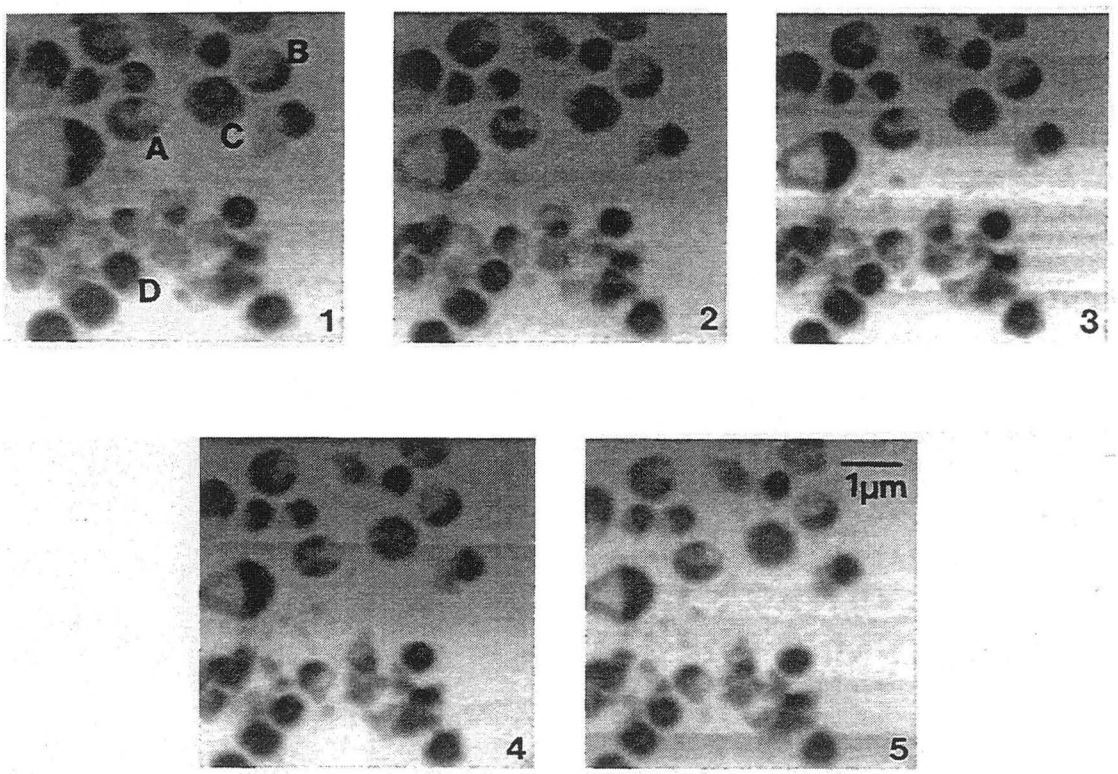

Figure 6.13. Field 1 from the June control experiment. As can be seen, all of the granules that are in the initial image can be seen throughout the time course. We also can see both UG and NUG type granules. The four granules that are indicated in the initial image are shown as protein density contour maps in figure 6.17. Pixel size = 39.9nm, image size 250x250 pixels. These images have been processed with a Robert's Edge Enhancement routine (see Chapter III).

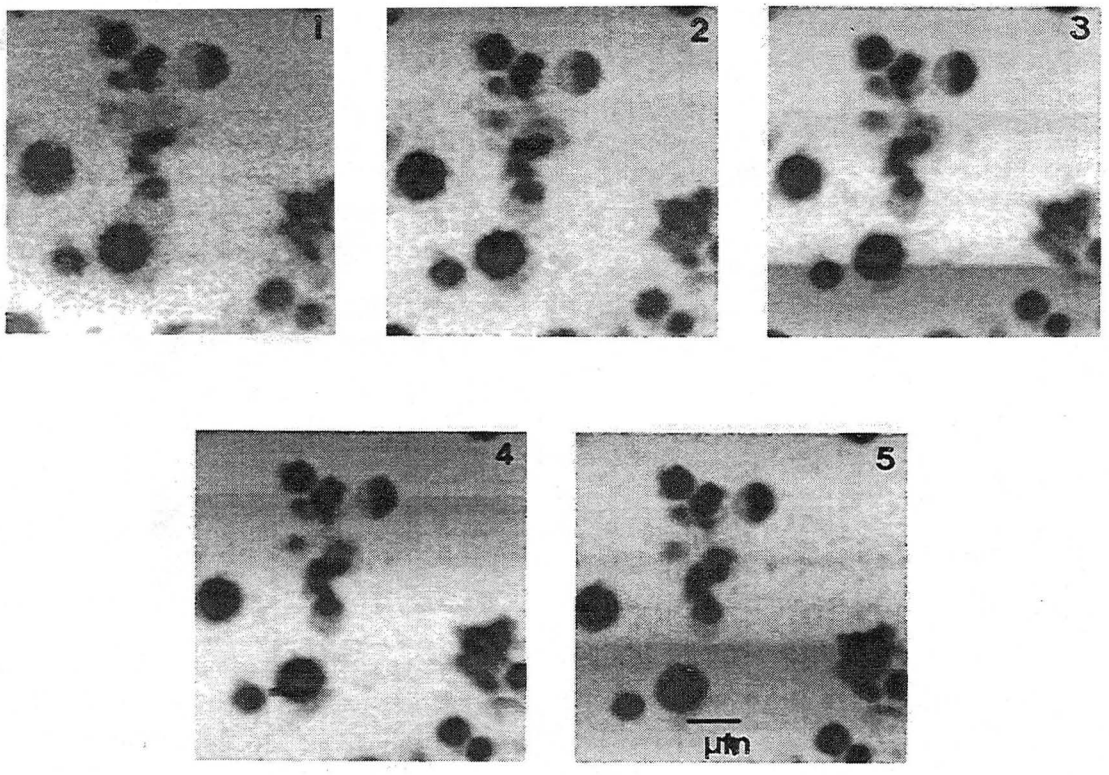

Figure 6.14. Field 2 from the June control experiment. As can be seen, all of the granules that are in the initial image can be seen throughout the time course. We also can see both UG and NUG type granules. Pixel size = 39.9nm, image size 250x250 pixels. These images have been processed with a Robert's Edge Enhancement routine (see Chapter III).

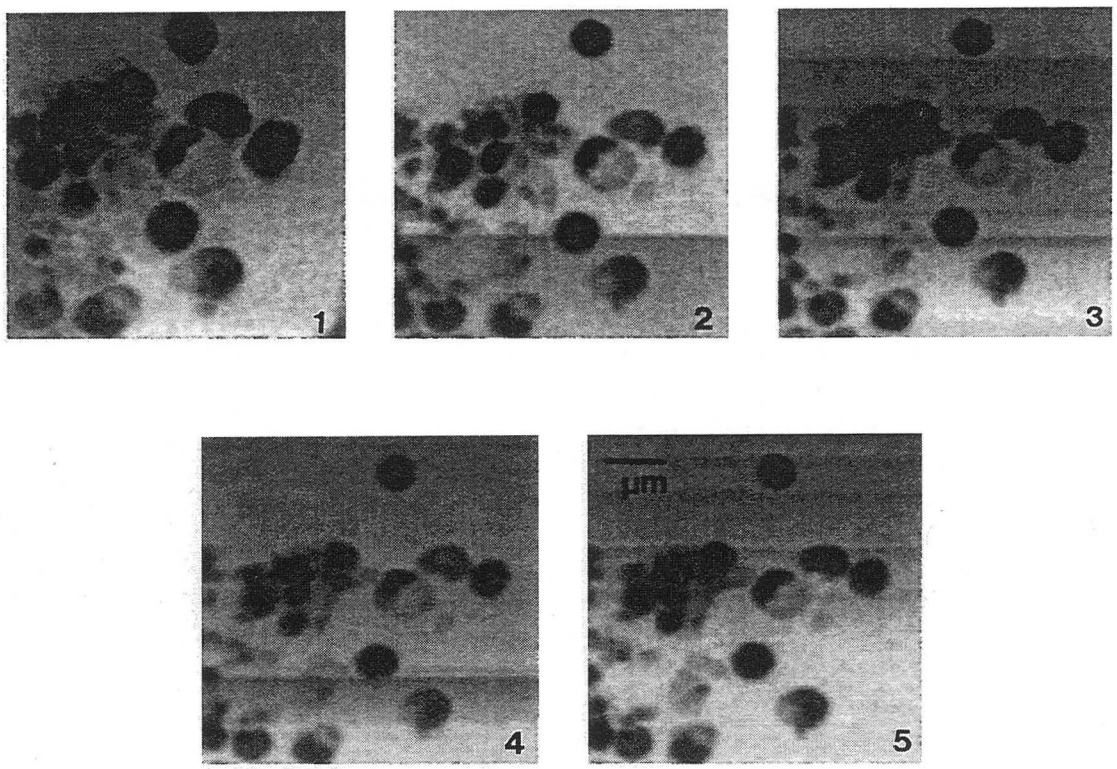

Figure 6.15. Field 3 from the June control experiment. As can be seen, all of the granules that are in the initial image can be seen throughout the time course. We also can see both UG and NUG type granules. Pixel size = 39.9nm, image size 250x250 pixels. These images have been processed with a Robert's Edge Enhancement routine (see Chapter III).

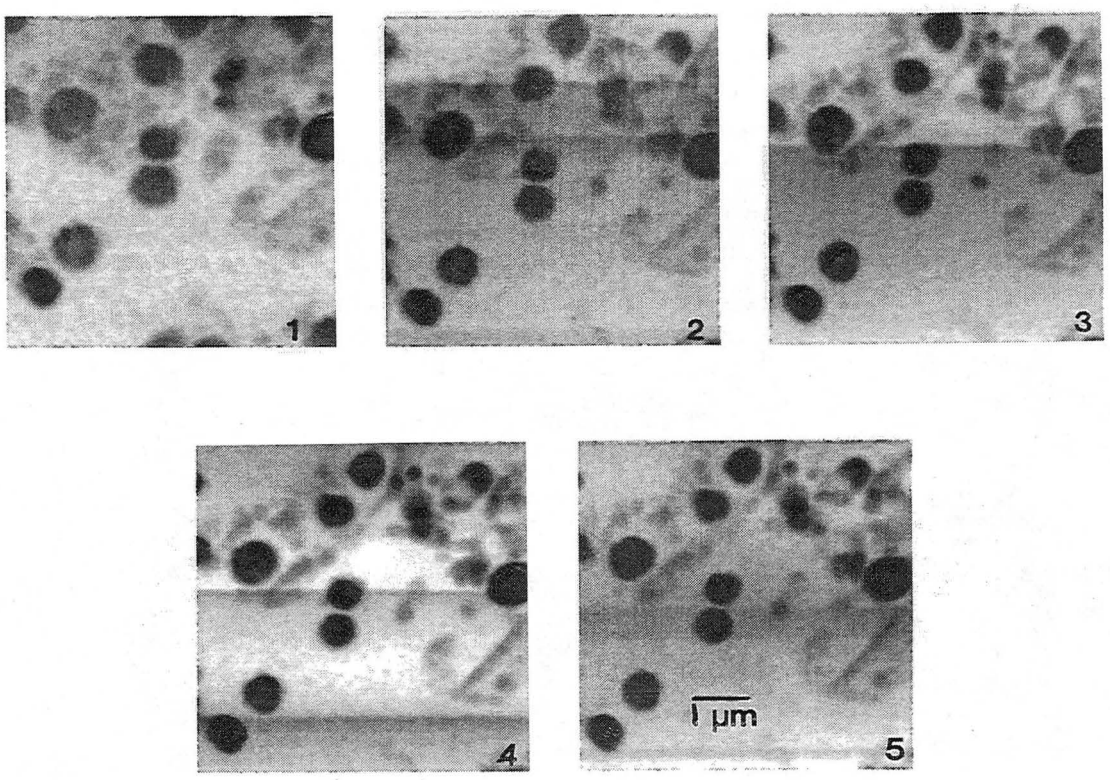

Figure 6.16. Field 4 from the June control experiment. As can be seen, all of the granules that are in the initial image can be seen throughout the time course. We also can see both UG and NUG type granules. Pixel size = 39.9nm, image size 250x250 pixels. These images have been processed with a Robert's Edge Enhancement routine (see Chapter III).

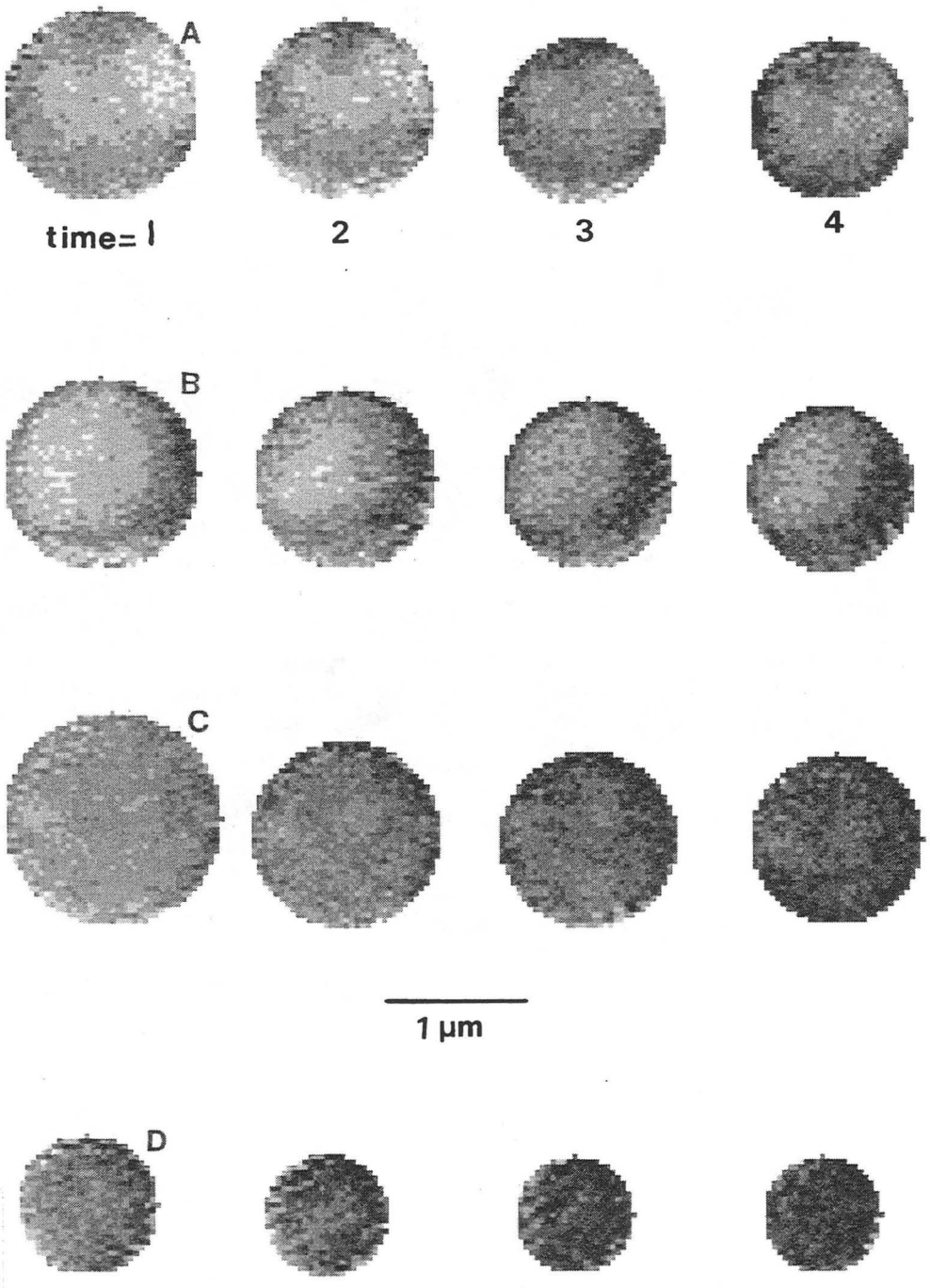

Figure 6.17 The protein density distributions of 4 granules from the June control experiment shown for the first 4 time points (for a total of 3 hours). The grey scale is uniform for all of the images and black represents protein densities that are between 350-400mg/ml and the lightest areas are between 0-50mg/ml.

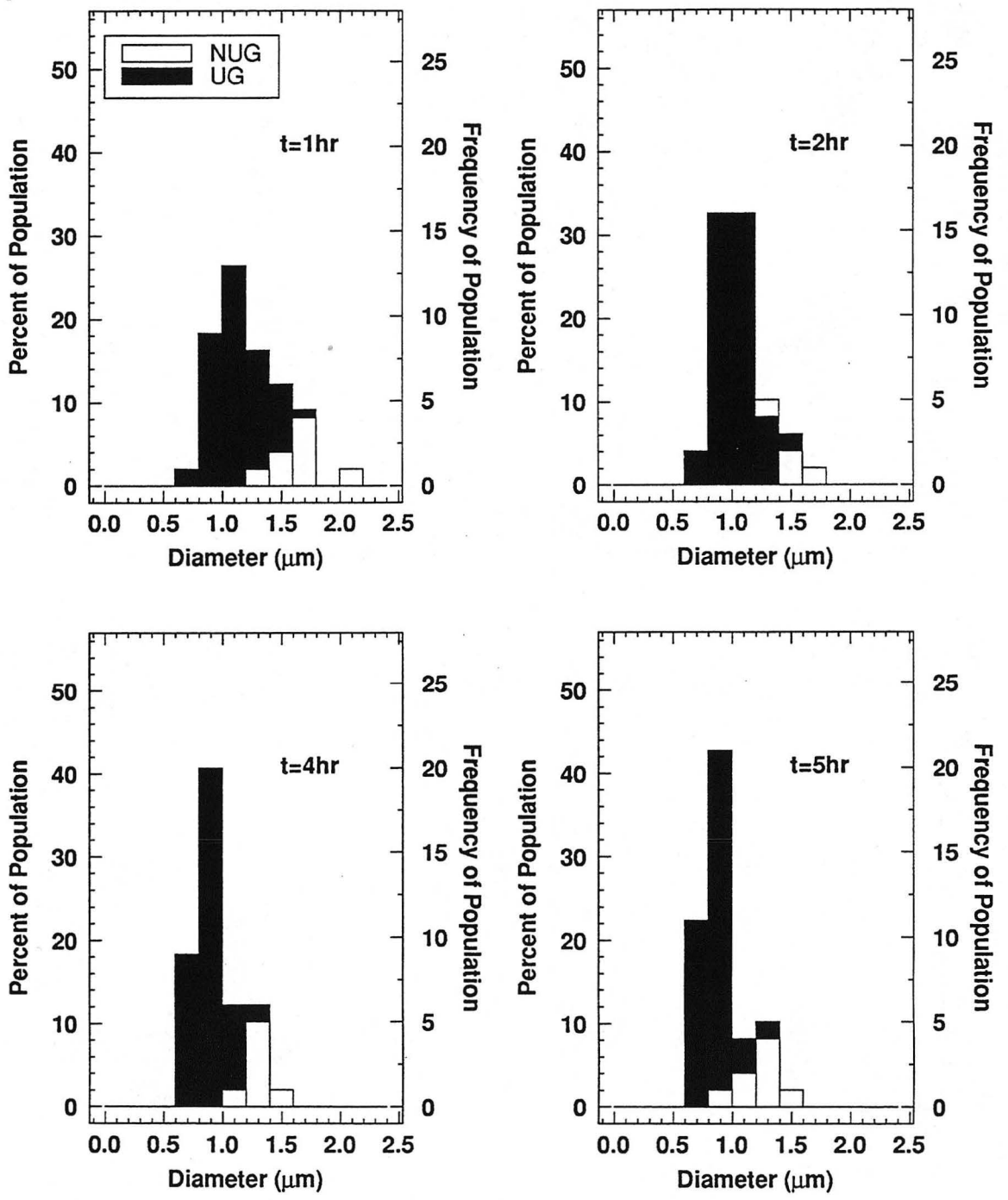

Figure 6.18. Distribution of diameters for both types of granules (UG and NUG) for four of the time points (1, 2, 4 and 5hr). We can see that over time that both distributions move toward smaller diameter values and merge.

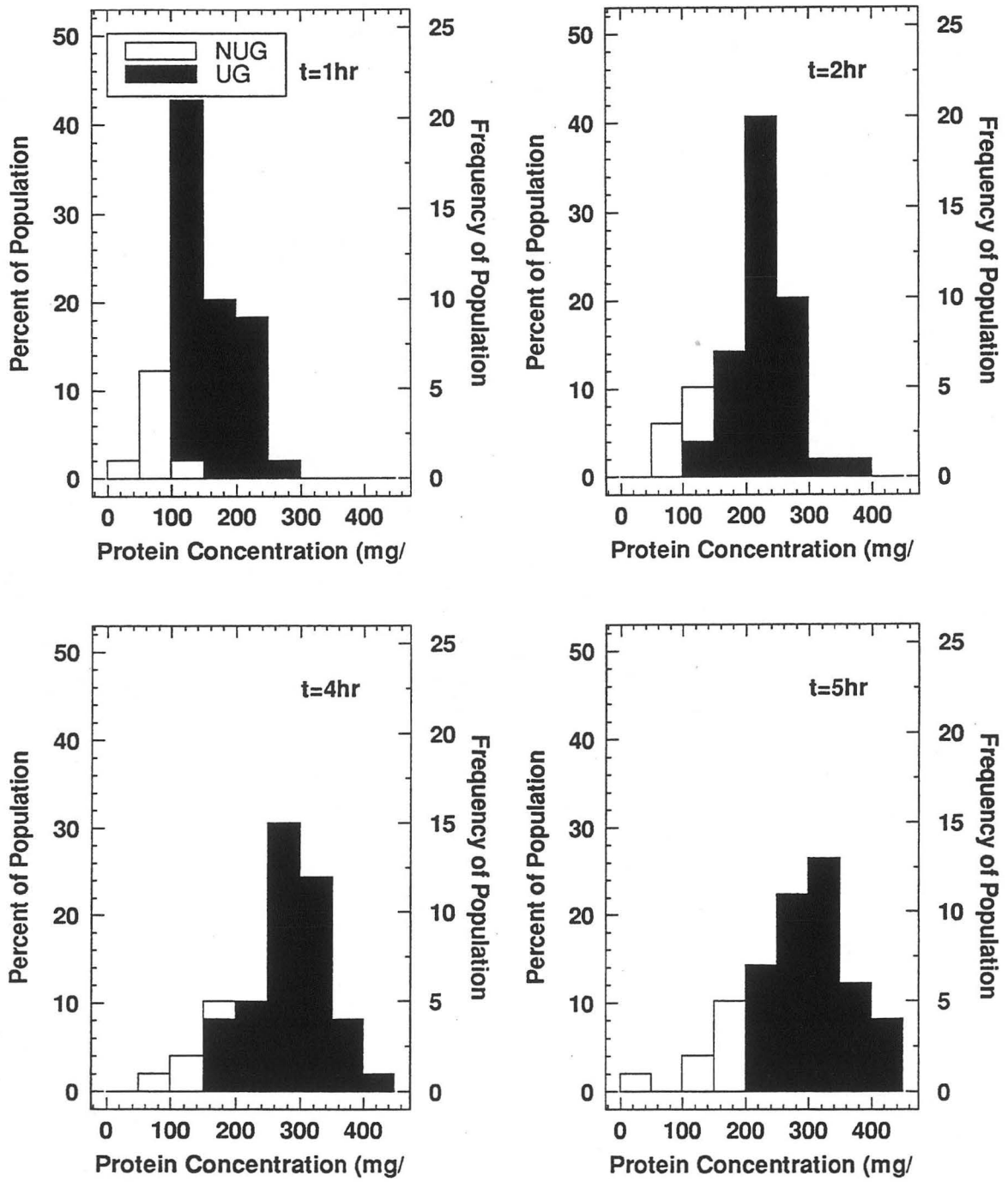

Figure 6.19. Distribution of protein concentration for both types of granules (UG and NUG) for four time points (1, 2, 4 and 5hr). Both distributions move towards higher protein concentrations over time and separate slightly in their range values.

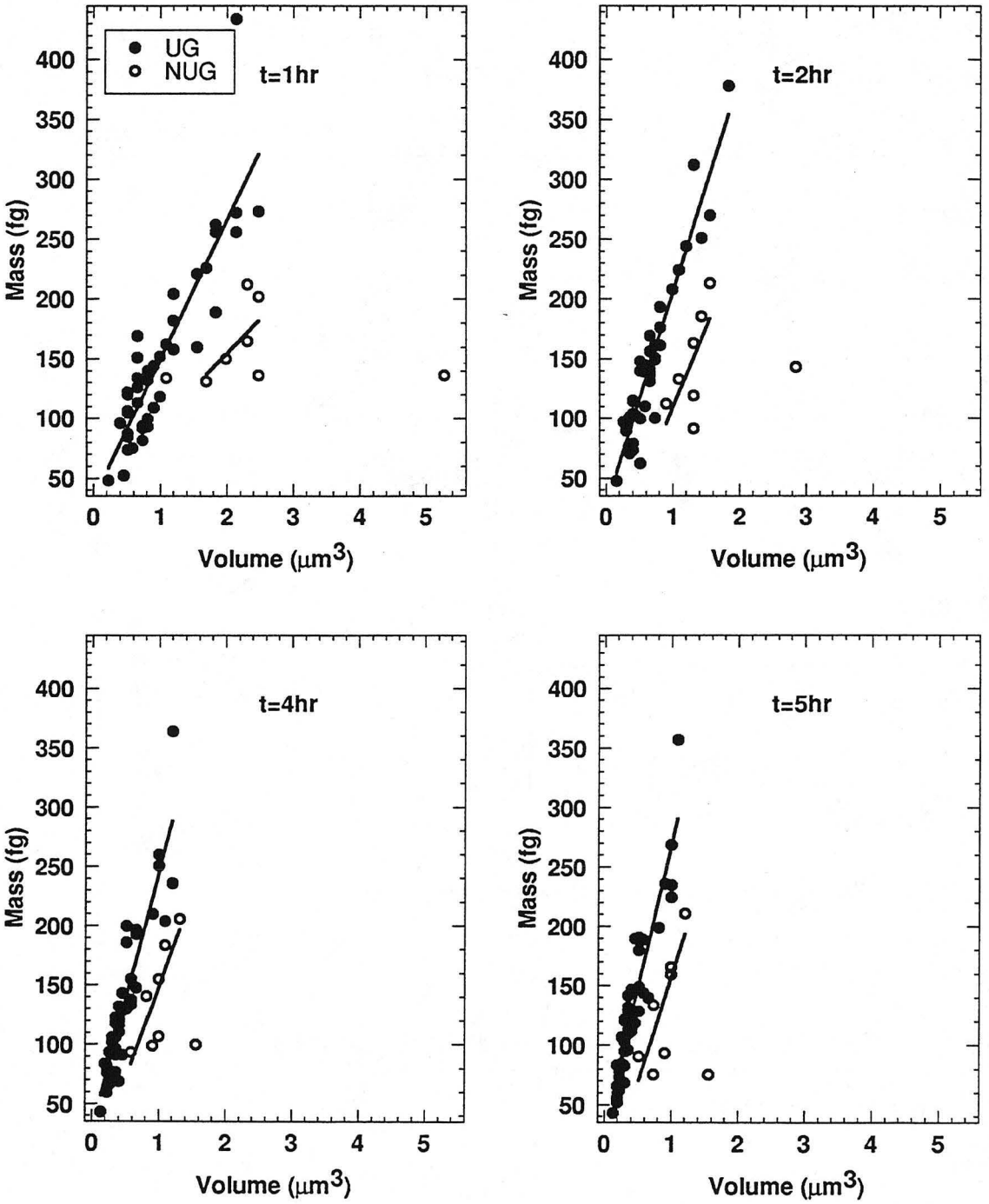

Figure 6.20 Protein mass versus granule volume for both types of granules for four time points (1, 2, 4 and 5hr.) The correlation coefficient and the slope (r,m) for each of the least squares lines are as follows: UG(1hr)=0.86, 140mg/ml; NUG(1hr)=0.57 ($P<0.10$), 80mg/ml; UG(2hr)=0.93, 207mg/ml; NUG(2hr)=0.66($P<0.05$); 114mg/ml; UG(4hr)=0.89, 243mg/ml; NUG(4hr)=0.81($P<0.01$), 142mg/ml; UG(5hr)=0.91, 284mg/ml; NUG(5hr)=0.82 ($P<0.01$), 154mg/ml - ($P << 0.01$ for UG granules at all time points). The least squares fit through the NUG granules does not include the point from the granules with the largest diameter value.

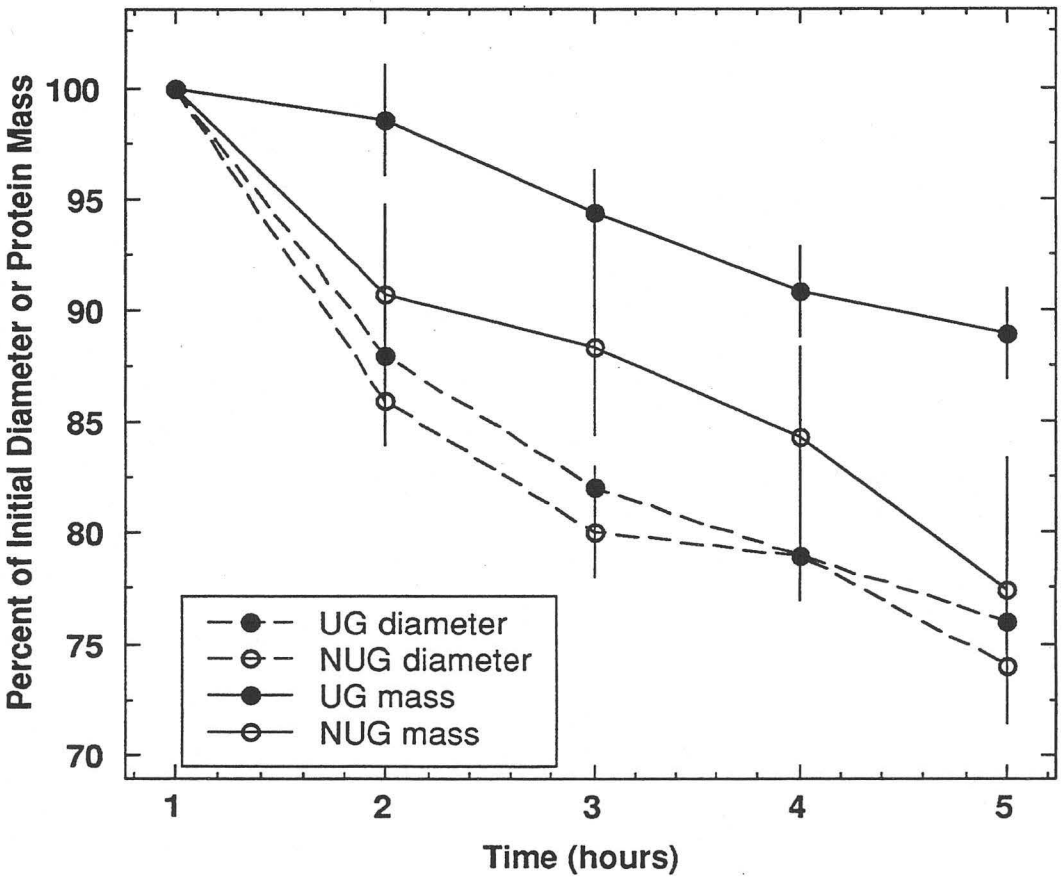

Figure 6.21. The percent protein mass and diameter loss for both types of granules from the June control experiment. Error bars are ± s.e.m.

December Control

We consider the results from the December and the June control experiments separately for two reasons. The first is that, because of a beam dump just as we were beginning the December experiment, the granules were at room temperature for 2 hours before we were able to begin imaging. Therefore, the initial time period is really "2" as opposed to "1." As we have seen, however, the delayed starting time only changes the initial characteristics of the population. The second reason is that there was also a slight flow of solution through the LBL-WC during the experiment. We had been experiencing evaporation problems and the constant flow alleviated this problem. Because we were circulating the suspending solution internally , including other granules in suspension, and not introducing a new solution into the LBL-WC, we still considered this a control experiment (that is, one in which the environmental conditions were not changed).

Table 6.5 shows the diameter, protein concentration and mass data for 15 granules over the time course. The granules were observed in 5 different fields from two different granule preparations; all of the images were taken with 18.8nm pixel sizes. The data from UG and NUG granules are reported separately as well as combined. From the table we can see that in this small sample, NUG granules represent 33% of the total population. They were not significantly different from UG granules in diameter for any of the time points ($P>0.05$, t test) although protein concentration differed. The UG granules are ~1.5 times as concentrated as the NUG granules for all of the time points. Both types of granules were observed to decrease in diameter and protein mass over time, although protein concentration increased. A notation is made on the chart when particular characteristics are not shown to be statistically significantly different between either the two groups of granules at a particular time point, or between the time points for a particular type of granule (UG or NUG).

Table 6.5. Results from the December control experiment. Values with the same letters are not significantly different (P>0.05, t test).

		Diameter (μm) average ± (s.e.m.)	Protein Concentration (mg/ml) average ± (s.e.m.)	Protein Mass (fg) average ± (s.e.m.)
Uniform				
(N=10)	**t=2hr**	0.80 ± 0.05	385 ± 25	106 ± 18
	t=3hr	0.73 ± 0.04	435 ± 21	93 ± 16[f]
	t=4hr	0.71 ± 0.04	465 ± 22[c]	92 ± 15[f]
	t=5hr	0.69 ± 0.04	447 ±28[c]	83 ± 14
Non-Uniform				
(N=5)	**t=2hr**	1.06 ± 0.10[a]	251 ± 23[d]	166 ± 41[g]
	t=3hr	0.97 ± 0.09[a,b]	262 ± 27[d]	147 ± 49[g,h]
	t=4hr	0.94 ± 0.08[b]	293 ± 27[e]	140 ± 40[h,i]
	t=5hr	0.90 ± 0.09	313 ± 26[e]	130 ± 35[i]
All				
(N=15)	**t=2hr**	0.88 ± 0.06	340 ± 25	126 ± 19
	t=3hr	0.81 ± 0.05	378 ± 27	111 ± 20
	t=4hr	0.79 ± 0.05	408 ± 27	108 ± 17
	t=5hr	0.76 ± 0.05	403 ± 26	99 ± 15

Diameter

The distribution of diameter for initial and final time points for the UG granules is shown in figure 6.22. The NUG granules are not shown because only 5 were examined. They ranged in value from 0.79-1.28μm for the initial time point to 0.66-1.13μm for the final time point. The UG granules diameter ranged from 0.55-1.09μm for the initial time point to 0.53-0.92μm for the final time point. No difference in variance of the diameter was observed (P>0.05, F test) between the time points.

Protein Concentration

The distribution of protein concentration for initial and final time points for UG granules is shown in figure 6.23. The NUG granules are again not shown. They ranged from 169-307mg/ml for the initial time point to 240-403mg/ml for the final time points. The NUG protein concentration in this population is relatively high as compared to the

General Population. The UG granules ranged in protein concentration from 313-535mg/ml for the initial time point to 324-656mg/ml for the final time point. The variance in these values was not significantly different (P>0.05, F test) between the time points. On average, protein concentration increased by a factor of 1.2. We can see from the figure that the initial distribution of protein concentration shifted to a distribution around a higher value. The NUG granules also became more concentrated by a factor of 1.2 over the time course.

A plot of protein mass versus granule volume is shown in figure 6.24. All of the time points for both populations of granules are shown on this graph as well as two lines with slopes that represent protein concentration values of 100 and 600 mg/ml. We do not see the distinction between NUG and UG granule distributions which was apparent in the June control experiment. This is because the protein concentration values of UG and NUG granules were initially more similar than in the June experiment.

Protein Mass and Diameter Change

Protein mass and diameter loss for both types of granules over time is shown in figure 6.25. The UG granules decreased in diameter to 88 ± 3% of the initial value and the NUG granules to 85 ± 4% over the 4 hours in which they were studied. This is a diameter loss rate of ~5%/hr for both granule types. The UG granules decreased in mass to 79 ± 4.5% of the initial value and the NUG granules to 79 ± 8.5% over the 4 hours. This is a mass loss rate of ~7.5%/hr and ~12.5%/hr, respectively.

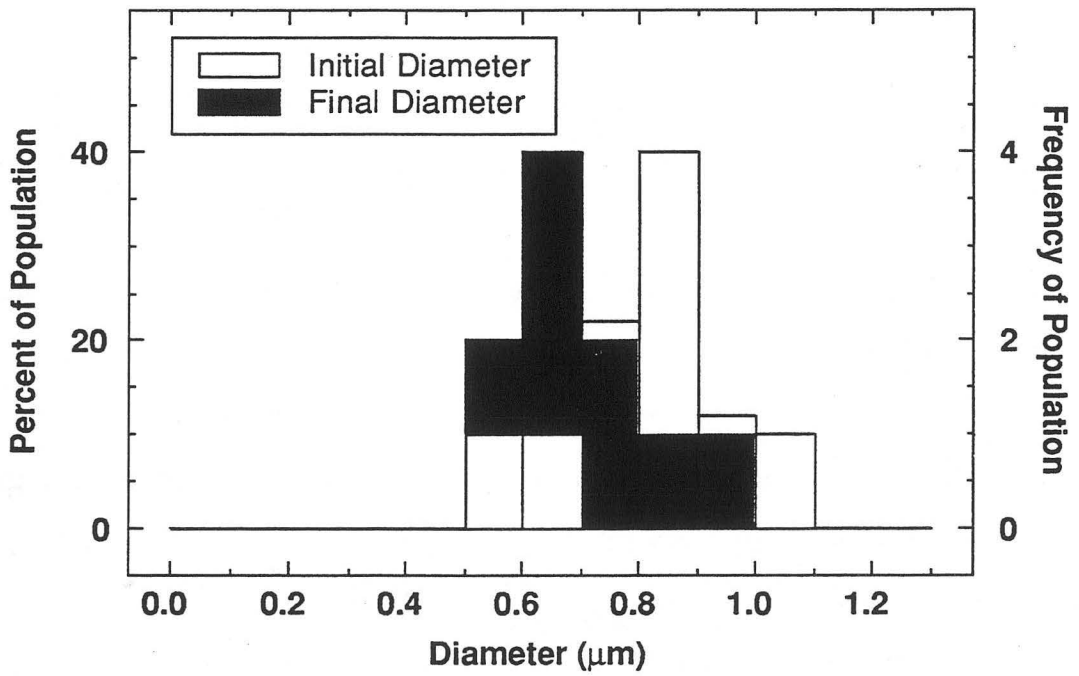

Figure 6.22 The diameter distribution for UG granules from the December control experiment for initial and final time points. The distribution shifted from an average diameter of 0.80 ± 0.05μm (± s.e.m.) to 0.69 ±0.04μm.

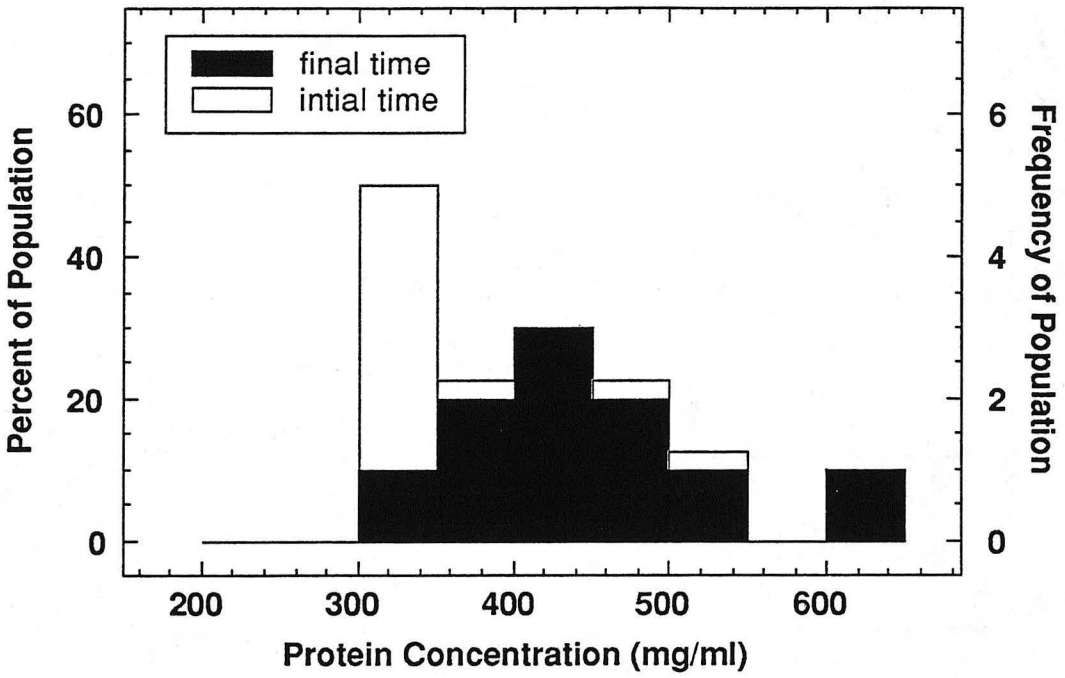

Figure 6.23 Protein concentration distribution for the UG granules from the December control for the initial and final time points. The distributions shifted from an average value of 385 ± 25mg/ml to 447 ± 28mg/ml. Over time there was a major decrease in the number of granules originally in the lowest protein concentration bin.

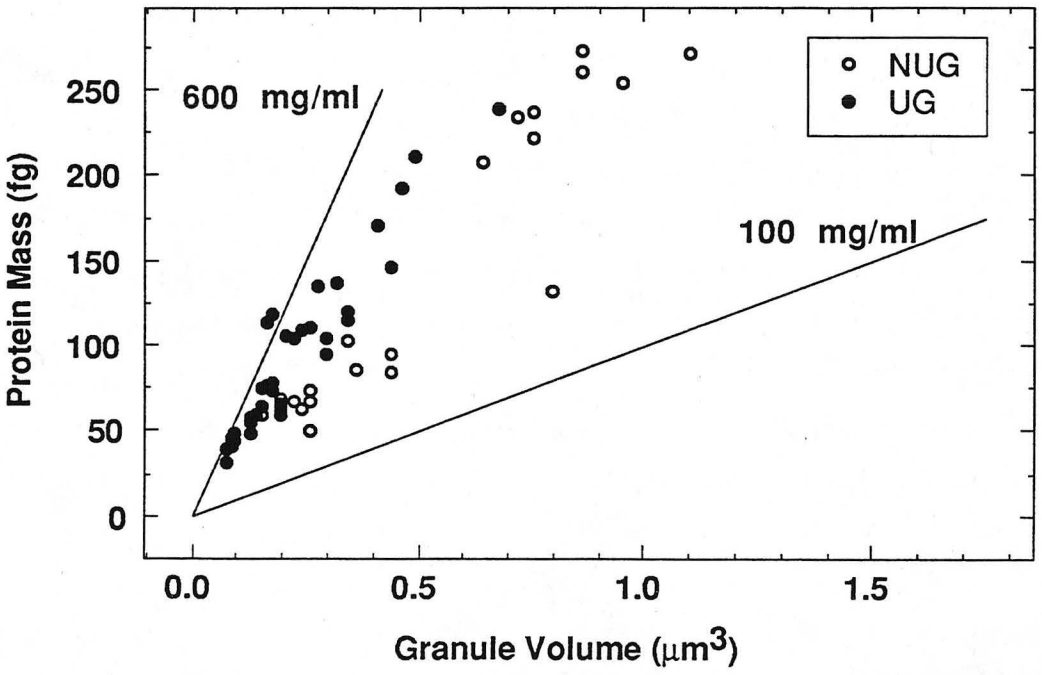

Figure 6.24 The protein mass versus the granule volume for both types of granules for all of the time points.

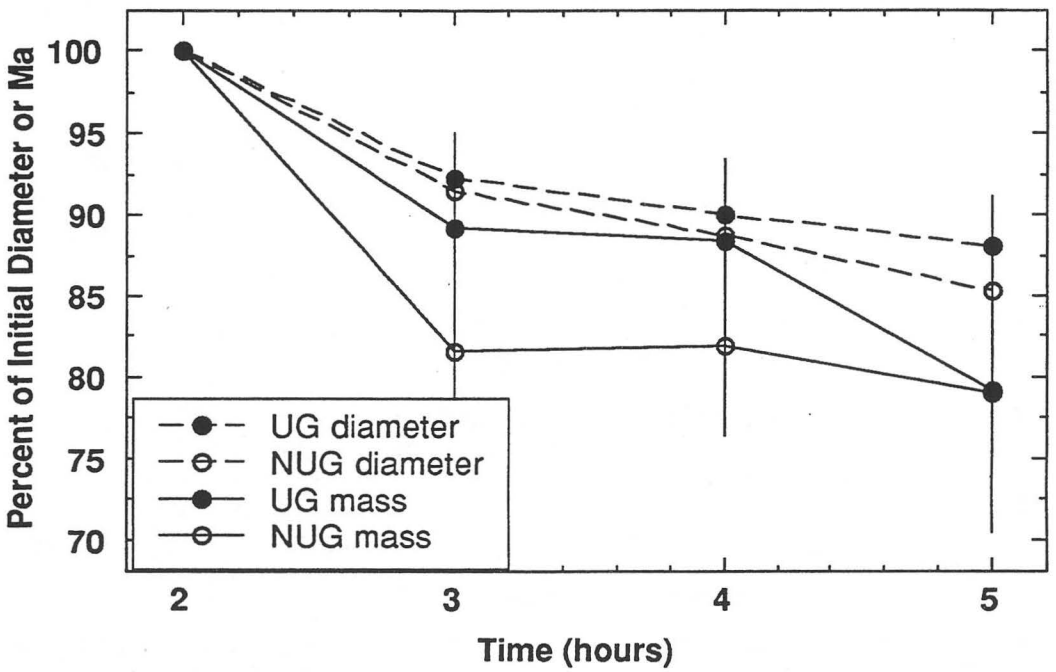

Figure 6.25 The percent protein mass and diameter loss for the UG granules over the time course for the December control experiment. The error bars are ± s.e.m.

VI.2.2c Summary of Control Experiments

The results of the control experiments confirm that zymogen granules release their enclosed protein into an isosmotic solution without the occurrence of lysis. Additionally, we observed that the granules changed in diameter and protein concentration over time.

This was first shown in the fixation experiment by observing that the characteristics of diameter and protein mass for populations of suspended, isolated granules - changed as a function of the amount of time the granules were held at room temperature. If protein was not released from individual granules then the population characteristics of the granules we observed in STXM would be the same no matter how long the granules were maintained at room temperature. From this experiment, we also saw that the protein that was released into solution was probably taken up by other granules in the population since the average protein mass of the UG granules increased for the different time points. However, because each time point in this experiment was from a different population of granules (although from the same initial preparation) we could not say for certain that particular individual granules took up or released protein .

However, in the fresh granule experiments, where we were able to observe individual granules over time, we see that on average, the granules in the May, June and December experiments lost protein over time. If we look at each granule individually in the June-control (data not shown), all NUG granules decreased in protein content over time whereas, some UG granules show an increase in protein mass. This confirms the observation from the fixed experiment that some granules take up protein released by other granules.

The low rate of protein release from the June-control experiment is similar to that measured using other techniques (Liebow and Rothman, 1976; Rothman, 1972). This small rate of release confirms that the granules are in a semi-equilibrium state with protein in the suspending solution and as we mentioned above, some granules are even

taking up protein. That the December control experiment shows a higher mass loss rate even though they too were suspended in the initial isolation solution, is because the suspending solution was circulated within the LBL-WC and the granules were not in a constant environment. The large mass loss rate from the May control experiment (~40% of the initial mass was lost) is also a result of the flow of the solution. At this time however, we were using pressurized gas to flow solutions through the LBL-WC. The flow rates were much greater than with the peristaltic pump, which was used in all other experiments, and as a result, the mass loss rate was higher. The difference between UG and NUG protein loss rate will be discussed in the summary of the next section.

In both June and December control experiments, protein concentration of both types of granules increased over the time course, even as the granules lost protein. The May control experiments did not show this same phenomenon, perhaps as a result of the large mass loss associated with the flow of solution during this experiment. In general, as we will see in other experiments, zymogen granules increase in protein concentration as they release protein. The distribution of protein concentration for the population in each experiment are easily visualized in the protein mass versus granule volume graph. We saw that, as compared to the General Population, the distributions for the June and December control experiments were relatively tight and this is a result of the fact that we used only one or two preparations of zymogen granules for these experiments. As the average protein concentration increased over time for these granule populations, the distribution remained tight and the relationship between protein mass and granule volume was maintained regardless of protein loss (or gain) or diameter loss. A discussion of this observation and diameter loss for all the experiments is given in the Discussion and Conclusion chapter (VIII).

VI.2.2 Dilute Isosmotic and Different Osmolarity Solutions

The experiments in this section were performed in order to observe the effects of dilution of the original suspension of granules as well as dilution plus an increase or decrease in the osmolarity of the suspending solution, on the diameter, protein mass and concentration of the granules. In this sense, dilution refers to increasing the volume of suspending solution to granule number and was accomplished by perfusion of a solution of isosmotic 0.3M sucrose, pH 6.0past the granules after an initial image. This solution displaced the original suspension medium already in the LBL-WC and established an essentially infinite reservoir of isosmotic solution to the granules that were already adhered to the silicon nitride windows. To increase osmolarity, a solution of 0.6M sucrose (pH 6.0) was used and to decrease osmolarity, water (pH 6.0) was used. Previous experiments have suggested that the granules do not behave as typical osmometers, i.e. like red blood cells that swell and lyse when suspended in water, or that shrink proportionately under osmotic stress in hyperosmotic solutions. Instead, they seem to be "osmotically inactive," although they do lose some of their protein content over time (Burwen and Rothman, 1972). After each type of solution was perifused through the LBL-WC (isosmotic, hyperosmotic and hyposmotic), the same fields of granules examined initially were re-imaged over time and changes in their diameter, protein concentration and mass were noted.

VI.2.2a 0.3 M Sucrose - Isosmotic Solution

As discussed in Chapter I, according to the equilibrium theory of protein release from granules (Rothman, 1975), protein efflux should increase in response to an increase in the protein concentration gradient across the granule membrane. From the previous chapter, we observed that protein loss from granules suspended in the original isolation solution was ~ 2.8%/hour (for UG granules, averaged over the entire observation time). In the isosmotic experiment we expect the rate of protein loss to increase because released

protein in the suspending solution is removed by perfusion maximizing the concentration gradient from the granules to the medium.

Table 6.6 shows the diameter, protein concentration and mass for 18 granules over the time course. These granules came from two different preparations and four different fields, the pixel size was 58.6nm for each image. All of the granules were initially identified as UG granules. The granules were observed to decrease in diameter and protein mass over the time course of the study although the protein concentration values increased. Values in this table compare to those seen for the General Population.

Table 6.6. The results of the dilution in isosmotic solution. All of the granules are of the UG type. The characteristics of the t=1hr time point are from the initial image where the granules are suspended in the original isolation solution. The experimental solution is flowed past the granules after this first time point and the characteristics of the other time points are measured when granules are suspended in this experimental solution. Values with the same letter are not significantly different (P>0.05, t test).

		Diameter (μm) average ± (s.e.m.)	Protein Concentration (mg/ml) average ± (s.e.m.)	Protein Mass (fg) average ± (s.e.m.)
(N=18)	t=1hr	0.93 ± 0.05	337 ± 23[a]	147 ± 24
	t=2hr	0.87 ± 0.05	355 ± 29[a]	126 ± 19
	t=3hr	0.82 ± 0.05	383 ± 30	116 ±19

Diameter

The distribution of diameters for the initial and final time points is shown in figure 6.26. The diameter ranged from 0.64-1.35μm for the initial time point and 0.58-1.35μm for the final time point. Variance in diameter did not change (P>0.05, F test) between the time points.

Protein Concentration

The distribution of protein concentration for initial and final time points are shown in figure 6.27. The granules range in protein concentration from 172-466mg/ml for the

initial time point to 193-557 mg/ml for the final time point. The average value of protein concentration increased over time by a factor of 1.15, somewhat less than observed in the control studies (1.8 and 1.2% for the June and December experiments, respectively). The variance did not change (P>0.05, F test).

A plot of protein mass versus granule volume is shown in figure 6.28. Again all of the data for all of the time points have been plotted together as well as two lines with slopes that represent protein concentrations of 600 and 100 mg/ml. We can see that the relationship between protein mass and granule volume is retained despite protein loss. Although there is substantial scatter in the plot, the average protein concentration did not change very much over time; not even significantly between the 1st and 2nd time point (P>0.05, t test).

Protein Mass and Diameter Change

Protein mass versus diameter loss is shown in figure 6.29. Over the time course, protein mass and diameter decreased. The granules decreased in diameter to 88 ± 1.5% (ave. ± S.E.M) of the initial value; a loss rate in diameter of ~6%/hr. And, the granules decreased in mass to 77 ± 3% of the initial value or a rate of mass loss of ~12%/hr. In this case, the average values of diameter and protein mass were significantly different (P>0.05, t test) between all time points.

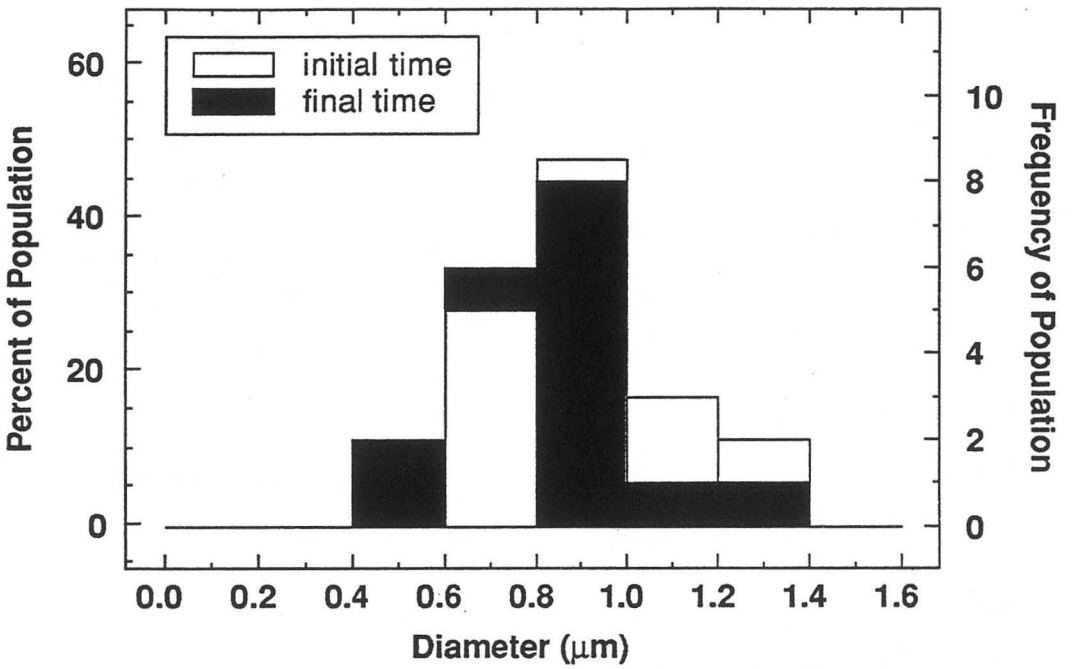

Figure 6.26 The distribution of diameter for initial and final time points for the isosmotic solution experiment. The peak does not change between the time points, although there is a shift towards smaller diameters.

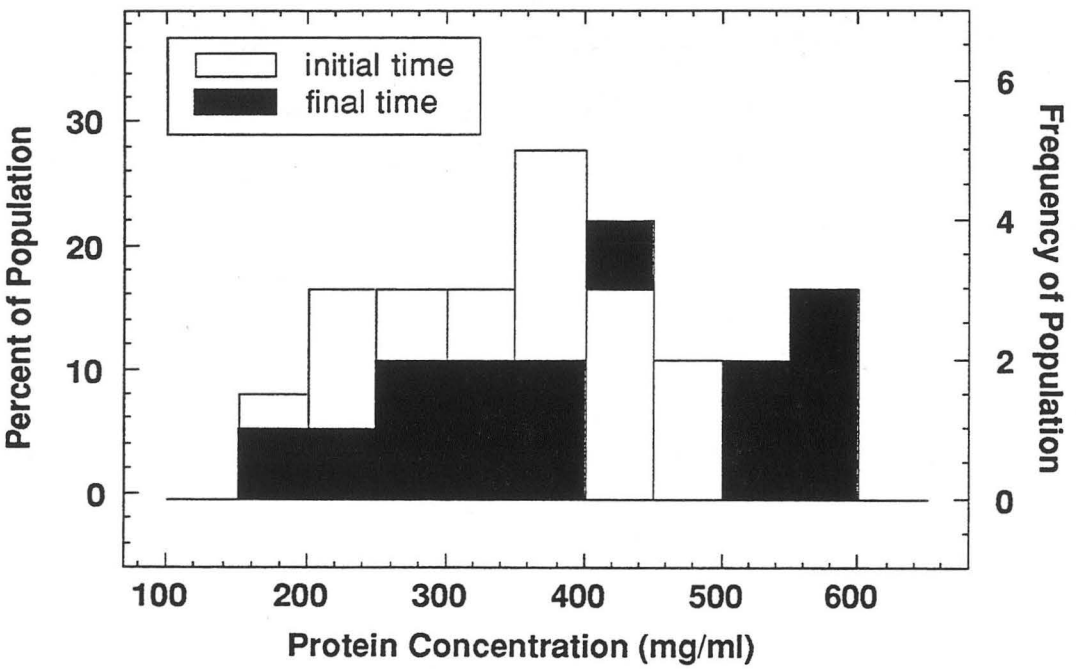

Figure 6.27 The distribution of protein concentration for the initial and final time points for the isosmotic solution experiment. The distribution shifts towards higher protein concentrations.

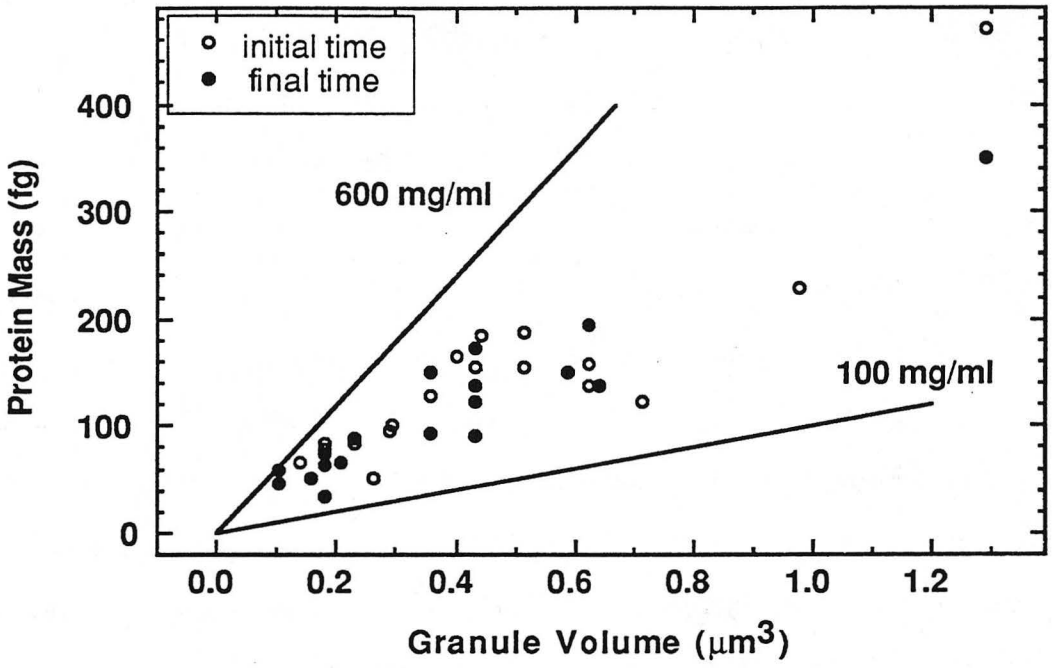

Figure 6.28 Protein mass versus granule volume for the initial and final time points. The relationship between the protein mass and granule volume is maintained between the initial and the final time.

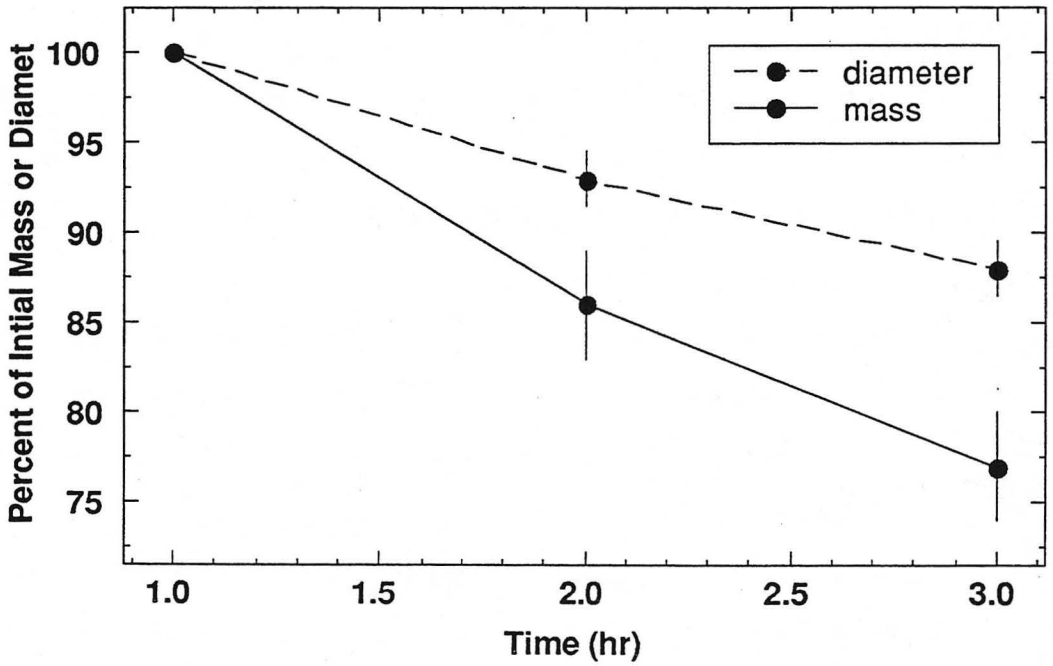

Figure 6.29 Diameter and protein mass loss for the isosmotic solution experiment. Error bars represent ± s.e.m.

VI.2.2b 0.6 M sucrose flow - Hyperosmotic Solution

Table 6.7 shows the diameter, protein concentration and mass data for 18 granules over the time course. These granules came from one preparation and three imaging fields. The pixel size in each field was 39.9nm. The data from the UG and NUG granules are reported separately as well as combined. From the table we can see that NUG granules represent 33% of the population. The NUG granules are larger than UG granules for all of the time points and UG granules are on average twice as concentrated as the NUG granules for all of the time points. Both types of granules were observed to decrease in diameter and protein mass over the time course although protein concentration values generally increased. A notation is made on the chart when particular characteristics are not shown to be statistically significantly different between either the two groups of granules at a particular time point, or between the time points for a particular type of granule (UG or NUG).

Table 6.7. The results from the hyperosmotic solution experiment. The characteristics of the t=1hr time point are from the initial image where the granules are suspended in the original isolation solution. The experimental solution is flowed past the granules after this first time point and the characteristics of all of the other time points are for granules in this solution. Values with the same letter are not significantly different (P>0.05).

		Diameter (μm) average ± (s.e.m.)	Protein Concentration (mg/ml) average ± (s.e.m.)	Protein Mass (fg) average ± (s.e.m.)
Uniform				
(N=12)	**t=1hr**	1.09 ± 0.06	305 ± 21	216 ± 26
	t=2hr	0.93 ± 0.06	383 ± 23[a]	164 ± 20
	t=3hr	0.90 ± 0.06	369 ± 17[a,b]	148 ± 21
	t=4hr	0.87 ± 0.06	378 ± 19[b]	136 ± 19
Non-Uniform				
(N=6)	**t=1hr**	1.36 ± 0.11	156 ± 11[a]	211 ± 38
	t=2hr	1.12 ± 0.11	184 ± 15[a,b]	154 ± 38
	t=3hr	0.98 ± 0.09	179 ± 15[b,c]	100 ± 29[d]
	t=4hr	0.92 ± 0.08	203 ± 10[c]	90 ± 19[d]
All				
(N=18)	**t=1hr**	1.18 ± 0.06	255 ± 22	215 ± 20
	t=2hr	1.00 ± 0.06	316 ± 28	160 ± 18
	t=3hr	0.93 ± 0.05	305 ± 25	132 ± 16
	t=4hr	0.89 ± 0.04	320 ± 24	120 ± 15

Diameter

The distribution of diameters for the initial and final time points for the UG granules is shown in figure 6.30. The NUG granules are not shown because only 6 were examined. They ranged in size from 1.00-1.68μm for the initial time point to 0.68-1.12μm for the final time point. The UG granules ranged in diameter from 0.64-1.48μm for the initial time point to 0.52-1.20μm for the final time point. The variance in diameter did not change (P>0.05, F test).

Protein Concentration

The distribution of protein concentration for initial and final time points for the UG granules is shown in figure 6.31. The NUG granules are not shown, but they ranged in value from 124-186mg/ml for the initial time point to 158-226mg/ml for the final time

point. The UG granules ranged in protein concentration from 171-397mg/ml for the initial time point to 284-529mg/ml for the final time point. The range of protein concentration shifted significantly between the initial and final time points. Both populations of granules became more concentrated over time; the UG granules increased in protein concentration on average by a factor of 1.2 and the NUG granules by a factor of 1.3.

A plot of the protein mass versus the granule volume is shown in figure 6.32. All of the time points for both populations of granules are shown on this graph. We can see that both types of granules show distinct distributions. The protein concentration values for both populations did not change dramatically between time points and, as we can see in Table 6.7, there was no significant change in the values ($P>0.05$, t test) between any of the time points for the NUG granules, although the values did increase overall from the initial to the final period for both UG and NUG granules.

Protein Mass and Diameter Change

Protein mass and diameter loss for both types of granules are shown in figure 6.33. The UG granules decreased in diameter to $82 \pm 2\%$ of the initial value and NUG granules to $77 \pm 1.5\%$ over the 3 hours of study. This is a diameter loss of ~4%/hr and ~8%/hr, respectively. The UG granules decreased in mass to $62 \pm 4\%$ of the initial values and NUG granules to $42 \pm 3.5\%$ over the 3 hours. This is a mass loss rate of ~13%/hr and ~19%/hr, respectively.

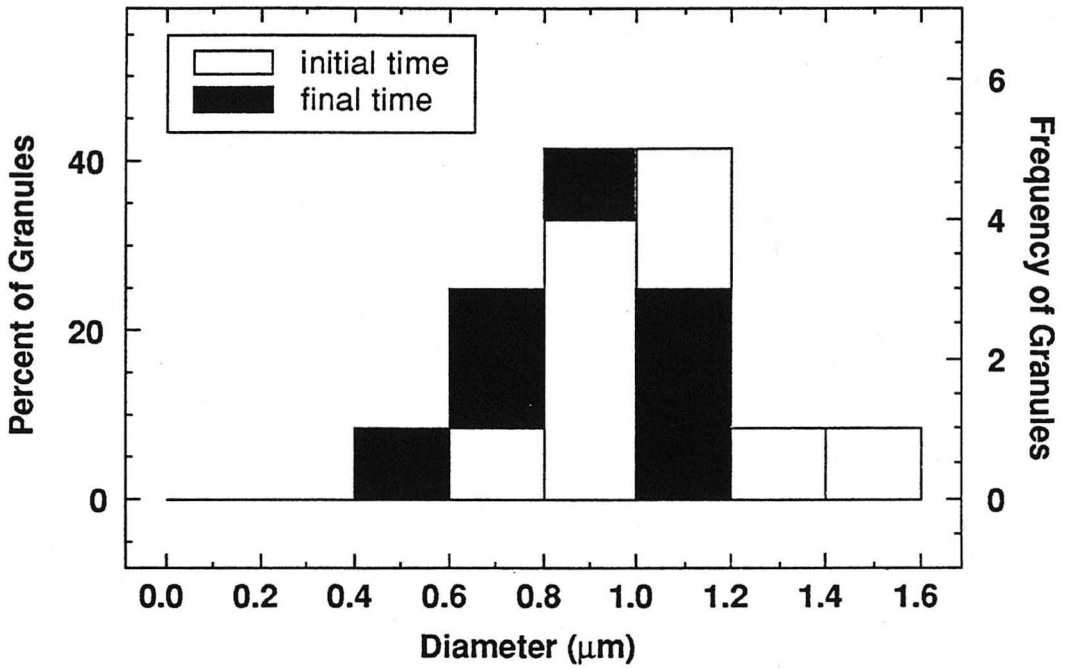

Figure 6.30 The distribution of granule diameter values for initial and final time points for the hyperosmotic solution experiment. The peak of the distribution shifts from 1.1μm at the initial time point to 0.9μm for the final time point.

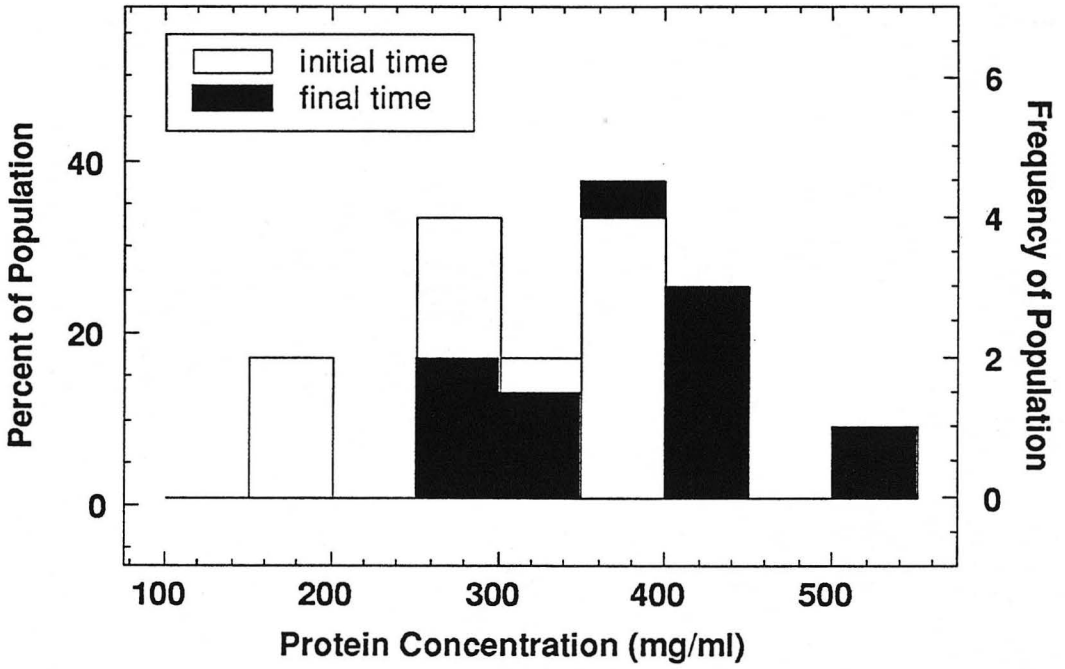

Figure 6.31 The distribution of protein concentration for initial and final time points for the hyperosmotic solution experiment. The distribution shifts to higher protein concentration over time.

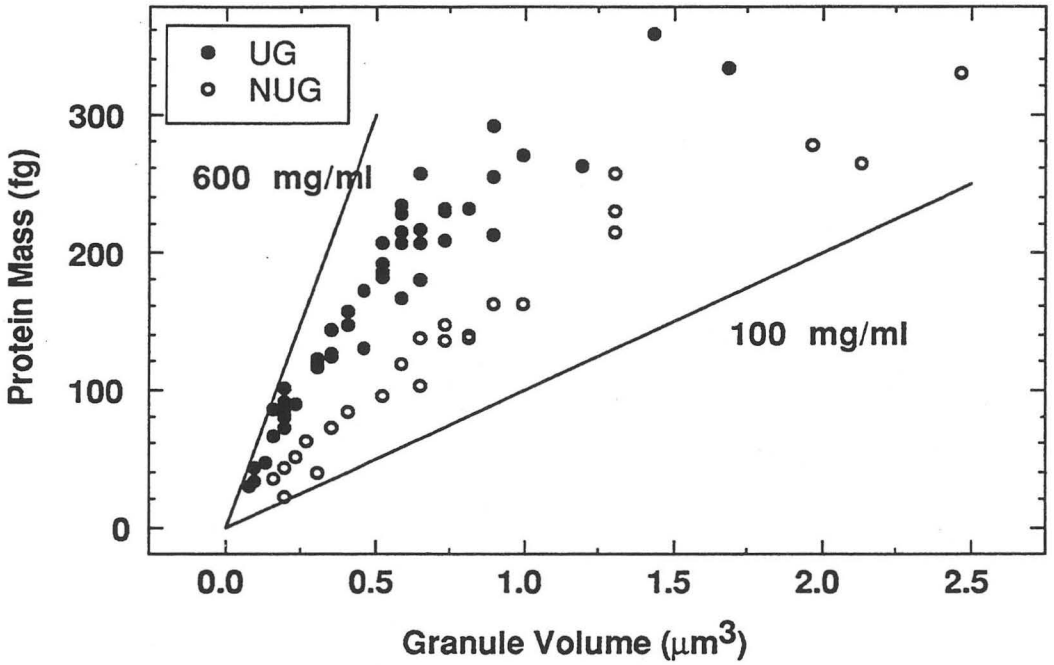

Figure 6.32 Protein mass versus granule volume for both types of granules for all of the time points. The relationship between protein mass and granule volume is different for the UG and the NUG granules and this relationship stays constant for the respective granules over the time course.

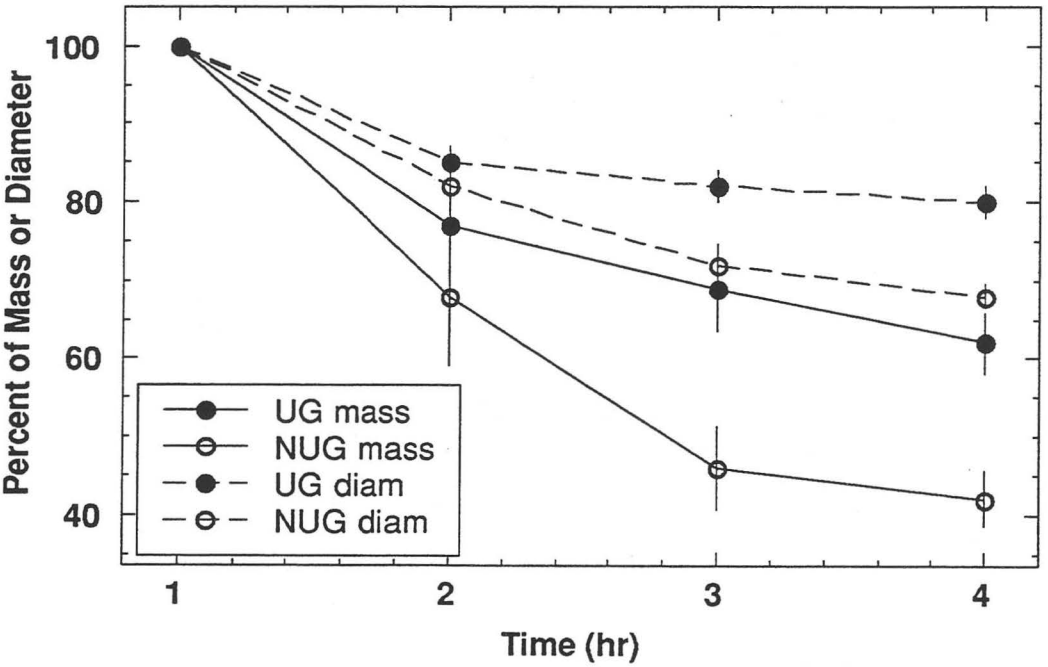

Figure 6.33 The protein mass and diameter loss curves for both types of granules for the hyperosmotic solution experiment. Error bars are ± s.e.m.

VI.2.2c Water - Hyposmotic Solution

This data set consists of 61 granules observed in 2 different fields from the same granule preparation once every hour over a period of 3 hours after the initial image. The pixel size was 63.3nm. The fields are shown in figures 6.34 and 6.35. We did not observe any lysis during the experiment and all of the granules that were in the initial field can be accounted for in the final field.

Table 6.8 shows diameter, protein concentration and mass data for the 61 granules over the time course. The data from the UG and NUG granules are reported separately as well as combined. From the table we can see that NUG granules represented 13% of the total population. They were not significantly different than the UG granules in diameter values for any of the time points ($P>0.05$, t test). Both populations were different in their protein concentration. Initially the UG granules were 2.2 times more concentrated that the NUG granules, but unlike the previous experiments, this factor did not stay constant and by the final time point the UG granules were only 1.6 times more concentrated because the final concentration of UG granules decreased. Both types of granules decreased in diameter and protein mass over the time course. The NUG granules increased in protein concentration, but the UG granules initially decreased in protein concentration after the immediate exposure to water and then slowly increased. A notation is made on the chart when particular characteristics are not shown to be statistically significantly different between either the two groups of granules at a particular time point, or between the time points for a particular type of granule (UG or NUG).

Table 6.8 The results from hyposmotic solution experiment. The characteristics of the t=1hr time point are from the initial image where the granules are suspended in the original isolation solution. The experimental solution is flowed past the granules after this first time point and the characteristics of the other time points are measured when granules are suspended in this experimental solution. Values with the same letter are not significantly different (P>0.05)

		Diameter (μm) average ± (s.e.m.)	Protein Concentration (mg/ml) average ± (s.e.m.)	Protein Mass (fg) average ± (s.e.m.)
Uniform				
(N=53)	**t=1hr**	0.93 ± 0.02	430 ± 10	183 ± 9
	t=2hr	0.87 ± 0.02	352 ± 12	129 ± 7
	t=3hr	0.82 ± 0.02	380 ± 12[c]	117 ± 7
	t=4hr	0.78 ± 0.02	391 ± 13[c]	104 ± 6
Non-Uniform				
(N=8)	**t=1hr**	1.00 ± 0.07[a]	195 ± 16[d]	109 ± 19
	t=2hr	0.94 ± 0.07[a]	202 ± 16[d]	91 ± 15[f]
	t=3hr	0.86 ± 0.06[b]	247 ± 26[e]	79 ± 11[f]
	t=4hr	0.82 ± 0.06[b]	251 ± 24[e]	71 ± 11
All				
(N=61)	**t=1hr**	0.94 ± 0.02	399 ± 14	173 ± 68
	t=2hr	0.88 ± 0.02	332 ± 13	124 ± 7
	t=3hr	0.83 ± 0.02	362 ± 13	112 ± 6
	t=4hr	0.79 ± 0.02	372 ± 13	100 ± 6

Diameter

The distribution of diameters for the initial and final time points for the UG granules is shown in figure 6.36. The NUG granules are not shown because only 8 were examined. They ranged from 0.76-1.39μm for the initial time point to 0.63-1.14μm for the final time point. The UG granules range in diameter values from 0.70-1.20μm for the initial time point to 0.51-1.08μm for the final time point.

Protein Concentration

The distribution of protein concentration for initial and final time points for the UG granules is shown in figure 6.37. The NUG granules are not shown. They ranged in value from 139-246mg/ml for the initial time point to 149-326mg/ml for the final time points.

The UG granules range in protein concentration values from 266-684mg/ml for the initial time point to 224-680mg/ml for the final time point. The protein concentration of the UG granules decreased by 20% after the first exposure to water and then gradually increased to 90% of the original value. Although, between the 3rd and 4th time point, there is no significant difference in the values ($P>0.05$, t test). We can see from figure 6.36 that the protein concentration distribution remains compact over time.

Protein mass versus granule volume plots are shown in figure 6.38 for each of the time points and for both types of granules. We can see that in the first time point, the UG and NUG granules show distinct distributions. But, as time goes on, even though the relationship between protein mass and granule volume is maintained, the two distributions merge. This is because the UG granules become less concentrated and the NUG granules become more concentrated.

Protein Mass and Diameter Change

The protein mass and diameter loss over time for both types of granules is shown in figure 6.39. Overall, UG granules decreased in diameter to 85 ± 1.5% of the initial value and NUG granules to 81 ± 3% over the 3 hours of study. This is a diameter loss of ~5.5%/hr for both types of granules. The UG granules decreased in mass to 58 ± 2.5% of the initial values and NUG granules to 68 ± 4.5% over the 3 hours. This translates to a mass loss of ~17%/hr and ~10%/hr, respectively.

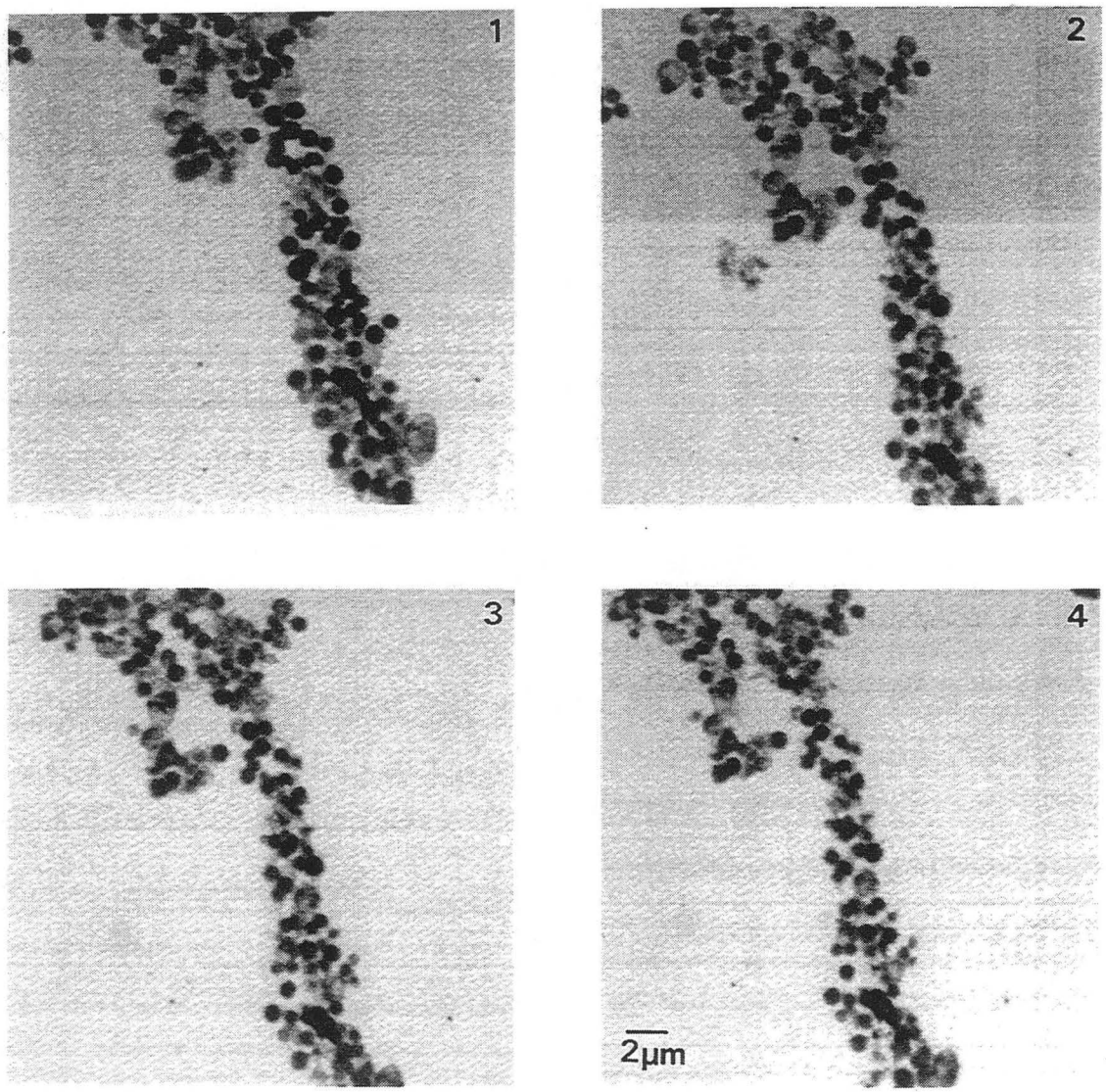

Figure 6.34 STXM images of all of the time points for the first field of granules in the water experiment. All of the granules that were present in the initial image can be found in the final image. The pixel size was 63.3nm.

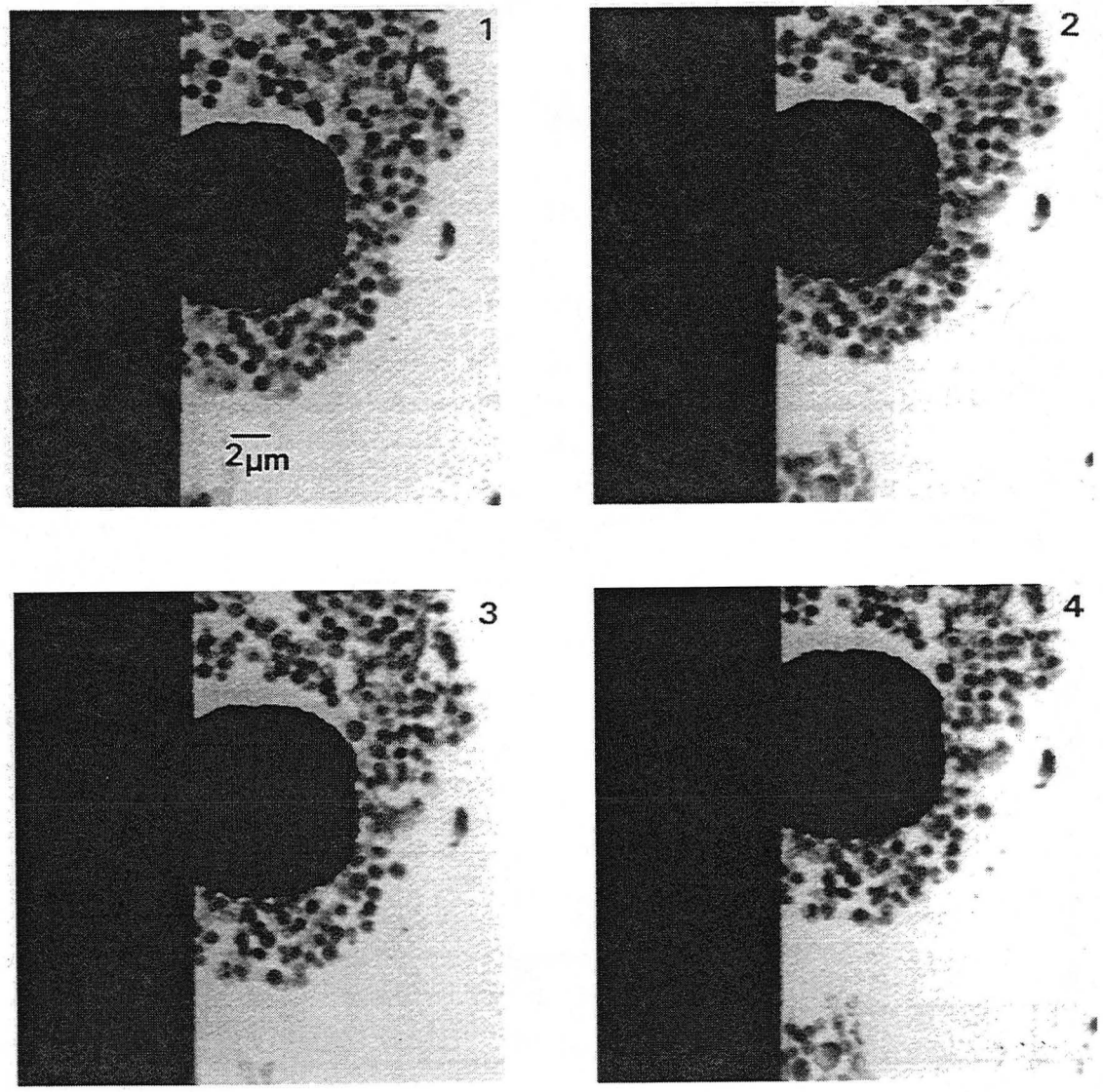

Figure 6.35 STXM images of all of the time points for the second field of granules in the water experiment. All of the granules that were present in the initial image can be found in the final image. The pixel size was 63.3nm.

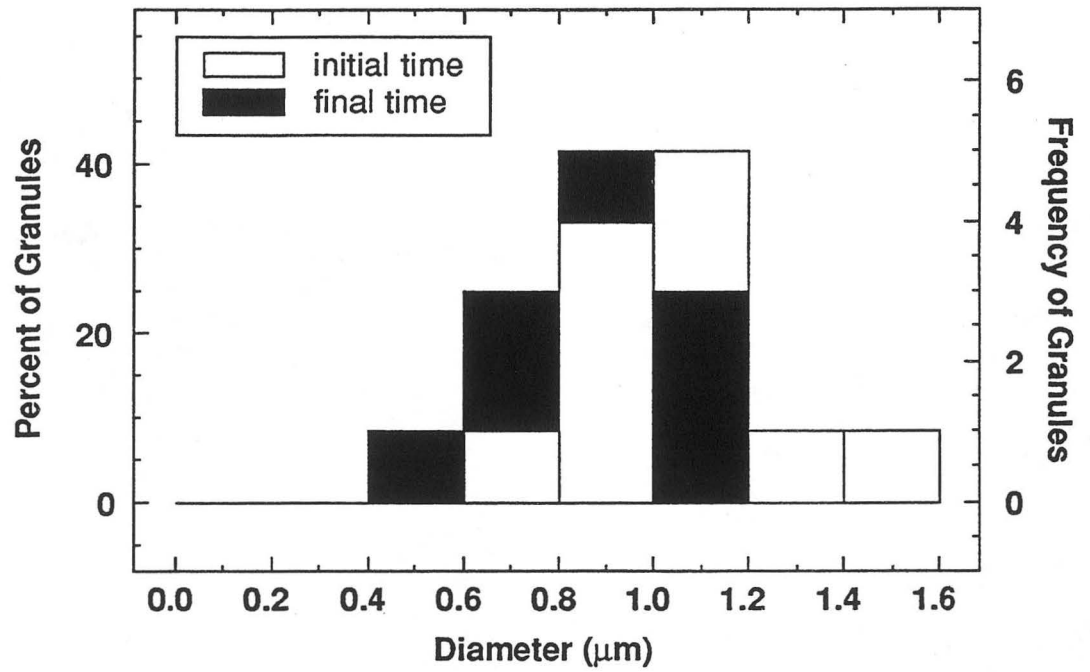

Figure 6.36 The distribution of diameters for UG granules in the hyposmotic solution experiment for initial and final time points. The distribution shifts to smaller diameter values over the time course.

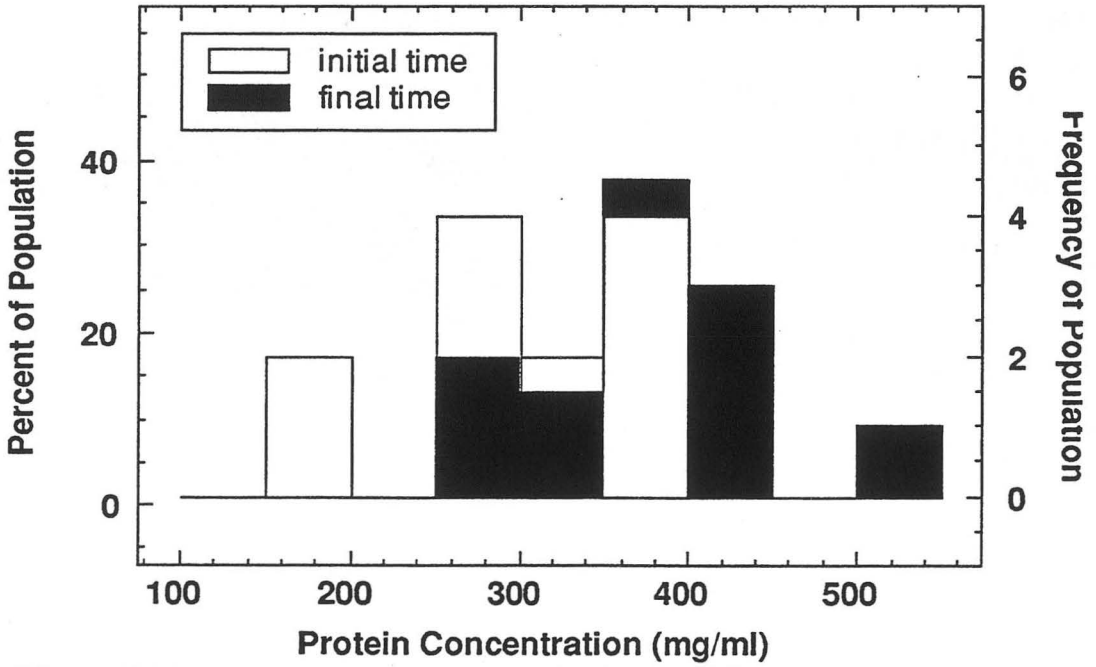

Figure 6.37 Protein concentration distribution for UG granules from the hyposmotic solution experiment the initial and final time points. In this case, the distribution shifts to lower protein concentration values over the time course. This is the only experiment in which we observe a drop in protein concentration.

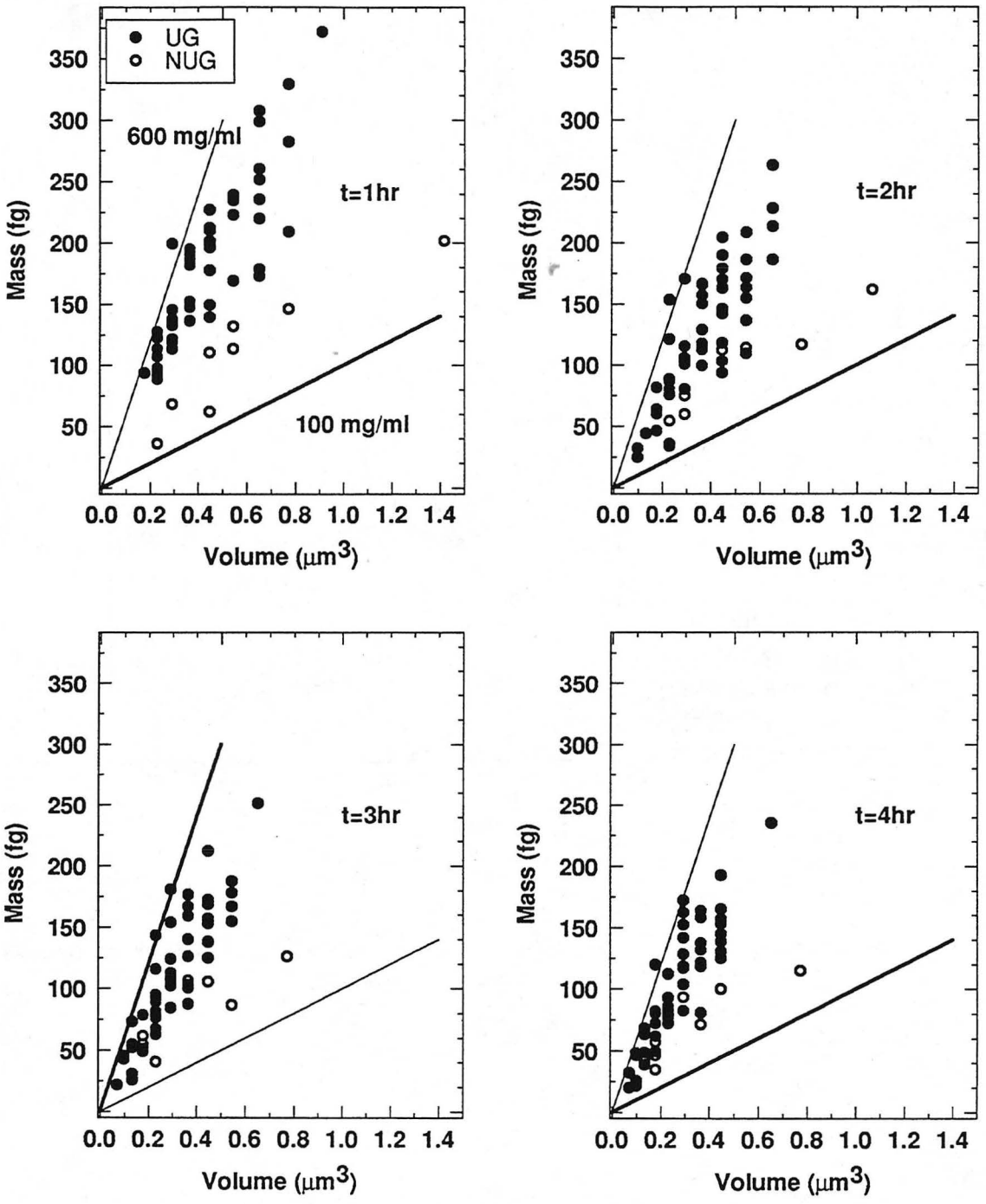

Figure 6.38 Plot of protein mass versus granule volume for all of the time points and both types of granules. In the first graph (time 1) we see that the distributions of UG and NUG granules are separate, but by the final graph, these distributions tend to merge. This is a result of the UG granules becoming less concentrated and the NUG granules becoming more concentrated.

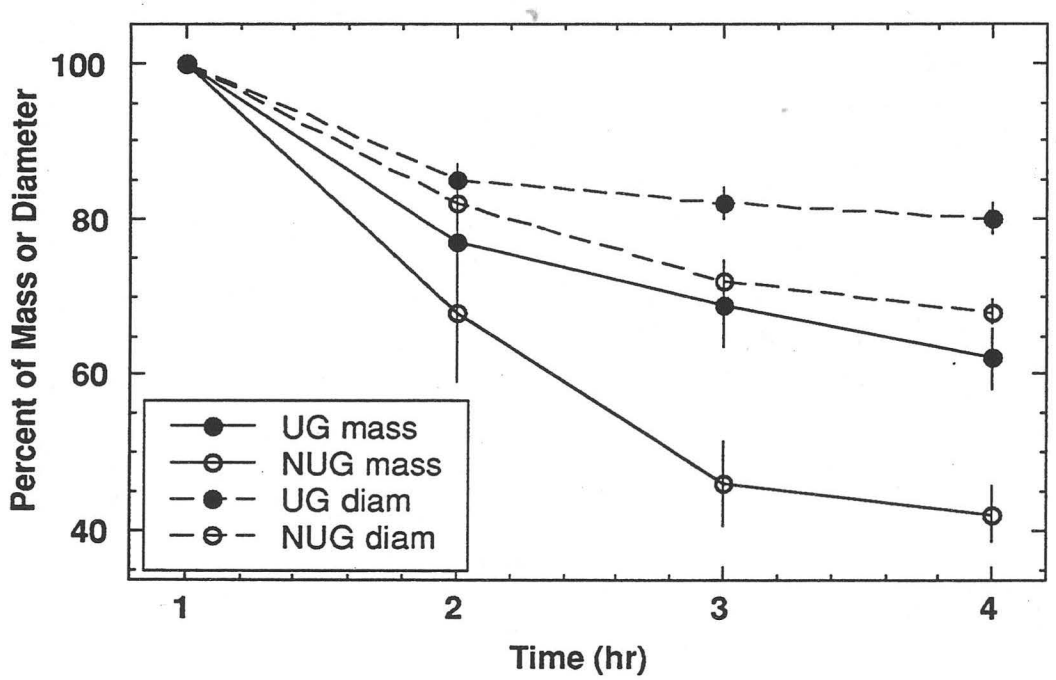

Figure 6.39 Diameter and protein mass loss for both types of granules over the time course for the hyposmotic solution experiment. The error bars are ± s.e.m.

VI.2.2d Summary of Dilution and Osmotic Experiments

The results from these experiments confirm that the rate of release of protein from isolated zymogen granules is affected by the nature of the suspending solution. By perifusing isosmotic, hyperosmotic or hyposmotic solutions past an initial field of granules, we observed that the rate of release of protein from these granules increased above that of the control experiments; e.g. no perfusion.

In order to compare these experiments to the controls, the results are compiled in Table 6.9 below. Both the initial rate of protein loss (the percent of the initial mass that the population of granules lost between the first and second image, when perfusion occurred) and the subsequent rate of protein loss (the average percent of mass lost per hour over the remainder of the experiment) are shown for UG and NUG granules from each experiment presented so far.

Table 6.9 The protein mass loss rates for the experiments we performed on isolated granules using STXM. The initial mass loss is the percent of the initial mass that the population of granules lost between the first and second image. The "subsequent" mass loss rate is rate at which the granules continued to lose protein after the second image and until the end of the time period of the study. Values shown are the averages for the population.

Experiment	UG granules		NUG granules	
	Initial mass loss	"Subsequent" mass loss rate	Initial mass loss	"Subsequent" mass loss rate
June-control	1.5%	3.0%/hr	9.2%	4.8%/hr
Dec.-control	10.7%	5.6%/hr	18.4%	0.5%/hr
Isosmotic (0.3M sucrose)	14.0%	10.3%/hr	---	---
Hyperosmotic (0.6M sucrose)	23.0%	9.4%/hr	31.7%	17.8%/hr
Hyposmotic (water)	29.2%	8.8%/hr	13.9%	10.2%/hr

From the table, we can see that perfusing isosmotic solution past the granules results in a higher initial rate of protein loss (UG-14.0%) than no perfusion (June-control; UG-1.5%). We can also see that circulating the suspending solution (December-control) has a

similar affect on the rate of release of protein as perfusion (10.7 versus 14% respectively, for UG granules). It would appear that the rate of release of protein from the granules is enhanced by exchanging the solution surrounding the granules. This result is expected as granules have been shown to release a greater proportion of their contents in response to an increase in the volume of the suspending solution (Liebow and Rothman, 1972). As both perifusion (or circulation) and a volume increase effectively decrease the concentration of protein released from other granules, it is apparent that the rate of release of protein from the granules is affect by local protein gradients.

The rate of protein loss was also affected by an increase in the osmolarity of the suspending solution. By perfusing a hyperosmotic solution (0.6M sucrose), the initial rate of protein release (23.0% for UG granules) was observed to increase over the isosmotic experiment (14.0% for UG granules). This was probably the result of "solvent drag." In other words, water that left the granule due to the osmotic forces carried with it protein in solution.

However, in the hyposmotic experiment, the increase in the rate of protein loss over the isosmotic experiment (29.2 versus 14%, respectively for UG granules) cannot be accounted for by solvent drag as water would enter the granule. In this case, water may have caused the release of protein from the internal aggregate by affecting its binding properties and therefore, more protein was able to be released from the granule. In this experiment, there was a possibility that we would have observed the granules swell as water entered the granules as the protein concentration within the granules was higher than outside. However, the fact that we did not observe this phenomenon indicates that protein in solution, which would contribute to an increase in the osmolarity of the granule interior, must quickly leave the granule and any remaining protein would remain in an aggregated form. The rate of protein release we observed in this experiment was similar to that measured by Hokin (1955) under similar circumstances.

In all of the experiments, except the hyposmotic, NUG granules lost a greater percentage of their protein than UG granules. This result is probably due to the fact that more protein is in solution within NUG granules than in UG granules, where it is primarily held in an aggregated form. As solubilized protein can more readily leave the granule, we would expect to observe a greater rate of protein release from NUG granules, even though, on average, they contain similar amounts of protein to UG granules. That this observation is reversed in the hyposmotic experiment is probably a result the water causing a partial dissolution of the aggregate in UG granules, as mentioned above, producing a greater percentage of solubilized protein.

In all likelihood, the above explanation accounts for the observed decrease in protein concentration for the hyposmotic (and the May control) experiment. This initially high rate of protein release without a simultaneous decrease in diameter, as observed in the hyperosmotic experiment, results in a decrease in the measured protein concentration. In all of the other experiments, the concentration increases over time. This increase in protein concentration and the observed changes in diameter will be discussed further in the Discussion and Conclusions Chapter (VIII).

VI.2.3 Triton X-100

In the Triton X-100 experiments, an initial image of a field of granules was taken and then a solution of either 0.025% or 0.5% Triton X-100 in 0.3M sucrose (pH 6.0) was flowed through the LBL-WC. The granules were then observed over a period of time and changes in their diameter, protein concentration and mass were noted. We were interested in how the changes in diameter, protein concentration and mass of granules were affected when granules were exposed to detergent at both a low concentration (0.025%) and a concentration that is known to solubilize the enclosing membrane of the granule. Unfortunately, we cannot show quantitative results for the 0.5% Triton-X experiment because, after the initial image, when the detergent solution was flowed past the granules, there were no granules left to image a second time. There were, what appeared to be, remnants of granules; clumps of indistinguishable biological material. We can conclude from this result that this concentration of detergent caused the dissolution of the granules because we know from other studies on populations of granules that the detergent causes the complete release of granule contents almost immediately, although it cannot be excluded that intact granules were released from the SiN windows by the detergent and were no longer visible.

Table 6.10 shows the diameter, protein concentration and mass data for 9 granules over the time course. All of the granules came from the same preparation and were imaged in three separate fields. The images had different pixel sizes, either 30.5 or 58.6nm. All except one granule was identified as an UG granule. The granules were observed to decrease in diameter and protein mass over time, although again protein concentration increased.

Table 6.10. Results from the 0.025% Triton X-100 experiment. The characteristics of the t=1hr time point are from the initial image where the granules are suspended in the original isolation solution. The experimental solution is flowed past the granules after this first time point and the characteristics of the other time points are measured when granules are suspended in this experimental solution. Values with same letter are not significantly different (P>0.05, t test).

		Diameter (μm) average ± (s.e.m.)	Protein Concentration (mg/ml) average ± (s.e.m.)	Protein Mass (fg) average ± (s.e.m.)
Uniform				
(N=9)	**t=1hr**	0.94 ± 0.05[a]	291 ± 30	126 ± 19
	t=3hr	0.80 ± 0.05[a]	362 ± 25[b]	99 ± 15
	t=4hr	0.75 ± 0.05	364 ± 23[b]	83 ± 12
Non-Uniform				
(N=1)	**t=1hr**	1.04	115	70
	t=3hr	0.92	146	59
	t=4hr	0.82	173	51
All				
(N=10)	**t=1hr**	0.95 ± 0.05	271 ± 34	119 ± 19
	t=3hr	0.81 ± 0.05	338 ± 33	95 ± 15
	t=4hr	0.76 ± 0.05	343 ± 30	80 ± 12

Protein Concentration

The UG granules ranged in protein concentration from 178-425mg/ml at the initial time point to 278-468mg/ml at the end of the study. On average they increased in protein concentration by a factor of 1.2. Although this increase took place between the 1st and the 3rd time point because there is no significant difference between the protein concentration values between 3rd and last time point (P>0.05, t test)

Figure 6.39 shows the plot of protein mass versus granule volume for all of the time points. The lone NUG granule is shown also. We can see that Triton X-100 at this concentration does not seem to affect the relationship although the variability of the data is somewhat greater than control and other experiments.

Protein Mass and Diameter Change

Protein mass and diameter loss for both types of granules are shown in figure 6.40. The UG granules decreased in diameter to 81 ± 2% of the initial value over the 3 hours of study. This is a diameter loss rate of ~9.5%/hr. The uniform granules decreased in mass to 70 ± 7% of the initial value. This translates to a rate of mass loss ~18%/hr.

Summary

The initial and subsequent rates of protein loss in the 0.025% Triton X-100 experiment are not significantly different from the rates we observed in the isosmotic 0.3M sucrose experiment (P>0.05, t test). As the 0.025% Triton X-100 is also in a 0.3M sucrose solution and we can conclude that at this concentration, the detergent is not sufficient to affect the permeability of the membrane of the granule and change the rate of protein release. It would have been interesting to try a detergent concentration between the two concentrations of 0.025 and 0.05%, however we did not have the opportunity.

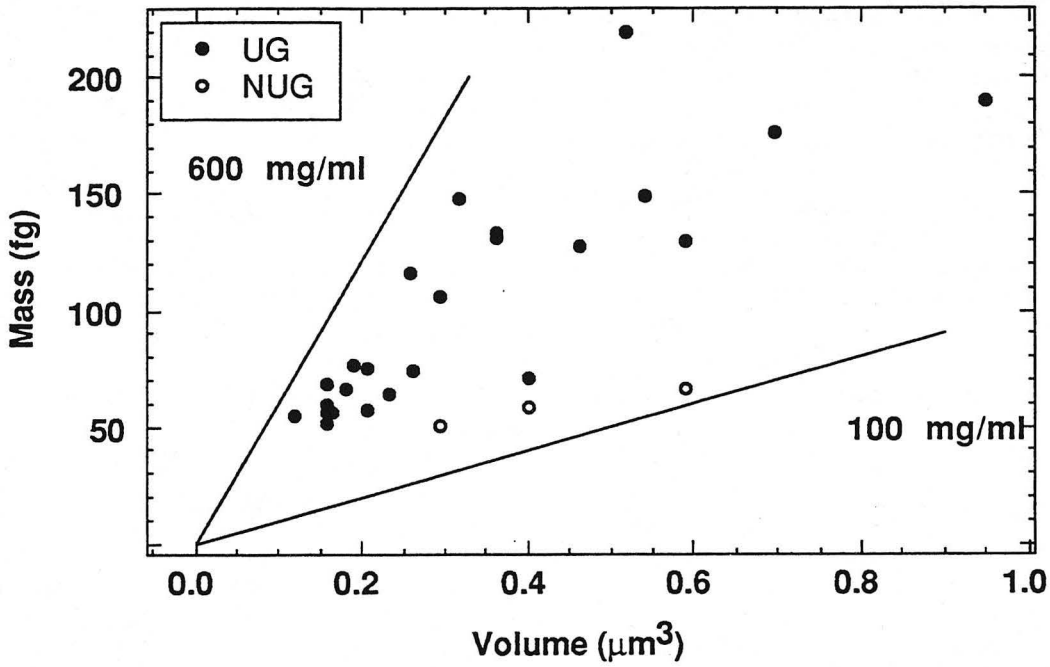

Figure 6.40 Protein mass is plotted against granule volume for all of the time points for both the UG and the lone NUG granule. The NUG granule show a correlation between protein mass and granule volume over the time course. The UG granules appear more variable in this experiment.

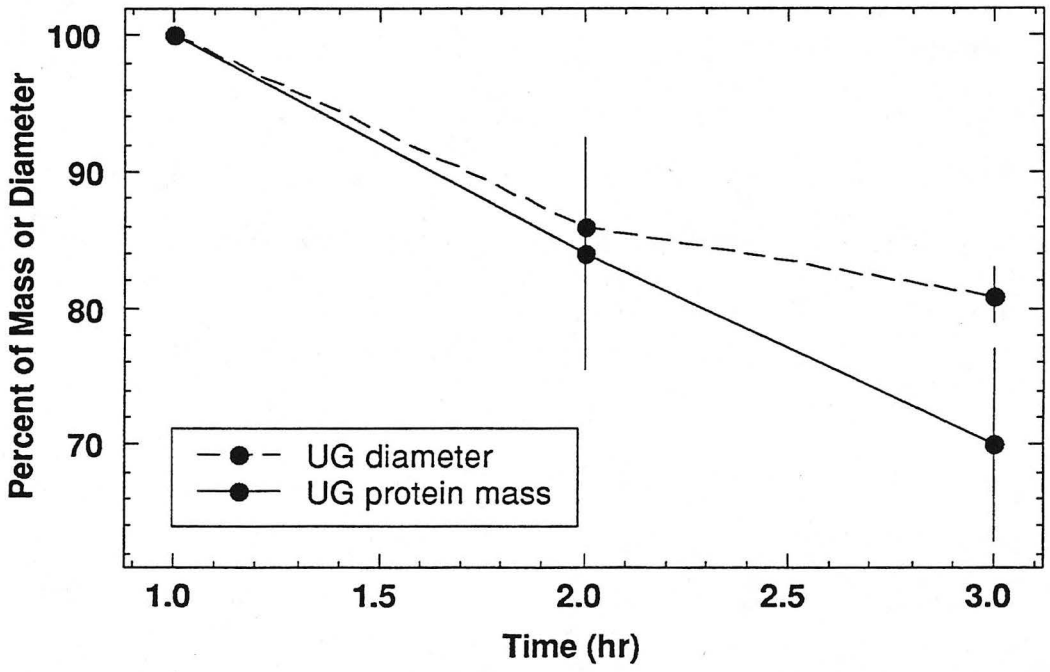

Figure 6.41 The percent loss of protein mass and diameter for the UG granules over the time course of the 0.025% Triton X-100 experiment. Error bars are ± s.e.m.

VI.2.4 Protein Uptake

All of the experiments in section VI.2&3 were designed to promote the release of protein from granules. We were interested in whether this was reversible and if the granules would take up protein if the concentration in the suspending solution was high enough. Re-uptake of chymotrypsinogen and total protein has been shown by Liebow and Rothman in granule suspensions (Liebow and Rothman, 1972, 1978). We chose to study only chymotrypsinogen, one of the 20 proteins contained within the granule. In these experiments, an initial image of a field of granules was taken and then a solution of either 50mg/ml or 250mg/ml α-chymotrypsinogen (bovine, Sigma) in 0.3M sucrose (pH 6.0) flowed into the LBL-WC. The granules were then observed over a period of time and the changes in their diameter, protein concentration and mass were noted.

VI.2.4a 50 mg/ml Chymotrypsinogen

Table 6.11 shows the diameter, protein concentration and mass data for 19 granules over the time course. These granules came from the same preparation and were imaged in two fields both of which had a pixel size of 58.6nm. All of the granules were identified as UG type. The granules decreased in diameter and increased in protein concentration until the 3rd time point, at which point they no longer changed significantly ($P>0.05$, t test). Protein mass decreased initially after the introduction of the 50mg/ml chymotrypsinogen, but remained unchanged for the remainder of the study.

Table 6.11 The results from the 50 mg/ml chymotrypsinogen experiment. The characteristics of the t=1hr time point are from the initial image where the granules are suspended in the original isolation solution. The experimental solution is flowed past the granules after this first time point and the characteristics of all of the other time points are measured when granules are suspended in this experimental solution. Values with the same letter are not significantly different (P>0.05, t test)

		Diameter (μm) average ± (s.e.m.)	Protein Conc. (mg/ml) average ± (s.e.m.)	Protein Mass (fg) average ± (s.e.m.)
(N=19)	t=1	1.05 ± 0.05	183 ± 13	104 ± 10
	t=2	0.85 ± 0.04	252 ± 16	84 ± 10[d]
	t=3	0.81 ± 0.04[a]	292 ± 19[c]	84 ± 10[d]
	t=4	0.80 ± 0.05[a,b]	299 ± 14[c]	84 ± 10[d]
	t=5	0.79 ± 0.04[b]	306 ± 16[c]	82 ± 10[d]

Diameter

A histogram of initial and final diameters for these granules is shown in figure 6.42. They ranged in diameter from 0.59-1.46μm for the initial time point to 0.47-1.00μm for the final time point. As can be seen in the figure, there is quite a substantial shift in the range of diameter values between the initial and final time point towards smaller sizes. In other words, the final time point does not have the same distribution of large diameter values as the initial time point

Protein Concentration

A histogram of protein concentration for the initial and final time points is shown in figure 6.43. The granules ranged in protein concentration from 93-348mg/ml at 1hr. to 193-440mg/ml at t=5hr. The change in concentration occurred mainly between the 1st and 2nd time point (a factor of 1.4) and did not change significantly at all between the 3rd & 5th time points.

Figure 6.44 shows protein mass versus granule volume for the initial and final time points. We can see that for both time points, the relationship between protein mass and granule volume holds, but suspension in 50mg/ml chymotrypsinogen increases the slope of the function or the average protein concentration in the granules.

Protein Mass and Diameter Change

Protein mass and diameter loss is shown in figure 6.45. The decrease in diameter was 76 ± 1.5% of the initial value over the 4 hours. This is a diameter reduction of ~6%/hr. The decrease in mass was 79 ± 4% of the initial value or a mass loss of ~5%/hr. Although, as mentioned before, most of the loss in both protein mass and diameter occurred between the 1st and 2nd time points.

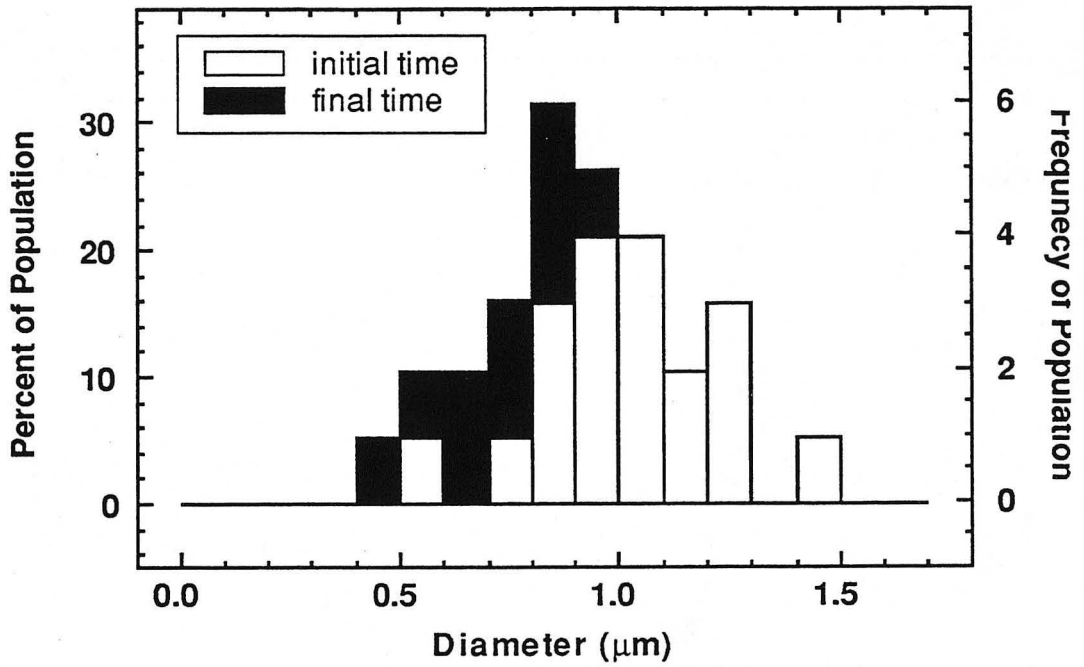

Figure 6.42 The diameter distribution for the 50mg/ml chymotrypsinogen experiment for initial and final time points. The final time point distribution is truncated in that there are no granules with diameters larger than 1micron. In the original distribution, 50% of the granules had diameters greater than 1micron.

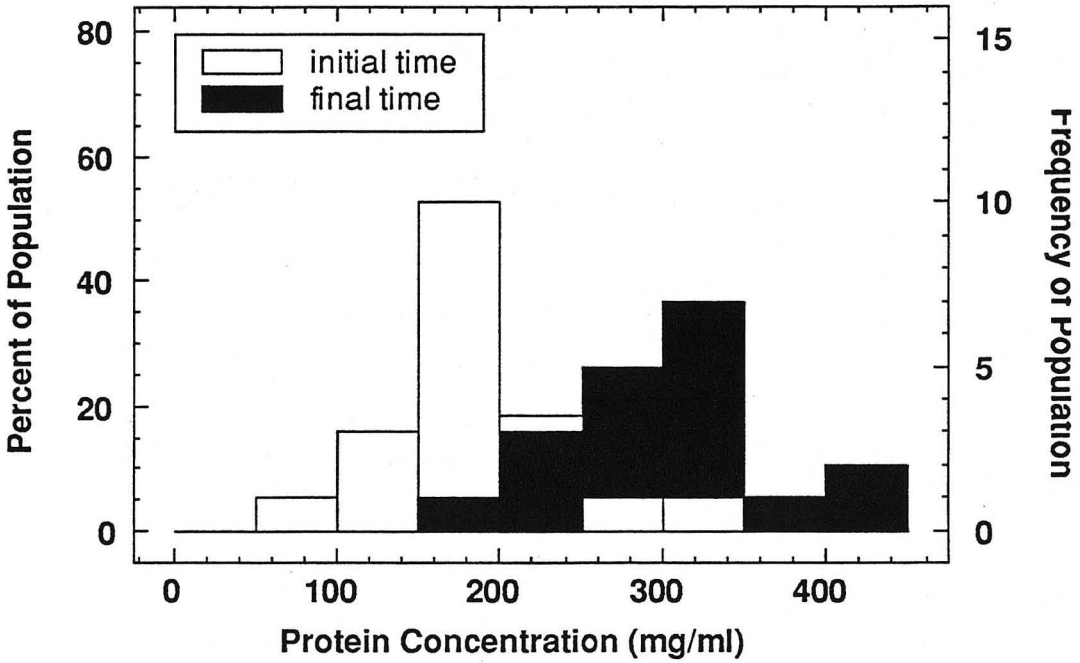

Figure 6.43 The protein concentration distribution for the 50mg/ml chymotrypsinogen experiment for initial and final time points. In the initial distribution less than 30% of the granules had a protein concentration greater than 200 mg/ml, but in the final distribution 95% of the granules had concentrations greater than 200 mg/ml.

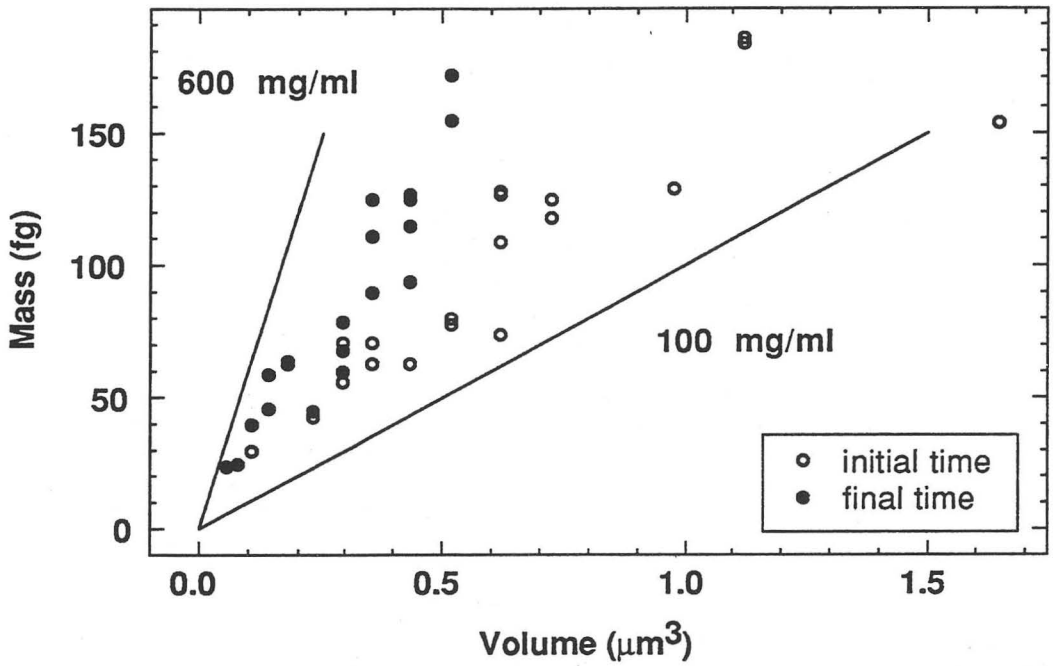

Figure 6.44 Protein mass versus granule volumes for initial and final time points for the 50mg/ml chymotrypsinogen experiment. While the relationship between the two variables holds for both time points, the distribution has shifted to higher concentrations at the end of the study.

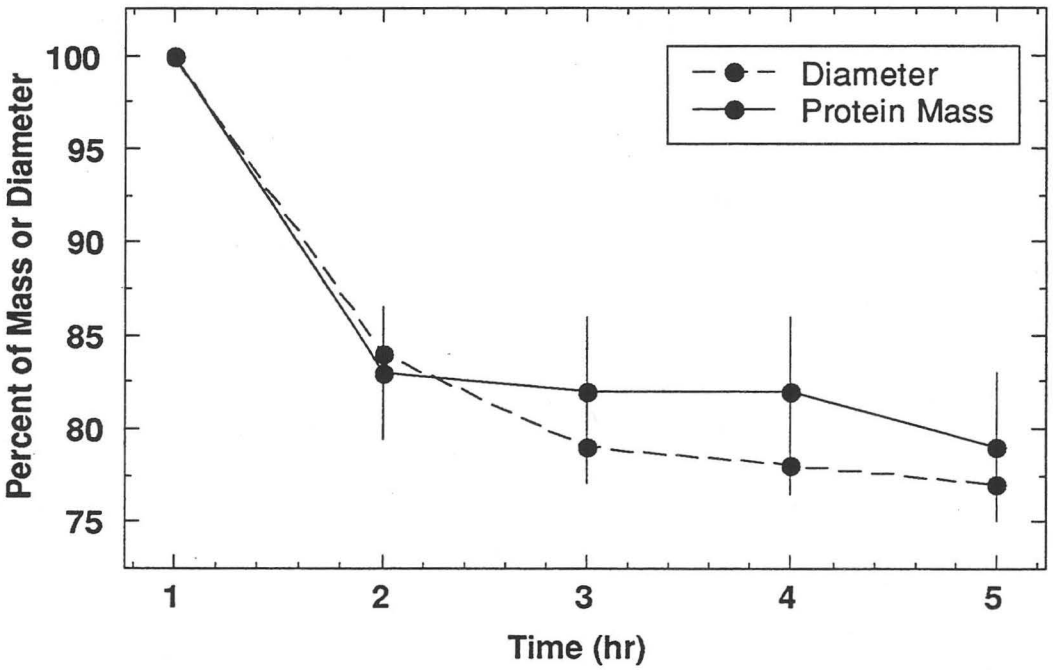

Figure 6.45 The protein mass and diameter loss curves for the 50mg/ml chymotrypsinogen experiment. Error bars are ± s.e.m.

VI.2.4b 250 mg/ml Chymotrypsinogen

In these experiments we increased the concentration of chymotrypsinogen in solution to 250 mg/ml. Table 6.12 shows the diameter, protein concentration and mass data for 35 granules taken from 3 different preparations and 7 different fields. The pixel size in all of the fields was 58.6nm. In the first experiment, oct22, the granules increased in protein mass and diameter, although there was an overall decrease in protein concentration. In the second experiment, oct28, granules increased in both diameter and protein mass while protein concentration stayed relatively unchanged. In a third experiment (apr), an increase in mass is again observed but there was a decrease in the diameter and an *increase* in protein concentration.

Table 6.12 250 mg/ml chymotrypsinogen. Results from three different experiments. The characteristics of the t=1hr time point are from the initial image where the granules are suspended in the original isolation solution. The experimental solution is flowed past the granules after this first time point and the characteristics of all of the other time points are measured when granules are suspended in this experimental solution. Values with the same letter are not significantly different (P>0.05, t test)

		Diameter (μm) average ± (s.e.m.)	**Protein Concentration (mg/ml)** average ± (s.e.m.)	**Protein Mass (fg)** average ± (s.e.m.)
oct 22	**t=1**	0.87 ± 0.05	175 ± 14	67 ± 12
(N=13)	**t=2**	1.30 ± 0.10	58 ± 4	86 ± 17
oct 26	**t=1**	1.09 ± 0.08	223 ± 35[b]	158 ± 32
(N=6)	**t=2**	1.36 ± 0.13	240 ± 14[b]	332 ± 68
	t=3	1.30 ± 0.11	226 ± 11[b]	278 ± 56
apr	**t=1**	1.20 ± 0.07	186 ± 14	167 ± 18[d]
(N=16)	**t=2**	1.04 ± 0.05[a]	283 ± 17[c]	177 ± 21[d]
	t=3	1.07 ± 0.05[a]	312 ± 24[c]	217 ± 28

Figure 6.46 shows the protein mass versus granule volume for all of the granules for all of the time points. We can see that the general relationship again holds regardless of protein mass gain, diameter loss/gain or protein concentration loss/gain. The only points not grouped with the others are from the second time point in the oct22 experiment.

These granules decreased in protein concentration by a factor of 3 (Table 6.12) and therefore show a different distribution.

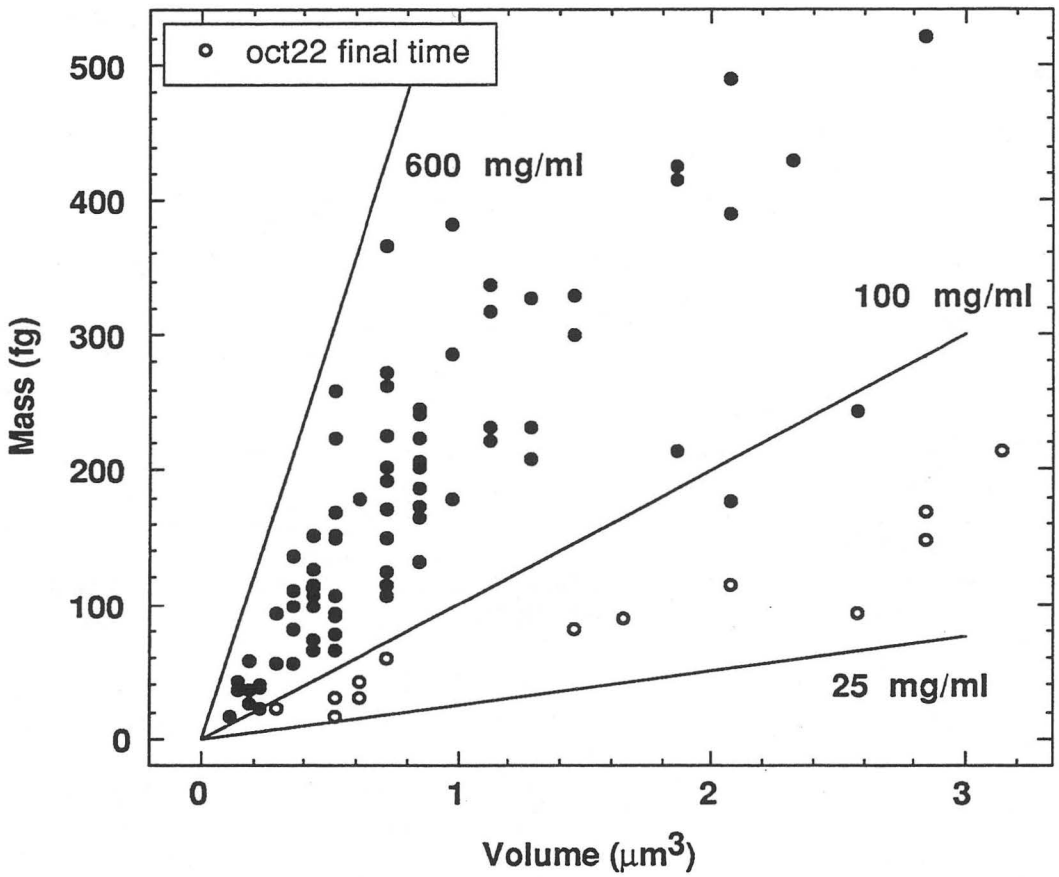

Figure 6.46 The protein mass for all of the 250mg/ml chymotrypsinogen experiments plotted against granule volume. Although there is a wide distribution of values, we still see that a relationship exists between these two variables. The granules from the oct22 experiment are no longer in this broad distribution after they were exposed to the chymotrypsinogen flow, because their protein concentration values fell dramatically (see Table 6.12).

VI.2.4c Summary of Protein Uptake

In the 50 mg/ml chymotrypsinogen study, while we did not observe the net uptake of protein in any of the granules after the solution had been flowed into the LBL-WC, we also did not observe any significant release of protein from the granules after the first time period. There was also no significant change in the diameter or protein concentration

of the population of granules. These results suggest the attainment of an equilibrium state between granules and the suspending solution, in that the flux of protein into the granule was the same as the efflux.

However, we did observe that granules increased in protein mass after exposure to the 250 mg/ml chymotrypsinogen solution - on average for all of the experiments between the first and the second time point by 30 ± 7% (±s.e.m), confirming that granules are able to take up exogeneously added protein (as opposed to protein released from other granules) as first seen by Liebow and Rothman (1978). This result indicates that protein is able to cross into and out of the granule across the membrane.

As protein entering the granule would also involve an influx of water in response to the increase in osmolarity within the granule, we would generally expect the diameter of the granules to increase and the protein concentration to decrease. And indeed, this phenomenon is observed in the oct22 experiment. However, it appears that some of the exogeneously added protein may also be taken up by the protein aggregate within the granule because in the other two experiments, the average protein concentration either stays approximately the same (oct26) or increases (apr) with a simultaneous increase in protein mass. This result indicates that excess water leaves the granules once protein is bound to the osmotically inactive aggregate. As such, we can see that as a result the average diameter value does not increase as much in the oct26 experiment (~20%) as it did in the oct22 experiment (~50%). Furthermore, in the apr experiment where we observe the largest increase in protein concentration, we also find that diameter decreases, probably as a result of water exclusion.

VI.2.5 NaCl

This experiment was designed to study the effect of suspending the granules in an ionic isosmotic solution (150mM NaCl, pH 6.0) instead of the usual nonionic isosmotic solution (0.3M sucrose). From previous work (Burwen and Rothman, 1972) is was demonstrated that ~36% of the total protein was released from granules after incubation in 150mM NaCl for 15min (37°C). Table 6.13 shows the average diameter, protein concentration and mass for granules suspended in NaCl in comparison to the General Population (GP) granules.

Table 6.13. Results of the experiments from resuspending isolated granules in 150mM NaCl, pH 6.0. Values with the same letter are not significantly different ($P<0.05$, t test)

	Diameter (μm) average ± (s.e.m.)	Protein Concentration (mg/ml) average ± (s.e.m.)	Protein Mass (fg) average ± (s.e.m.)
Gen. Pop. (N=388)	1.08 ± 0.02^a	253 ± 7	150 ± 4
NaCl (N=19)	1.06 ± 0.06^a	138 ± 14	86 ± 13

From the table we can see that comparing the results to the GP population, the diameter values are not significantly different, but protein concentration and mass values are significantly less than the GP population. The NaCl population has an average protein mass that is ~57% of the GP population. The protein concentration of the granules suspended in NaCl is also less than the General Population. This result may reflect the fact that NaCl causes the dissociation of protein from the internal granule aggregate, which is maintained by means of electrostatic interactions, so that much of the protein is in solution within the granule. This would explain the substantial release of protein from the granules and it would also explain their appearance compared to controls in STXM; which is uniform but of low density.

VI.2.6 Nigericin

Nigericin is a cation exchange ionophore that exchanges K^+ for H^+. It readily inserts itself into membrane bilayers and can be used to increase the internal pH of a membrane bound organelle by suspending said organelle in a solution containing free K^+. This technique has been used on isolated zymogen granules (LeBel, 1988) to study the "stability" of the granules as their internal pH increases. LeBel et al. observed that the optical density of a suspension of granules decreased after the addition of Nigericin and they concluded that the granules lysed as a result of the increased internal pH. The present experiments were carried out to determine if granules lysed or if the decrease in optical density was a result of either a decrease in diameter or refractive index (protein concentration) as predicted by Mie scattering theory (see Chapter I). The results are shown in Table 6.14. Two populations of granules were imaged from the same preparation. One group was the control to the other population to which 15μM Nigericin was added Then we imaged as many granules as we could in an hour (Pixel size:100nm).

Table 6.14 The results from the Nigericin experiment. Values with the same letter are not significantly different (P>0.05, t test)

	Diameter (μm) average ± (s.e.m.)	Protein Concentration (mg/ml) average ± (s.e.m.)	Protein Mass (fg) average ± (s.e.m.)
Control (N=16)	1.07 ± 0.07[a]	164 ± 15	112 ± 21
Nigericin (N=12)	0.97 ± 0.06[a]	110 ± 16	48 ± 6

From the table, we can see that although the diameters of both populations were not significantly different, the protein concentration and mass values were. The control sample has a protein concentration 50% greater than the Nigericin group and a protein mass that was slightly more than a factor of two bigger. These results demonstrate clearly that the change in optical density observed in a suspension of isolated granules upon the

addition of Nigericin was the result of a change in the refractive index of the granules (protein concentration) not to a reduction in the number of granules (lysis) as originally proposed LeBel (1988).

VI.3 The Effect of Fixation

Much of what we currently know about the size and structure of zymogen granules has come from electron microscopic (EM) studies. The standard EM procedure requires specimens to be stained, fixed and dried (usually with plastic substitution); techniques which may alter the natural structure of biological material on a sub-micron level. From section VI.1, "A general description of fresh zymogen granules," we have seen that STXM images of fresh zymogen granules seem different from EM images of fixed zymogen granules in that the fresh granules are heterogeneous in appearance. In some we can identify structures, or at least clumps of protein, giving a non-uniform appearance. But, conclusions about the effects of fixation are difficult to make based on experiments using two different techniques. So, here we examine the changes in appearance, diameter, protein mass and concentration of granules in the X-ray microscope before and after fixation.

This section contains two studies. The first compares a population of fixed granules to a population of fresh granules. The second presents the results of experiments in which fresh granules were imaged and then an isosmotic solution containing 1 1/2% glutaraldehyde was flowed past the granules - fixing them in place.

VI.3.1 As compared to the General Population

Appearance

We have already seen many STXM images of fresh granules (figures. 6.1, 6.13-6.16 and 6.34, 6.35) and figure 6.8 showed four images of fixed granules. From figure 6.8, it is immediately apparent that the two populations of granules that were originally identified

in the fresh granule image are again seen in these images (UG and NUG). However, there are some slight differences. While the UG granules in the fresh granule images were uniform in appearance, it was generally possible to distinguish at least some slight variations in the density across the granule. In the fixed images, UG granules are extremely uniformly dark in appearance - almost to the point of being indistinguishable from each other. Their sphericity is also much more perfect than the fresh UG granules, which were "generally" round. This is consistent with the fact that fixation causes protein cross-linking to membranes and each other. Moreover, in UG granules, since they already have such a high concentration of protein, it is not difficult to imagine that fixation cross links all of the protein within the granule giving the granules a very appear uniform appearance. This would also "smooth" the edges of the granule making them more circular in appearance.

Given that we are still able to identify NUG granules, we can conclude that the fixation is not able to cross link and draw together the protein clumps that we see in NUG granules, into one uniformly dark clump. Fixation, however, does appear to have the effect of making the clumps and reticulations within NUG granules stand out more clearly and this is probably the result of cross-linking within the clumps.

From these observations, it appears that fixation has the effect of smoothing the appearance of some features, e.g. eliminating slight variations in density that are visible in UG granules. That we could see these variations in fresh granules when we were imaging at resolutions at ~50nm implies that fixation may eliminate our ability to distinguish features that are about 50nm due to cross linking whatever the resolution of the method may be.

Diameter, Protein Concentration and Mass

Fixation had the effect of enhancing the affinity of the granules for the silicon nitride windows. This facilitated being able to image *hundreds* of granules. Table 6.15 shows

the diameter, protein concentration and mass data for the 210, 1/2hr time point fixed granules taken from Table 6.2[2] compared to granules from General Population (GP - Table 6.1). The data is divided into UG, NUG and the combined results for fixed and fresh granules.

From the table below we can see that the NUG granules represent a similar fraction of the total population for the fixed and fresh populations, 20% and 23% respectively. We can also see that for both populations the NUG granules are bigger than the UG granules and have lower protein concentration and mass values.

Table 6.15. Fixed and fresh granules. This table presents the average values for the characteristics of a fixed populations of granules and from Table 6.1 General Population) for comparison. The granules have been divided into two sub-classes; uniform and non-uniform. Values with the same letter are not significantly different (P>0.05)

	Diameter (μm) ave. ± (s.e.m)	Prot. Con. (mg/ml) ave. ± (s.e.m)	Protein Mass (fg) ave. ± (s.e.m)
1/2hr Fixed			
Uniform (N=167)	1.03 ± 0.02^{a}	300 ± 5^{c}	180 ± 7
Non-Unif (N=43)	1.49 ± 0.05	96 ± 6	163 ± 13^{e}
All	1.13 ± 0.02^{b}	256 ± 7^{d}	176 ± 6
GP			
Uniform (N=300)	1.00 ± 0.01^{a}	294 ± 7^{c}	153 ± 3
Non-Unif. (N=88)	1.36 ± 0.04	115 ± 6	142 ± 10^{e}
All	1.08 ± 0.02^{b}	253 ± 13^{d}	150 ± 4

From the table, we can see that the diameter and protein concentration for the combined data of each population (fresh and fixed) and UG granules are not significantly different (P>0.05, t test). Although, the same cannot be said of the protein mass. It would appear from this population study that fixation may increase the mass of the granules, presumably by the binding of glutaraldehyde within the granule. However, as this is a

[2]As mentioned in chapter 3, the 1/2hr time point refers to the population of granules that were left at room temperature for 1/2hr after their isolation. They were then fixed with 1 1/2% glutahaldehdye at 4C overnight. The results from this particular population of fixed granules are used here so that a comparison can be made with the GP population that was also at room temperature on average for 1/2hr before imaging.

population study, it is impossible to determine if individual granules increased in mass, thus we performed the following real time experiments to observe the affects of fixation on individual granules.

VI.3.2 Real Time Fixation

From the previous section, we saw that fixation appears to affect the appearance of granules at the level of resolution we can see in STXM but does not seem to affect the measured characteristics of diameter and protein concentration, and may increase the mass of the zymogen granules by ~18%. These results are based on comparing different granules and are therefore subject to sampling variations, although a substantial number of granules was included in the comparison. We were therefore interested in observing the effects of fixation on individual granules. In this experiment an initial image of isolated granules was taken and then a solution of 1 1/2% glutaraldehyde was flowed past the granules and subsequent images made. The results from two of these experiments are presented here separately; oct1 and oct2. Images from both experiments used 31nm pixels.

The diameter, protein concentration and mass values for the initial (t=0.63) and final time points (t=4) are shown in Table 6.16 for the three granules analyzed in the oct1 image.

Table 6.16 The results of the first fixation in real time experiment. Values with the same letter are not significantly different (P>0.05, t test)

	Diameter (μm) average ± (s.e.m.)	Protein Concentration (mg/ml) average ± (s.e.m.)	Protein Mass (fg) average ± (s.e.m.)
oct1 (N=3) initial	0.86 ± 0.16^{a}	231 ± 37^{b}	79 ± 28^{c}
final	0.74 ± 0.17^{a}	297 ± 91^{b}	54 ± 16^{c}

From the table we can see that there was no significant change in the diameter, protein mass or protein concentration values between the initial image and 3 hours after the introduction of the glutaraldehyde. However, the number of observations (n=3) do not really allow a satisfactory statistical distinction and this experiment was performed again.

The results of the second experiment (oct2) are shown in table 6.17, which shows the average diameter, protein concentration and mass for the initial (t=2.5hr)[3] and final time (t=6hr) for the 8 granules studied. In this experiment, images were taken, on average, every ten minutes for the first half hour and then once every hour for 5 more hours. From the table we can see that the average diameter and protein mass decreased over the time course and protein concentration increased.

Table 6.17 The results from the second real time fixation experiment, oct2.

	Diameter (μm) average ± (s.e.m.)	**Protein Concentration (mg/ml)** average ± (s.e.m.)	**Protein Mass (fg)** average ± (s.e.m.)
oct2 (N=8) initial	0.83 ± 0.09	165 ± 16	52 ± 13
second	0.83 ± 0.09	146 ± 15	47 ± 12
third	0.76 ± 0.08	222 ± 28	46 ± 10
final	0.70 ± 0.08	225 ± 25	41 ± 10

The percent protein mass and diameter change for all of the granules for all of the time points is shown in Figs. 6.47 and 6.48 respectively. In figure 6.47 we see an immediate and substantial decrease in protein mass. This decrease may be a result of the sudden flow of solution past the granules and not an effect of glutaraldehyde.

[3] The initial time point was at 2 1/2 hrs because the beam dumped just as we were beginning the experiment. We decided to leave the granules at room temperature until we had beam again, and this was 2 1/2 hrs after we had initially taken them off of ice.

The granules had been sitting at room temperature for 2 1/2 hours previous to the initial image were probably close to a "semi-equilibrium" state with the suspending solution (as seen in the control experiments). This new flow of solution, after the initial image, changed the equilibrium state resulting in the initial large loss of mass we see at the second time point (similar to the isosmotic 0.3M sucrose experiment). Therefore, the average protein mass value at the second time point is considered to be our initial mass before the fixative was in the LBL-WC.

After the second time point, we see an increase in protein mass. At this point the glutaraldehyde is in the LBL-WC. This mass increase may be either a result of glutaraldehyde binding directly to the granules or granule protein in solution binding to the granule surface via glutaraldehyde. Either way, the granules increased in mass above their original values but then proceeded to lose mass again slowly over time until the rate of mass loss appeared to reach a plateau by the 6hr time point. From table 6.17, we see that the final protein mass is not significantly different ($P>0.05$, t test) from the second protein mass value, or what we consider to be the initial protein mass. Figure 6.48 shows that the granule diameter values were not initially affected by the flow of solution but then changed dramatically at the third time point. After this abrupt change, diameter did not change significantly for the remainder of the experiment.

From both of these experiments, it appears that fixation does not change the protein mass of the granules during the time period of the experiment. In the first study we saw that after 4 hours of fixation, the initial characteristics of diameter, protein mass and concentration were the same. In the second experiment, although we saw the diameter, protein mass and concentration changed after the first time point, this was probably not a result of the fixation and was probably due to the fact that the granules had been sitting at room temperature for 2 1/2 hours before the experiment. After the initial drop in these

characteristics, we see that they do not change significantly over the 6 hours that the 1 1/2% glutaraldehyde was in the LBL-WC.

However, as we did observe a significant increase in the protein mass of the population of fixed granules (NUG type) compared to the population of fresh granules (previous section), it is possible that in our system, the effect of glutaraldehyde fixation on the mass of an object are only apparent after an extended period of time. The enclosing membrane of the granule may serve as a barrier to the influx of glutaraldehyde. Indeed, recent results have shown that fixation with 1% glutaraldehyde for one hour at room temperature increased the mass of fixed chromosomes over fresh chromosomes by 15% (Williams et al., 1993). This is comparable with the ~18% greater protein mass we measured and as there is no enclosing membrane to the chromosomes, the increase in mass was observed after only 1hour of incubation time.

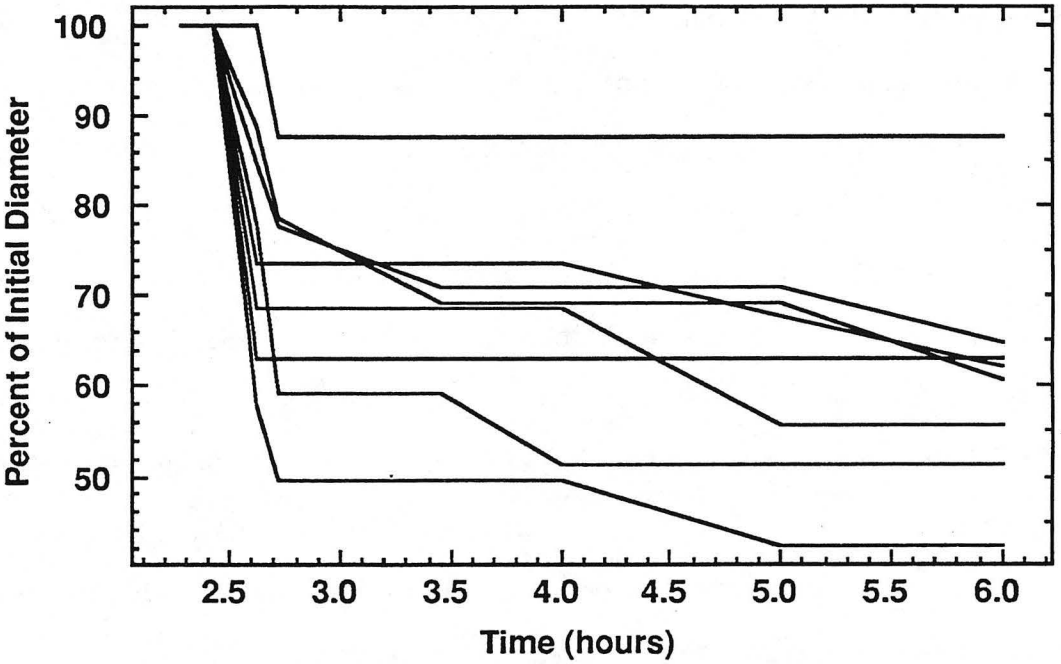

Figure 6.47 The percent diameter loss for the oct2 real time fixation experiment. The curves for all of the granules are shown. Glutaraldehyde was added after the initial image was taken but was probable not "seen" by the granule until the third time point.

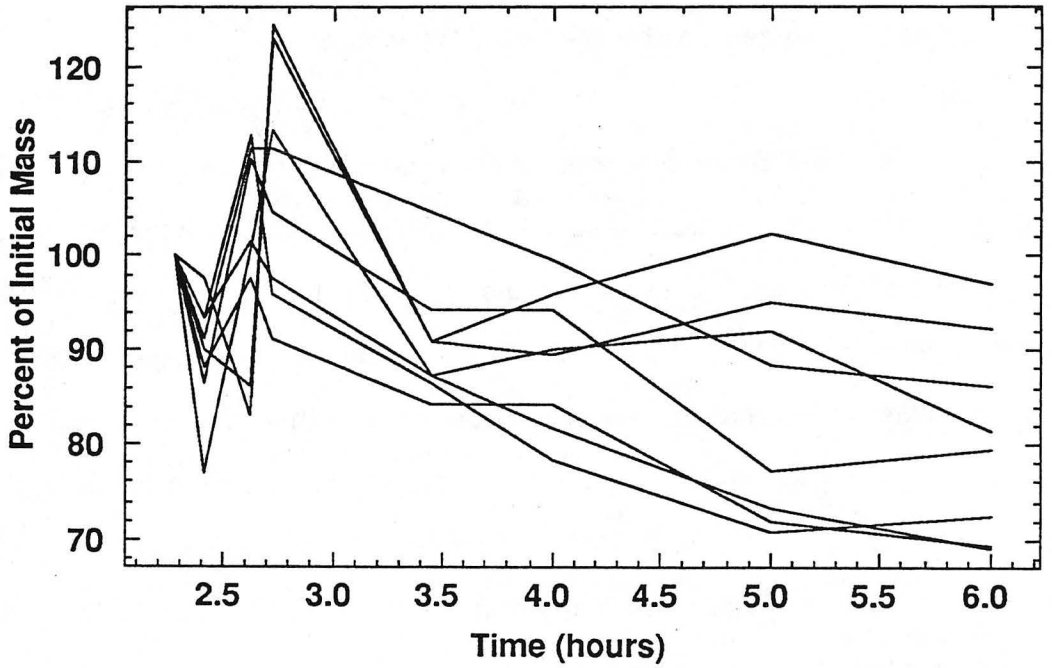

Figure 6.48 The percent protein mass loss for the oct2 real time fixation experiment. The curves for all of the granules are shown. Glutaraldehyde was added after the initial image was taken but was probably not "seen" by the granule until the third time point.

VI.4 The Permeability Coefficient

In this section we present the results of calculations which determine the permeability coefficient (P) of the zymogen granule membrane to its enclosed proteins. The permeability coefficient of a membrane to a particular molecular species is a commonly used phenomenological constant that can help relate the penetrability of different species to a membrane bilayer. For example, permeability coefficients for urea and glycerol to a particular lipid bilayer is ~5 x 10^{-6} cm/sec, considerably less than for water, 5 x 10^{-3} cm/sec. This indicates that water moves more easily through the membrane than either urea or glycerol.

The permeability coefficient can be calculated from the Fick equation which relates the efflux of protein from the granule to membrane permeability by

$$\text{Flux} = P * A * (C_{in} - C_{out}) \qquad (6.1)$$

where A is the membrane area and (C_{in} - C_{out}) is the protein concentration gradient that provides the driving force for protein efflux across the membrane.

There has been little work done on calculating the permeability coefficients of bio-membranes to large proteins. However, the technique of STXM offers us the opportunity to measure the protein content of each granule, and therefore to determine the change in the protein content of the granule over time, or the flux and calculate P for the proteins enclosed within the granule. The area is determined from diameter values. Unfortunately, we still do not know the relevant concentration value within the granule. The concentration values that we have reported in the previous sections were for the total amount of protein within the granule divided by the volume of the granule. But, most of this protein is bound in an aggregate (~90% according to Rothman, 1971) and is therefore not active and does not provide the driving force for transport. To determine the true concentration gradient, we need to know protein activity, not concentration, within the granule, that is, the concentration of solvated, unassociated protein solute. In order to

determine this value, we need to know the ratio of bound to free (active) protein. Fortunately, for granules at pH 6.0 it is already known. From the literature (Liebow and Rothman, 1976), we know that a suspension of granules is at equilibrium with the suspending solution when the protein concentration in the solution is ~75 μg/ml. If we assume that the interior of the granule is at equilibrium with the medium, then the free protein concentration inside the granules must also be 75μg/ml. Furthermore, if we assume that protein translocation out of the granule is the rate limiting step, then the interior of the granule will always be in equilibrium and will have a free protein concentration of 75μg/ml no matter how much of the protein is bound in the aggregate. This will hold true as long as the state of aggregation is not changed, e.g. by pH or salt. If there is no, or minimal protein in the suspending solution, then $(C_{in}-C_{out}) = 75\mu g/ml$.

In four experiments, protein in the suspending solution was minimal. These were the perifusion studies: 0.3M sucrose, 0.6M sucrose, water and 0.025% Triton-X. The control experiments had a significant amount of protein in solution because the suspending medium was not replaced and so protein lost from granules accumulated in the solution. From the four experiments just mentioned, we calculated an average P value for both populations of granules (UG and NUG) using equation 6.1. The flux rate used was that between the initial and second images in order to best estimate the initial rate of release.

Table 6.18. The permeability coefficient of the granule membrane to its enclosed proteins as calculated from equation 6.1 for the different experiments listed. The values were calculated using the protein efflux measured between the initial time point and the second time point. Values with the same letter are not significantly different (P>0.05, t test).

	Permeability Coefficient (ave. ± S.D.)	
Experiment	**Uniform**	**Non-Uniform**
0.3M sucrose	$3.2 \pm 0.5 \times 10^{-6}$ cm/sec[a]	-----
0.025% Triton-X	$2.5 \pm 0.9 \times 10^{-6}$ cm/sec[a]	-----
0.6M sucrose	$5.4 \pm 1.1 \times 10^{-6}$ cm/sec[c,d]	$4.0 \pm 1.1 \times 10^{-6}$ cm/sec[d,e]
water	$7.2 \pm 0.7 \times 10^{-6}$ cm/sec[c]	$2.1 \pm 0.6 \times 10^{-6}$ cm/sec[d,e]

From the table, we can see that the permeability coefficients for the 0.025% Triton X-100 and the 0.3M sucrose are not significantly different. This result confirms our earlier observation that at this concentration of detergent the permeability of the granule membrane is not compromised and protein release from the granules is not affected. However, the permeability for the isosmotic solutions was significantly smaller than the non-isosmotic solutions of water and 0.6M sucrose. This indicates that the permeability of the granule membrane to its enclosed membranes is affected by the osmotic strength of the suspending solution. And as we saw earlier, the rate of protein release when granules are exposed to water or 0.6M sucrose is higher than in the 0.3M sucrose and 0.025% Triton X-100 experiments.

Most interesting is the fact that the permeability coefficients for the 0.6M sucrose and water, were both elevated even though one solution was hyper-osmotic and the other hypo-osmotic. We can also see that the permeability of UG granules is substantially higher than that of NUG granules, at least for the water experiment. In figure 6.54 the distributions of the permeability coefficients for the granules for the two groups are shown: A=(0.3M sucrose/0.025% Triton X-100) and B=(0.6M sucrose/water). In Group

A, we see that the permeability coefficients are tightly distributed around the mean value. In group B, the distribution takes on more of a bimodal or even a trimodal appearance due to the permeability coefficients for NUG granules being similar to that of group A. By whatever mechanism protein is "normally" released from the granules, as shown by the distribution in A, it appears that this same mechanism exists in group B, however the nature of the solutions appears to have affected the mechanism in such a manner that the permeability of some granules is twice to three times normal.

We can compare our calculated permeability coefficient to the permeability coefficients of other molecular species. For example, comparing it to that of water across a lipid bilayer, because our value is 3 orders of magnitude smaller than for water, this suggests that the granule membrane provides a substantial barrier to the release of protein. Thus, release is probably not occurring through large holes or breaks in the membrane. On the other hand, although the magnitude of the permeability coefficient for both for urea and glycerol across a lipid bilayer is similar to those we calculated for protein, because of the enormous electrical and mechanical barriers to transporting hydrophilic proteins though lipid bilayers, it is unlikely that proteins are able to cross the granule via the same mechanism as urea and glycerol. Therefore, we can conclude that there must be some mechanism within the granule membrane by which transport is accomplished. A discussion of potential mechanisms is given in the Discussion and Conclusion chapter (VIII).

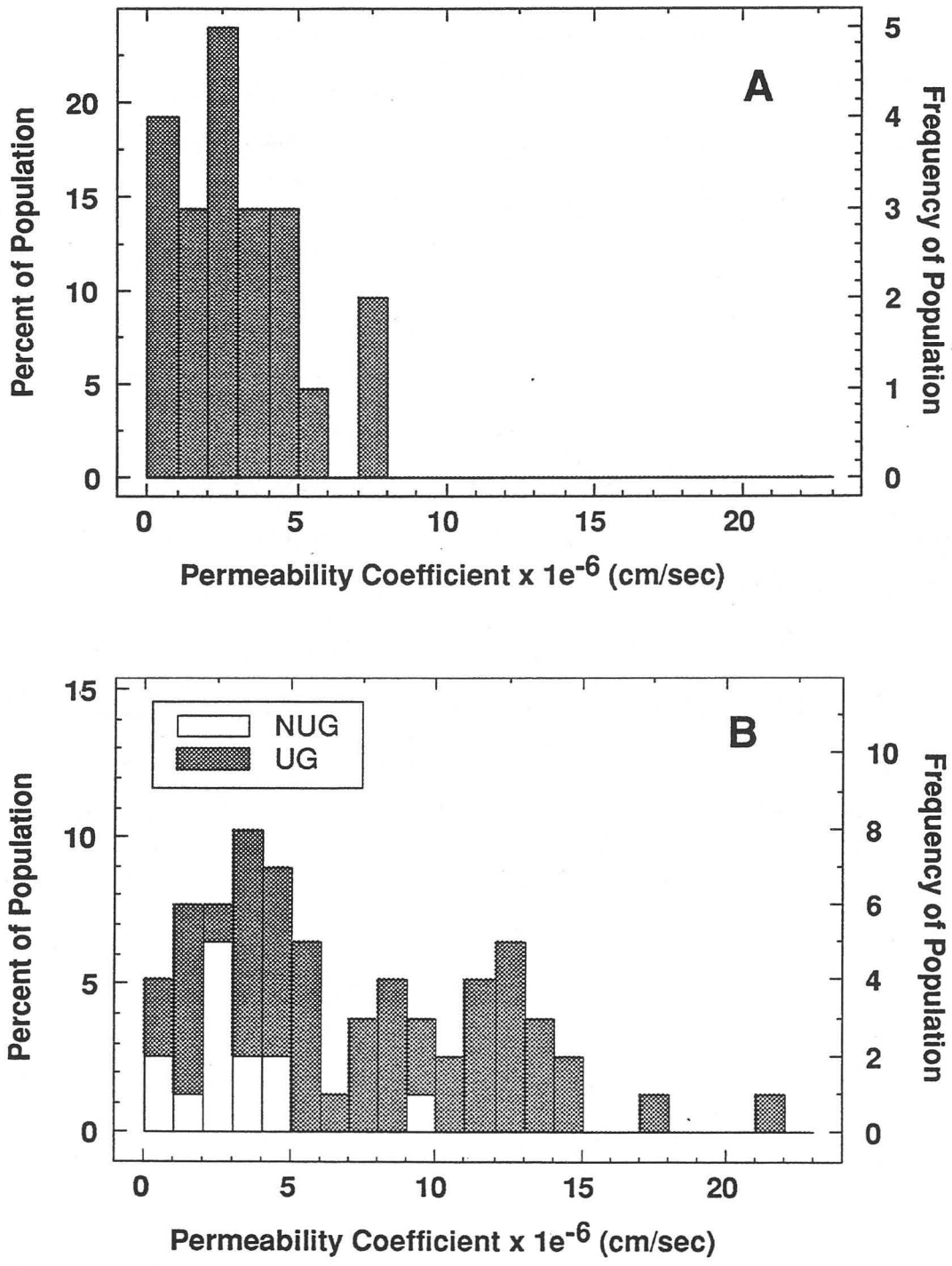

Figure 6.49 Distribution of the permeability coefficients calculated from the experiments shown in Table 6.20. **A** is the combined values of the 0.3M sucrose and 0.025% Triton X-100 in 0.3M sucrose experiment and **B** is the combined values of the 0.6M and water experiments. These values were combined because they were not significantly different (P>0.05, t test).

Chapter VI - References

Burwen, S.J. and S.S. Rothman, Zymogen granules: osmotic properties, interactions with ions, and some structural implications, Am. J. Physiol. (1972) **222**:1177-1181.

LeBel, D. G. Grondin and J. Paquette, In vitro stability of pancreatic zymogen granules: roles of pH and calcium, Biol. Cell (1988) **63**:343-353.

Liebow, C. and S.S. Rothman, Membrane transport of proteins, Nature (1972) **240**:176-178.

Liebow, C. and S.S. Rothman, Equilibrium of pancreatic digestive enzymes across zymogen granule membranes, Biochim. Biophys. Acta (1976) **455**:241-253

Rothman, S.S., The behavior of isolated zymogen granules: pH-dependent release and reassociation of protein, Biochim. Biophys. Acta (1971) **241**:567-577.

Williams, S., C. Jacobsen, S. S. Lamm, V. Oehler, J. Van't Hof, S. Wirick and X. Zhang, Metaphase chromosome DNA mass fraction is a constant, independent of species, To be published (1993).

Chapter VII. Radiation Damage

In the field of microscopy, it is a fundamental fact that in order to observe a specimen, the illuminating light or "radiation" must somehow interact with the object. This interaction can mean the absorption, reflection, diffraction, scattering or refraction of the light by the sample - all of which can involve the transfer of some of the light's energy to the sample. Understanding how this transferred energy can affect the structure and function of biological objects is the study of radiation damage and is extremely important because the type of damage incurred by a specimen can limit the use of that particular type of microscopy. For example, in visible light microscopy the sample may be damaged by heat through the absorption of radiation. In electron microscopy specimens are elaborately prepared with heavy metals in order to protect the structure from the radiation damaging effects of electrons.

In X-ray microscopy, the radiation effects are from the interaction of soft X-rays with water and organic material. These have been addressed theoretically, but there is little in the way of experimental results. This is primarily because X-ray microscopy is still a relatively new field. Therefore, each researcher must establish for themselves the structural and functional constraints for their individual specimens due to exposure to soft X rays in order to use the microscope successfully. This chapter presents the results of our studies on the damaging effects of soft X-ray radiation to the structure and function of zymogen granules.

The first section discusses the method used to determine how much radiation our specimen received. This measurement of "dose" is used then in reference to actual structural and function damage. The second section presents experimental results on the damage that can occur to zymogen granules and how we determined the dose we eventually exposed the granules to. The third section is a discussion of the mechanisms by which X-rays interact with organic material and how these interactions may lead to the

type of damage that was observed, as well as "non-visible" damage. The final section is a review of the results of radiation damage studies performed by other researchers on their biological systems and how these results are beginning to define some of the limitations for imaging biological specimens using X-ray microscopes.

VII.1 Determining radiation exposure or "Dose."

Traditionally, the amount of radiation that a sample is exposed to, or "dose," regardless of the type of radiation, is expressed as the amount of absorbed energy divided by the mass of the sample. The SI unit of absorbed dose is "gray," defined as

absorbed dose: 1gray = 100 erg/g = 6.25×10^{15}eV/g. (7.1)

However, X-ray microscopists have been using units of "rad" instead of gray when reporting on radiation dose where 1gray = 100 rads. Therefore, in order to be consistent within the field, rad will be used. In the X ray wavelength range that we have used, the incident radiation is transmitted through the sample unattenuated, scattered, or the energy of the X ray photons is completely absorbed by sample. As the scattered photons are elastically scattered and do not transfer any energy to the sample they are counted by the proportional counter as "transmitted" photons[1]. Therefore, the absorbed dose (D_{ab}) can be easily calculated from the following relationship,

$$D_{ab} = N \bullet \frac{(\text{energy / photon})}{(\text{mass} - \text{of} - \text{sample})} \tag{7.2}$$

where N is the number of absorbed photons. It would also be possible to calculate the abosrbed dose to our sample using the LET value for photons, however as the total LET is not significantly different than the LET of photoelectron absorption in this energy range (Cullen et al., 1989), we use equation.

---

[1]The scattered photons are still counted by the proportional counter because the proportional counter has such a large collection area that even though the photons are scattered to some degree relative to the transmitted photons, the proportional counter is still able to detect them.

In order to calculate the absorbed dose a sample receives in a scanning transmission X-ray microscope (STXM) image, we need to calculate the dose to each pixel in the image, and then the total dose to the sample is the average of the pixel values. We have already shown how we can calculate the mass of sample in each pixel for our STXM images, now all we need to do is determine the number of photons that were absorbed by the sample in each pixel (Ns) and we can calculate the absorbed dose.

We can determine (Ns) from the information in our STXM images and a few approximations. From Chapter III, we recall that the pixels in the STXM images are a record of the number of photons that have passed through the wet cell (LBL-WC) and have been detected by the PC. The number of transmitted photons through the sample in the LBL-WC at a particular pixel is designated as (Is) and the number of transmitted photons through the background suspending solution is (Ib). This is schematically shown below in figure 7.1.

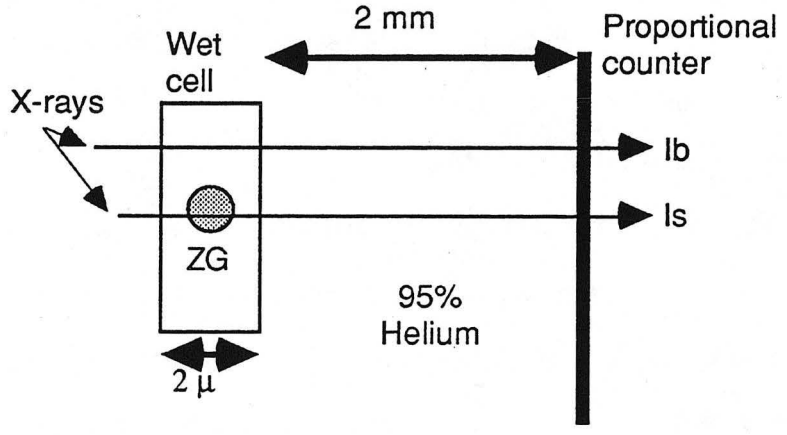

Figure 7.1 The path of X-rays through the microscope before being finally counted at the proportional counter. I(b) represents the number of photons per pixel that have transmitted through the background solution in the wet cell. I(s) represents the number of photons per pixel that have passed through the sample.

The difference between these two values, times a factor γ that corrects for the loss of the photons between the sample and the proportional counter, is the number of photons that

have been absorbed by the sample of thickness t (Ns) plus the number of photons that have been absorbed by an equal thickness of background solution (Nb) and can be written as

$$\gamma(Ts - Tb) = Ns + Nb \qquad (7.3)$$

We can get Ts and Tb from our STXM images, as mentioned above, but there are still 2 unknown variables, Nb and γ, that need to be dealt with before we can solve for Ns.

The variable Nb is the number of photons absorbed by a thickness of the background solution that is the same thickness as the sample. The ratio of Nb to Ns is the ratio of the absorption of X-rays by the background and the sample. The absorption factor (A) can be written from equation 3.3 as

$$A = 1 - \text{transmission} = 1 - \exp^{-(\mu\rho t)} \qquad (7.4)$$

where μ is the mass absorption coefficient (cm^2/g), ρ is the density and t is the thickness of the material and so we can write

$$Nb/Ns = Ab/As \text{ or } Nb = Ns \bullet (Ab/As) \qquad (7.5)$$

We can calculate Ab and As for different thicknesses of the sample using the values for μ and ρ from Table 3.2 and now equation 7.3 can be written as

$$\gamma(Ts - Tb) = Ns + Ns \bullet (Ab/As) = Ns\,(1 + Ab/As) \qquad (7.6)$$

The second unknown variable, the correction factor γ, is determined by approximating how much each structural element in the microscope downstream of the sample has contributed to the attenuation of the X rays detected at the PC. These elements are, as shown in figure 7.1, the suspending solution[2], the LBL-WC SiN exit window, the pathlength of He between the exit window of the LBL-WC and the PC, and the PC SiN window. The attenuation of the X rays by these components can be calculated using equation 3.3 which describes relative transmission through a material:

---

[2]Because we do not know if the zymogen granule is on the upstream or the downstream window, there could be as little as no suspending solution between the sample and the exit window or as much as 1µm, so in calculating attenuation, we have used an average value of 0.5µm.

$$\text{transmission} = \exp-\left[(\mu\rho t)_b + (\mu\rho t)_{SiN} + (\mu\rho t)_{He}\right] = \gamma^{-1} \qquad (7.7)$$

The variables are; μ, the mass absorption coefficient (cm^2/g); ρ, the density and t, the thickness of the material. The subscripts are as follow: b=background suspending solution, SiN=silicon nitride and He=helium. The values for μ and ρ for all of the elements are given in Table 3.2 for the different wavelengths and the values for the thicknesses are given below in Table 7.1.

Table 7.1. Thicknesses of absorbing elements in the microscope. The components have attenuated the X ray beam and therefore the number of photons that are counted at the proportional counter are only a fraction of the total number that were incident on the sample.

variable	value	error
t_σ	0.5 μm	±100%
t_{Si} LBL-WC	60 nm	±10%
PC	100 nm	±10%
t_{He}	2mm	±50%

In Table 7.2, we present the attenuation of the X rays between the sample and the PC by the absorbing elements as calculated by equation 7.4 for different wavelengths used and also the corresponding correction coefficient γ. The minimum and the maximum values for γ, which were calculated from the estimated errors shown in Table 7.1, are also shown.

Table 7.2. The attenuation factor for the detected number of photons at the proportional counter and the corresponding correction factor γ.

wave - length	atten- uation	γ value	γ min-max range	wave - length	atten- uation	γ value	γ min-max range
3.4nm	0.39	2.5	1.9 - 3.4	3.55nm	0.36	2.8	2.0 - 4.0
3.5nm	0.37	2.7	2.0 - 3.8	3.6nm	0.33	3.0	2.1 - 4.3

We are now in a position to solve equation 7.6 for Ns, the number of photons that are absorbed by the sample in each pixel, which we will do based on the characteristics of a model granule - diameter, 1.08 ± 0.01μm, (± s.e.m.) and protein concentration, 253 ± 7mg/ml - which has been taken from the General Population presented in Chapter VI. Equation 7.6 is rewritten below

$$Ns = \gamma(Ts - Tb) / (1 + Ab/As) \qquad (7.8)$$

For our model sample, the average protein concentration per pixel is 253 mg/ml and the average sample depth per pixel[3] is 0.15 μm. We can then calculate the variables in the above equation for the different wavelengths used and solve for Ns; this is shown in Table 7.3

Table 7.3. The average number of photons that are absorbed in a pixel with a protein concentration of 253 mg/ml. The number of photons that were detected at the PC through the sample (Ts) was held at 1000 photons in order to expose the sample to as little radiation as possible while still collecting sufficient statistics to meet the Rose criterion, as discussed in Chapter III, for a minimum detection of ~24mg/ml protein per pixel.

wavelength	Ab (%)	As (%)	$\frac{Ab}{As}$	Ts (photons)	Tb (photons)	Ns (photons)
3.4nm	6.0	26	0.23	1000	1276	**561**
3.5nm	6.0	28	0.21	1000	1297	**660**
3.55nm	7.0	29	0.24	1000	1307	**693**
3.6nm	7.0	30	0.23	1000	1328	**800**

From Table 7.3, we can now calculate the average absorbed dose that a pixel in a STXM image of an average zymogen granule receives using equation 7.2. The absorbed dose per pixel will vary depending on the size of the pixel. This is because the mass of sample in each pixel depends on the volume of that pixel even though the average protein concentration remains the same. Table 7.4 shows the average absorbed dose per pixel (in

[3] Calculated from the average protein concentration per pixel and the density of protein (1.2gm/ml)

Mrads) for different pixel sizes used and for the different wavelengths. The mass per pixel is calculated by multiplying the average protein concentration times the volume of the pixel.

Table 7.4 Average absorbed dose for an average pixel in an average granule. The number of photons absorbed in each pixel is taken from Table 7.3. These values are based on the average value of γ from Table 7.2. Given the error range of γ, we can expect the average absorbed dose given in this table to vary by ±40%.

pixel size (nm)	ave mass/pix (fg)	Average Absorbed Dose per Pixel Mrad			
		3.4nm (364eV)	3.5nm (354eV)	3.55nm (349eV)	3.6nm (341eV)
18.8	0.06	50.8	58.0	60.0	67.7
27.0	0.13	24.6	28.1	29.1	32.8
30.5	0.17	19.3	22.0	22.8	25.7
31.0	0.18	18.7	21.3	22.1	24.9
31.6	0.18	18.0	20.5	21.2	15.0
39.9	0.29	11.3	12.9	13.3	9.8
49.3	0.44	7.4	8.4	8.7	9.8
58.6	0.63	5.2	6.0	6.2	7.0
63.3	0.73	4.5	5.1	5.3	6.0

From the table, we can see that the absorbed dose ranged from 4.5-67.7 Mrad depending primarily on pixel size. If the granule was imaged more than once, then the total absorbed dose was the addition of the absorbed dose per image.

The actual absorbed dose that each granule received will of course vary depending on the protein mass and the actual number or photons (Ts) that were detected through the sample. But, to the degree that the current method of calculating the absorbed dose depends on the accuracy of our measurement for γ (±40%), it is not useful to calculate the dose for each granule however accurate it may seem. It is more informative to get a general idea of average absorbed dose. The problem of determining the absorbed dose more accurately for a sample is currently being addressed at BNL.

VII.2 Our experiments - the limits of Dose

In the previous section, we presented our methodology for estimating the average absorbed dose that the granules received in STXM. In this section we will discuss how we decided the dose that was acceptable for our experimental purposes and what we considered an unacceptable dose.

The final decision of how much X ray exposure was appropriate for our sample came from trying to minimize absorbed dose without greatly compromising the counting statistics (the number of photons detected at the proportional counter). Counting statistics were important because we were interested in calculating the protein mass of each granule and the accuracy of these calculations of course depends on the number of photons that are counted at each pixel (see Chapter III). Unfortunately, general radiation damage studies using soft X rays were not useful in trying to determine acceptable absorbed dose levels. In such studies, it was found that 400 Rads of 386eV photons can kill 90% of a cell population after three cycles of replication. Exposing our samples to 400 Rads, would mean counting only ~0.1photons per pixel which is definitely not sufficient counting statistics. Moreover, we weren't concerned about killing cells or generational survival. We were only interested in observing the release of protein from the granules and no studies addressed at what level of absorbed dose this activity or "function" is affected. So, after some experimentation with different levels of exposure, we decided that counting ~1000 photons/pixel gave us sufficient statistics for our quantitative work and a dose range that did not appear to affect the rate of protein release.

That protein release is not affected by this exposure can be seen from the results of the June control experiments. In these experiments, granules were imaged over a period of 4 hours, each hour. From Table 7.4, for the pixel size and wavelength used we can see that, on average, each granule received an absorbed dose of 9.8Mrad for each image. Over the course of the experiment, the granules lost an average of 10% of their initial

protein mass at rate of loss ~2.5%/hour; approximately the same rate of release isolated granules measured by other techniques in the complete absence of radiation have shown (Rothman, 1971). Although some investigators have used mass loss as an indicator of radiation damage (see final section this chapter) this is not an appropriate symptom of radiation damage in our case because we expect to witness some degree of mass loss. The question is at what dose radiation increases the rate of protein release. And, mass loss is not always observed. In the June control experiments, the average mass of 48 granules did not change significantly ($P>0.05$, t test) between the 1st&2nd and the 3rd&4th images after a final estimated total dose of 40Mrads. Moreover, protein loss tends to reach an equilibrium over time. If loss was the result of absorbed dose, then it would continue to decrease linearly as a function of the accumulated absorbed dose. This clearly does not occur.

Additionally, protein release and granule structure were affected differentially by exposure to a variety of solutions (e.g., they showed different protein mass release rates). This implies that the mechanism by which protein is being released from the granules is influenced by the different environments, not the radiation.

Although we are confident that protein loss in these studies is not due to radiation damage, this is not to say that the granules have not sustained any structural or functional damage. We are simply claiming that whatever structural or functional damage may occur, it does not cause the granules to release their contained proteins, nor produce change in the size of the object.

We have measured the absorbed doses at which we can observe obvious, and sometimes not so obvious, structural damage that does affect protein loss and the results of these experiments are presented below. There are four experiments ranging from the extreme to the sublime.

Figure. 7.2 shows a series of images of the same group of zymogen granules over a period of forty-five minutes. The initial image was taken with 2.7nm pixel sizes and from Table 7.4, corresponds to each granule receiving an average dose per image of ~30Mrad. After the first image, the focused spot of X-rays (~50nm in diameter) was centered on granule (**B**) and the shutter left open for 5 min. As can be seen, the effect is quite dramatic and the granule is obviously structurally damaged We cannot calculate the absorbed dose that this granule received because as can be seen, there is no sample left where the focused spot of X rays was placed. But, that spot was exposed to X rays a factor of ~1.0×10^5 times greater than the granules in the initial image. We were able to repeat the effect on granule (**D**), but when we attempted it on granule (**A**) it disappeared entirely although this was probably the result of its disassociation from the silicon nitride window.

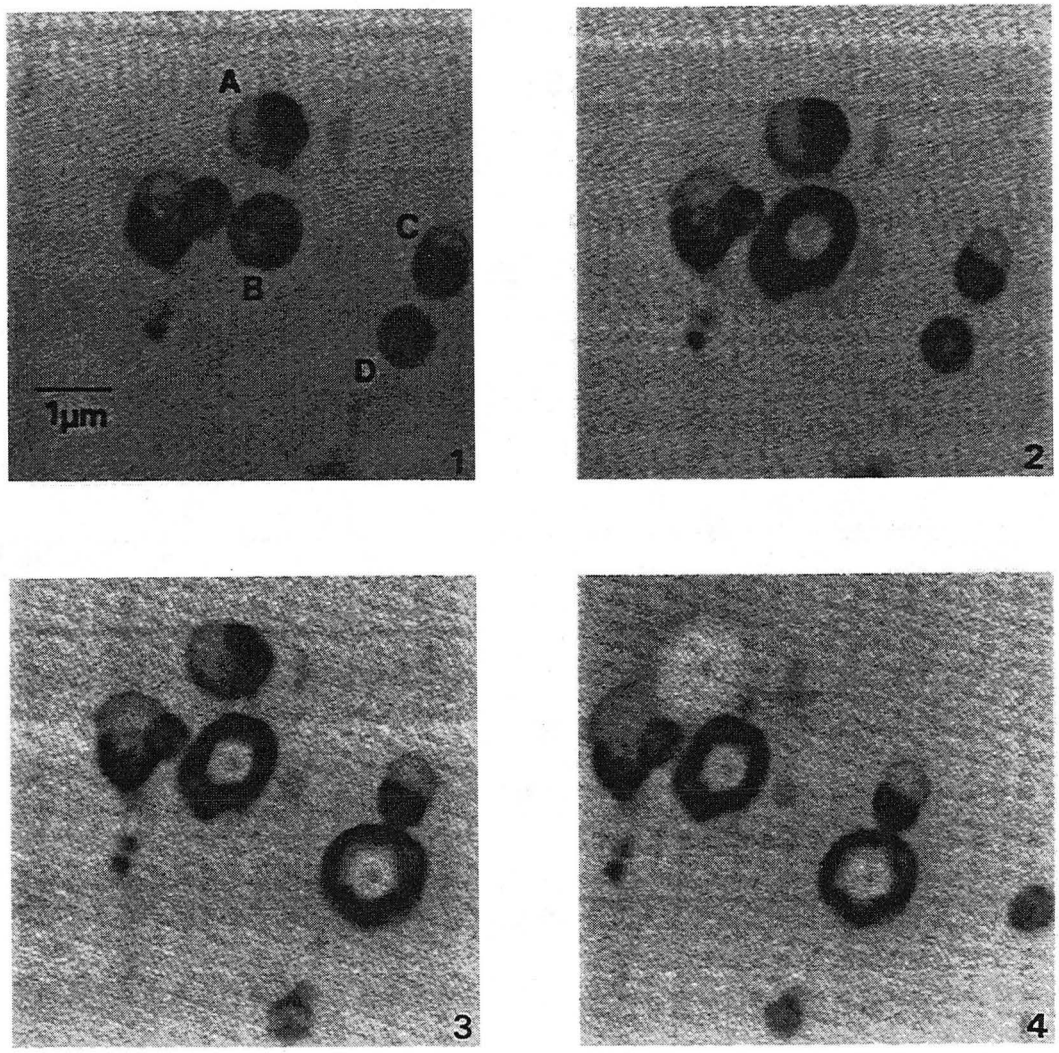

Figure 7.2 A group of zymogen granules suspended in 0.3M sucrose. After the initial image (**1**) image, the focused beam of X-rays was left on granule **B** for 5 min and then the second image was taken. After this image, the X rays were then focused on granules **D** for 5 min and the third image was taken. Again, after this image, the X rays were focused on granule **A** for 5min and the final image was taken. The total time between the first and last image was 45 minutes.

Mass loss for these granules before they were subjected to the spot of focused X-rays is shown below in figure 7.3. The granules that are represented in the figure were not exposed directly to any more radiation than necessary to image them. Regardless, mass loss rate was much more rapid than would be expected for granules suspended in the original isolation solution, 0.3M sucrose (pH 6.0). This is probably a result of the indirect effects of radiation damage which will be discussed at the end of the third section. Even so, granule C, which received a cumulative dose of some 120Mrads, approaches a steady state with its mass still at 60% of the initial value. Which indicates that the accelerated rate of protein lose was due to an increase in the permeability of the membrane (hastening attainment of a steady state) and not mass loss due to "vaporization."

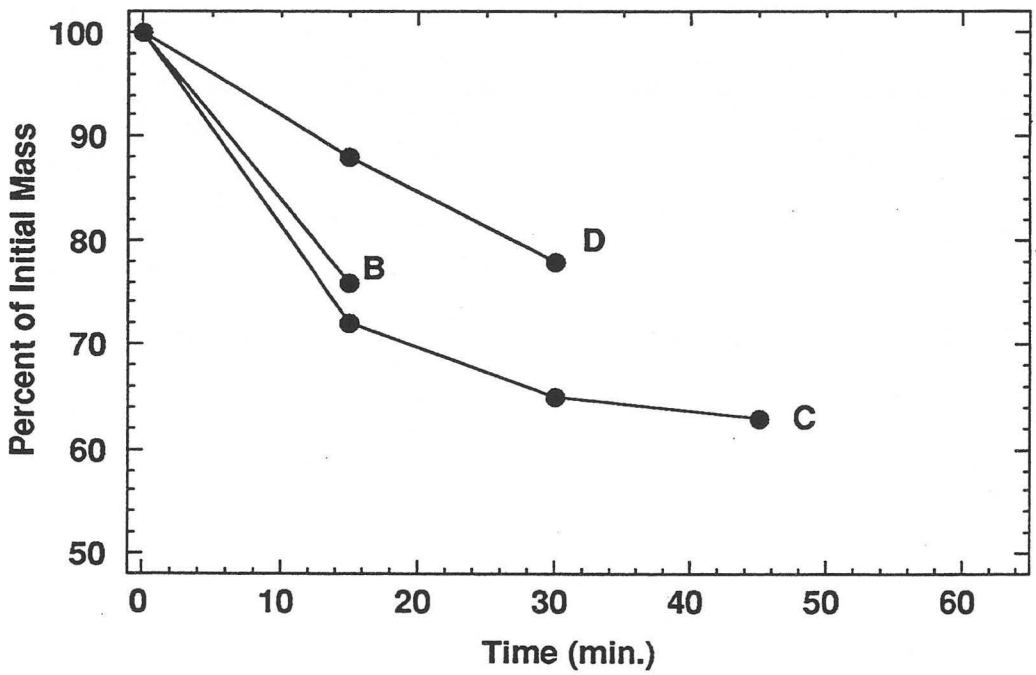

Figure 7.3 The mass loss rate for the granules shown in figure 7.2.

After this dramatic performance, we were interested in determining what the maximum dose was that we could subject the granules to without observing any obvious structural damage to the zymogen granule. We experimented with leaving the focused spot of X-rays on different granules for 10, 5 and 2sec and the results are shown below. All of the experiments presented used granules from the same preparation and were imaged in the same LBL-WC. Figure 7.4 shows a series of a granule where the shutter was left open, exposing the center of the granule to the focused beam of X-rays for 10sec. The exposure time was ~2500 times greater than for a regular image which is ~30Mrads. We can see that the damage is not as severe as figure 7.3, although an obvious hole has been formed in the granule. The hole is ~0.2μm in diameter which is larger than the focused spot of X-rays (~0.05μm) indicating that the radiation damage effects can spread.

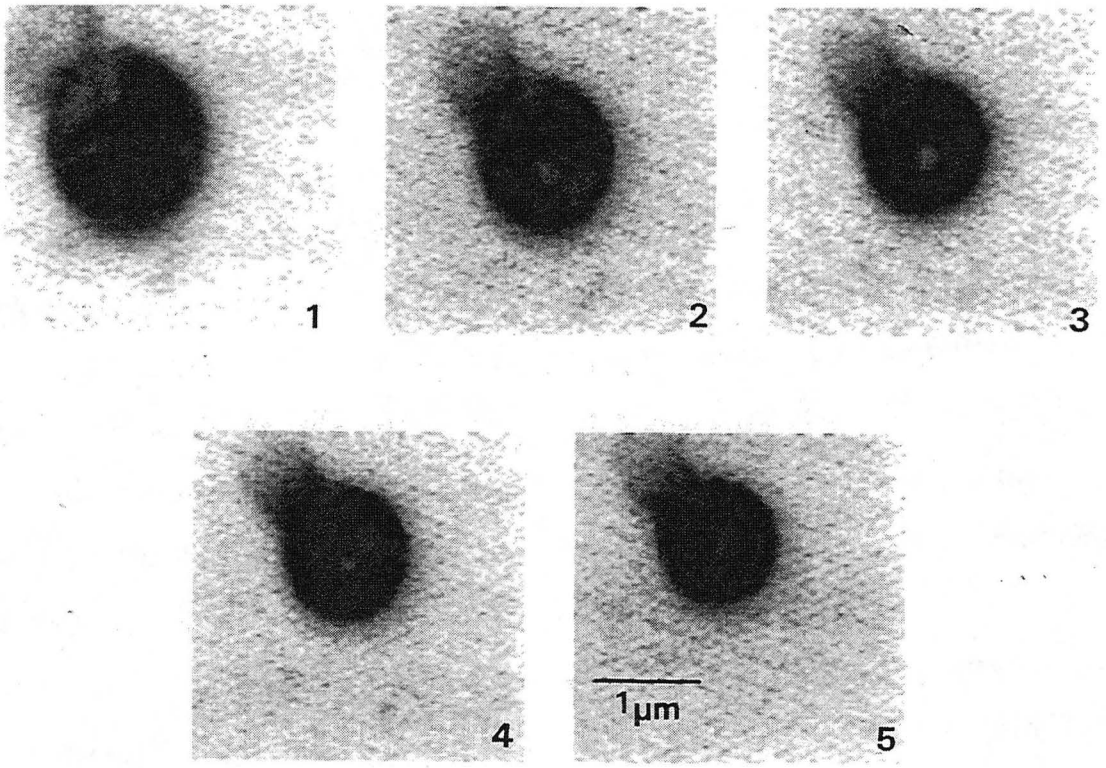

Figure 7.4 This is a series of images taken of the same zymogen granule suspended in 0.3M sucrose. After the first image was taken, the focused beam of X-rays was allowed to dwell on the granule for 10 sec and the second image was taken. The subsequent three images were taken within a half hour without any further overexposure. The pixel size in each image was 2.7nm.

Figure 7.5 shows the mass loss for this granule over the time course. As compared to figure 7.3, we can see that the mass loss rate of this exposed granule is initially four times faster than granules that were not exposed in this manner.

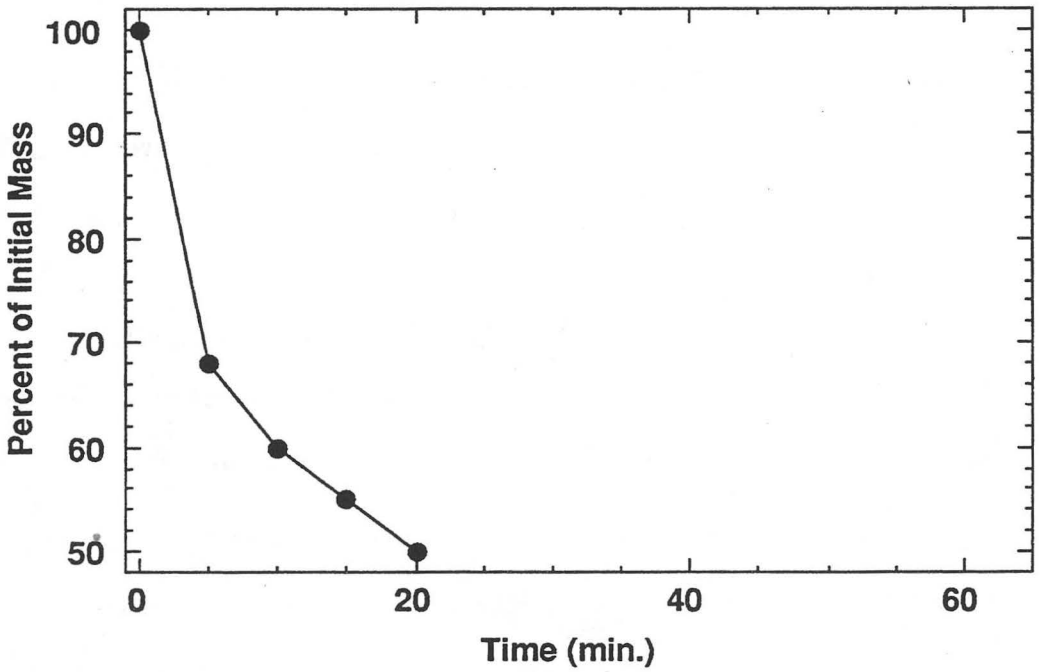

Figure 7.5 The mass loss rate of the granule shown in figure 7.4. The focused spot of X-rays was directed on the granule for 10sec after the initial image was taken.

The next experiment involved exposing granules to the focused spot of X-rays with the shutter left open for 5 sec. The images from this experiment are shown in figure 7.6. The initial image was again taken with 2.7nm pixels (~30Mrads). After this initial image, the focused spot of X-rays was directed onto granule A for 5 sec. The exposure time was ~1250 times that of a regular image. We did not observe any obvious hole in the granule after this, although as can be seen in figure 7.7, mass loss increases noticeably after the exposure as compared to the controls. We exposed a second granule, E, to the focused spot of X-rays after the second image and in the third image it is possible to discern what might be a hole, although E does have a lucent area visible in the first image that may be what we think is a hole. Nonetheless, we can see in figure 7.7 that the exposure has resulted in an increased rate of mass loss.

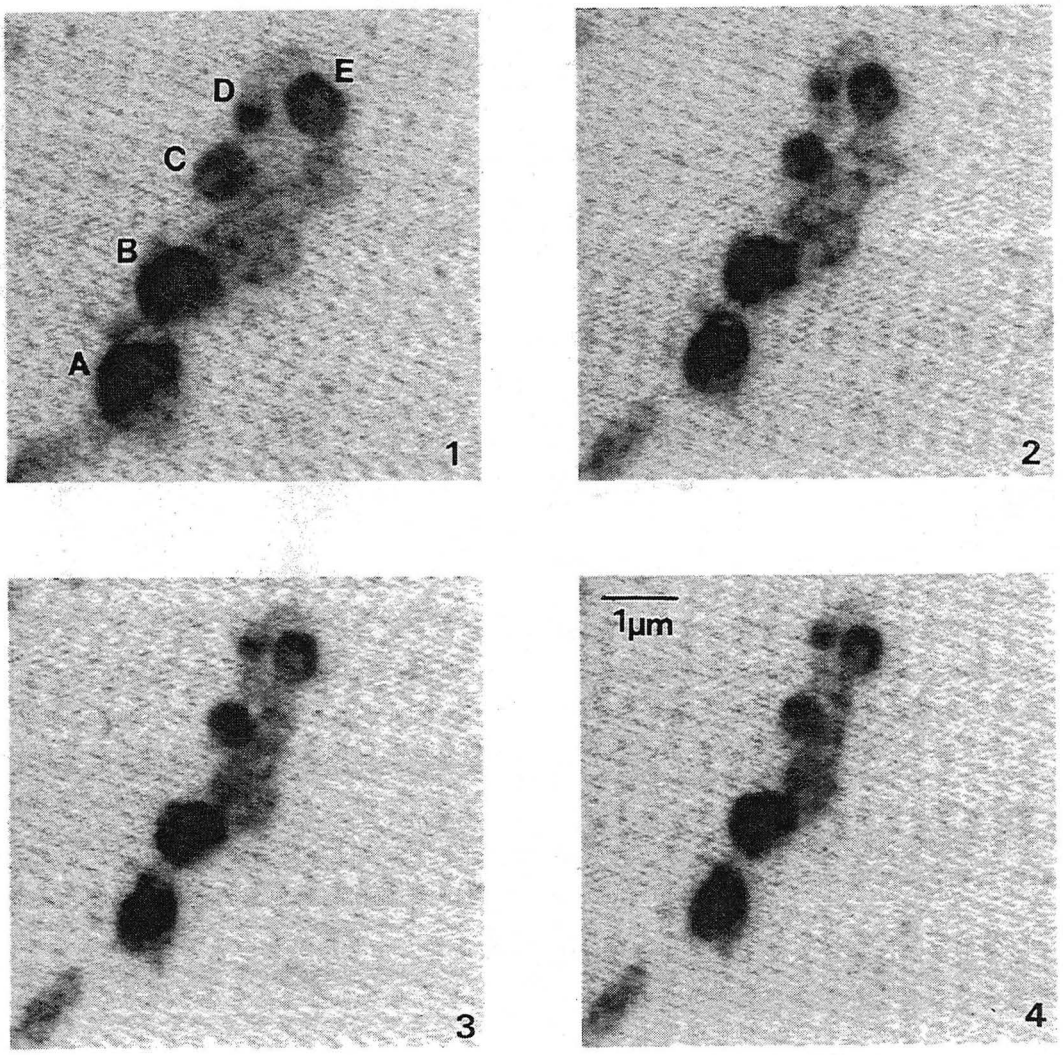

Figure 7.6 After the initial image the shutter was left open for 5sec on granule A. A second image was taken 6 minutes later and then the shutter was left open for 5 sec on granule E.

We can see that the rate of mass loss of granule **A** was initially only 2.5 faster than the granules from figure 7.3 (recall that the granule from Figure 7.5, which was exposed twice as long, had an initial mass loss rate that was 4 times as fast as those from figure 7.3). We can also see that after granule **E** was exposed, its mass loss rate also increased by a factor of 2.5 from its initial rate between the 1st and 2nd image.

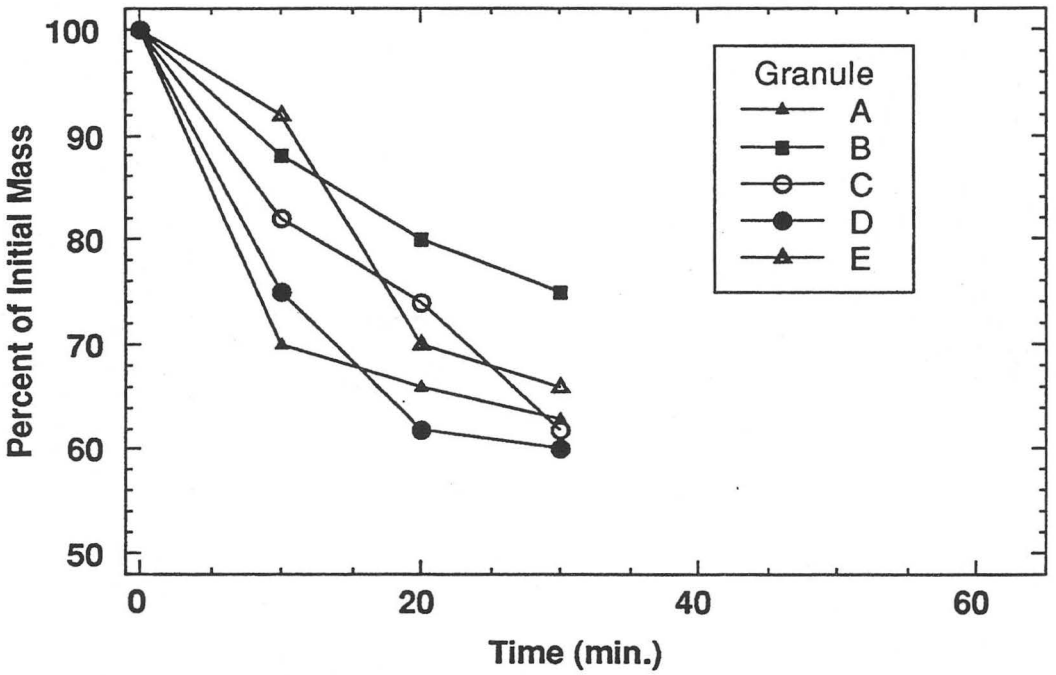

Figure 7.7. Mass loss rate from figure 7.6. Granule **A** had the spot of X rays left on it for 5 sec after the initial exposure and granule **E**, after the second exposure. We can see that after the irradiation, the mass loss rate increased dramatically, but then plateaus.

The final experiment involved leaving the focused spot of X rays on a granule for 2 sec, which is an exposure only 666 times greater than normal (again, ~30Mrad). The series of images from this experiment is shown in figure 7.8. Granule B was chosen and was exposed for 2sec after the initial image. We cannot discern any obvious structural change in the granule in the second image.

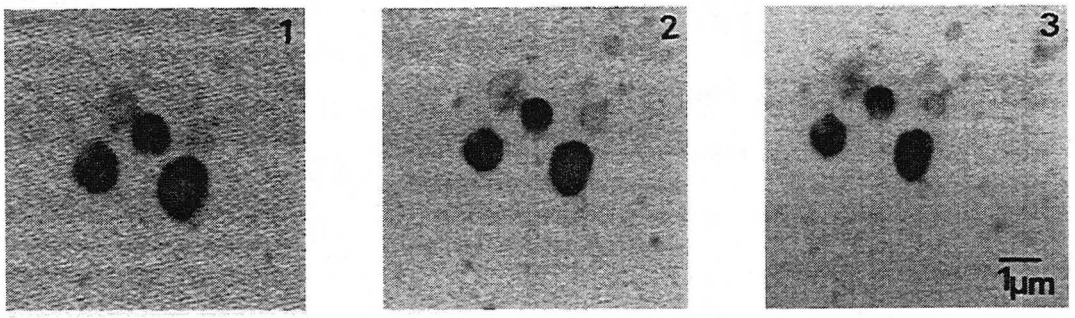

Figure 7.8. The initial image was taken with 2.7nm pixel sizes. After the initial image, the probe of X-rays was centered on granule **B** for 2 sec. Then two additional images were taken. We do not observe the type of structural damage that was visible in the previous studies.

The rate of mass loss for these is shown in figure 7.9. We can see that the mass loss for the exposed granule **B** does not appear different from the mass loss rates of the other two granules in the image. And the average initial mass loss rate for all of the granules in this experiment is not remarkably different from the granules in figure 7.3 (18% versus 14%, respectively in the first 10 minutes) but still greatly elevated as compared to the controls.

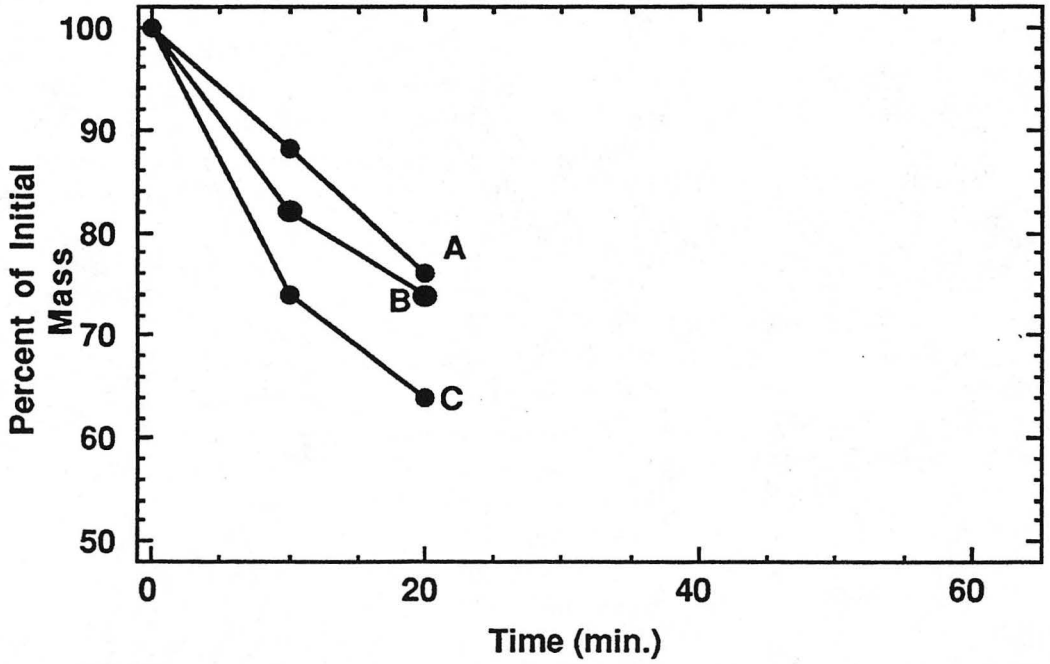

Figure 7.9 The mass loss rate for the granules shown in figure 7.8. Granule B was exposed for 2sec to the focused spot of X rays after the initial image.

From the results of these experiments it would appear that we can expose areas of our granules to doses of X rays that are almost 1000 times higher than what other areas in the same granule receive and do not see any gross structural damage. There also doesn't appear to be a change in the release of protein from granules at these dose rates. For example, the protein mass loss rate from a granule exposed to a 2sec spot of focused X rays was similar to those in the same field that were not exposed.

But in all of these experiments we observed a higher rate of protein loss, even from the granules than in control experiments; about 15 times higher! This is probably the result of oxidative damage to the membrane due to free radicals produced from the radiolysis of water molecules exposed to the focused spot of X rays and that diffused to the membrane from the site of their production. These indirect effects of radiation will be discussed in the next section.

VII.3 Damage Mechanisms

From the previous section, we can see that exposure to X rays can result in the structural and functional damage to a specimen. It is important to understand how the structural damage is occurring and what types of functional damage are possible in order to 1) understand the limitations of the method and 2) develop techniques that can be used to protect specimens.

All of the damage to a specimen incurred by the X-ray photons in STXM must be either a direct or indirect result of the absorption of the X ray photons by the sample. This is because in the energy range of X rays we are using, the scattered photons are elastically scattered and therefore do not transfer any energy to the sample and so photons are either innocuously transmitted through the sample or absorbed (Henke, 1981). The process of X-ray absorption involves the transfer of the energy of the photon to an orbital electron of an atom. If the photon contains sufficient energy, then the electron is ejected from the atom, now called a **photo-electron**, with an energy equal to the difference between the photon energy and the binding energy of the electron. This is a **primary ionization** process as the atom is left ionized. If there is not enough energy, then the electron is merely excited to a higher orbital state and the atom is considered **excited**. The formation of a photo-electron and the primary ionizations are a result of the **direct effect** of the absorption of the X ray photons. They in turn lead to a chain reaction of further ionizations at other atoms and more photo-electron production that propagates until the initial energy of the photon has been dispersed. These secondary processes are called the **indirect effects** of the absorption of X rays.

We would like to know two things in order to predict the type of structural or functional damage that can occur as a result of these direct and indirect effects. The first is to understand the extent of the direct effect; what atoms are most likely to absorb the X rays? how does the primary ionization affect these atoms? and what is the energy of the

photoelectrons? And the second is to understand the indirect effects; how the primary ionization's affect other molecular species and what further damage do the photoelectrons inflict?

We will address the direct effects first. We can predict the probability that a particular atom will absorb a photon based on the atomic subshell photoionization cross sections for that particular atom. Then, by knowing the binding energies of the electrons, we can determine the primary ionization state that the atom is left in after the absorption event and calculate the energy of the photo-electron. Table 7.5 shows the cross sectional values for the different shell electrons in some atoms that we would find in a typical biological system - H, C, N and O would be the most common atoms although we might find trace amounts of the other atoms listed - and the binding energies of the different shell electrons for a 350eV (3.5nm) photon. Silicon is also shown as a matter of interest because it is a major element in the windows used in the STXM.

Table 7.5. Cross section values for atom species encountered in our system. These values are taken from (Yeh and Lindau, 1985). The most commonly encountered species are H, C, N and O. The other atoms are only present in trace amounts. Si is shown because it is found in the silicon nitride windows. Values in parenthesis are the binding energies for the particular shell electron.

atom	Cross Section (Mb*) for Electron Shell for X ray photon = 350eV and binding energy [eV] for the electron				
	1s	2s	2p	3s	3p
H	$4x10^{-4}$ [13.6]				
C	$6x10^{-1}$ [290.9]	$3x10^{-2}$ [17.5]	$4x10^{-3}$ [9.0]		
N		$4x10^{-2}$ [23.1]	$1x10^{-2}$ [11.5]		
O		$6x10^{-2}$ [29.2]	$3x10^{-2}$ [14.2]		
Na		$1x10^{-1}$ [64.3]	$2x10^{-1}$ [36.3]	$4x10^{-3}$ [5.1]	
Si		$2x10^{-1}$ [150.8]	$7x10^{-1}$ [108.2]	$2x10^{-2}$ [13.6]	$1x10^{-2}$ [6.5]
S		$3x10^{-1}$ [224.6]	$1x10^{-0}$ [171.8]	$3x10^{-2}$ [20.8]	$5x10^{-2}$ [10.3]
Cl		$3x10^{-1}$ [266.2]	$2x10^{-0}$ [208.2]	$4x10^{-2}$ [24.6]	$9x10^{-2}$ [12.3]
K			$2x10^{-0}$ [299.4]	$6x10^{-2}$ [40.2]	$2x10^{-1}$ [23.6]

*Mb = $1x10^{-18}$ cm^2

From the table we can see that the most probable absorption event for 350eV photons is by the core shell electrons of carbon. This event has a probability of occurring 10 times more often (if there are equal numbers of atoms in the system) than the next most frequent event, which would be the absorption of the photon by the 2p electron shell of oxygen. The direct effect of absorption by the core shell electron of carbon leads to a double ionization of the atom; the production of an Auger electron and a very low energy photoelectron, 59 eV(Halpern, 1982). Whereas the direct effect of absorption by the core shell of oxygen leads to a single ionization of the atom and a photo-electron with energy of 321 eV!

Even though absorption by a carbon atom is the most probable event, it is not the most common one because we are not working in a system where there are equal numbers of all of the atoms. In our system, the average protein concentration of zymogen granules is 253 ± 7mg/ml (±s.e.m.). The depth of the sample chamber is ~2μm which means that approximately half of the thickness is the suspending solution and half the granule (the average diameter being 1.08 ± 0.01 μm). Therefore, in a typical pixel volume, there is 10% protein by mass and 90% water. This is roughly the same situation found in hydrated cells so this discussion can be extended to include cells. The molecular formula for a typical granule protein (chymotrypsinogen) is $C_{1157}H_{2378}N_{318}O_{585}S_{22}$ and it has a MW=25,000. From this information we can calculate that in a typical pixel volume, there is ~20 times more oxygen than carbon atoms. Therefore, even though the probability of the photon being absorbed by an oxygen molecule is 10 times less than carbon, because there are so many oxygen atoms, the effective absorption with oxygen being favored is more like 2:1. Or in other words, if we consider only absorption by oxygen and carbon then 66% of the total absorbed photons would be absorbed by oxygen, primarily in water, and 33% would be absorbed by carbon, primarily in carbon.

For our typical pixel, from Table 7.4 we determined that 700 photons were absorbed solely by the sample, or essentially in carbon. As there are ~5,000 protein molecules in this pixel (considering the average protein concentration is 253 mg/ml), this means that one carbon atom in every 8 protein molecules would be doubly ionized, producing an Auger and a low energy photo-electron. But, it was also determined that ~1400 photons were absorbed by water (primarily in oxygen) and one of these ionization's would produce a photo-electron, as mentioned above, with energy of 321 eV! A photoelectron of this energy could ionize ~10 more oxygen molecules. In effect the 1400 photons that are absorbed by water/oxygen could eventually ionize 11*1400 oxygen molecules, which is one in every 7000 water molecules in the pixel. After the photo-electrons have dissipated most of their energy and are at ~100eV or less, they can be captured by the process shown in figure 7.10 or they can attract the permanent dipoles of several water molecules to form the hydrated electron, e_{aq}^-. This entity is more stable than the free electron.

Of course, not only carbon and oxygen absorb photons. A more rigorous model of the probable absorption events, photo-electron production and subsequent ionization's would be overwhelming and clearly beyond the scope of this thesis. But, from this basic analysis, we can get a general idea of the maximum number of carbon and oxygen atoms that could be ionized by the absorption of X-ray photons.

The next question is how does this ionization of atoms affect the structure and function of the biological system. First we will consider the effect of ionization on carbon atoms, or other atoms that are part of bio-molecules. The ionization has the effect of changing the original charge distribution of the molecule and this is noted as (R•). The affected molecule may attempt to regain its original charge distribution by "stealing" from a neighboring molecule. This is called restitution and occurs by

$$R\bullet + R\text{-}SH \rightarrow R\text{-}H + R\text{-}S\bullet$$

but it only has the effect of leaving a second molecule reactive. Structural damage can occur when R• attempts to regain its original charge distribution by stealing charge from a bond. This results in broken bonds and potentially "freeing" the molecule, or part of the molecule to diffuse away (note: this can only occur if there is a suspending solution).

Functional damage can occur simply through intra-molecular charge redistributions that take place due to electrostatic repulsion as a result of the ionization of atoms within the molecule repelling one another. A doubly ionized atom (as occurs in the absorption of the photon by a carbon) will cause a tremendous shift in the original shape of the molecule and can lead to its dysfunction (Halpern, 1982). Functional damage can also occur through peroxidation if the damaged molecule grabs an oxygen molecule, and occurs as follows

$$R\bullet + O_2 \text{ --> } R\bullet\text{-peroxide}$$

The peroxidated radical cannot undergo restitution but is more stable than the original radical.

The ionization of water affects the biology in our system because the species that are produced through the radiolysis of water can diffuse through the medium and attack the bio-molecule. So having a hydrated specimen, as opposed to a dry sample, increases the amount of radiation damage that can occur to the specimen. This is an unfortunate side-effect of attempting to perform experiments in a natural environment but the alternative is to avoid observations on the natural state we wish to learn about. Water radiolysis has been studied in detail and the following discussion is based on a review by Alpen (1990). The radical species formed as a result of either the direct absorption of X rays or a photoelectron (e^-) produced from another atom, on water are shown below in figure 7.10

Event			Radical Species	
Excitations:	H_20 + (X ray or e^-)	-->	H_20^*	--> H• + OH•
Ionization:	H_20 + (X ray or e^-)	-->	$H_20^+ + e^-$	
Propagation:	H_20^+	-->	H^+ + OH•	
	e^- + H_20	-->	H_20^-	--> H• + OH^-
		-->	e_{aq}^-	
	e^- + H^+	-->	H•	

Figure 7.10. The products formed by the interaction of ionizing radiation with water. After the initial event, the excited or ionized water molecules dissociate to form the primary products shown. e^- represents the photo-electron. These species react with water or hydrogen ions. The symbol (*) indicates an excited and (•) indicates a radical species and (+) or (-) gives the charge of the atom. The radical species e_{aq}^- is also called a hydrated electron and was discussed in the text.

Not all of these species will interact with bio-molecules. For one thing, they may be far away, i.e. in the bulk suspending medium. Reactive species may recombine before they affect other molecules. But if this does not occur within the first 10^{-11}sec, then it won't happen because of diffusion. Although, they will react with other water molecules or with bio-molecules until stable products are formed. Some of the stable products formed from the interaction with other water molecules (or hydrogen) are H_3^+, H_2, OH^-, HO_2•, O_2, O_2^-, HO_2^-, H_2O_2 and O_2^-.

Some possible reactions of radical species on bio-molecules are shown below in figure 7.11 where R represents the bio-molecule.

Extraction of hydrogen atoms:

$$R\text{-}H + H\bullet \rightarrow R\bullet + H_2$$
$$R\text{-}H + OH\bullet \rightarrow R\bullet + H_2O$$

Dissociation reactions:

$$R\text{-}NH_3^+ + eaq^- \rightarrow R\bullet + NH_3$$
$$R\text{-}NH_2 + H\bullet \rightarrow R\bullet + NH_3$$

Addition reactions:

$$R\text{-}CH{=}CH\text{-}R + OH\bullet \rightarrow RCHOH\text{-}CH\bullet\text{-}R$$

Figure 7.11 The reactions that the radical species produced from the radiolysis of water can participate in with bio-molecules (R).

All of these reactions leave the molecule in a highly reactive state (R•) with an altered charge distribution. Thus, in general, water acts to increase the effectiveness of ionizing radiation in producing damage to the bio-molecule.

We have already seen how water radiolysis increases the effectiveness of the indirect effects of the absorption of X rays in the radiation studies we presented in the previous section. In these studies, massive doses of X rays directed onto isolated granules probably caused the ionization of many water molecules. The radical species that were produced from this exposure diffused through the water and affected the rate of mass loss of other granules in the image.

Unfortunately, while it is possible to predict the type of atoms that may be affected by the absorption of X rays and the subsequent number of ionization's and photoelectrons produced, given the range of reactions that can occur as reported above, it would be near impossible to predict how much structural and more importantly, what type of functional damage will come about as a result of the absorbed dose. And so, in the end, it is the result of actual experiments that have been performed that contribute to our understanding of the extent of radiation damage and relating the absorbed dose to either the observed structural damage or functional damage.

VII..4 Radiation Damage Experiments by Others

There had been no radiation studies performed using scanning X-ray microscopes before we began our research at BNL, although there had been several theoretical studies (Sayre et al., 1977; Kirz, 1980). During the time period that we were at BNL, two other users were performing research that concentrated on the effects of radiation damage (Williams et al., 1993; Gilbert, 1992). Since then research has continued and at the latest X-ray Microscopy Conference, September 20-24 1993, Moscow, many new radiation damage studies were presented. In this section, we will review many of these studies and

discuss some of the similar results. The studies are of two types, those that measure mass loss as an indicator of radiation damage and those that observe functional changes as a result of absorbed dose. There have been no studies on the amount or type of molecular byproducts produced as a result of exposure.

In terms of measuring the mass loss of samples as a result of exposure to X-rays, we report here three experiments, all on different systems. Gilbert (1992) has done a comprehensive study determining what the limits of STXM (at BNL) are in terms of the resolution and contrast in wet, fixed and fresh cells (chick fibroblasts), taking into consideration the amount of absorbed dose that these cells can sustain. Radiation damage was measured as a function of mass loss and he concluded that mass loss is a linear function with respect to the cumulative energy absorbed. This means that the damage that each photon does is independent of all other photons, and is consistent with what others have found when studying radiation inactivation of enzyme function (Kepner and Macey, 1968). Gilbert calculated what he called a hardness factor "α = -0.78" which is in units of carbon atoms lost/ eV deposited. This factor translates to about 450 carbon atoms worth of absorption lost to each 3.6nm photon or about a 15% mass loss would be observed for an absorbed dose of 30Mrad in fixed, wet cells.

Williams et al. (1993) studied the effect of radiation damage in STXM (at BNL) by measuring changes in the measured mass of isolated *Vicia faba* (bean) chromosomes, wet and dry. All of the wet specimens were fixed with either glutaraldehyde, formaldehyde or osmium tetroxide. Williams et al. found that the dried samples were extremely resistant to mass loss and only after 150Mrad of absorbed dose, was there any noticeable change in mass. Wet chromosomes fixed with 0.1% glutaraldehyde retained 99.0-99.5% of their original mass during exposure to 5-10Mrad. At higher doses, 50Mrad, 95% of the initial mass was retained and 89% of the mass was retained after 100 Mrad. They noticed also that the type of fixative had an effect on the radiosensitivity of the sample;

chromosomes fixed with formaldehyde or osmium tetroxide were much more radiation sensitive and a complete loss of the sample was observed at 40Mrad. The concentration of glutaraldehyde also made a difference in the radiosensitivity of the sample. Chromosomes fixed in 1% glutaraldehyde at room temperature for one hour were more stable than those fixed at 0.1% for 24 hours at 4°C. Finally, Burge et al. (1993) have observed, using the STXM at Daresbury (England), a 20% mass loss in fresh, unfixed sarcomeres after 2Mrad.

From these results it is apparent the mass loss of a sample as a result of exposure to soft X-rays depends on two things. The first of these is the state of the sample and whether its dry, wet or fixed. Dry samples are the most radioresistant and this is no surprise because as was discussed earlier, the indirect effects of the radiolysis of water can contribute greatly to the radiation damage of a sample. The fixed samples are also fairly radio-resistant although this can depend on the type of fixative and the concentration of the fixative due to the cross linking of molecules preventing diffusion. It is interesting to note that even though both samples are fixed, the mass loss rates are quite different for Gilbert's cells and Williams' chromosomes - 15% at 30Mrad and 5% at 50Mrad respectively. Apparently particular types of samples are affected very differently under similar conditions.

There have been two viability experiments performed using the scanning transmission microscope. The first was done by Foster et al. (1992) at Daresbury. In this experiment, hydrated myofibrils were exposed to various doses of soft X-rays. Afterwards, ATP and calcium were added to the suspension and the proportion of myofibrils that contracted was monitored in a light microscope. Approximately 70% of a population of myofibrils failed to contract after 2Mrad of radiation. The second experiment was performed by Jacobsen et al. (1993). Using the STXM at BNL, CHO (chinese hamster ovary) cells are exposed to various doses of soft X-rays. After the exposure, a vital dye is added to the

suspension and the cells are observed under a light microscope. The dye has the characteristic of only being able to enter through damaged membranes, and once inside the cell it changes color from green to red. From these experiments, they found that cells remain intact after ~1Mrad of absorbed dose. After several Mrads, the cells still appear intact, but after a period of time the dye enters the cells. After ~10Mrad, the dye immediately enters the cells. Both of these experiments indicate that the kinetic aspects of cells can be extremely sensitive to dose. Although, once again we see that different aspects show different radiosensitivities. While many of the myofibrils fail to contract after 2Mrad, the membrane barrier of the cells remains unaffected. This difference in the sensitivity of each specimen is why it is so important to understand the effects of radiation system by system and not to generalize from single examples.

These studies are just beginning to scratch the surface of our understanding of what limits soft X-ray radiation damage imposes on our ability to image biological specimens. Moreover, the limits are different depending on whether only high resolution images are the goal (no kinetic aspect) or if the experiment involves wet, hopefully viable samples. The damage that occurs in the later type of experiment is much easier to inflict.

There is some hope in terms of increasing the resistance of samples to the effects of radiation and this is through the use of free radical scavengers. These molecules generally contain NO or R-SHH• groups and are particularly handy in "mopping up" the OH• and H• radicals produced by the radiolysis of water. In the myofibril experiment reported above (Foster et al., 1992) when 25% DMSO (dimethyl sulphoxide) was added to the buffer, 100% of the myofibrils were able to contract after the same 2Mrad of dose that resulted in 70% of the population being *unable* to contract in its absence. These free radicals also contribute to reducing the mass loss rate observed in a given specimen (Williams).

Chapter VII - References

Alpen, E.L., Radiation Biophysics, Prentice Hall: Englewood Cliffs, NJ. (1990).

Burge, R.E., G. Foster, C.J. Buckley and P. Bennet, Sarcomere structure by X-ray microscopy, In: X-ray microscopy IV (to be published).

Cantafora, A., M. Ceccarini, L. Guidoni, F. Ianzini, M. Minetti and V. Viti, Effects of gamma-irradiation on the erythrocyte membrane: ESR, NMR and biochemical studies, Int. J. Radiat. Biol. (1987) **51**:59-69.

Cullen, D.E., M.H. Chen, J.H. Hubbell, S.T. Perkins, E.F. Plechaty, J.A. Rathkopf and J.H. Scofield, Tables and graphs of photon-interaction cross sections from 10eV to 100GeV derived from the LLNL evaluated photon data library (EPDL), Part A: Z=1 to 50, UCRL-50400 vol. 6, University of California, Lawrence Livermore Laboratory: Springfield VA, National Technical Information Service (1989).

Edwards, J.C., D. Chapman, W.A. Cramp and M.B. Yatvin, The effects of ionizing radiation on biomembrane structure and function, Prog. Biophys. Molec. Biol. (1984) **43**:71-93.

Foster, G.F., C.J. Buckley, P.M. Bennett and R.E. Burge, Investigation of radiation damage to biological specimens at water-window wavelengths, Rev. Sci. Instrum. (1992) **63**:599.

Gilbert, J.R., Soft X-ray microimaging of whole wet cells, Ph.D. Thesis, California Technical Institute: Pasadena, California (1992).

Halpern, A., Damage to biomolecules and cells by low-energy X-rays and vacuum ultraviolet light, In: Uses of Synchrotron Radiation in Biology (H.B. Stuhrmann, Ed.) Academic Press: San Francisco (1982).

Henke, B.L. Low energy X-ray Interactions: Photoionization, Scattering, Specular and Bragg Reflection, (1981) 146-155.

Hutchison, F. and E. Pollard, In: Mechanisms in Radiobiology (M. Errera and A. Forrsberg, Eds.), Volume 1, Academic Press, Inc.: New York.

Kepner, G.R. and R.I. Macey, Membrane enzyme systems molecular size determination by radiation inactivation, Biochim. Biophys. Acta (1968) **163**:188-203.

Lea, D., Actions of Radiations on Living Cells, Cambridge University Press, London (1955).

Pollard, E.C. Am. Scientist (1969) **57**:206-236.

Pollard, E.C., W.R. Guild, F. Hutchinson and R.B. Setlow, The direct action of ionizing radiation of enzymes and antigens, Prog. Biophys. (1955) **5**:72-108.

Raleigh, J.A., W. Kremers and B. Gaboury, Dose-rate and oxygen effects in models of lipid membranes: linoleic acid, Int. J. Rad. Biol. (1977) **31**:203-213.

Rothman, S.S., The behavior of isolated zymogen granules: pH-dependent release and reassociation of protein, Biochim. Biophys. Acta (1971) **241**:567-577.

Schneider, G., Investigation of soft X-ray radiation induced structural changes in wet biological specimens, In: X-ray Microscopy IV (to be published)

Williams, S., X. Zhang, C. Jacobsen, J. Kirz and S. Lindaas, Measurements of wet metaphase chromosomes in the scanning transmission X-ray microscope (1993) **171**:155-165..

Wolters, H., C.A.M. van Tilburg and A.W.T Konings, "Radiation-induced lipid peroxidation:influence of oxygen concentration and membrane lipid composition," Int. J. Radiat. Biol. (1987) **51**:619-628.

Yeh, J.J. and I. Lindau, Subshell photoionization cross sections, Atomic data and nuclear tables, Vol. 32 (1985).

Chapter VIII. Discussion and Conclusions

Using X-ray microscopy, we have been able to successfully image freshly isolated zymogen granules (diameter ~1μm), from the acinar cell of the pancreas, suspended in isosmotic solution at a resolution that is ~3-5 times better than light microscopy without the use of stains or fixatives. We have also been able to follow individual granules over a period of time and monitor changes in the structure of these granules while changing the environmental conditions (suspending solution). In fact, this is the first time it has been possible to perform a direct time resolved experiment on such a small bio-object; not only obtaining visual images, but also quantitative information on the characteristics of diameter, protein concentration and mass of each object over the time course. The first section of this chapter will discuss what we have learned about zymogen granules from these studies and the second section will present our views on the general technique of X-ray microscopy.

VIII.1 The zymogen granule

The change in protein mass and granule volume

Our measurements showing a change in the protein content of isolated zymogen granules and the images taken simultaneously provide direct evidence for the permeability of isolated zymogen granule membranes to the protein contained within the granules. As such, the measured change in mass of individual zymogen granules over time was taken to be a direct consequence of protein either leaving or being taken up by the granule. In addition, these observations invalidate the contention that protein is released from granules by lysis, or the breaking open of the granule and the releasing of all its contents at once. The granules in our experiments remained intact throughout the study and were observed to change in their measured protein mass over the time at a relatively slow and measurable rate. That the results are not due to damage from the X-ray microscope is verified by the fact that our measured rates of protein loss, mentioned

in the Results chapter (VI), are similar to rates measured using other techniques (Liebow and Rothman, 1976, 1972; Rothman, 1971; Hokin, 1955).

The driving force behind the release of protein was determined to be simple mass action. In other words, protein moved in response to local protein gradients; from regions of high protein concentration to low concentration until, if possible, an equilibrium was reached. Granules suspended in isosmotic solution were observed to reach a quasi-equilibrium as the protein gradient between the interior of the granule and the suspending solution steadily decreased as a direct consequence of granules releasing their protein into the solution (June-control experiments). Moreover, the rate of protein release could be increased by increasing the protein gradient by either circulating the isosmotic suspending solution (December-control experiments) or perifusion (isosmotic dilution experiments). This increased rate of protein release was able to return to a quasi-equilibrium state once the protein gradient was decreased by halting the circulation of fluid (December-control). In the isosmotic dilution experiment, the elevated protein gradient was maintained and as expected, the rate of protein release remained linear and did not approach an equilibrium value.

The release of protein from the granules is a reversible process and granules are able to take up protein when the concentration in the suspending solution is elevated. In the June-control experiment, some granules showed an increase in mass (data not shown) that could only be accounted for by these granules taking up "released" protein from other granules in the same suspension. As such, this indicates that a true equilibrium state can be achieved by isolated zymogen granules where the rate of protein efflux is balanced by the rate of influx of protein . Moreover, granules were also observed to take up exogeneously added protein (chymotrypsinogen). This bi-directional movement implies that a simple mechanism must be involved in the transport of protein across the membrane, possibly a pore such as will be discussed later.

In mass action processes, the amount of protein released from the granules depends on the concentration of soluble protein within the granule. However, in the zymogen granules, this concentration is constant and so the rate of protein release from the granules is influenced more by the total amount of protein in solution - or the volume of the protein solution. The remaining volume within the granule is occupied by protein in an aggregated form. A standard by which we can calculate the percent volume of the granule occupied by soluble protein is given by the protein concentration of the granule; for example, a protein concentration of 600mg/ml indicates that the volumes of aggregate and soluble protein are equal, however for a protein concentration of 100mg/ml, the soluble protein will occupy ~90% of the granule volume[1]. As such, NUG granules, which on average have a low protein concentration and therefore a generous percentage of their volume in soluble protein, consistently show a higher rate of protein loss than UG granules.

The observation that granules release protein at different rates actually requires further exploration in light of the fact that granule protein is able to move from an aggregated to a soluble form, and vice versa (Liebow and Rothman, 1976). As such, we would expect to observe the continuous release of protein from the granules as protein from the aggregate is solubilized and, given the existence of a concentration gradient. However, we observe that there is a limit to the amount of released protein as demonstrated in both the hyper- and hyposmotic experiment where the rate of protein release reached a quasi-equilibrium state (for both types of granules, UG and NUG) even though protein was still visible in the granules. Although some of this remaining protein is not enzymatic in nature and, as mentioned in the Chaper I, may be structural. However, as this type of protein accounts for only ~5-10% of the total protein most of the remaining protein would be digestive enzyme.

---

[1] Assuming the density of protein to be 1.2 gm/ml and the concentration of protein in solution within the granule (as discussed in the results section) to be 75µg/ml.

The different rates and the limit to protein release from the granules are, in fact, a consequence of the particular binding and solubility properties of the granule protein despite mass action; protein will only be released from the granule if it is in a soluble form. Although it is not currently known how proteins are bound in the aggregate or what are their binding and solubility properties, the binding has been shown to be electrostatic in nature (Rothman et al., 1974). Therefore, we would expect different solutions with different ionic properties to affect the electrostatic binding and to change the rate of protein release from the granules. Indeed, when granules are exposed to salt (150mM NaCl) or the internal pH is increased by using the ionophore Nigericin, the rate of protein release from the granules is elevated . Additionally, when all of the soluble protein is released from the aggregate, the rate of protein release reaches an equilibrium value - as mentioned above.

Moreover, because each protein has a different isoelectric point (see the Chapter I), we can assume that each of the 20 different enzymes that are known to be contained within the granules would have unique binding and solubility properties. As such, they would behave independently of each other and would either be bound or soluble depending on the nature of the environmental conditions. This suggests that under certain conditions, only particular proteins would be released from the aggregate and be free for release from the granule. In other words, release of protein from the granules would be non-parallel.

The fact that we observed differences in the measured rate of protein release from individual granules under the same experiment conditions (data shown as statistical variation) may have been a direct result of this phenomenon. If each zymogen granule contained different proportions of each protein and some of the proteins were more soluble in the particular environmental conditions of the experiment than others, then granules containing greater amounts of the soluble proteins would show a rate of protein

release that was relatively higher than other granules. As it has already been reported that granules appear to contain various amounts of the enzymes (Tobler et al., 1991; Adelson and Miller, 1989; Mroz and Lechene, 1986), the scenario described above appears plausible. It may be possible in the future to label individual enzymes and track their movement using STXM to further characterize the distribution of enzymes from granule to granule.

The character of the protein aggregate, up to this point, has not truly been addressed and this is partially because it is not well understood. As mentioned above, each granule contains 20 different types of enzymes and it is yet unclear if such a heterogeneous aggregateis formed by enzyme-enzyme binding or by non-specific binding to each other or to structural proteins. In our experiments, we have noticed that for each preparation (a combination of two pancreases) the protein concentration values for all granules of a particular type (UG or NUG) are tightly grouped together. Additionally, if we plot the protein mass against the granule volume for each granule, all of the data fit a line, the slope of which is the average protein concentration, regardless of the size or "weight" of the granule (see for example, figure 6.20). However, if we combine the results of many different experiments, as in the General Population, we do not observe this relationship (figure 6.7). It would appear that the protein concentration of the granules is a characteristic of the particular pancreas and as such implies that all of the granules are subject to be filled equally and therefore have similar protein concentrations. Because it is known that the proportions of the different enzymes varies from granule to granule and since the characteristic protein concentration of a particular preparation is maintained, in all likelihood the proteins are bound non-specifically within the granules.

The observed change in the diameter of the granules is influenced by both the change in protein content and the size of the protein aggregate. Protein release results in a decrease in the diameter as water, associated with the solubilized protein, leaves the

granule. As protein release occurs in isosmotic solutions, the decrease in diameter cannot be attributed to osmotic shrinking in this case. However, granules are sensitive to hyperosmotic forces as an increase in the osmolarity of the suspending solution will result in a decrease in the diameter of granules above that of the isosmotic solution. Alternatively, when granules take up protein, as observed in one of the chymotrypsinogen experiments, granules increased in mass *and* in diameter. The increase in volume can be attributed to the influx of water along with protein and a subsequent decrease in protein concentration is noted.

In general, the protein concentration of the granules increases as granules lose protein. This indicates that granules are losing the aqueous region of their volume more than the protein aggregate. This is shown in figure 6.17 where protein density maps of granules as they lose protein and diameter indicate that the lucent regions in the granule are decreasing in size. However, there is no clear correlation between the amount of protein and volume lost in any of these experiments and granules do not increase in protein concentration in a manner suggesting volume loss is connected linearly with protein release. As such this implies that while a certain amount of water may be lost with each protein molecule released, the protein aggregate provides a substantial barrier to the shrinking of the granule volume. This result has previously been observed when granules did not to shrink as theoretically expected in response to an increase in osmotic strength of the suspending solution (Warashina, 1981).

However, the protein aggregate does appear to be flexible and may be able to shrink (exclude water) and swell (take up water) according to the environmental conditions. That it shrinks can be seen in the granules shown figure 6.17. The general shape of high dense regions (the aggregate) appears to stay the same even though they get smaller. And that the aggregate may also be able to swell is shown in the NaCl and Nigericin experiments. In these cases, ~50% of the protein was released after the granules were

exposed to these isosmotic solution but the diameters were not significantly different (P>0.05, t test). Given the electrostatic nature of these solutions, the aggregate's charge distribution may have been sufficiently altered changing its osmolarity and enabling it to take up water to compensate for the loss of protein. It is possible that the granule protein aggregate is a sol-gel.

However, even though individual protein loss (or uptake) and osmotic strength both contribute to the decrease in the diameter of a granule, it appears that all granules in an experiment are affected in a similar manner such that, regardless of the change in mass or diameter, the relationship between protein content and granule volume is maintained over time (see for example figure 6.20). As mentioned above, this relationship appears to be a characteristic for a particular preparation of granules.

The change in protein concentration of the granules can be diagrammed using the protein mass versus granule volume graphs and shown below in figure 8.1.

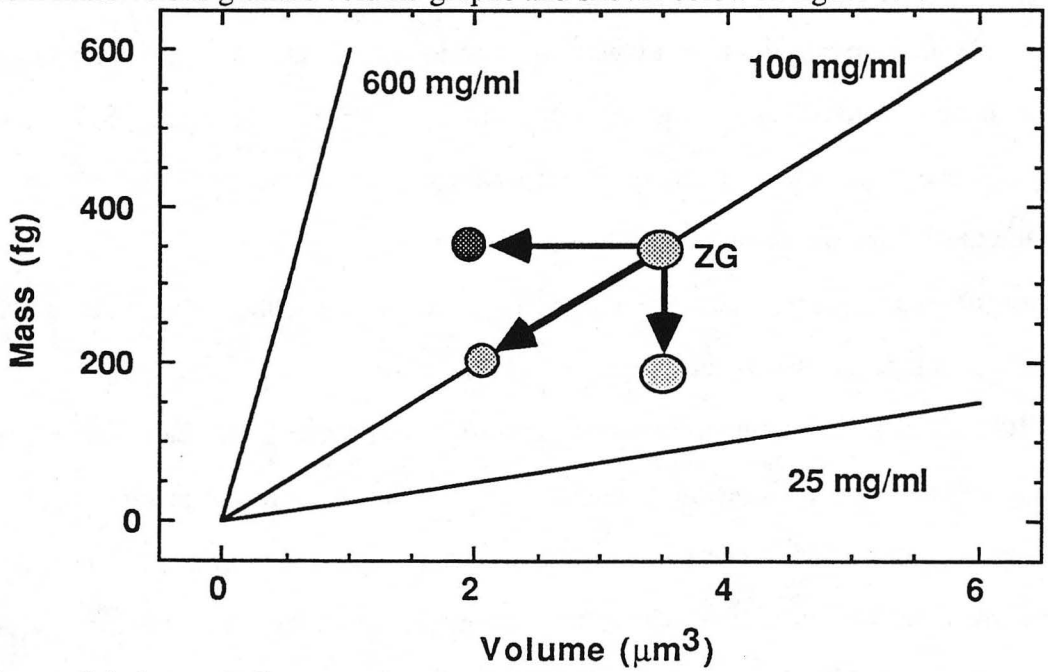

Figure 8.1 A graph diagramming the relationship between protein mass and granule volume. The slope of a line through the data point of granule ZG and the origin is the protein concentration of the granule. As either the volume or mass of the granule changes, so will the protein concentration. It is possible for the granule to become either less or more concentrated, or stay the same - as indicated by the shading of the granule.

From this figure, we can see that the protein concentration of a granule will increase when the decrease in volume of the granule dominates the decrease in mass and that the protein concentration will decrease when the decrease in mass dominates the decrease in volume. However, if the change in volume and mass vary together, the protein concentration will be maintained. The changes in protein mass and diameter occur, as mentioned aboved, as a result of mass action and the permeability of the granule membrane to its proteins. In the majority of our experiments, we observed an increase in the average protein concentration of a population of granules indicating that the rate of protein release was greater than the rate of diameter loss. And, as mentioned above, this is an indication that the structure of the protein aggregate limits the amount of granule shrinking.

Thus, using STXM we have observed that isolated secretion granules are not inert objects. They can change in size, as well as protein mass; shrinking (or enlarging) in response to non osmotic disequilibrium states as they release (or increase) their protein contents. These experiments provide direct evidence for the permeability of granule membrane to its enclosed proteins.

Many of our observations on isolated granules are consistent with similar observations made in situ. For example: (1) labeled chymotrypsinogen added to extracellular fluid accumulates in zymogen granules within the acinar cell (Liebow and Rothman, 1972), (2) the secretion of at least some of the 20 different proteins found in the zymogen granule can occur independently of each other (Rothman, 1985) and (3) granules are observed to shrink within the cell when secretion is augmented with a stimulant (Ermak and Rothman, 1981). These results indicate that zymogen granules are permeable to their enclosed proteins in situ.

Mechanisms of protein release

However, the central question is now "what is the mechanism whereby protein is able to cross the membrane of the zymogen granule?" Currently, the topic of membrane protein transport, or how protein molecules pass through biological membranes is an active and growing area of research and there are a host of mechanisms that have been discovered in pro- and eukaryotic cells involved in the transport of proteins across membranes.

It is generally considered that there are three mechanisms by which proteins are able to cross membranes; pores, chaperones and "dissolution" - the ability of the protein to cross through the membrane unaided. In the following section, we will briefly discuss the evidence for these mechanisms.

The discovery of the nuclear pore (Bonner, 1978) was the first time it was shown that a pore was capable of transporting protein. Previously, it was though that pores were only capable of transporting ions and very small molecules. Since then, other protein transporting pores have been discovered. There is currently a family of proteins, called multi-drug resistant (MDR) proteins that have been shown to form pores in membranes (Bradley, 1988). These pores are able to engage in the protein transport of a variety of different proteins in a variety of pro- and eukaryotic cells. The evidence suggests that either single protein molecules, or perhaps oligmers, form the transmembrane pores through which other proteins can pass.

The chaperones are molecular proteins and behave more as a helper in protein transport than an actual mechanism. They act to unfold certain proteins and as such prepare them for entrance into and transport across membranes (Pelham, 1989; Kumamoto, 1991). The unfolding may expose internal hydrophobic regions of the protein thus allowing the protein to pass through the hydrophobic membrane. Alternatively, as the unfolding process results in a smaller diameter protein, the protein may now be able

to cross through small diameter pores that were previously inaccessible to the tertiary structure of the protein. The chaperones may also function to retain proteins within a membrane enclosed region by holding onto or folding proteins once they enter a membrane bound compartment and therefore preventing them from being transported again.

The fact that proteins are also able to cross membranes on their own (dissolution) is the most recently accepted mechanism by which proteins are able to cross membranes. As mentioned above, it may be that chaperones assist in this process by helping to unfold proteins and exposing hydrophobic regions of the protein which are more apt to pass into the lipid bilayer. However, recent experiments show that some proteins are able to "dissolve" through lipid bilayers without any assistance. The bacterial toxins, colicins, are known to exit bacterial cells and re-enter other of their species across the outer membrane either by apparently embedding themselves in the inner plasma membrane or passing through it (Cramer et al., 1990; Lazdunski et al., 1988). This has recently been proposed to occur without the need for any special processes (Shin et al., 1993). Apparently the outer amphipathic charge-containing segments of the protein adsorbs to the charged moieties on the bilayer's surface. And this is followed by penetration of the bilayer by the protein's internal hydrophobic helices.

Unfortunately, when Rothman first proposed that proteins were able to cross bio-membranes, there was no evidence that any of these mechanisms existed and the theory was discounted. Possibly, had he made his observations today, even without direct evidence for a mechanism, the idea that proteins can cross membranes would not be quickly discounted. Currently, there is evidence that at least one, if not more, of the above mentioned mechanisms exist in zymogen granules and can aid in protein transport.

Of the three candidates for a mechanism by which the protein could cross the membrane; two of these are pores and the third is a chaperone. We have already

mentioned that a large pore, ~5nm, was reported by Cabana (1988) to be visible in the membrane of the zymogen granule in EM images. This pore would be large enough to allow the passage of protein. However, since this report, there have been no further studies pertaining to this particular pore. There is also recent evidence that a Cystic Fibrosis Transmembrane Regulator (CFTR) protein may be present in the membrane of rat zymogen granules (Tseng). This is one of the family of MDR proteins, mentioned earlier, and is known to form a pore that could be a protein transporter.

The third candidate is the chaperone and two such proteins have recently been discovered in the zymogen granule (Yeiaz-Granell et al., 1993). The authors of this abstract did not speculate as to the function the chaperone may serve in the granules, but in light of our results, it is possible that the chaperones could aid in the unfolding of the enclosed granule proteins and their subsequent transport across the ZG membrane.

VIII.2 A discussion on the technique of STXM for biology

The capability of imaging whole, viable biological samples in aqueous environments at high resolution has been a major driving force for the development of X-ray microscopy. And while this technique is still considered in the developmental stage, the results that we discussed reflect some of its potential for biologists. As such, our experience with zymogen granules enables us to raise some of the issues that need to be kept in mind if biologists are to obtain valuable results from the technique.

In terms of the type of specimen best suited for STXM, the zymogen granule is ideal and, in general, the technique is probably best used for micron sized objects. One reason for this is because the depth of focus of STXM is ~2 μm and an image of a thicker object would not be completely in focus. In addition, there is a size limit to the field of view of the microscope. When Gilbert (1992) imaged fibroblasts, multiple images had to be taken of different areas to construct a mosaic. The zymogen granule was also well suited

because it has a relatively simple structure; i.e. it predominately contains protein in various clumps and configurations. This is an advantage because the images are two-dimensional projections of three dimensional objects. If an object is complex and contains many different kinds of features at different depths, then interpreting what these features are or where they are in the sample is difficult. Furthermore, to quantitatively determine the amount of material present in the sample from the STXM image, we must know the type(s) and *relative* amount(s) of different materials present, such as nucleic acids and proteins.

In using STXM, it is also important to keep in mind the effects that the absorption of X-ray radiation can have on the particular specimen. In the radiation damage chapter (VII) it was shown that live cells are sensitive to radiation damage and after tens of Megarads of absorbed dose, cells die (Jacobsen). However in our situation, the particular kinetics of the zymogen granule which we wanted to observe, release of the contained protein, did not appear to be affected by the dose of soft X-rays the granules received. This is not to say that there was no radiation damage, only that it did not interfere with the process we were investigating.

Ultimately, the sensitivity of an object to damage due to interaction with soft X-rays dictates the experiments that can be performed with a particular sample using STXM. And, while is may be impossible to observe live cells functioning at high resolution in STXM over time, high resolution native state imaging or the ability to calculate amount of organic material present in an object may still be of value. For example, research is currently being performed on fixed cells that uses STXM to 1) map the calcium content of the cells (Buckley, 1993) and 2) detect at high resolution the location of fluorescence markers (Moronne, 1993).

In order to perform experiments on zymogen granules with STXM, it was first necessary for us to design a sample chamber (LBL-WC). Our chamber allowed for the

sample to be suspended in an aqueous environment for the duration of the experiment as well as permitting the fluid environment to be exchanged during the course of an experiment. The LBL-WC is well suited for imaging any biological object that is <2μm in size and requires a fluid environment. Other sample chambers have been developed specifically for cell cultures (Gilbert, 1992).

In our experiments, we relied on the affinity of zymogen granules for silicon nitride in order for our sample to remain still during imaging. In the future, the use of "biological glues," such as poly-L-lysine, to be coated on the viewing windows will aid in the adherence of samples . Another approach is to immobilize samples by using the thin, flexible silicon nitride windows as "tweezers." This is accomplished simply by placing a small negative pressure in the LBL-WC to pull the two windows closer together. This can be effective for samples as small as 1μm in diameter. The newly developed method of optical tweezers may also prove to be a useful specimen manipulator in the future. Finally, although this technique is just now being tested in our laboratory, it may be possible to immobilize the specimen in agar gel. It would then be possible to flow solutions over thin slabs of the gel and allow solutes to diffuse towards the specimen.

The primary problem with the development of this technique is its accessibility. Currently, there are only two STXM type microscopes that are performing biological experiments, Brookhaven and Daresbury in England, and one IXM (imaging X-ray microscope) located at BESSY in Berlin. Although recently, the Advanced Light Source synchrotron at Lawrence Berkeley Laboratory produced its first X rays and two more X-ray microscopes (a STXM and IXM) will be built there. All of the above mentioned microscopes require a synchrotron source in order to produce the X-rays. But X-ray microscopes are not limited to using these sources; the field of X-ray lasers has been growing making "table-top" X-ray microscopes a reality and there are other techniques in

the works which would use a laser plasma source (Hirsch). However, it is important to remember that the development of this technique is as much investigational as it is instrumental . The more biology that is performed using these microscopes, the faster the technique will be developed in terms of what kind of biological questions are best addressed using this method.

Chapter VIII - References

Adelson, J.W. and P.E. Miller, Heterogeneity of the exocrine pancreas, Am. J. Physiol. (1989) **256**:G817-G825.

Bonner, W.M., Protein migration and accumulation in the nuclei, In: The Cell Nucleus (Ed. H. Busch) Vol. 6, Academic Press: New York (1978).

Bradley, G., P.F. Juranka and V. Ling, Mechanism of multidrug resistance, Biochim. Biophys. Acta (1988) **948**:87-128.

Burwen, S.J., Zymogen granules: Structure and properties, Ph.D. Dissertation (1972) Harvard University, Cambridge, MA.

Buckley, C.J., N. Khaleque, S.Y. Ali, C.A. Scotchford, C. Downes and L. DiSilvio, Scanning X-ray microscopy of cartilage and bone, In: X-ray Microscopy IV (to be published).

Cabana, C., P. Magny, D. Nadeau, G. Grondin and A. Beaudoin, "Freeze-fracture study of the zymogen granule membrane of pancreas: two novel types of intramembrane particles," Eur. J. Cell Biol. (1988) **45**:246-55.

Ermak, T.H. and S.S. Rothman, Large decrease in zymogen granule size in the postnatal rat pancreas, Cell Tiss. Res. (1981) **214**:51-66.

Gilbert, J.R., Soft X-ray microimaging of whole wet cells, Ph.D. Thesis, California Technical Institute: Pasadena, California (1992).

Hirsch, G. U.S. Patent number 4,829,177.

Ho, J.J.L. and S.S. Rothman, Protein concentration in the pancreatic zymogen granule, Biochem. Biophys. Acta (1976) **755**:457-466.

Hokin, L.E., Isolation of the zymogen granules of dog pancreas and a study of their properties, Biochim. Biophys. Acta (1955) **18**:379-388.

Jacobsen, C.J. Personal communications.

Kumamoto, C.A., Molecular chaperones and protein translocation across the Escherichia coli inner membrane, Mol. Microbiol. (1991) **5**:19-22.

Liebow, C. and S.S. Rothman, Equilibrium of pancreatic digestive enzymes across zymogen granule membranes, Biochim. Biophys. Acta (1976) **455**:241-253.

Liebow, C. and S.S. Rothman, Membrane transport of proteins, Nature (1972) **240**:176-178.

Moronne, M.M., Development Fluorescent probes for soft X-ray microscopy, In: X-ray Microscopy IV (to be published).

Mroz, E.A. and C. Lechene, Pancreatic zymogen granules differ markedly in Protein concentration, Science (1986) **232**:871-873.

Pelham, H.R.B., Heat shock and the sorting luminal ER proteins, Emb. J. (1989) **8**:3171-3176.

Rothman, S.S. In: Protein Secretion: A critical analysis of the vesicle model, John Wiley and Sons (1985) New York.

Rothman, S.S., S. Burwen and C. Liebow, The zymogen granule: Intragranular organization and its functional significance, Advances in Cytopharmacology, Vol. 2 (eds: B. Ceccarelli, F. Clementi and J. Meldolesi) Raven Press, New York (1974).

Rothman, S.S., The behavior of isolated zymogen granules: pH-dependent release and reassociation of protein, Biochim. Biophys. Acta (1971) **241**:567-577.

Tobler, M., J. Kassner, R.W. Ammann and A.U. Freiburghaus, Heterogeneity of zymogen granules - Are all granules filled equally?, In: Abstracts of the XXII Meeting of the European Pancreatic Club (1991) 182.

Tseng, H.C., Personal communication

Shin, Y.K., C. Levinthal, F. Levinthal and W.L. Hubbell, Colicin E1 binding to membranes: Time-resolved studies of spin-labeled mutants, Science (1993) **259**:960-963.

Velez-Granell, C., A.E. Arias, J.A. Torres-Rulz and M. Bendayan, Involvement of chaperones in the secretory activity of the pancreatic anciar cells, Pancreas (1993) **8.**

Warashina, A., Properties of pancreatic zymogen granules studied by quasi-elastic light scattering, Biochim. Biophys. Acta (1981) **672**:158-164.

LAWRENCE BERKELEY LABORATORY
UNIVERSITY OF CALIFORNIA
TECHNICAL INFORMATION DEPARTMENT
BERKELEY, CALIFORNIA 94720